

AD-A101 360

TRW DEFENSE AND SPACE SYSTEMS GROUP REDONDO BEACH CA
EVALUATION OF DCS III TRANSMISSION ALTERNATIVES, PHASE 1A REPORT--ETC(U)
MAY 80 T M CHU
TRW-35142-APP-A

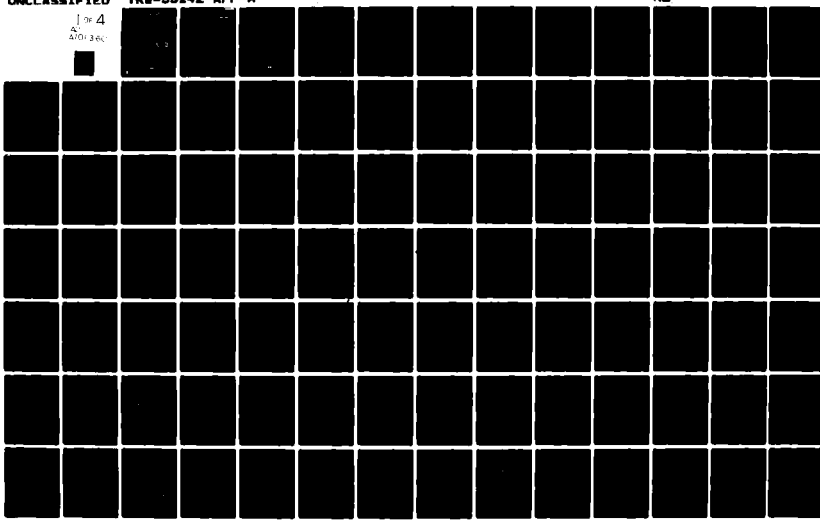
F/0 17/2.1

DCA100-79-C-0044

NL

UNCLASSIFIED

1 of 4
470136C



AD A101360

(12)

LEVEL III

P101369

DEFENSE COMMUNICATIONS
DEPARTMENT OF DEFENSE

(10)

EVALUATION OF DCS III
TRANSMISSION ALTERNATIVES
PHASE 1A REPORT.

APPENDIX A.
TRANSMISSION MEDIA.

26 MAY 1980

(12) 388

DTIC
SELECTED
JUL 14 1981

D

B

Prepared for
Defense Communications Agency
Defense Communications Engineering Center
Reston, Virginia 22090

Contract No. DCA 100-79-C-0044

DISTRIBUTION STATEMENT A
Approved for public release;
Distribution Unlimited

TRW.
DEFENSE AND SPACE SYSTEMS GROUP

ONE SPACE PARK, REDONDO BEACH, CALIFORNIA 90278

ONE FILE COPY

441637

81608082

UNCLASSIFIED

SECURITY CLASSIFICATION OF THIS PAGE (When Data Entered)

REPORT DOCUMENTATION PAGE		READ INSTRUCTIONS BEFORE COMPLETING FORM
1. REPORT NUMBER TRW No. 35142	2. GOVT ACCESSION NO. <i>AD-A102 360</i>	3. RECIPIENT'S CATALOG NUMBER [REDACTED]
4. TITLE (and Subtitle) EVALUATION OF DCS III TRANSMISSION ALTERNATIVES - PHASE 1A REPORT	5. TYPE OF REPORT & PERIOD COVERED Final Phase 1A Report	
7. AUTHOR(s) T. M. Chu	6. PERFORMING ORG. REPORT NUMBER DCA 100-79-C-0044 ✓	
9. PERFORMING ORGANIZATION NAME AND ADDRESS TRW, Inc.; Defense and Space Systems Group One Space Park Redondo Beach, CA 90278	10. PROGRAM ELEMENT, PROJECT, TASK AREA & WORK UNIT NUMBERS N/A	
11. CONTROLLING OFFICE NAME AND ADDRESS Defense Communications Engineering Center Transmission Engineering Division, R200 1860 Wiehle Ave., Reston, VA 22090	12. REPORT DATE 26 May 1980	
14. MONITORING AGENCY NAME & ADDRESS (if different from Controlling Office) N/A	13. NUMBER OF PAGES 1044	
16. DISTRIBUTION STATEMENT (of this Report) Approved for public release; distribution unlimited	15. SECURITY CLASS. (of this report) Unclassified	
17. DISTRIBUTION STATEMENT (of the abstract entered in Block 20, if different from Report) N/A	15a. DECLASSIFICATION/DOWNGRADING SCHEDULE N/A	
18. SUPPLEMENTARY NOTES Four Volumes: Main and Appendixes A, B, and C.		
19. KEY WORDS (Continue on reverse side if necessary and identify by block number) Defense Communications System Digital Transmission System Millimeter Wave LOS System	EHF Satellite System Airborne Relay Platform Cable/Optical Fiber System	
20. ABSTRACT (Continue on reverse side if necessary and identify by block number) This report covers DCS III requirements, transmission media characteristics, regulatory factors, and DCS III transmission system alternatives. Appendix A documents results of transmission-media investigations. Appendix B presents a detailed review of rules, procedures, regulations, standards, and recommendations established by national/international organizations. Appendix C provides a description of topographic and climatic conditions in Germany, Turkey, and Hawaii.		

EVALUATION OF DCS III TRANSMISSION ALTERNATIVES PHASE 1A REPORT

APPENDIX A TRANSMISSION MEDIA

26 MAY 1980

Prepared by



Dr. T.M. Chu
Manager
DCS III Project

Approved by



N. Estersohn
Manager
Communications Architecture

Prepared for

Defense Communications Agency
Defense Communications Engineering Center
Reston, Virginia 22090

Contract No. DCA 100-79-C-0044



ONE SPACE PARK . REDONDO BEACH, CALIFORNIA 90278

CONTENTS

	Page
A.1 TRANSMISSION MEDIA	A.1-1
A.1.1 >Coaxial Cable Characteristic, and	A.1-2
A.1.2 Mean Real Part of 1.2/4.4-mm Cable Impedance	A.1-5
A.1.3 Future Trend in the Coaxial System Development	A.1-15
A.1.4 Intrinsic Limitation of Coaxial Systems,	A.1-16
A.1.4.1 Bandwidth Limitation Due to Attenuation	A.1-16
A.1.4.2 Cable Irregularities	A.1-17
A.2 MILLIMETER WAVEGUIDE	A.2-1
A.3 BEAM WAVEGUIDE ;	A.3-1
A.4 TERRESTRIAL MICROWAVE LINE-OF-SIGHT (LOS) TRANSMISSION; . . .	A.4-1
A.4.1 Description of Medium	A.4-1
A.4.2 Intrinsic Technical Limitations	A.4-15
A.4.3 Development Trends	A.4-23
A.5 TROPOSPHERIC SCATTER COMMUNICATIONS	A.5-1
A.5.1 Description of Medium	A.5-1
A.5.2 Fading and Diversity Reception	A.5-13
A.5.3 Digital Troposcatter	A.5-19
A.5.4 Summary	A.5-19
A.6 MM-WAVE TECHNOLOGY	A.6-1
A.6.1 Transmitters	A.6-1
A.6.1.1 MM Traveling Wave Tubes	A.6-2
A.6.1.2 Gyrotrons	A.6-2
A.6.1.3 Low-Power Sources	A.6-7
A.6.2 Modulation of Semiconductor Sources	A.6-20
A.6.3 Receiver Technology	A.6-22
A.6.4 Circuit Fabrication Technology	A.6-25
A.6.5 Antennas	A.6-27
A.6.6 Atmospheric Effects	A.6-27
A.6.7 Point-to-Point Transmission	A.6-33
A.6.8 Fading Due to the Atmosphere	A.6-45

RE: DISTRIBUTION STATEMENT.
EVALUATION OF DCS III TRANSMISSION
ALTERNATIVES.
STATEMENT A PER JANET ORNDORF
DCA TECHNICAL LIBRARY CODE 312
WASHINGTON D. C. 20305

• .	A.6-22	
• .	A.6-25	
• .	A.6-27	
• .	A.6-27	
• .	A.6-33	<input type="checkbox"/>
• .	A.6-45	<input checked="" type="checkbox"/>

By _____

Distribution/

Availability Codes

Avail and/or

Dist Special

A

CONTENTS (Continued)

	<u>Page</u>
A.7 EHF SATELLITE COMMUNICATIONS	A.7-1
A.7.1 Introduction	A.7-1
A.7.2 Major Features of Current EHF Technology	A.7-1
A.7.2.1 Hardware Technology	A.7-1
A.7.2.2 Propagation Losses	A.7-3
A.7.3 Other EHF SATCOM System Features	A.7-4
A.7.4 Applications	A.7-7
A.7.5 EHF SATCOM Network Performance Capability	A.7-7
A.7.5.1 Performance Bounds Under Benign Conditions	A.7-7
A.7.5.2 Network Problem	A.7-15
A.7.5.3 Traffic Capability	A.7-18
A.7.5.4 Technology Availability for ECCM Performance and Survivability	A.7-18
A.7.6 Summary and Conclusions	A.7-20
A.8 PACKET RADIO; CIVILIAN COMMUNICATIONS PROGRAM	
A.8.1 Packet Radio Technology	A.8-1
A.8.1.1 Packet Switching	A.8-1
A.8.1.2 Packet Radio	A.8-2
A.8.1.3 Related Techniques	A.8-3
A.8.2 Packet Radio System	
A.8.2.1 Signaling in the Ground Radio Environment	A.8-3
A.8.2.2 Multiple Access and System Performance	A.8-8
A.8.2.3 Network Elements	A.8-10
A.8.3 Experimental Packet-Radio Developments	A.8-12
A.8.3.1 ARPA Packet-Radio Experimental Program	A.8-12
A.8.3.2 Experimental Packet-Radio Unit	A.8-14
A.8.3.3 Upgraded Packet Radio Unit	A.8-16
A.8.4 Packet Satellite Experiment	A.8-19
A.8.4.1 Atlantic Packet Satellite Experiment	A.8-19
A.8.4.2 Wideband Experimental Integrated Switched Network	A.8-36

CONTENTS (Continued)

	<u>Page</u>
A.9 OPTICAL FIBER COMMUNICATION	A.9-1
A.9.1 Introduction	A.9-1
A.9.2 Optical Fiber Communication System	A.9-5
A.9.3 Optical Fiber	A.9-7
A.9.3.1 Fiber Propagation Modes	A.9-7
A.9.3.2 Optical Fiber Attenuation	A.9-14
A.9.3.3 Dispersion and Pulse Broadening	A.9-17
A.9.4 Optical Sources	A.9-23
A.9.4.1 Light-Emitting Diodes	A.9-24
A.9.4.2 Injection Laser	A.9-29
A.9.5 Modulation Techniques	A.9-35
A.9.5.1 Direct Modulated Light Emitting Diodes LED	A.9-36
A.9.5.2 Direct Modulated Injection Lasers	A.9-38
A.9.6 Optical Detector	A.9-40
A.9.6.1 Detection Process and Detector Requirements	A.9-40
A.9.6.2 PN Photodiode	A.9-41
A.9.6.3 PIN Photodiode	A.9-43
A.9.6.4 Avalanche Photodiode	A.9-45
A.9.7 Research Trends and Systems Capability	A.9-49
A.9.7.1 Fiber Optics Research Areas	A.9-50
A.9.7.2 Fiber Optics Components	A.9-51
A.9.7.3 Predicted System Capability	A.9-53
A.10 SUBMARINE CABLES	A.10-1
A.10.1 Development of Submarine Cable	A.10-1
A.10.1.1 Development of Submarine Telegraphic Cable	A.10-3
A.10.1.2 Development of Submarine Telephone Cables	A.10-3
A.10.1.3 Major Submarine Cable Routes	A.10-4
A.10.2 Submarine Cable Technology Development	A.10-7
A.10.3 Recent Growth of Submarine Cable	A.10-11

CONTENTS (Continued)

	<u>Page</u>
A.11 METEOR-BUST COMMUNICATIONS SYSTEM	A.11-1
A.11.1 Introduction	A.11-1
A.11.2 System Concept	A.11-2
A.11.2.1 Physical Properties of Meteors	A.11-2
A.11.2.2 Meteor Trails	A.11-6
A.11.2.3 Scattered Signal of an Idealized Trail . .	A.11-7
A.11.2.4 Scattered Signal from Meteor Trails . . .	A.11-9
A.11.3 Meteor Communications Systems	A.11-12
A.11.3.1 Canadian JANET Buffer-Burst System	A.11-13
A.11.3.2 STC COMET System	A.11-16
A.11.3.3 Boeing Data Acquisition System	A.11-23
A.11.3.4 Other Related Experimental Systems	A.11-?
A.12 RADIO FREQUENCY SPECTRUM	A.12-1
A.12.1 Wave Propagation Mechanism	A.12-2
A.12.1.1 Wave Propagation Mechanism	A.12-2
A.12.1.2 Nature of Radio Signals	A.12-3
A.12.1.3 Characteristics of Radio Waves	A.12-4
A.12.2 ELF and VF Propagation Characteristics	A.12-4
A.12.2.1 Boundary Characteristics	A.12-9
A.12.2.2 Waveguide Modes	A.12-11
A.12.3 VLF and LF Propagation Characteristics	A.12-11
A.12.3.1 VLF and LF Propagation Mechanisms	A.12-12
A.12.3.2 Waveguide Theory	A.12-13
A.12.3.3 Wave Hop Theory	A.12-14
A.12.4 Medium Frequency Propagation Characteristics .	A.12-17
A.12.5 High-Frequency Wave Propagation Characteristics	A.12-18
A.12.5.1 HF Propagation Mechanism	A.12-18
A.12.5.2 HF Signal Predictions	A.12-23
A.12.5.3 HF Frequency Management	A.12-23
A.12.6 VHF, UHF, and EHF Bands	A.12-26
A.12.6.1 Ionospheric Scattering	A.12-27
A.12.6.2 Sporadic-E Propagation	A.12-28
A.12.6.3 F ₂ Propagation	A.12-28

CONTENTS (Concluded)

	<u>Page</u>
<i>Alternatives to Electromagnetic Communication; Particular Emergency Considerations</i>	
A.13 ALTERNATIVES TO ELECTROMAGNETIC COMMUNICATION LINKS	A.13-1
A.13.1 Basic Considerations	A.13-1
A.13.2 Gravitational Waves and Subnuclear Particles	A.13-5
A.13.3 Conclusions on Non-Electromagnetic Communications Options	A.13-8
A.14 MANNED AND UNMANNED AIRCRAFT	A.14-1
A.14.1 Manned Aircraft	A.14-1
A.14.1.1 EC-135 Aircraft	A.14-2
A.14.1.2 Other Manned Relay Aircraft	A.14-2
A.14.1.3 Utility of Manned Aircraft for DCS III . .	A.14-5
A.14.2 Unmanned Aircraft	A.14-6
A.15 TETHERED BALLOON CHARACTERISTICS AND CAPABILITY	A.15-1
A.15.1 Tethered Balloon	A.15-1
A.15.2 System and Components Description	A.15-1
A.15.2.1 Balloonet System	A.15-1
A.15.2.2 Stabilizers	A.15-3
A.15.2.3 Materials	A.15-3
A.15.2.4 Powered Tether System	A.15-5
A.15.2.5 Mooring System	A.15-5
A.16 HIGH-ALTITUDE POWERED PLATFORM CHARACTERISTICS AND CAPABILITY	A.16-1
A.16.1 Introduction	A.16-1
A.16.2 Power System	A.16-3
A.16.3 Potential Applications of HAPP	A.16-4
A.16.4 Summary	A.16-6

REFERENCES

R-1

BLANK PAGE

FIGURES

	<u>Page</u>
A.1-1 Attenuation of 9.5 cm (3/8 in.) Coaxial Cable at 55°C . . .	A.1-4
A.1-2 Growth of Bell Coaxial System	A.1-6
A.1-3 The Hierarchy of Digital Channels on the North America System	A.1-10
A.1-4 Evaluation of DCS III Transmission Alternatives Digital Hierarchies	A.1-12
A.1-5 System Configuration for PCM-100M System and PCM-400M System	A.1-14
A.2-1 Model Coupling of Circular Waveguide	A.2-2
A.2-2 Attenuation of Millimeter Waveguide	A.2-3
A.2-3 Attenuation of Millimeter Waveguides of Different Size . .	A.2-4
A.2-4 Typical Constructions of Millimeter Waveguide	A.2-6
A.3-1 Iris Beam Waveguide	A.3-2
A.3-2 Lens Beam Waveguide	A.3-2
A.3-3 Reflection Mirror Beam Waveguide	A.3-2
A.3-4 Typical Relationship Between Bandwidth and Refelcting . .	A.3-4
A.4-1 Summary of Frequency Allocations	A.4-3
A.4-2 Two-Path Interference Caused by Reflection at the Surface of the Intervening Ground	A.4-6
A.4-3 Multipath Caused by Ground Based Ducting Layer	A.4-6
A.4-4 Multipath Caused by Elevated-Duct Reflection	A.4-7
A.4-5 Atmospheric Multipath	A.4-7
A.4-6 Atmospheric Absorption	A.4-8
A.4-7 Ground Obstruction Caused by a Combination of Insufficient Ground Clearance and Upward Bending of the Rays	A.4-8
A.4-8 Deflection of a Microwave Signal by a Duct Boundary at the Elevation of a Path Line	A.4-9
A.4-9 Deflection of a Microwave Signal by an Elevated Duct . . .	A.4-9

FIGURES (Continued)

	<u>Page</u>
A.4-10 Rain Attenuation for Different Frequencies	A.4-12
A.4-11 Space Diversity Configuration	A.4-20
A.4-12 Frequency and Space Diversity Improvements	A.4-21
A.4-13 Frequency Response Versus Differential Absolute Delay for Space Diversity	A.4-22
A.4-14 Trends of Transmission Capacity	A.4-27
A.4-15 Frequency Utilization Efficiency	A.4-27
A.4-16 Repeater Spacing	A.4-28
A.5-1 Typical Troposcatter Path Geometry	A.5-2
A.5-2 Median Basic Propagation Loss for Groundwave Tropospheric-Scatter Mode of Propagation Over a Smooth Spherical Earth	A.5-4
A.5-3 Transmitter Power Requirement for 24-Voice-Channel Tropospheric Scatter Circuit over Smooth Earth	A.5-5
A.5-4 Expected Maximum Ranges vs Frequency for Various Types of Service and Antenna Diameters	A.5-6
A.5-5 Aperture-to-Medium Coupling Loss	A.5-7
A.5-6 Standard Deviation of Scattered Field for Various Climates	A.5-8
A.5-7 Median Attenuation by Scattering	A.5-9
A.5-8 Plots of Bandwidth Versus Range with Antenna Gain as Parameters	A.5-10
A.5-9 Path Loss Vs Frequency from the NMS Model and from the Turbulent Scatter Theory with Type Parameter	A.5-11
A.5-10 Aperture-to-Medium Coupling Loss Vs Antenna Diameter . . .	A.5-12
A.5-11 Path Profile with Optimized Vertically Offset Beams . . .	A.5-18
A.5-12 2S/2A Configurations	A.5-22
A.6-1 Distributed Interaction Gyrotron	A.6-3
A.6-2 Gyrotron Power Tube State-of-the-Art	A.6-5

FIGURES (Continued)

	<u>Page</u>
A.6-3 GaAs FET State-of-the-Art	A.6-7
A.6-4 CW Power Output of Negative Resistance Diodes	A.6-9
A.6-5 Efficiency of CW Negative Resistance Diodes	A.6-9
A.6-6 Pulses Power and Efficiency of Double Drift Silicon IMPATT Diodes Pulse Width = 100ns	A.6-10
A.6-7 FM Noise of CW InP IMPATT OSCILLATOR QX 130	A.6-10
A.6-8 Injection Locking Gain-Bandwidth Characteristics of a Millimeter-Wave IMPATT Oscillator	A.6-12
A.6-9 Millimeter-Wave Phase Locking Technique	A.6-15
A.6-10 Frequency Tuning Characteristics of an IMPATT Oscillator	A.6-16
A.6-11 Peak Power Capability Decreases with Increasing Pulse Width Due to Heating During the Pulse	A.6-16
A.6-12 Predicted Transferred Electron Device Efficiency Versus Frequency	A.6-18
A.6-13 IMPATT Device Efficiency Versus Frequency	A.6-18
A.6-14 Output Power Versus Input Power for InP Notch Device Biased for Low Noise	A.6-19
A.6-15 Gain Versus Frequency for InP Notch Diode. Maximum Measured Noise Figure Across Band is 10.9 dB	A.6-19
A.6-16 Performance of Hughes Gunn VCOs	A.6-21
A.6-17 Typical Performance of Millimeter IMPATT Sweeper with 20 GHz Sweep Bandwidth	A.6-21
A.6-18 Sweep Bandwidth Capability for Hughes IMPATT Sweepers . .	A.6-21
A.6-19 Receiver Technology	A.6-22
A.6-20 Noise Figures of 0.5 m Gate GaAs FETS	A.6-23
A.6-21 Noise Figure of Narrow Band Transistor Amplifiers as a Function of Frequency and Time	A.6-23
A.6-22 Loss Comparison for Various Waveguide Sizes	A.6-26

FIGURES (Continued)

	<u>Page</u>
A.6-23 Antenna Selection Requirements	A.6-28
A.6-24 Attenuation Due to Rain	A.6-29
A.6-25 Atmospheric Attenuation	A.6-30
A.6-26 Millimeter Wave Attenuation	A.6-26
A.6-27 Sky Noise Temperature Due to Reradiation by Oxygen at Water Vapor	A.6-32
A.6-28 Transmission Loss for a MM Wave LOS Link	A.6-35
A.6-29 Maximum Repeater Spacing for 16 dB S/N Rain as Heavy Pour (150 mm/Hr) using a 200 Milliwatt Transmitter	A.6-39
A.6-30 Peak Fade with a Large Number of Repeaters in Line Due to Mutual Interference	A.6-44
A.7-1 Simplified Diagram of European DCS	A.7-8
A.7-2 EHF Satellite Network for Replacing European Long Haul DCS Network	A.7-9
A.7-3 Coverage of an Elliptical Satellite Antenna	A.7-10
A.7-4 Coverage of a Multiple Feed Antenna with Three Foot Offset Reflector	A.7-11
A.7-5 Six Beam MNA Long Haul Coverage	A.7-13
A.7-6 Satellite Translation Transponder	A.7-17
A.8-1 Packet Format	A.8-2
A.8-2 Pseudonoise Spread Spectrum System	A.8-6
A.8-3 Frequency Hopping Spread Spectrum System	A.8-7
A.8-4 Traffic Versus Throughput for a Bare ALOHA Channel and a Slotted ALOHA Channel	A.8-9
A.8-5 Channel Utilization of Various Multiple Access Methods of Packet Radio	A.8-10
A.8-6 Packet Radio Network Elements	A.8-11
A.8-7 Location of Major Elements of the 1977 Packet Radio Testbed	A.8-13

FIGURES (Continued)

	<u>Page</u>
A.8-8 Experimental Packet Radio (EPR) Configuration	A.8-15
A.8-9 Upgraded Packet Radio (UPR) Configuration	A.8-17
A.8-10 Schematic of SATNET Experiment	A.8-20
A.8-11 Earth Station Equipment Associated with SATNET Experiment	A.8-21
A.8-12 Block Diagram of SATNET System	A.8-22
A.8-13 Schematic of Satellite IMP Software	A.8-24
A.8-14 Elements of the Gateway	A.8-25
A.8-15 Topology for Experimental Wideband Network	A.8-27
A.8-16 Subsystems for Experimental Network	A.8-28
A.9-1 Progress in Reliability Reduction of Optical Fiber Transmission Loss	A.9-2
A.9-2 Progress in Reliability Improvement of Semiconductor Injection Laser	A.9-3
A.9-3 Optical Fiber Communication System	A.9-6
A.9-4 Repeater of an Optical Fiber Communications System	A.9-6
A.9-5 Types of Optical Fibers	A.9-8
A.9-6 Normalized Modal Propagation Constant Versus Modal Parameter V and Field Distribution Patterns	A.9-10
A.9-7 Fiber Attenuation Versus Wavelength	A.9-12
A.9-8 Attenuation Spectrum for a High Silica Waveguide	A.9-16
A.9-9 Fiber Material Dispersion	A.9-19
A.9-10 Dispersion of a Single Mode Optical Fiber	A.9-22
A.9-11 Comparison of Pulse Spread of Various Types of Optical Fiber	A.9-23
A.9-12 Edge Emitter DH LED	A.9-26
A.9-13 Surface Emitting LED	A.9-27

FIGURES (Continued)

	<u>Page</u>
A.9-14 Couples Power Versus NA for LEDs	A.9-29
A.9-15 Board Are Injection Laser	A.9-30
A.9-16 Stripe Injection Laser	A.9-30
A.9-17 Geometry of a Stripe Injection Laser	A.9-33
A.9-18 Far-Field Pattern of a Edge Emitter Laser	A.9-33
A.9-19 Modes of An Injection Laser	A.9-35
A.9-20 Output Characteristics of ADP LED	A.9-39
A.9-21 PN Photodiode	A.9-42
A.9-22 PIN Photodiode	A.9-43
A.9-23 Front Illuminated PIN Diode	A.9-44
A.9-24 Side Illuminated PIN Diode	A.9-44
A.9-25 Avalanche Photodiode	A.9-45
A.9-26 Mesa APD	A.9-46
A.9-27 N+PP+ Guard APD (GAPD)	A.9-47
A.9-28 Reach-Through APD	A.9-48
A.9-29 Epitaxial Reach-Through APD	A.9-48
A.9-30 Project Progress of Optical Fiber Transmission Capacity. .	A.9-52
A.9-31 Projected Optical Fiber Price	A.9-54
A.9-32 Projected Power Output of Optical Sources	A.9-54
A.9-33 Projected Mean Time to Failure of Optical Sources	A.9-55
A.10-1 Commonwealth Backbone Network	A.10-2
A.10-2 Major Transoceanic Submarine Cable Route	A.10-5
A.10-3 Growth of Submarine Cable System Bandwidth	A.10-10
A.10-4 Submarine Capacity and Relative Cost Progress	A.10-12

FIGURES (Continued)

	<u>Page</u>
A.11-1 Temporal Variation of Meteor Rates	A.11-4
A.11-2 Frequency-Height Distributions of Long Enduring Meteor Trails	A.11-6
A.11-3 Geometry of Forward-Scattering	A.11-8
A.11-4 Low Frequency Underdense Meteor Trail	A.11-11
A.11-5 Long Frequency Overdense Meteor Trail	A.11-12
A.11-6 Simplified Block Diagram of JANET System	A.11-14
A.11-7 Distribution Information Rate - Percentage of Time the Information Rate Exceeded a Given Value	A.11-15
A.11-8 Diurnal Variation of Average Mean Information Rate	A.11-15
A.11-9 Block Diagram of Terminal Equipment of STC COMET System	A.11-17
A.11-10 Number of Transmission Burst Per 7.5 Minute Period	A.11-19
A.11-11 Probability Distribution of Burst Length	A.11-19
A.11-12 Probability of Distribution of Interval Duration	A.11-20
A.11-13 Probability Distribution of Transmiission Delay	A.11-21
A.11-14 Block Diagram of Boeing Meteor Burst Data Acquisition System	A.11-24
A.11-15 Boeing System Waiting-Time Statistics	A.11-26
A.11-16 Signal Duty Cycle Versus Threshold Level	A.11-28
A.11-17 Character Error Rates Versus Transmission Speed	A.11-28
A.11-18 Block Diagram of SRI Meteor Burst Voice System	A.11-30
A.11-19 Locations of Meteor Burst Link and Monitoring Stations . .	A.11-35
A.11-20 Cumulative Distribution of Propagation Time Percentages for Stations A, C, D, E,, and F	A.11-36
A.11-21 Statistical Distribution of Normalized Values of P for Stations C, D, E, and F	A.11-36

FIGURES (Concluded)

	<u>Page</u>
A.11-22 Cumulative Distribution of Interception Ratio for Stations C, D, E, and F	A.11-37
A.12-1 Geometry for Wave Hop Propagation Model	A.12-15
A.12-2 Single-Hop Ionospheric Transmission Paths	A.12-20
A.12-3 Multiple-Hop Ionospheric Transmission Paths	A.12-21
A.12-4 Ionospheric Transmission Paths with Sporadic-E, E_s , Layers Reflection	A.12-22
A.13-1 Energy Propagation Modes	A.13-2
A.14-1 Major Dimensions of L-450 Aircraft	A.14-7
A.14-2 Typical L-450 Flight Profile	A.14-9
A.15-1 Aeorstat Balloon	A.15-2
A.15-2 Balloon Hull-Material Construction	A.15-4
A.15-3 Powered Tethered System	A.15-6
A.16-1 Concepts of High Altitude Powered Platform	A.16-1
A.16-2 HAPP Baseline Airship Designs	A.16-2
A.16-3 Diameter of Area Seen from a HAPP Versus Sensor Angular F(V (For 70,000 Foot Altitude	A.16-5
A.16-4 LOS Range as a Function of Ground Antenna Evaluation Angle	A.16-5

LIST OF TABLES

	<u>Page</u>
A.1-1 CCITT Recommended Nominal Cable Attenuation	A.1-3
A.1-2 Mean Real Part of 1.2/4.4-mm Cable Impedance	A.1-5
A.1-3 Growth of the Bell L-System	A.1-7
A.1-4 CCITT Recommendations on Transistorized Coaxial Cable Systems	A.1-8
A.1-5 Bell System Digital Coaxial Cable System in North America	A.1-11
A.1-6 Japanese PCM-100M and PCM-400M System Parameters	A.1-13
A.1-7 Summary of the State-of-the-Art Coaxial Cable Transmission Systems	A.1-15
A.2-1 Comparison of Waveguide Transmission Systems	A.2-8
A.4-1 Rain Attenuation in dB/mi at 11 GHz	A.4-11
A.4-2 Fade Margins in dB Required for Protection Against Multipath Fades at 12 GHz	A.4-11
A.4-3 Expressions for Redundant-Equipment Availability	A.4-14
A.4-4 Carrier to Interferences (C/I) Ratios in dB into Different Systems	A.4-18
A.4-5 Efficient Spectrum Utilization	A.4-26
A.4-6 DRAMA Radio Configurations	A.4-30
A.5-1 S/N-Ratio Improvement Using Diversity	A.5-15
A.5-2 S/N-Ratio Improvement Induced by Diversity System	A.5-15
A.6-1 Current Developmental TWTs	A.6-2
A.6-2 Reported Gyrotron CW Results	A.6-4
A.6-3 Current Power Outputs Available from Off-the-Shelf Single-Device IMPATT Source	A.6-8
A.6-4 TRW MM-Wave IMPATT-Circuit Developments	A.6-11
A.6-5 Diode Performance	A.6-25
A.7-1 Current Technology Development Programs	A.7-2

LIST OF TABLES (Continued)

	<u>Page</u>
A.7-2 SATCOM Attenuation at 30° Elevation as Function of Season in Representative Climate Zones	A.7-5
A.7-3 Beam Pattern and Weather Attenuation for Typical Terminal Locations	A.7-6
A.7-4 Performance Comparison of Two Spacecraft Antenna Systems with a Single Frequency Translation Transponder	A.7-14
A.7-5 Performance Capability at Typical Station Location (Single Transponder)	A.7-16
A.9-1 Milestones of Optical-Fiber Communications Development	A.9-3
A.9-2 Representative Test and Operational Optical Fiber Systems	A.9-4
A.9-3 Predicted Capability of Fiber Optic Communication System	A.9-56
A.10-1 Some Typical Transoceanic Submarine Telephone Cables . .	A.10-6
A.10-2 Bell System Submarine Cable	A.10-8
A.10-3 Varying Cable Bandwidth and System Capacity	A.10-9
A.10-4 Distribution of Submarine Cables	A.10-14
A.10-5 Cable-Network Growth in 1974-1978 Period	A.10-14
A.10-6 Planned Submarine Cable Systems	A.10-15
A.11-1 Characteristics of Sporadic Meteors	A.11-3
A.11-2 Transmission-Delay Statistics	A.11-22
A.11-3 Characteristics of Boeing Data Acquisition System	A.11-24
A.12-1 Frequency Bands Summary	A.12-5
A.12-2 Characteristics of Radio Waves	A.12-6
A.13-1 Communication Carriers Summary	A.13-3
A.13-2 Energy Propagation Modes	A.13-4
A.13-3 Properties of Various Subnuclear Particles	A.13-6
A.14-1 Major Characteristics of 70	A.14-3

LIST OF TABLES (Concluded)

	<u>Page</u>
A.14-2 Relay Aircraft Communications Equipment Complement . . .	A.14-3
A.14-3 Specification of EC-130 Q	A.14-4
A.14-4 Annual Operation and Support Costs	A.14-7
A.14-5 L-450 Specifications	A.14-10
A.14-6 Comparison of Three Types of RPVs	A.14-10

APPENDIX A

TRANSMISSION MEDIA

Appendix A documents results of transmission-media investigations undertaken in connection with the Evaluation of DCS III Transmission Alternatives study.

A brief but rather broad categorization and preliminary examination of the entire transmission spectrum covering guided as well as radiated transmission modes has been conducted. This approach was adopted so that no potentially promising transmission medium would be overlooked or missed and that no effort is wasted on intensive study of media not suitable for DCS. To achieve those goals this preliminary effort categorizes media into the following two groups:

- Most promising media meriting further detailed investigation
- Media to be discarded.

Results of detailed investigation of promising media are documented first, followed by brief descriptions of discards. Reasons for discard are also included for each medium.

A.1 COAXIAL CABLE

Coaxial cables are used to transmit signals in the TEM propagation mode. The outer and inner conductors are usually copper, with dielectric medium between. To enhance mechanical strengths as well as to provide additional magnetic shielding, lead or steel tapes are applied over the outer conductor. Additional dielectric insulation is wrapped around the outer conductor.

A.1.1 Coaxial Cable Characteristic

At normal operating frequencies current flows on the surface of the inner conductor and on the inner surface of the outer conductor. The outer conductor serves as shielding between adjacent transmission channels due to skin effect of the good conductor, thus reducing crosstalk and interferences. At low frequencies, where the skin depth is comparable to the thickness of the outer conductor, the coaxial cable is not a satisfactory transmission medium and excessive magnetic shielding and insulation are required to reduce the interferences. For frequencies above several hundred kHz the cable is an excellent transmission medium as far as crosstalk and interference are concerned.

Skin effect controls the effective resistance of the cable conductor. For an air-insulated coaxial cable, attenuation due to resistive loss is found to be proportional to the square root of the operating frequency and inversely proportional to the cable diameter. Minimum loss occurs at where the ratio of the outer-conductor and inner-conductor diameters is approximately 3.6, but imperfection in the dielectric used will contribute additional attenuation. This dielectric effect is more profound in higher frequencies than in the lower frequencies.

Attenuation of a 3/8-in polyethylene-disk-supported coaxial cable used by Bell Systems is given as:

$$3.9 \sqrt{f} + 0.0047f + 0.024 + 0.0043(T-55) \sqrt{f} \text{ dB/mi}$$

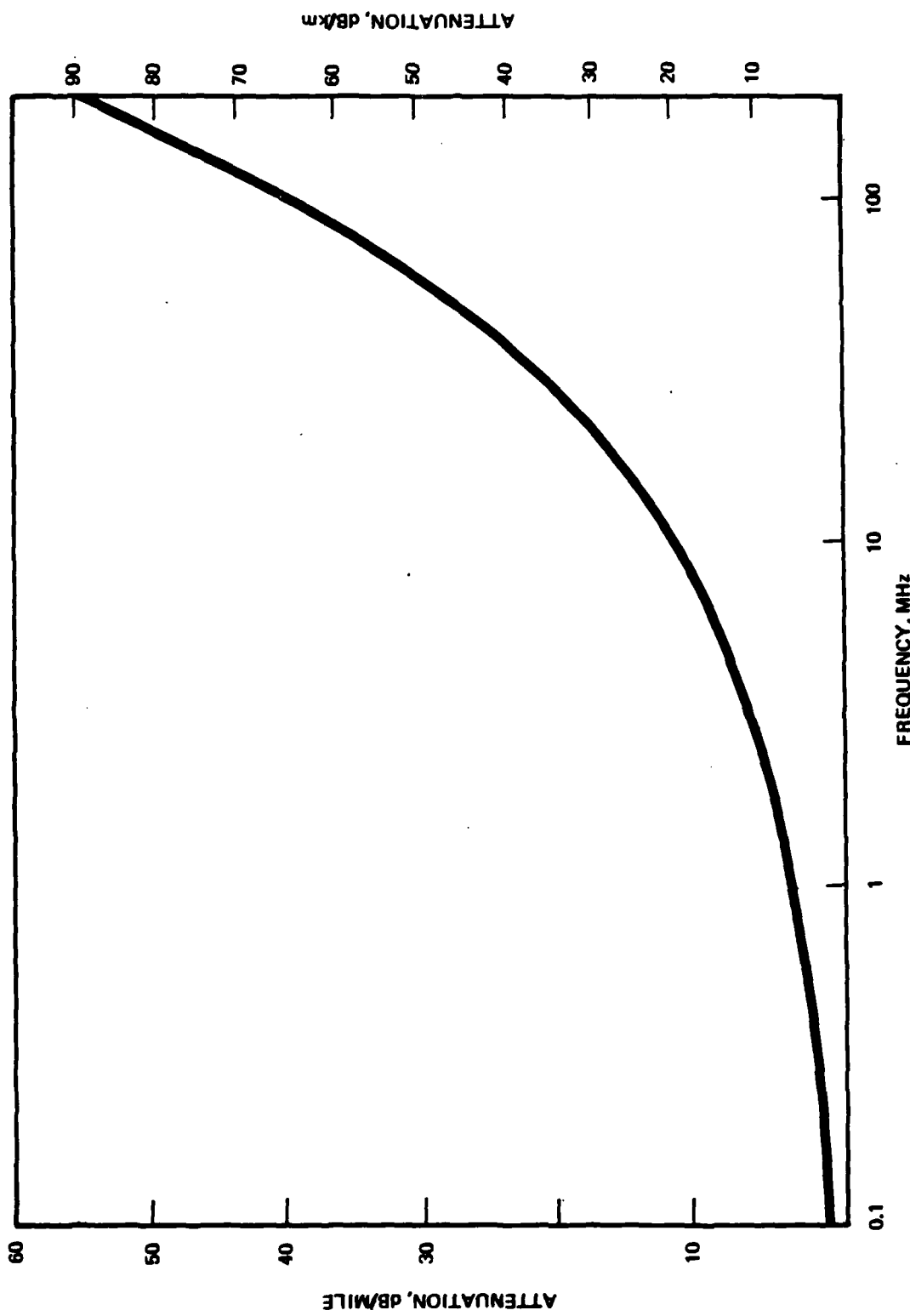
where f is the operating frequency in MHz and T is the cable temperature in $^{\circ}\text{F}$. The first term is caused by the skin effect and the last term is introduced by the temperation variations. The f term, which is due to the dielectric used, is small at low frequencies and increases significantly as the frequency increases to hundreds of MHz. Figure A.1-1 is a plot of the attenuation of the 3/8-in cable as a function of frequency, and Table A.1-1 identifies CCITT recommended attenuation values at some specific frequencies.

Table A.1-1. CCITT Recommended Nominal Cable Attenuation

Parameter	Attenuation at Given Frequency							
(Cable Size 2.6/9.6 mm)								
Frequency (MHz)	0.06	0.3	1.0	4.0	12.0	20.0	40.0	60.0
Attenuation (dB/km)	0.59	1.27	2.32	4.62	8.0	10.35	14.67	18.0
(Cable Size 2.6/4.4 mm)								
Frequency (MHz)	0.06	0.1	0.3	0.5	1.0	1.3	4.5	
Attenuation (dB/km)	1.5	1.8	2.9	3.7	5.3	6.0	11.0	

Characteristic impedance of the coaxial cable can be made to have any specified value, but usually is at approximately 50 ohms or 75 ohms depending on the cable application. The theoretical characteristic impedance for the air-insulated dielectric cable dimensioned for minimum attenuation is approximately 77 ohms. However, cables with dielectric spacers are subject to certain modification in both impedance and cable loss. The CCITT-recommended impedance characteristic for 2.6/9.5-mm coaxial cable is given by

$$Z = 74.4 \left[1 + \frac{0.0123}{\sqrt{f}} (1-j) \right] \text{ ohms}$$



A.1-1. Attenuation of 9.5 cm (3/8 in.) Coaxial Cable at 55°C

where frequency, f , is measured in MHz and the value of 74.4 ohms is subject to a tolerance of ± 1 ohm. The CCITT specification of the smaller 1.2/4.4-mm cable impedance is given in Table A.1-2. The mean real part of the impedance measured at 1 MHz must not differ from the nominal value given by more than 1.5 percent for telephony or 1 percent for cables that may be used for television transmissions.

Table A.1-2. Mean Real Part of 1.2/4.4-mm Cable Impedance

Parameter	Mean Real Part of Impedance for Given Frequency						
Frequency (kHz)	60	100	200	500	1000	1300	4500
Impedance (\$)	79.8	78.9	77.4	75.8	75.0	74.8	74.0

A.1.2 Coaxial-Cable System Capabilities

Coaxial-cable transmission systems for analog and digital signals have been in service for many years. At the present time the two common types of coaxial cable used for long-haul transmission are the 1.2/4.4-mm and the 2.6/9.5-mm cables which are used to carry 2700 and 10,800 voice channels respectively. The 50-MHz 2.6/9.5-mm (3/8-in) cable system represents the most advanced high-capacity analog transmission system ever developed. Its capacity has been extended from 10,800 to 13,200 voice channels by better use the frequency-spectrum allocation and by optimizing the repeater and equalizer performance. This highest-capacity analog long-haul transmission system was put in service in 1978 by the Bell System.

History of the development of the coaxial-cable system can be represented by the installation of the Bell L-Systems. As the demand increased and the technology advanced, the L-System grew from the 600-channel vacuum tube L1 to the most advanced 13,200-channel transistorized and microprocessor-controlled L5E (Ref. A.1-1). Figure A.1-2 and Table A.1-3 provide brief descriptions of the growth of the Bell L-Systems (Ref. A.1-2).

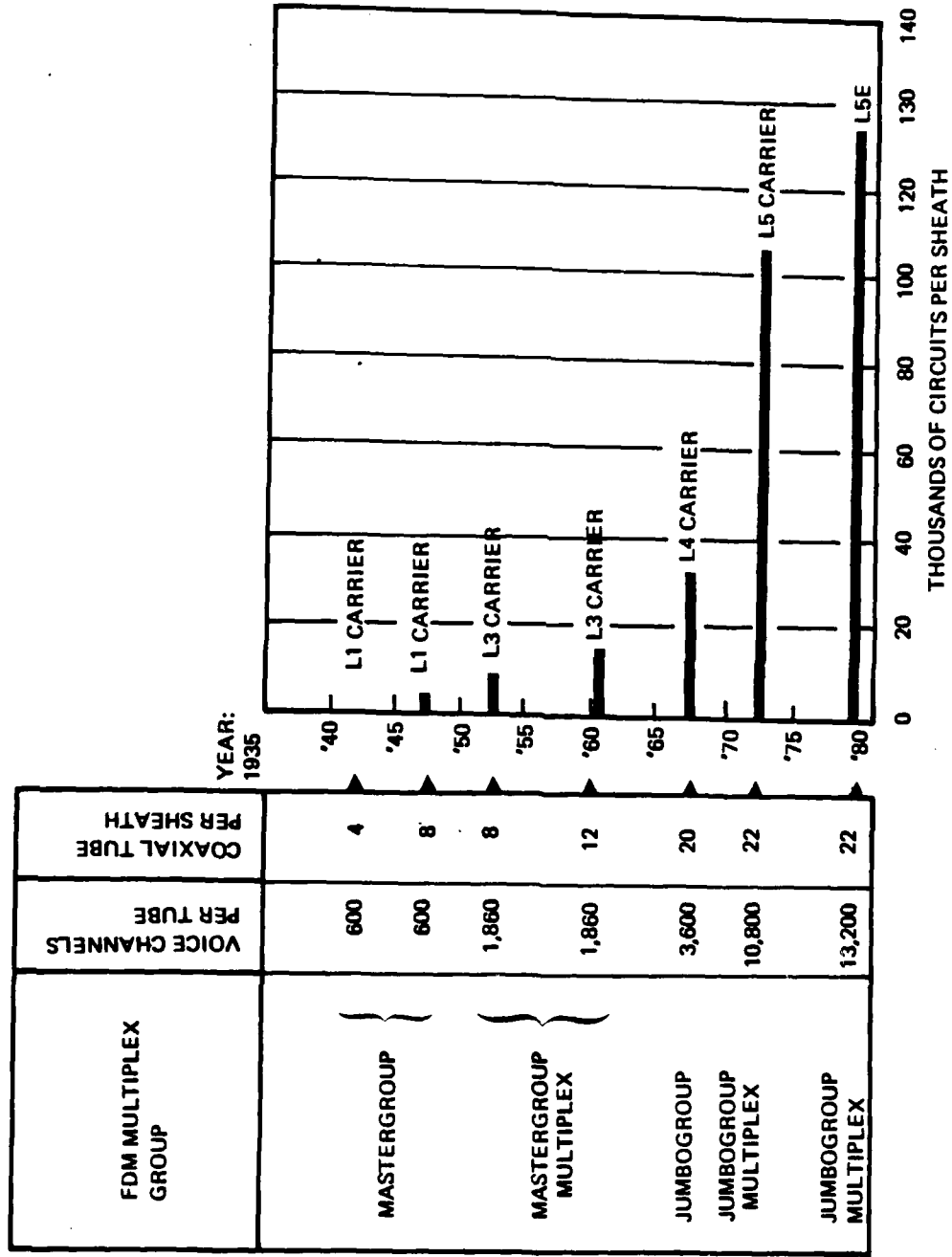


Figure A.1-2. Growth of Bell Coaxial System

Table A.1-3. Growth of the Bell L-System

Parameter	System				
	L1	L3	L4	L5	L5E
Start of Service	1941	1953	1967	1974	1978
Two-Way Message Capacity/ Cable Pair	600	1,860	3,600	10,800	13,200
Frequency Band (kHz)	60- 2,788	312- 8,284	564- 7,548	159- 68,780	159- 68,780
Nominal Repeater Spacing (mi)	8	4	2	1	1
Number of Cable Pairs Working vs. Protection	3/1	5/1	9/1	10/1	10/1
Total 2-Way 4-kHz Message Channel	1,800	9,300	32,400	108,000	132,000

Although the 9.5-mm (3/8 in) coaxial cable has been the only standard cable used in the Bell System for the long-haul transmission, both of the two types of cable are used in many other countries coexistantly. In European countries and in Japan the standard 2.6/9.5-mm cables are used in the high-capacity 12-MHz and 60-MHz systems, whereas the smaller 1.2/4.4-mm cables are used extensively in serving the 1-12 MHz systems. Table A.1-4 lists the capabilities recommended by CCITT for the buried-transistor repeater systems.

Table A.1-4. CCITT Recommendations on Transistorized Coaxial Cable Systems

Parameter	Description					
	1.2/4.4-mm Cable			1.6/9.5-mm Cable		
Bandwidth (MHz)	1.3	4.0	6.0	12.0	12.0	60.0
Repeater Spacing (km)	8(6)*	4.0	3.0	2.0	4.65	1.55
Data Capacity (voice channel per coaxial pair)	300	960	1260	2700	2700	10,8000

* 6-km spacing for future expansion into 6-MHz, 3-km system.

The 60-MHz, 10,800-channel analog system has been pushed one step ahead by the Bell System. Further expansion in bandwidth might possibly depend on circuit demand and technology improvement. The increase of channel capacity of Bell-System L5E over L5 was accomplished by reducing the guard band between adjacent Mastergroups and Jumbogroups. To combat increasing intermodulation due to crowding of channels the following three modifications are required:

1. Reduction of the number of equalizers to minimize noise
2. Incorporation of a 180^0 -phase-shift module in the line to partially cancel the 2nd-order intermodulation
3. Optimization of the transmission level to accommodate the tightly packed signal

The additional two guardband modifications also are necessary:

1. Reduction of the guardband between adjacent Mastergroup from 186-616 kHz to fixed 186 kHz
2. Reduction of the guardband between adjacent Jumbogroup from 11 percent to 5 percent of the message bandwidth.

The broadband signal can be transmitted in both analog and digital forms. Although economic reasons as well as higher channel capacity have favored the analog FDM type signal in the past and even at the present time, the significant progress realized in digital techniques and semiconductor integrated circuits render the digital transmission economically feasible.

The trunk circuits of the digital transmission are designed to use the existing repeater locations that also are used in the analog operation. Data rates of 100, 140, 173, and 400 Mbps are used in different systems.

In digital transmission analog inputs are filtered, sampled, and encoded to form a basic digital stream and then multiplexed with other data at the appropriate multiplexing levels. If the input data are already digital, they will be synchronized with the operating system and then multiplexed with many other data streams. Data rates at different points in the system occur in accordance with the hierarchy of the digital system used.

The typical hierarchy of digital channels used in North America is shown in Figure A.1-3. The basic input is the 64-kbps PCM voice channel, and the first or primary PCM multiplexer produces an output at 1.544 Mbps with 24 voice channels. After three more levels of multiplexing the final output data stream is at 274.176 Mbps, corresponding to 4032 voice channels or three television channels. Possible transmission media for each level of multiplexing also are shown. Standard 9.5-mm coaxial cable is used to transmit the 274.176-Mbps data. The repeater spacing is about 1 mile, which is in common with the standard 60-MHz analog system. The typical digital system in North America is characterized in Table A.1-5.

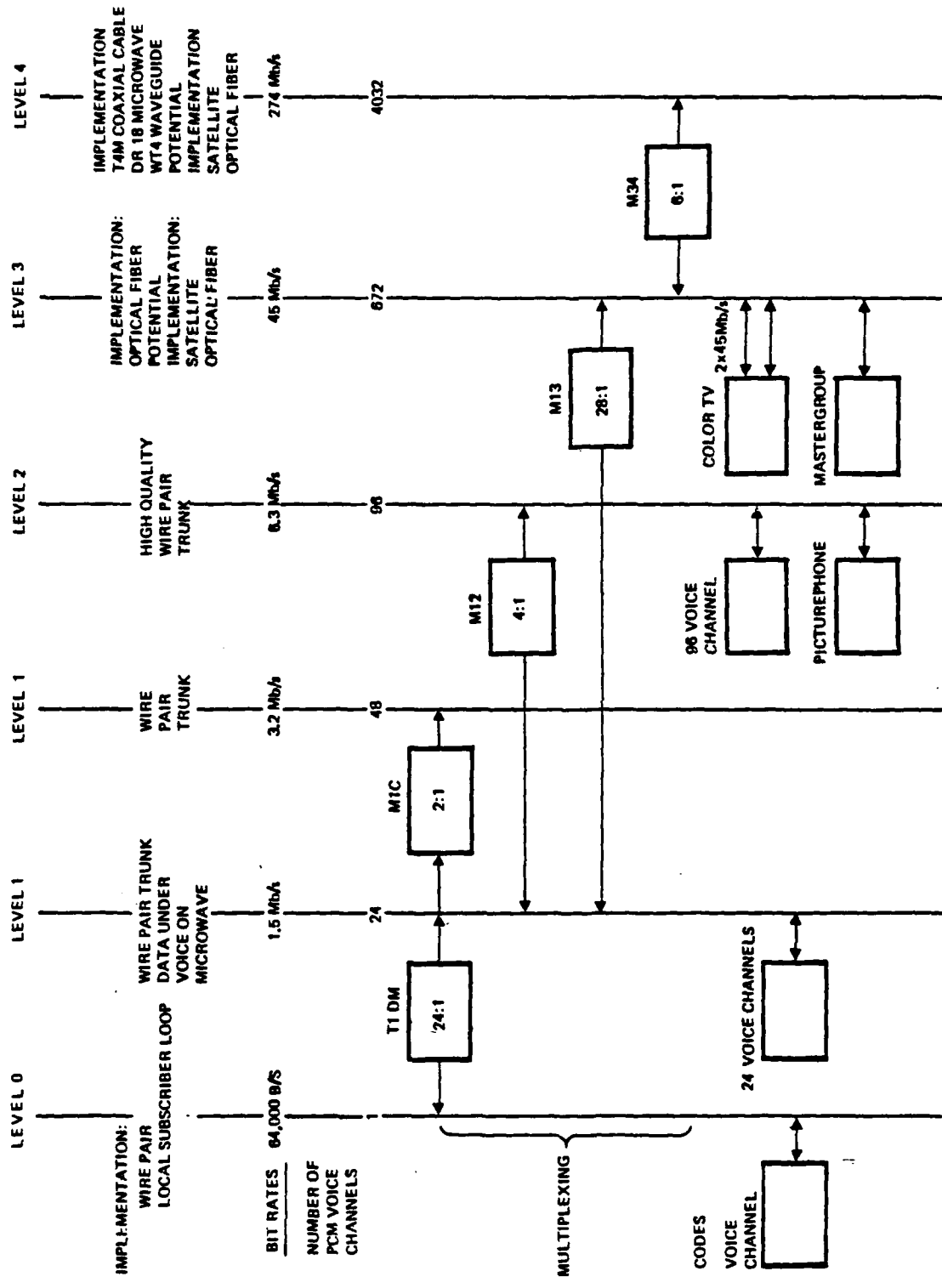


Figure A.1-3. The Hierarchy of Digital Channels on the North America System

Table A.1-5. Bell System Digital Coaxial Cable System in North America

Parameter	Description	
	LD4 (Montreal - Ottawa)	T4M (New York - Newark)
Start of Service	1975	1975
Cable Size (in)	3/8	3/8
Number of Cable Pairs Working vs. Protection	5/1	10/1
Repeater Spacing	6,000 ft	1 mi
Data Rate (Mbps)	274.176	274.176
Telephone Channels per Cable Pair	4,032	4,032
Total Channel Capacity	20,160	40,320

The hierarchies of digital transmission used in Europe and Japan are different from those used in North America, as seen in Figure A.1-4 (Refs. A.1-3, A.1-4). The data rate of 64 kbps PCM remains the building block in all the systems, but the level of multiplexing and data rate are different. The CEPT system yields 139.264 Mbps at the end of the fourth multiplexer, which corresponds to 1920 voice channels (Ref. A.1-5). The data streams are transmitted over the smaller 1.2/4.4-mm cable with repeater spacing of 2 km, or over the standard 2.6/9.5-mm cables with repeater spacing of 4.65 km.

In Japan, development of digital transmission is most advanced, and in 1977 the first high-capacity 400-Mbps long-haul transmission system in the world was put into service (Ref. A.1-6). This system provides 5760 voice channels, or 60 interframe-coded 4-MHz color television signals similarly as in America, except that the standard 9.5-mm (3/8-in) coaxial cables are used for long-haul digital transmission in Japan. Table A.1-6 and Figure A.1-5 summarize Japanese PCM-100 and PCM-400 system parameters and configurations.

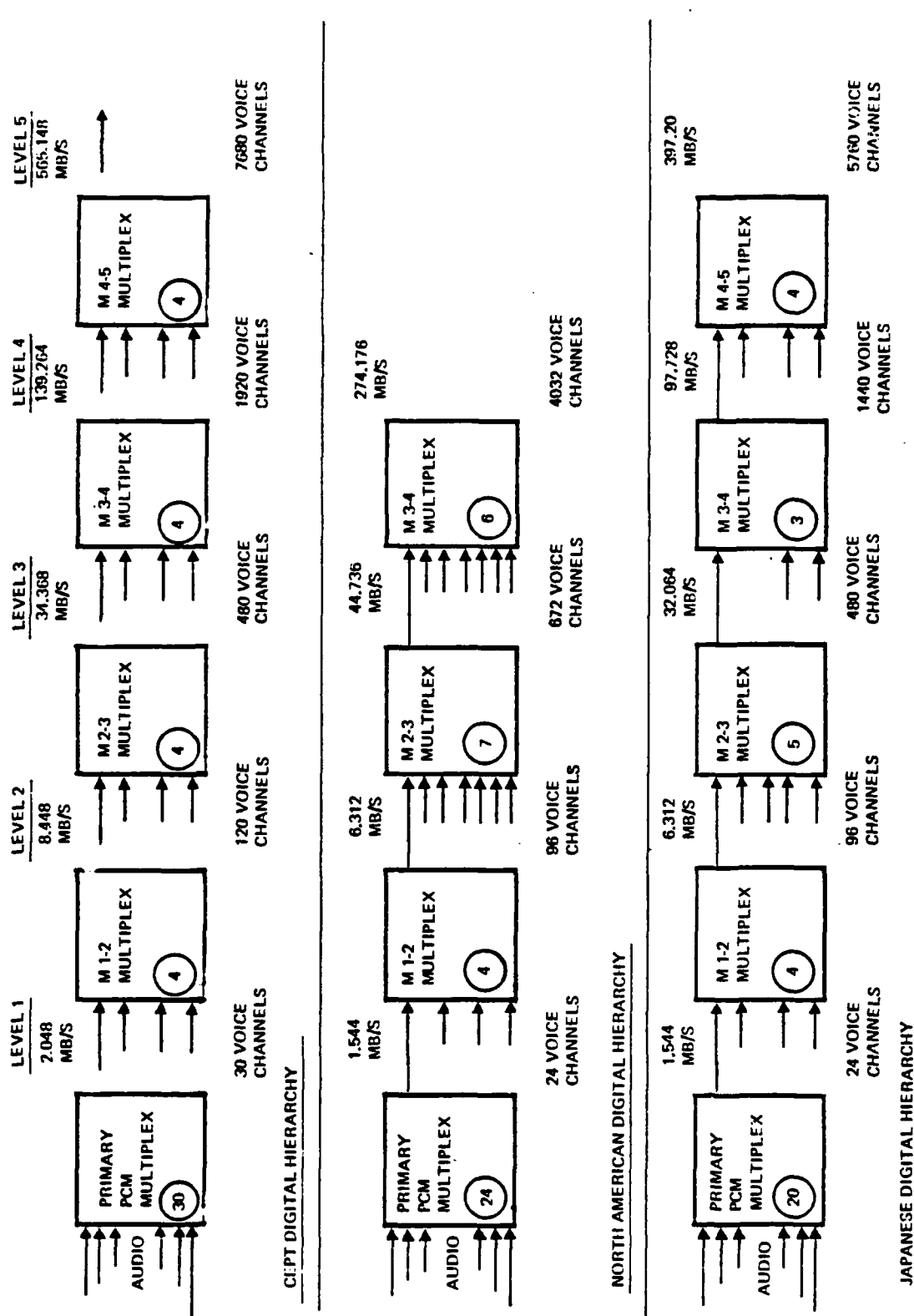


Figure A.1-4. Evaluation of DCS IIII Transmission Alternatives Digital Hierarchies

Table A.1-6. Japanese PCM-100M and PCM-400M System Summary

Parameter	Specification	
	PCM-100M System	PCM-400M System
Transmission Medium	2.6/9.5 mm Coaxial Cable	2.6/9.5 mm Coaxial Cable
System Capacity Voice Channel 4-MHz TV Signal	1,400 ch 12 ch	5,760 ch 60 ch
Transmission Bit	97.728 Mbps	400.352 Mbps (Terminal Interface: 397.200 Mbps)
Error Rate	10^{-9} per 300 km	10^{-8} per 2,500 km
Repeater Spacing	1.2 km - 3.7 km	0.1 km - 1.6 km
Signal Code	Scrambled AMI	Scrambled AMI
Power Feeding	DC250 mA at +350 V	DC550 mA at + 650 V
Line Supervisory System	Detection of AMI violation	Detection of AMI violation
Line Protection	--	8 to 1 protection and switching
Multiplexing	Positive justification bit by bit multiplication	Positive justification bit by bit multiplication
Repeater Zero-to-Peak Output Voltage	2.0 V	3. V
Repeater Size	160 x 80 x 270 mm	160 x 80 x 270 mm

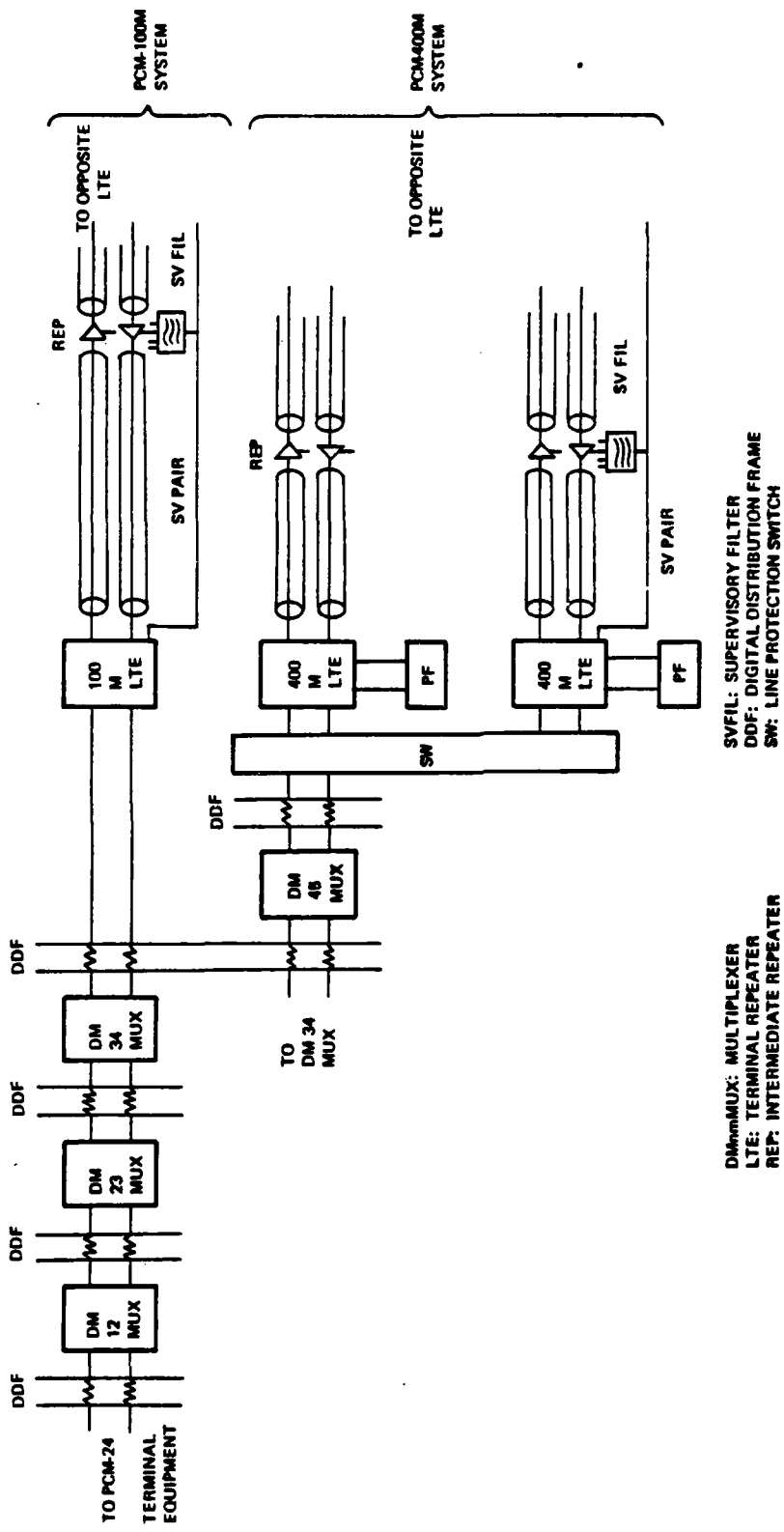


Figure A.1-5. System Configuration for PCM-100M System and PCM-400M System

A summary of the state-of-the-art of the coaxial cable system is given in Table A.1-7, from which it may be seen that the most advanced analog system is the Bell L5E System covering a bandwidth from 3 to 63 MHz with a capacity of 13,200 channels. The most advanced digital system is the NTT PCM-400 Mbps system with a capacity of 57,600 voice channels. Expectation regarding future expansion of the cable system capability is also noted.

Table A.1-7. Summary of the State-of-the-Art Coaxial Cable Transmission Systems

Parameters	Cable Size	
	1.2/4.4 mm	2.6/9.5 mm or 3/8"
Present Data Rate	140 Mbps (1)	400 Mbps (3)
Present Bandwidth	12 MHz (2)	60 MHz (4)
Repeater Spacing	2 Km	1.6 Km
Capacity (Voice Channel)	1920, 2700	57600, 10800, 13200
Future Data Rate	210 Mbps	565 Mbps - 800 Mbps
Future Bandwidth	18 MHz	120 MHz

Remarks:

- (1) Digital Systems in Europe. (3) Japanese PCM-400 System.
(2) Analog System in Europe and Japan. (4) Bell L5E.

A.1.3 Future Trend in the Coaxial Cable System Development

Future growth of the coaxial cable system will be centered on the existing cables with their existing repeater spacing, and advances in technology, careful planning of the spectrum, and extensive application of microprocessors will enhance channel capacity beyond the current limit. Increase of bandwidth from 60 MHz to 120 MHz might be possible for the 2.6/9.5-mm cables, and bandwidth of the 2.1/4.4-mm cable might be expected to increase to 18 MHz from the current standard of 12 MHz.

The rapid-growth area will be associated with digital transmissions, studies having indicated that the following are among the advantages of digital systems (Refs. A.1-4, A.1-7, A.1-8):

- All types of information are translatable into a uniform signal format, tending to simplification of network and equipment requirements
- Introduction of new services is simplified
- System transmission performance is improved
- Economies are realized through use of available technology developed for other applications (e.g., computer science and space exploration).

Expansion of the digital capability to 560 Mbps in the near future is possible as the result of field testing of the 560-Mbps system that has been in operation in Germany (Refs. A.1-9, A.1-10).

A.1.4 Intrinsic Limitation of Coaxial Systems.

A.1.4.1 Bandwidth Limitation Due to Attenuation. The bandwidth that can be transmitted over the coaxial cable medium, and hence its channel capacity, is limited by the high attenuation at frequencies at the upper bandedge, so that repeaters must be placed at constant intervals to compensate for the cable losses. At present the standard repeater spacing is at about 1.55 km for the 2.6/9.5-mm, 60-MHz systems and at about 2 km for the smaller 1.2/4.4-mm, 12-MHz systems. Any decrease from these values in the long-haul transmission systems seems unlikely.

One option to increase bandwidth in the coaxial cable is to increase the coaxial tube size. However, this is rather impractical due to the high expenses associated with creating a new standard within the cable family.

Special consideration will be given to techniques whereby the existing 2.6/9.5-mm coaxial cable systems may be used more effectively. Successful extension of the bandwidth beyond 60 MHz and increase of channel capacity beyond the 10,800 standard will depend on advances realized in other technology areas such as repeater and equalizer design, methods to reduce intermodulations, and innovations in effective use of the available spectrum.

A.1.4.2 Cable Irregularities. In the manufacturing of coaxial cables unintentional irregularities may be introduced. These may be caused by dimensional tolerances of the inner and outer conductors and/or periodic variation in the application of steel or paper tapes to the outer conductor. Use of periodically-spaced polyethylene disks also will introduce periodic variation of cable impedance, the most important imperfection being the periodic cable deformation caused by the cable stranding process.

When stranding the individual coaxial tubes and the twisted-pair order wires in forming a single coaxial cable each tube is periodically pressed against the stranding guides briefly, which thus deforms the cable dimensions. Also in the stranding process a uniform trend force acts upon the cable, which results in irregularities that are spaced approximately one meter apart.

The high return loss due to cable periodic irregularities does not affect the present analog transmission system because its maximum frequency is at approximately 68 MHz, which is below the first return-loss spike frequency. However, when system capacity grows and other component technology warrants extension of analog transmission to higher frequencies, the effect of the additional return loss at certain frequency bands may introduce additional loss and interference. Also, if the same cable system is used for high-data-rate digital transmission, extra degradation will be introduced.

To minimize the periodic irregularities produced in the stranding process, various improvements in fabricating coaxial cable have been adopted by the cable manufacturers. For example, a method called "Stranding Pitch Length Modulation" adopted by a Japanese firm has been reported as the source of cable characteristics improvement noted during cable test and installation.

A.2 MILLIMETER WAVEGUIDE

It is well known that attenuation of TE₀₁ mode transmission in a circular waveguide decreases with frequency. In practice, a waveguide with diameter of many times of the TE₀₁ cutoff wavelength will be used to guide the electromagnetic waves to take advantage of even smaller attenuation at larger waveguide sizes. The oversized waveguide can support many high-order waves in addition to the excited TE₀₁ mode.

Imperfection in the circular geometry and deviation of waveguide axial straightness will cause mode conversion from TE₀₁ mode to high-order modes and back to TE₀₁ mode at different phase and time delay, thus increasing transmission attenuation. In general, attenuation is small at lower frequencies with negligible mode conversions and increases due to domination of the mode conversions at higher frequencies.

Waveguide curvature was found to be the significant source of the mode-conversion loss (Ref. A.2-1). The dominant modes of conversion and re-conversion are among the TE₀₁ to TE₁₂ and TM₁₁ directly and then to TM₂₁ indirectly, as shown in Figure A.2-1. Other high-order mode conversions contribute to the total loss. A typical plot of the attenuation and its contributors as a function of frequency is shown in Figure A.2-2.

The attenuation curve of the circular waveguide can be approximated by the expression (Ref. A.2-2),

$$\alpha = K_1 a^{-3} f^{-3/2} + K_2 a^2 f^2$$

where

a = inner radius of the guide

f = frequency

K₁, K₂ = suitable constants

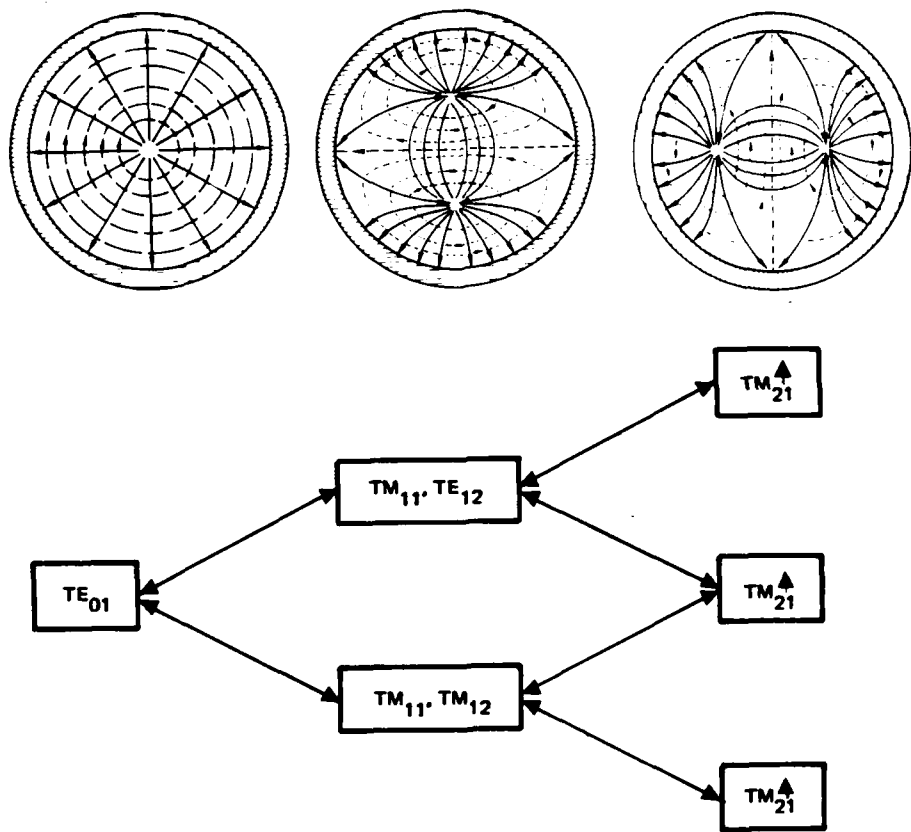


Figure A.2-1. Model Coupling of Circular Waveguide

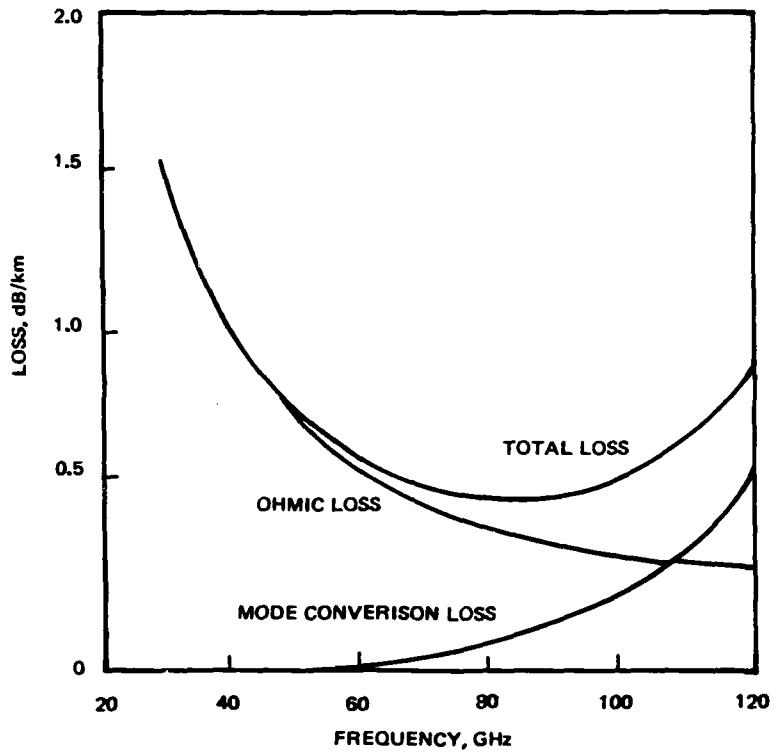
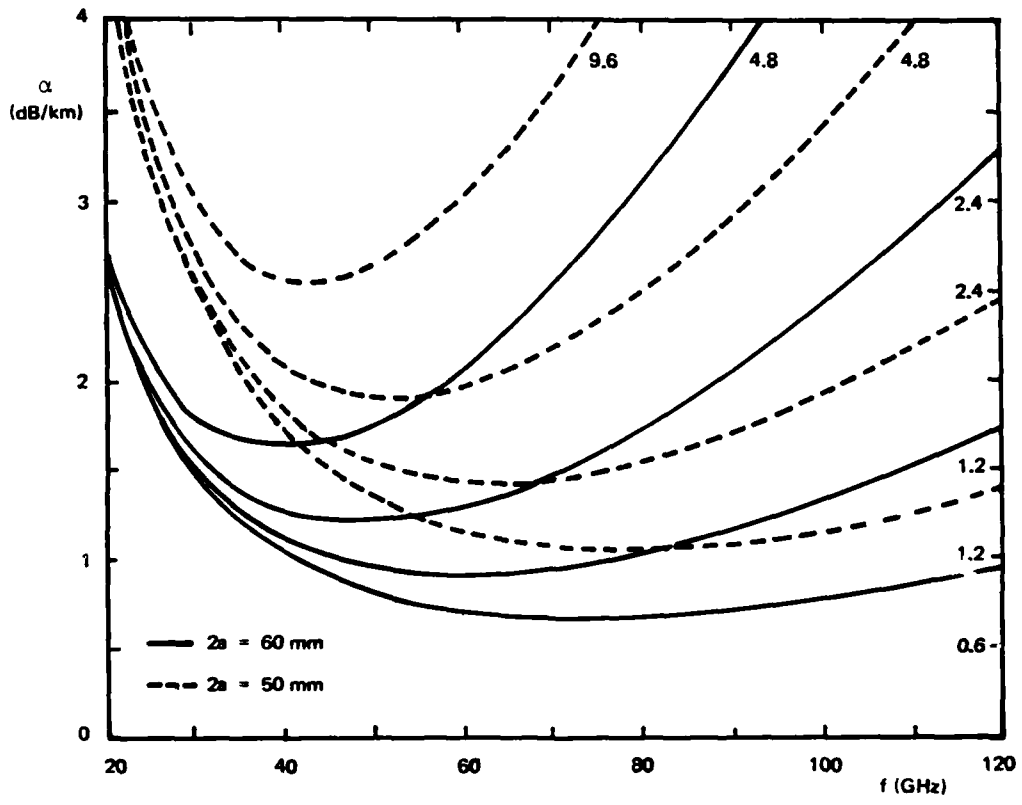


Figure A.2-2. Attenuation of Millimeter Waveguide

The constant, K_1 , accounts for the theoretical ohmic loss for the TE_{01} mode in a perfect circular waveguide. The first term justifies the advantage of using oversized waveguides for low-attenuation transmission, and the second term is partially due to the unavoidable deformation of the waveguide in circular diameter and mostly to deviation of axial straightness. Therefore K_2 is a function that depends on the degree of imperfections. It is known that the large-diameter waveguides are more sensitive to deformations than the small-diameter ones, as may be seen in Figure A.2-3.



$$\alpha \text{ (dB/km)} = K_1 a^{-3} f^{-3/2} + K_2 a^2 f^2$$

Figure A.2-3. Attenuation of Millimeter Waveguides of Different Size

To minimize the conversion and re-conversion process and to suppress the high-order mode propagation, the waveguide is constructed of steel tube with an inner conducting surface of plated copper covered with a thin layer of polyethelene lining. The steel tube provides sufficient precision of waveguide-wall smoothness as well as necessary strength and rigidity to resist bending, and the dielectric lining serves to lessen generation of the unwanted modes in bends. Sections of helix waveguide used as filters are inserted in the waveguide run at regular intervals in order to absorb high-order spurious-mode energy (caused by intentional and unintentional bends, waveguide junctions) and thereby prevent its conversion back to the TE_{01} mode. Figure A.2-4 shows typical construction of the waveguides.

The steel waveguide is placed inside another steel pipe or other protective pipe that serves as a sheath for underground laying and assures straightness of the waveguide. The steel sheath and the spring supports installed between the sheath and the waveguide function as mechanical filters to smoothe out the loading irregularities imposed by surrounding soil.

Bends of relatively large curvatures are necessary to accommodate the terrain and right of way. Small sections of special short flexible waveguide are used for sharp curves and turns (Ref. A.2-3). The amount of helix waveguide or filter used will depend on the overall waveguide design.

Waveguides of different inner diameter were used in studies for mm-waveguide transmission systems in different countries. CCITT suggested that size would be limited to 70, 60, 51, 50, 40, and 30 millimeters. Although the large waveguides have advantages of lower basic attenuation and allow increased repeater spacing for the relatively straight route, they also are more costly to manufacture, more critical to bends, and therefore critical to laying requirements. On the other hand, although the small-diameter waveguides are cheaper to produce, more tolerant to bends, less critical to laying requirements, thus offering advantages in urban areas and rough terrain, they also require closer repeater spacing.

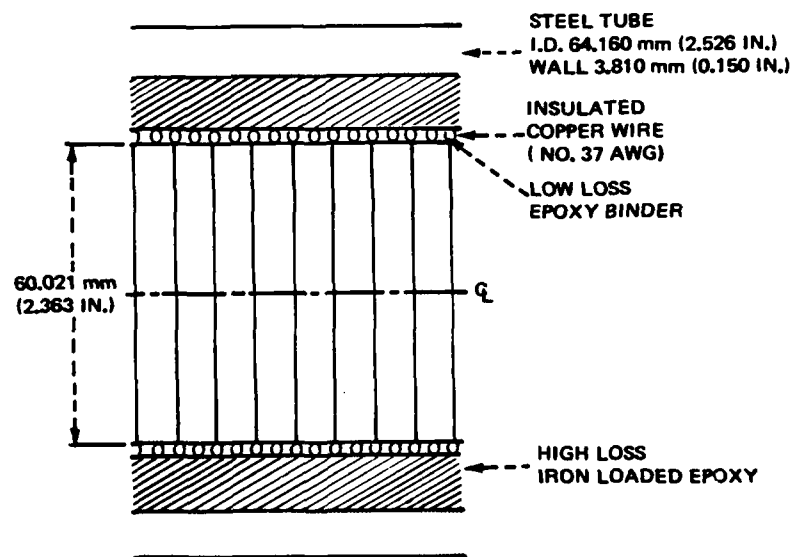
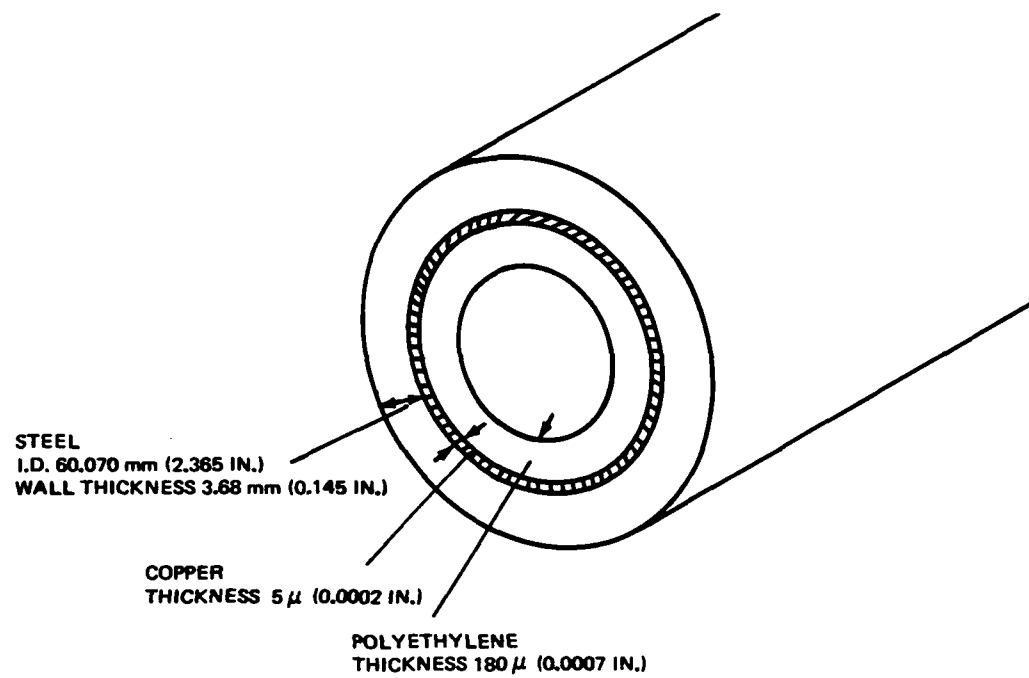


Figure A.2-4. Typical Constructions of Millimeter Waveguide

Design of the millimeter circular waveguide transmission system will deal with aspects such as operating frequency band, type of terrain, production and laying precision, repeater gain and spacing, and waveguide size. A few waveguide systems have been proposed by different countries. However, each one is unique and there is no standard design.

In the United States the Bell System has had a 14-km experimental millimeter waveguide system in operation since 1974. The WT4 system was designed to use solid-state regenerative repeaters spaced at approximately 60 kilometers for relatively gentle terrain and at 50 kilometers for rugged terrain. The system incorporates 59 message channels and 3 protection channels each way for the 2-way communication. Each channel is a transmitter-receiver pair and carries one DS-4 digital signal stream at 274 Mbps. Initial system capacity is 238,000 voice channels which can be expanded to 476,000 channels as traffic increases by converting from 2-PSK to 4-PSK coding without changing the repeater spacing. A summary of the WT4 and other proposed systems is given in Table A.2-1.

The millimeter-waveguide system offers advantages in high capacity, high reliability, and low attenuation, and can handle many times more messages than any of the known communication media. To realize these advantages high precision in manufacture and laying are essential. If there is sufficient traffic to feed the system and to fully utilize its high-capacity potential it would be an ideal transmission medium (data rate at tens of Gbps). However, its prohibitively high cost would force designers to favor other alternatives.

The waveguide system is a closed system buried underground and consists of two layers of steel pipe. Its electronics, except for its power supply, are enclosed within the steel pipes. Therefore the electromagnetic field configuration inside the waveguide cannot be altered by any external disturbance and the electronic hardware is protected electrically and magnetically by the steel barriers.

Table A.2-1. Comparison of Waveguide Transmission Systems

Parameter	France	Japan	U.S.A.	U.K.
Waveguide	Helix	Tandem (20% helix)	Tandem (1% helix)	Helix
Diameter	50 ⁽¹⁾	51	60	50
Bandwidth (GHz) for Maximum Attenuation (dB/km)	60	45	70	70 ⁽²⁾
Capacity (telephone channels)	>200,000	300,000	228,000	225,000
Developed bandwidth	30-60	43-87	40-110	32-49 ⁽²⁾
Bit Rate per Carrier (Mbps)	580	800	274	560
Telephone Channels per Carrier	7,680	11,250	4,032	7,680
Minimum Frequency (GHz)	30	43	40	32
Modulation	4-PSK indirect	4-PSK indirect	2-PSK direct	4-PSK indirect
Demodulation	Differential	Coherent	Differential	Differential coherent
Repeater Gain (dB at 40 GHz)	79	70	78.2	74
Repeater Spacing (km)	20	15	50-60	20-30 ⁽²⁾
Intermediate Frequency (GHz)	1.45	1.7	1.371	1.25

(1) 60-mm diameter is also studied.

(2) Several bandwidth and repeater spacing under consideration.

A strong rigid waveguide can sustain relatively high stress without significant damage to the system. However, because system attenuation is sensitive to the physical configuration of the system any intentional modification is easily detectable. Therefore, the waveguide system is an anti-jamming, interference-free, EMP-immune and physically-rigid transmission system. Although even these advantages may not serve to provide the final commercial high-density long-distance transmission medium (coaxial cable and optical fiber are expected to be used instead), the buried waveguide may fit some specific applications in special situations.

Millimeter-waveguide communication applied to DCS will be considered as a narrowband technique, as it then will be possible to trade bandwidth capability of the circular waveguide system against its quality and its rigorous laying requirements. The waveguide also will tolerate frequent bends and sharper curvatures, and because the narrow-band repeater will be a single-channel unit instead the huge multiple-channel one used in the regular waveguide system there is no need for multiplexing, demultiplexing, and channelization, so that the repeater unit will be small and cheap. In addition, more repeaters (shorter repeater spacing) can be used to combat the increasing attenuation.

To assess feasibility of the millimeter-wave circular waveguide system for DCS increased understanding of the following is necessary:

- Manufacturing Technology: The waveguide is the major expense element of the waveguide system. Any improvement in the manufacture process therefore will accelerate realization of the system. Areas of improvement must emphasize low cost, ease of handling, and laying.
- Statistics of Signal Attenuation: Statistics of signal attenuation must be studied with respect to number of bends, and curvature of the bends for a specific size of waveguide because it is impossible to establish a system baseline design in the absence of such information.
- Trade-Off Study of mm-Waveguide System: Trade-off studies for a mm-waveguide system conceptual design should be conducted in such areas as waveguide size, repeater spacing, cost, etc. in order to gain expanded insight of such systems and to determine whether such a system is a desirable resolution of the DCS requirement.

A.3 BEAM WAVEGUIDE

In ordinary electromagnetic wave propagation in free space the cross-section of the beam diverges once it is launched from the antenna. Wave intensity then decreases in proportion to the square of the distance it travels. Divergence of the beam and hence attenuation of the wave can be corrected by preventing the beam from monotonically spreading out from its axis by introducing periodic discontinuities along its path, whereby divergence and convergence of the beam occur in alternating fashion. Periodic reconstruction of the beam shape subsequently produces acceptable attenuation at the receiving end of the transmission path.

A beam waveguide is a periodic structure consisting of irises, lenses, or, reflection mirrors, as shown in Figures A.3-1, A.3-2, and A.3-3 respectively. The electromagnetic wave beam traversing such a waveguide then will be modified either by diffraction or by refraction at the apertures, and the wave is guided to its destination. An electromagnetic wave at any frequency can be guided by the beam waveguide, but larger apertures are required at lower frequency. Optical communication using a beam waveguide is more practical.

The iris-type beam waveguide shapes or iterates the beam by diffraction, so that when the beam passes through the iris the field is limited in diameter. In the lens-type waveguide, iteration is performed by redistribution of the phase on the lens cross-section, each lens resetting the phase distribution to that which is the same at the output of the preceding lens. Diffraction at the edge of the lenses plays a minor role in the iteration process. In the reflector-type beam waveguide the reflector reflects the beam in direction and at the same time performs the phase transformation in the same manner as the lens. The three categories of beam waveguide attenuations are 1) aperture diffraction loss, 2) aperture-material absorption loss, and 3) attenuation due to misalignment. Both the aperture diffraction and material losses can be minimized to certain extent by using large, oversized apertures. Misalignment is the major contributor to the overall attenuation.

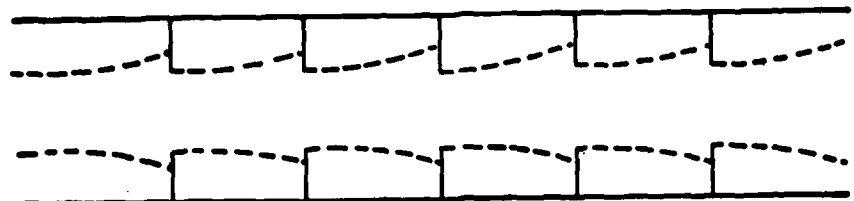


Figure A.3-1. Iris Beam Waveguide

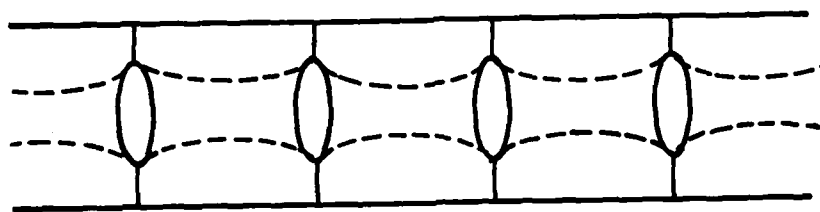


Figure A.3-2. Lens Beam Waveguide

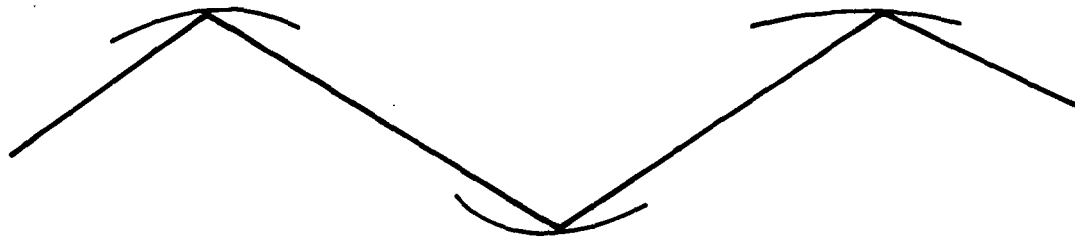


Figure A.3-3. Reflection Mirror Beam Waveguide

Diffraction loss in a beam waveguide can be made negligibly small by using larger apertures with the aperture radius $r^2 \lambda \gg$, where λ is the wavelength and the aperture spacing. It has been shown that the iris-type beam guide is more subject to diffraction loss than the lens type (Ref. A.3-1). To achieve iteration loss comparable to that of the lens type, the aperture of the iris must be a minimum of ten times larger than the lens. Because of its large size the iris-type beam waveguide is not a favorable choice in practical applications.

One important aperture loss in lens-type beam waveguides is due to reflection of the beam from the lens surface, which occurs when there is mismatch in wave impedance at the boundary of free space and the lens material. In such cases impedance-matching techniques of multiple-coating of the lens surface must be used to create quarter-wavelength impedance transformers to reduce reflection losses, whereby the transmission bandwidth will be reduced. Figure A.3-4 shows the typical relationship between bandwidth and reflection.

Dissipation or absorption loss of the lens is determined by the material used and is proportional to the lens thickness, and can be reduced by using a high-purity lens with the minimum lens thickness that meets phase iteration requirements. Scatter loss due to lens surface irregularities can be minimized by using oversized lenses because the irregularities due to polishing are most severe at points furthest from the lens center.

Ability of a beam waveguide to guide an electromagnetic beam is severely limited by tolerance of the lens positions relative to the guide axis. Transverse displacement of the lenses causes the beam to deviate from the axis of the waveguide. As the deviation grows in proportion to the number of lenses, lens alignment becomes the critical element in beam-waveguide communication. It has been shown that for a system with random longitudinal lens displacement and with variations in lens focal length coupled with transverse lens displacement, RMS beam displacement grows exponentially with the number of lenses through which the beam has passed and only a small portion of the transmitted energy will be intercepted by the axially-aligned receiver (Ref. A.3-2).

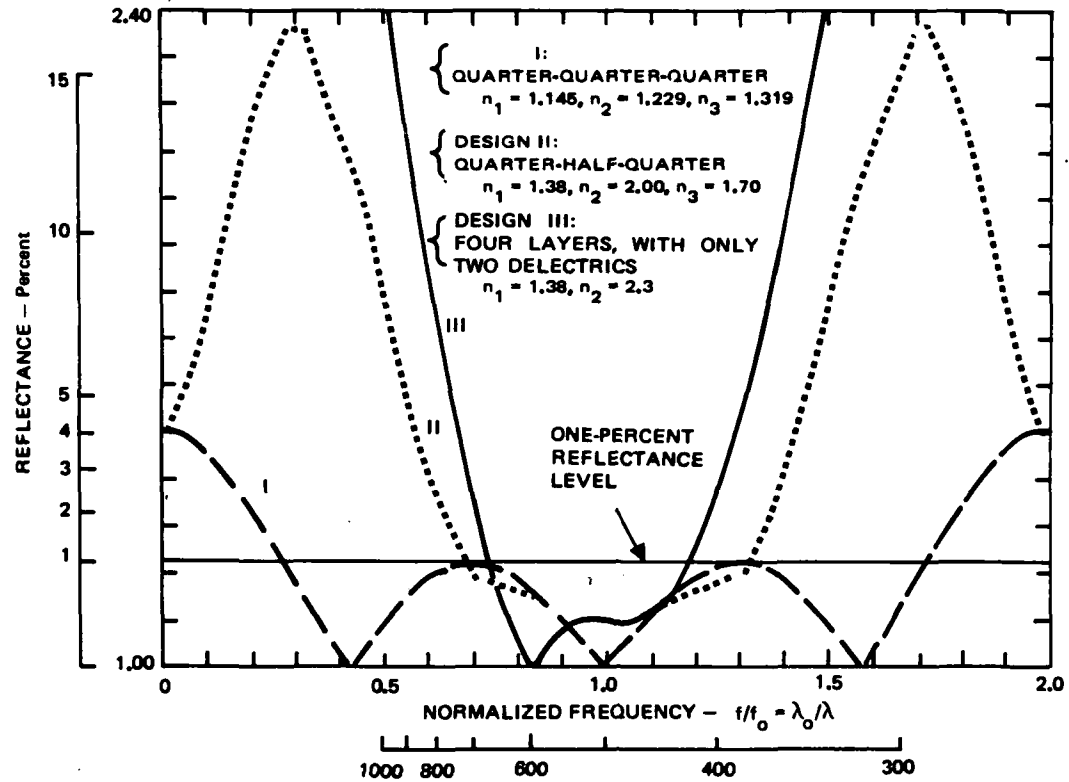


Figure A.3-4. Typical Relationship Between Bandwidth and Reflection

Beam waveguides require absolute straightness except where an intentional bend is introduced, and lens position longitudinal and transverse variations must be kept at a minimum. Any structural variations in temperature, aging, earth movement, and medium turbulence caused by temperature gradient also are causes of beam attenuations. Therefore, in order to maintain long-term waveguide stability automatic control, methods must be employed to sense and to realign the lenses once noticeable lens displacement occurs. Unfortunately, such a scheme may be impractical and too expensive even for very-large-capacity systems and special applications.

Experiments in both the microwave and optical frequencies have been conducted, with typical attenuation of 1 db/km or less obtainable for optical transmission (Refs. A.3-3, A.3-4, A.3-5). It appears promising that long-distance, extremely-high-density traffic can be handled by the beam waveguide if associated problems in the areas of long term stability, automatic control, and realignment of lenses and circuits (filter, amplifier, modulator, and multiplexer) can be resolved. However, due to advances in fiber optics and lack of demand for very-high-density circuits, little activity has been reported in beam-waveguide research in the last ten years. Consequently it is concluded that little to no chance exists for the beam waveguide to play any role at this stage of future communications development.

A.4 TERRESTRIAL MICROWAVE LINE-OF-SIGHT (LOS) TRANSMISSION

A.4.1 Description of Medium

Electromagnetic energy can be radiated and received in narrow antenna beams (1° to 2.5°) both in the UHF region (248 MHz) and especially in the microwave region (1 to 13 GHz). This is advantageous in that radiation of interference at frequencies may be kept low and that the large antenna gain (up to 50 dB) produced as a result of the narrow beam requires only small transmitter powers of a few Watts. However, an overly narrow antenna beam would impose excessive demands on the torsional stiffness of the antenna structures used for the system, as the horizontal offset from the beam axis of a steel tower antenna by wind loading is approximately $\pm 1.4^{\circ}$ to $\pm 1.0^{\circ}$ maximum.

Most terrestrial microwave transmission systems use line-of-sight (LOS) propagation between radio relay stations (i.e., between antenna towers), typically resulting in approximately 30 miles distance between towers, a difference that keeps the influence of ground reflections sufficiently small. LOS distances of 30 miles are useful for up to 10 GHz, but attenuation of LOS radio links due to rain, snow, fog, or hail increases very fast at higher frequencies. For example, additional attenuation with 100-mm/hr rain intensity during approximately 0.001-percent of the time exceeds 4 db/km at 11 GHz, 10 dB/km at 18 GHz, and 20 dB/km at 30 GHz, thereby reducing LOS path distances for frequencies above 10 GHz to spans of 35 km (21.7 mi) for 11 GHz, 15 km (9.3 mi) for 15 GHz, and 3 km (1.9 mi) for 18 GHz (Ref. A.4-1).

Lack of available frequencies and demand for increased frequency bandwidth results in expansion into higher frequency regions (e.g., 13 GHz and 20 GHz in some existing systems). Microwave LOS transmission will take place below 20 GHz and also in the frequency "windows" of 28-42 GHz and 75-95 GHz because of absorption bands of atmospheric gases whose first maximum values are 02 dB/km at 22 GHz (through water vapor), 20 dB/km at 60 GHz (through oxygen), and 2 dB/km at 120 GHz (through oxygen) (Ref. A.4-1).

The lowest applicable radio frequency (RF) for LOS radio relay links depends on antenna gain (i.e., whether the required (large) antenna can be mechanically realized in view of strength requirements imposed on the antenna tower by its structure and the wind load). This results in a lowest frequency of about 300 MHz, at which frequency the LOS distance can be exceeded by 30 percent.

In general, most LOS links presently in use operate between 2 and 8 GHz. The LOS microwave links are of equal value in comparison to cable links with respect to quality, reliability, and constancy. The frequency carriers of present microwave LOS systems are mostly frequency modulated (FM) by a large number of voice frequency (VF) channels (i.e., 1500 to 3600 channels and up to 6000 VF channels with single-sideband AM (SSB-AM) modulation). These systems are called analog systems. In addition, there are the newer digital radio relay systems by which the carrier is digitally modulated (e.g., with phase-shift key (PSK) modulation) by binary data from 90 to 200 Mbps or by 1300 to 2900 VF channels digitized by pulse code modulation (PCM) (Ref. A.4-1). In analog systems the VF channels are combined by frequency division multiplex (FDM) before they FM-modulate the carrier. In digital systems the data or VF channels (after being digitized) are transmitted in time division multiplex (TDM) before digital modulation (PSK) of the carrier.

The trend is toward microwave LOS systems above 10 and 15 GHz which can transmit more than 10,000 PCM-VF channels. Microwave LOS systems also are used to transmit an equivalent number of TV or wideband channels (relative to VF channels) VF groups, and TV programs can be transmitted over the same LOS links and with the same equipment. U.S. and international frequency allocations, their channel capacities, and other data are given in Figure A.4-1 (Ref. A.4-2).

Advantages of microwave LOS systems include the following (Ref. A.4-3):

- Extremely wide transmission bandwidth of atmospheric transmission medium used
- Low interference because of high antenna directivity

U. S. FREQUENCY ALLOCATIONS

U.S. (MWh)	1710	1850	1990	2110	2130	2150	2160	2180	2200	2290	3700	4200	5925	6425	6575	6875	7125	8400	10700	11700	12200	12700	13250
	U.S. Govt.	Op. Fixed Pvt. MW	TV Aux		Pvt. MW	GC		CC	Pvt. MW	U.S. Govt	Common Carrier (ICC)		Common Carrier (ICC)		Op. Fixed Pvt. MW	TV Aux.		U.S. Govt		CC	Op. Fixed Pvt. MW	TV Aux CARS	
600	600			252				252		600													
96	96	PCM	PCM		96	PCM		96	PCM														
				TV							1800/TV			1800/TV		600	TV	1200/TV		1800/TV		1200	TV
											1500/TV			2400/TV		600	TV	1200/TV		2400/TV		1200	TV

INTERNATIONAL FREQUENCY ALLOCATIONS

FREQUENCY ALLOCATIONS									
INT'L (MHz)	2100	3100	4200	5225	6250	7110	7425	7725	8275
		Rec. 382 Annex		Rec. 383		Rec. 384	Rec. 385	Rec. 386 Annex	Rec. 388
CCIR Rec. 283/382									Rec. 387
300/800									
80 PCM									
TV				1800/TV	1280/TV ②	300	1280/ TV ②	680	1800/ TV
		1800/TV		2400/TV ①	2400/TV ②		1280/ TV ②		2400/ TV ①

NOTES:

- Numbers in box indicate max. channel capacity. (No. of voice channels per rf channel).
① CCIR Rec. 383 and Rec. 387 channel capacity is 1800 telephone channels.
② CCIR Rec. 384 channel capacity is 2700 or 1260 telephone channels.
③ CCIR Rec. 386 (Annex) channel capacity is 960 telephone channels.

Figure A.4-1. Summary of Frequency Allocations

- External noise negligible
- LOS links relatively easily implemented and modified
- Geographical barriers easy to overcome
- VF channels and video channels can be transmitted by the same equipment
- LOS links highly resistant to disasters.

Disadvantages of LOS systems include the following:

- Number of VF channels or video channels that can be transmitted limited by available (assigned) frequency spectrum
- Signal degradation due to different types of interference.

Microwave LOS signals are susceptible to occasional fluctuations, even on clear LOS paths and with adequate ground clearance. Deep fades in the signals occur from time to time and momentarily increase the noise level. On rare occasions signal amplitude in one or more channels on a microwave link falls below the permissible limit and causes an interruption.

In many cases, microwave LOS-system performance is limited by natural parameters of the transmission medium such as the following (Ref. A.4-4):

- Attenuation by rain, snow, hail, clouds, etc.
- Scattering by irregularities in refractive index structure of the atmosphere
- Refraction, ducting, and multipath resulting from atmospheric layers
- Dispersion resulting from frequency-dependent properties of the atmosphere
- Reflection, scattering, multipath, and lower atmosphere perturbations resulting from irregular terrain and man-made structures.

The importance of each of the above propagation phenomena depends in part upon the radio frequency used and the characteristics of the system employed.

Most microwave paths are subject to at least a small amount of multipath and attenuation fading throughout the year. Multipath fading is a relatively rapid type of fluctuation in the received signal strength that usually is caused by interference between two or more slowly varying replicas of the desired signals arriving via different paths. Attenuation fading is a relatively slow fluctuation in the mean level of the received signal normally caused by the signal passing through atmospheric media having varying attenuation properties (variations in air density and dielectric constant). Attenuation fading results from intervention absorption of the signal or deflection of the signal away from the receiving antenna. The three main causes of attenuation fading are atmospheric absorption, ground obstruction, and duct reflection.

Multipath fading may be classified as reflection multipath fading or as atmospheric multipath or "Rayleigh" fading. In reflection multipath fading the signal arrives at the receiver via at least two paths including a direct path and an indirect path. The indirect path can result from ground surface reflection, water surface reflection, reflection from physical objects, reflection from an inversion layer or ducts, or reflection from a spurious object such as an aircraft. Atmospheric multipath fading or "Rayleigh" fading is rapid fading caused by reflection/refraction of the signal from many small discontinuities of the radio refractive index in the atmosphere. The period of time atmospheric multipath fading occurs depends on geographic location, whereas the depth and number of fades are dependent on the LOS path length and frequency of operation. Typical examples of multipath fading are shown in Figures A.4-2 through A.4-9 (Ref. A.4-5).

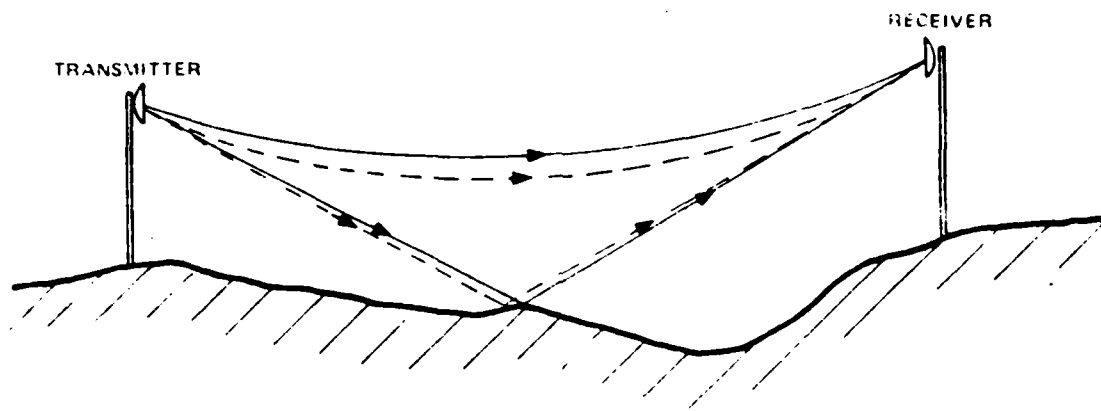


Figure A.4-2. Two-Path Interference Caused by Reflection at the Surface of the Intervening Ground

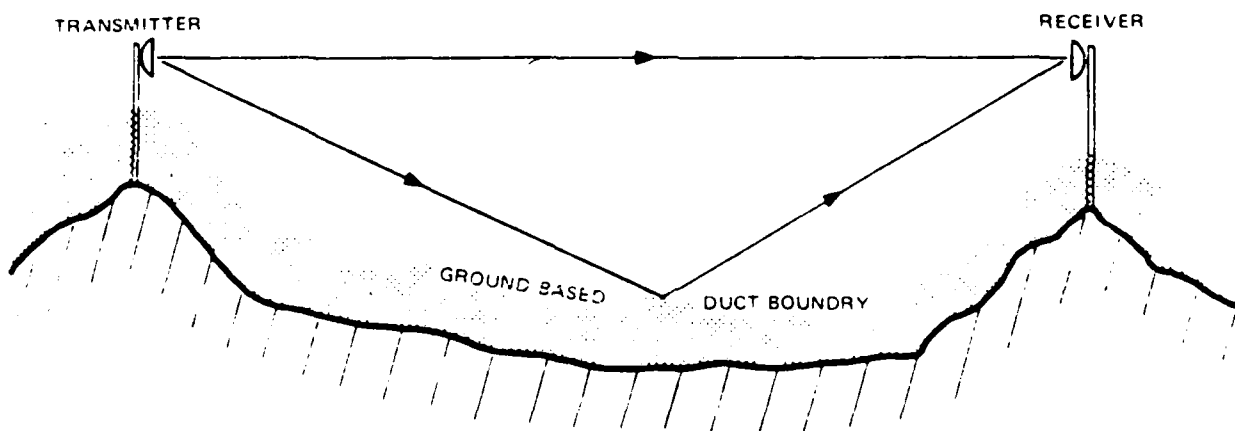


Figure A.4-3. Multipath Caused by Ground Based Ducting Layer

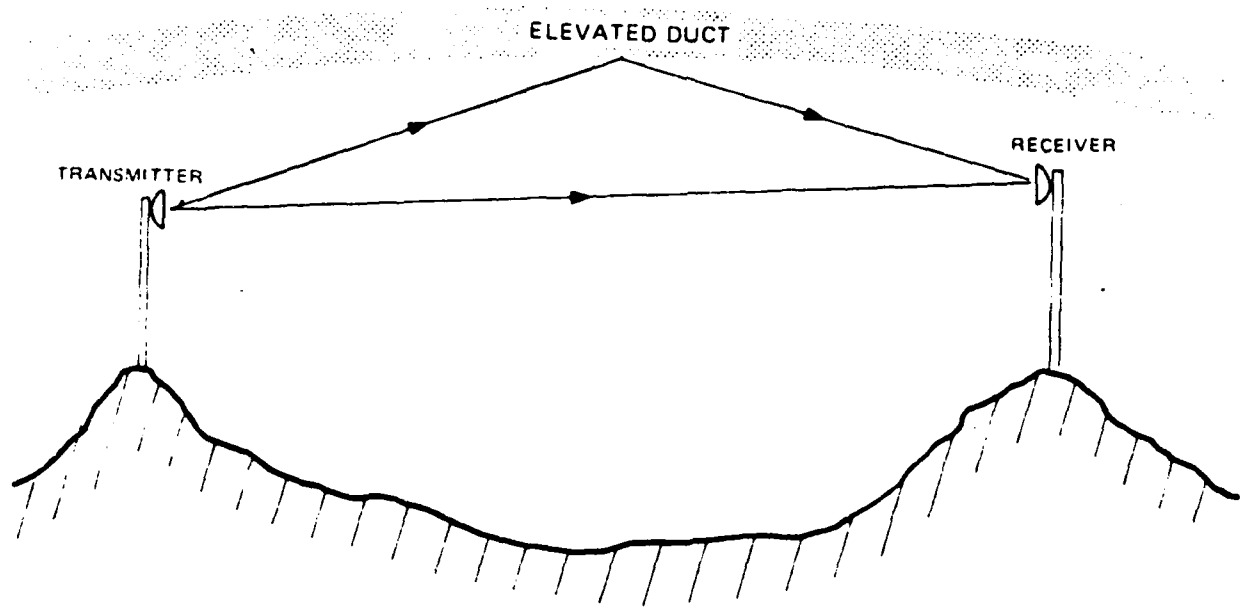


Figure A.4-4. Multipath Caused by Elevated-Duct Reflection

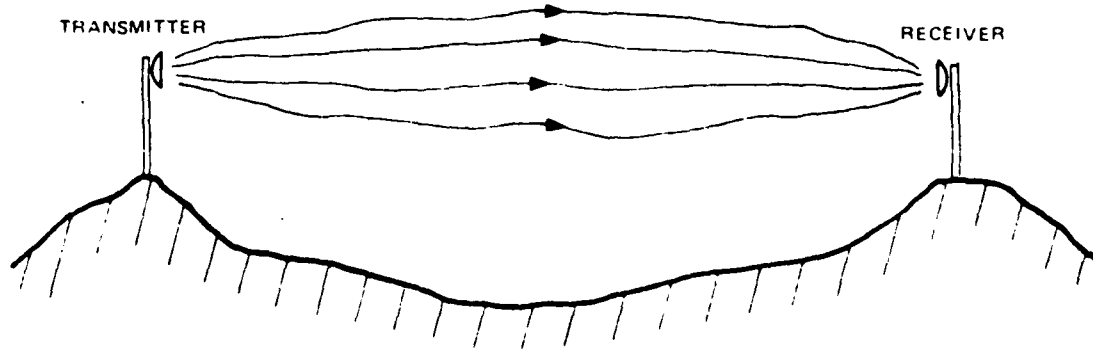


Figure A.4-5. Atmospheric Multipath

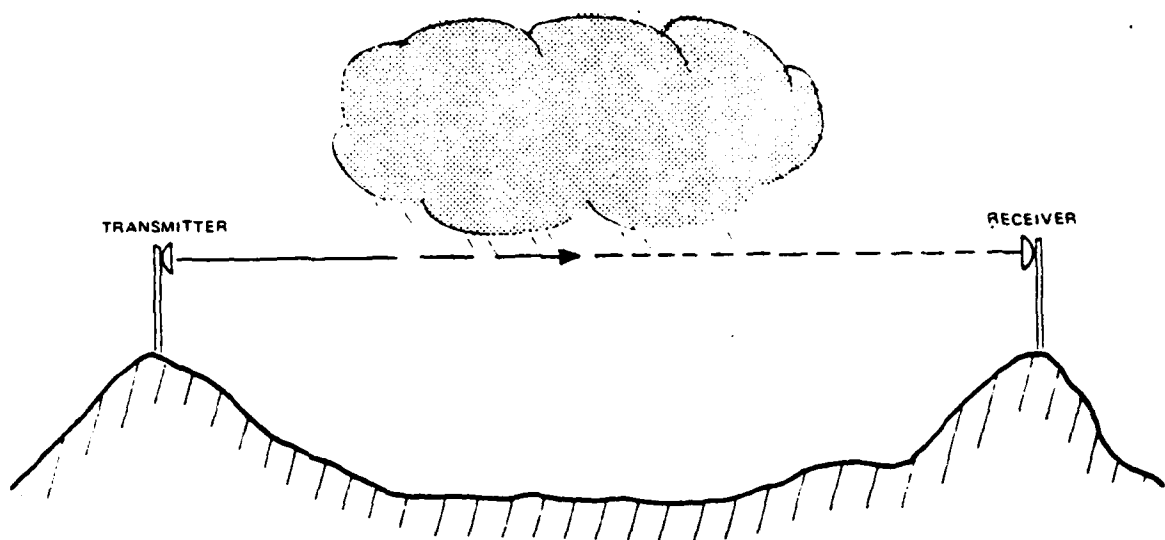


Figure A.4-6. Atmospheric Absorption

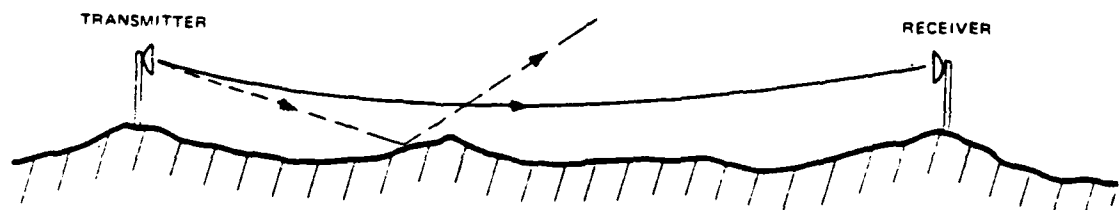


Figure A.4-7. Ground Obstruction Caused by a Combination of Insufficient Ground Clearance and Upward Bending of the Rays

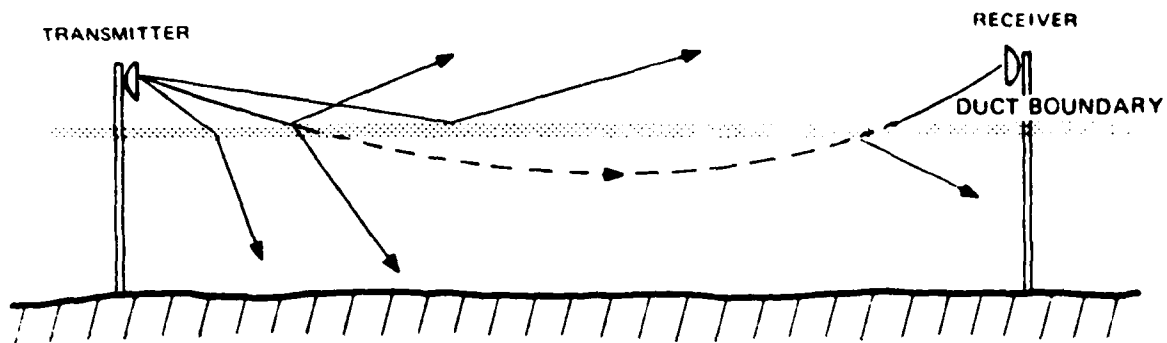


Figure A.4-8. Deflection of a Microwave Signal by a Duct Boundary at the Elevation of a Path Line

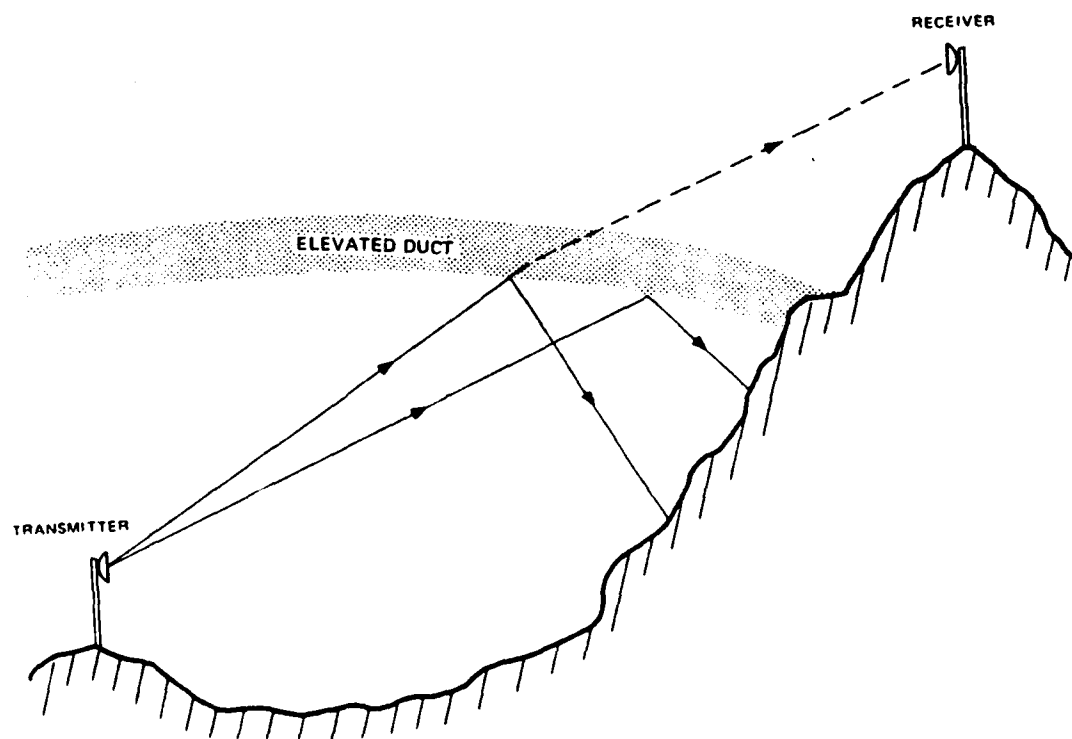


Figure A.4-9. Deflection of a Microwave Signal by an Elevated Duct

Path reliability as influenced by propagation effects is a major design factor in determining transmitter power, antenna gain, and receiver noise figure. For example, a microwave path can fail because of rain, multipath fading, or beam bending, and rain attenuation caused by scattering of the microwave energy by the water droplets also becomes a significant problem in the higher frequency regions starting at about 9 GHz. Table A.4-1 compares rain attenuation per mile (in dB/mile) versus the probability of outage per year in hours, minutes, or seconds for various regions of the U.S. Table A.4-2 shows fade margins required for protection against multipath fades at 12 GHz. Figure A.4-10 shows rain attenuation for different frequencies, path lengths, and percent of outage for various locations in the Federal Republic of Germany (curves are statistical predictions and bar graphs are measured values) (Ref. A.4-6).

LOS path reliability (and availability) is influenced by absorptions and reflections along the path which degrade the signal by attenuation of the signal amplitude, and which is known as fading. Interference fading is particularly critical for frequencies below 10 GHz. Interference fading is frequency- and time-dependent and occurs in the form of relatively short-duration (up to several seconds) but relatively frequent (10 to 100 times per month) signal-level reductions. Sometimes several microwave co-channels or adjacent channels may be affected by the same interference fading. Effects of interference fading or equipment failure, or both causes together, can lead to interruptions in the LOS link, although interruptions due to fading disappear when the fading phenomena die away. Also, the cause of fading can be corrected by proper planning of the microwave path, or by use of diversity reception (space and frequency diversity) or of multiline protection switching. Equipment reliability and link availability also can be improved by use of equipment redundancy (Ref. A.4-7).

Microwave equipment availability or outage calculations are based on concepts of "mean time between failures" (MTBF) and "mean time to restore" (MTTR). The relationship between these concepts determines the outage ratio, or

$$U = \frac{MTTR}{MTBF} \quad (A.4-1)$$

Table A.4-1. Rain Attenuation in dB/mi at 11 GHz

REGION	OUTAGE PER YEAR						
	10 HRS	5 HRS	1 HR	30 MIN	6 MIN	3 MIN	30 SEC
A	2.3	2.6	4.8	5.8	8.2	9.4	11.8
B	2.0	2.2	3.45	4.1	5.7	6.35	7.8
C	1.9	2.0	2.4	2.6	3.15	3.45	4.7
D	1.4	1.5	1.8	2.0	2.85	2.9	4.5
E	1.25	1.3	1.5	1.6	1.95	2.15	2.7
F	1.1	1.15	1.3	1.4	1.6	1.75	2.1
G	.8	.9	1.2	1.3	1.5	1.6	2.0
H	.7	.8	1.05	1.15	1.4	1.5	1.7
	.1	.05	.01	.005	.001	.0005	.0001
	% OF TIME FOR SYSTEM OUTAGE						

Table A.4-2. Fade Margins in dB Required for Protection Against Multipath Fades at 12 GHz

OUTAGE PER YEAR	PATH LENGTH IN MILES						% OF TIME OUTAGE PER YEAR
	5	10	15	20	25	30	
10 HOURS	0 dB	4dB	15dB	22dB	29dB	35dB	.1
5 HOURS	0	7	18	25	32	38	.05
1 HOUR	0	14	25	32	39	45	.01
30 MINUTES	0	17	28	35	42	48	.005
6 MINUTES	5	24	35	42	49	55	.001
3 MINUTES	8	27	38	45	52	58	.0005
30 SECONDS	15	34	45	52	59	65	.0001
MOST MULTIPATH OCCURS IN EARLY DAWN HOURS							

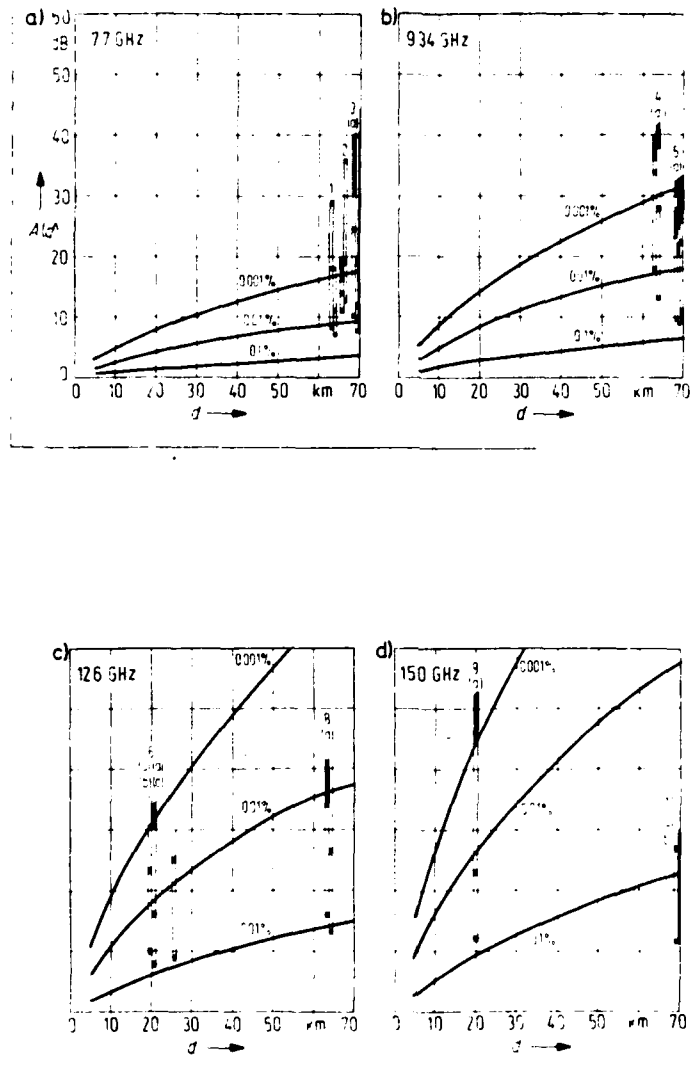


Figure A.4-10. Rain Attenuation for Different Frequencies

wherein MTTR is assumed to include modification time, travel time, diagnostic time, and actual repair or replacement time. The "innage ratio" or availability, A, consequently may be written as

$$A = 1 - U \quad (A.4-2)$$

which also may be expressed as percentage when multiplied by 100. For example, for MTBF = 5000 hours and MTTR = 5 hours, the outage ratio is $U = 5/5000$, or 0.001, and availability is $A = 1 - 0.001 = 0.999$, or 99.9 percent. Availability for a single equipment alternatively can be expressed as

$$A = \frac{\text{MTBF}}{\text{MTBF} + \text{MTTR}} \quad (A.4-3)$$

On the other hand, for equipment redundancy it is more convenient to calculate availability in terms of failure rate, λ (reciprocal of MTBF), and of restoration rate, μ (reciprocal of MTTR), whereby availability for single equipment would be written as

$$A = \frac{\mu}{\mu + \lambda} \quad (A.4-4)$$

Expressions for redundant-equipment availability are summarized in Table A.4-3.

Primary power sources for microwave LOS relay stations (and terminals) traditionally have consisted of AC commercial power, batteries, and emergency engine-driven generators. For remote relay stations where AC power cannot be made available, the following newer types of sources have been developed for various power requirements:

- Solar power systems of from 4 to 350 Watts output, with MTBF exceeding 200,000 hours
- Thermolectric (solid-state) generators of from 10 to 300 Watts output
- Rankine-cycle (dynamic) turbogenerators of from 50 to 6,000 Watts output.

Table A.4-3. Expressions for Redundant-Equipment Availability

No. of Equipment	Conditions		Steady-State Availability	Av. for $\lambda = 0.01$ $\mu = 0.2$
	Type of Redundancy	Type of Repair		
1	---	--	$\frac{\mu}{\mu + \lambda}$	0.95
	Standby	Single*	$\frac{\mu^2 + \mu\lambda}{\mu^2 + \mu\lambda + \lambda^2}$	0.998
2	Parallel	Single*	$\frac{\mu^2 + 2\mu\lambda}{\mu^2 + 2\mu\lambda + 2\lambda^2}$	0.996
	Standby	Single*	$\frac{\mu^3 + \mu^2\lambda + \lambda^2\mu}{\mu^3 + \mu^2\lambda + \lambda\mu + \lambda^3}$	0.9999
3	Parallel	Single*	$\frac{\mu^3 + 3\mu^2\lambda + 6\mu\lambda^2}{\mu^3 + 3\mu^2\lambda + 6\mu\lambda^2 + 6\lambda^3}$	0.9993

* Failed branches can only be repaired one at a time.

All of the above sources are capable of 24-hour continuous operation. The thermoelectric generators and turbogenerators are fuel-driven, whereas the solar and thermoelectric power systems are limited to small and medium-size remote repeater stations. Larger power requirements could be filled by the turbogenerator, which has only one moving part. Other energy sources may be realized by hybrid power systems such as wind generators and batteries or other combinations (Ref. A.4-8).

Antennas for microwave LOS links are usually mounted on microwave towers of from about 50- to 300-ft heights. Type of tower construction depends on height of the tower, number of antennas to be mounted, wind load, radio equipment housing, and other technical, economic, topographical, and aesthetic factors. The three types of antenna towers generally in use are light-construction, guy-wire towers, self-supporting steel towers, and steel-reinforced concrete (ferro-concrete) towers. The limitations of guyed towers are the size and number of antennas (dishes) which can be mounted. Self-supporting tower construction is ordinarily used for large towers or to accommodate many antennas, limitations being antenna size, number of antennas, and the wind load. The limitation of the taller concrete towers is need to cluster all antennas at the tower top, which results in excessive antenna height and waveguide (transmission line) attenuation. The magnitude of forces involved may readily be visualized by realization that the loading on one 12-ft-diameter dish antenna from a wind gust of 140 mph can exceed three tons. Fortunately such wind speeds are not common, although they are statistically likely to occur at many exposed radio stations as gusts of three-second duration once in 50 years (Ref. A.4-9).

A.4.2 Intrinsic Technical Limitations

Several important technical limitations of LOS transmission such as multipath propagation and rain attenuation have been addressed in Section A.4.1. Section A.4.2 describes additional limitations as well as possible techniques for their resolution or mitigation.

One area wherein conventional techniques normally used to combat fading (e.g., switching) are virtually ineffective is that of abnormal or anomalous propagation which is characterized in its most extreme form by the catastrophic phenomenon known as blackout fading.

Conventional fading phenomena consist of reflection from the smooth surface of water or ground, of diffraction, whereby loss depends on the Fresnel-zone radius of the wavefront compared to the area obstructed and the reflectivity of the obstruction, and of refraction, which causes the microwave path to be bent toward the denser atmosphere. The amount and direction of bending to which the microwave beam is subjected is defined by the effective radius factor of the earth, k (k -factor), which when multiplied by the actual earth radius gives the radius of a fictitious earth curve that is equivalent to the relative curvature of the earth (i.e., equal to the actual earth curvature minus the curvature of the microwave beam). Any change in the amount of refraction caused by atmospheric conditions can then be expressed as a change in k . Typical k -factors are from 1.2 in dry elevated areas and $4/3$ in typical inland areas to 2 or 3 in humid coastal areas. With k less than 1 the path could become obstructed and vulnerable to extreme multipath fading, and when negative values of k occur the path may become trapped and susceptible to blackout fading (Ref. A.4-10).

Blackout fading results from formation of unusually steep, negative atmospheric density gradients due to a dramatic drop in humidity or to an increase in temperature with height. Blackout fading also can be caused by signal trapping within a ground-based superrefractive layer on low-clearance microwave paths, which often limits the path length in LOS systems located in buried regions. Still another cause of blackout fading may be the result of antenna decoupling (i.e., even if the antenna is within the radio horizon, presence of a superrefractive layer will cause the radio beam to arrive at a greater elevation angle than it normally would). Antenna decoupling has been identified as a major cause of severe nocturnal fading on many microwave links. However, careful antenna alignment following a special procedure will correct most decoupling problems (Ref. A.4-10).

A further type of intrinsic limitation may be caused by signal degradation due to interference, of which the most common types include threshold degradation (receiver threshold), co-channel interference, adjacent-channel interference, and interference resulting from spurious receiver responses.

Threshold degradation becomes apparent when the RF signal falls below the improvement threshold (in FM), at which time the S/N ratio of the output of the receiver decreases so rapidly that circuit performance becomes unacceptable. Penetration of receiver selectivity by interference has the same effect as thermal noise, and if interference power is greater than thermal-noise power a new, higher improvement threshold will be established. Threshold degradation can also be caused by co-channel or adjacent-channel interference as noted below.

Co-channel interference originates from the difference in frequency between the desired and undesired carrier signals. Interference is present whenever the frequency difference between these signals causes a beat to fall in the baseband spectrum. This situation occurs in 2-way frequency plans because use of the same frequency on alternate hops requires receiving of that frequency from two directions. The fact that the transmitters as well as the receivers of a relay station operate on the identical nominal frequency as well as that the front-to-back ratio of the antennas has a finite value must lead to interference in one direction of transmission. Objectionable co-channel interference therefore is an indication that the antenna-to-antenna isolation is inadequate for use in 2-frequency plans (Ref. A.4-7).

Adjacent-channel interference can be caused by sideband overlap (carriers close together so that the sidebands occupy the same frequency spectrum) or by "direct" adjacent-channel interference, which introduces intelligible cross-talk into the baseband of the victim receiver and is more disturbing than the garbled noise resulting from sideband overlap.

Spurious receiver response will convert an adjacent-channel signal into the desired IF band. Such signals will appear as co-channel or adjacent-channel interference insofar as receiver action is concerned.

In analyzing interference between terrestrial systems, accepted practice is to use the carrier-to-interference ratio, C/I. This follows directly from the fact that a certain amount of noise may be permitted in the derived voice channels due to the interference, and also depends on the levels of desired as well as of undesired carriers (i.e., on their difference). Table A.4-4 identifies effects of introducing various C/T ratios into different systems (Ref. A.4-11).

Table A.4-4. Carrier to Interference (C/I) Ratios in dB into Different Systems

Number of Channels of Interfacing System	Spacing Between Interfacing and Victim ⁽³⁾ System (MHz)				
	0.0	7.4 ⁽¹⁾	14.8	22.2 ⁽²⁾	29.6 ⁽²⁾
1800	68.0	90.0	65.0	47.0	27.0
1200	70.0	90.0	64.0	47.0	27.0
960	74.0	90.0	63.0	47.0	27.0
300	81.0	90.0	63.0	50.0	30.0

Notes:

- (1) Carrier beat
- (2) Threshold
- (3) Victim System has 1800 channels

Frequency diversity uses two different frequencies to transmit the same information, with two vertically separated antenna transmitting or receiving the information over two different paths through space. Figure A.4-11 portrays an example of a space-diversity configuration (only one direction is shown). Typical antenna spacings are 30-40 feet at 6 GHz, 45-50 feet at 4 GHz, and 60-80 feet at 2 GHz. At 11 GHz, spacings of 25-30 feet would be adequate, and experience indicates that even small spacings of 10-20 feet provide good diversity, at least in the 6-GHz bands. Space diversity can be applied only on a point-to-point (per-hop) basis (Ref. A.4-5).

Frequency-diversity systems have the advantage that a complete end-to-end protection channel can be automatically switched in to replace a failed channel, regardless of whether the failure was caused by fading or equipment outage (100-percent equipment redundancy). RF combining and switching have been used to improve problem paths on multiline systems where frequency-diversity protection has been inadequate and additional propagation protection in the form of space diversity is needed over a particular path. Equipment redundancy in the form of hot-standby or protection-channel switching also continues to be an economical method of improving system reliability. However, hot-standby and space-diversity configurations have the problem of differential absolute delay, which must be corrected by equalization.

Figure A.4-12 identifies improvement factors for frequency and space diversity at 4 and 6 GHz, and Figure A.4-13 the frequency response versus differential absolute delay for space diversity (Ref. A.4-5). Other factors which impose physical limitation on system capability are maximum repeater spacing and antenna height. Also, the limited availability of frequencies in the preferred frequency bands necessitates use of higher frequencies.

NOTE: ONE DIRECTION ONLY IS SHOWN

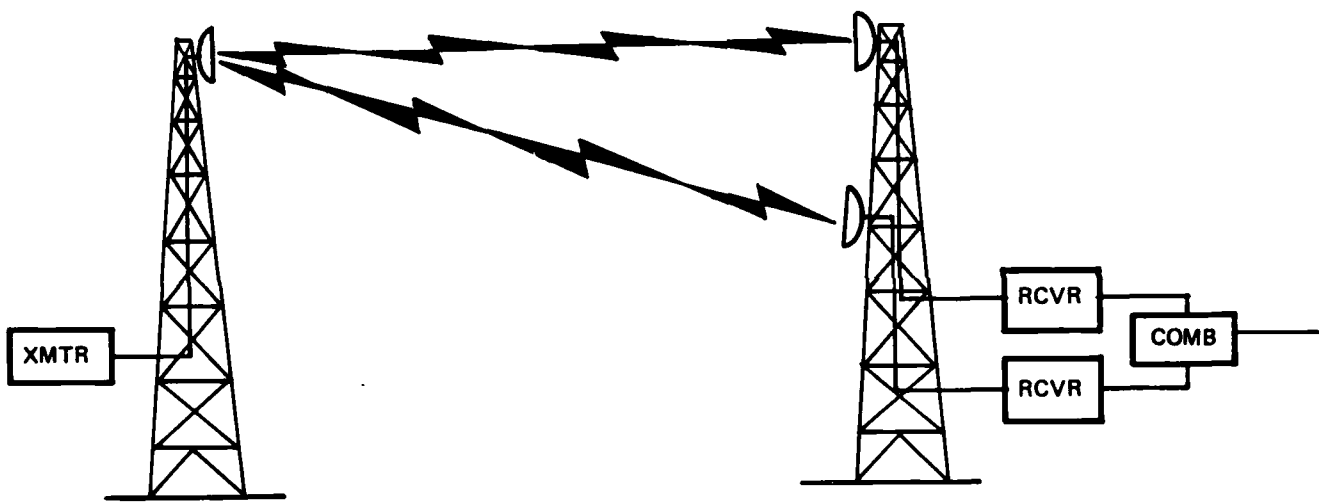


Figure A.4-11. Space Diversity Configuration

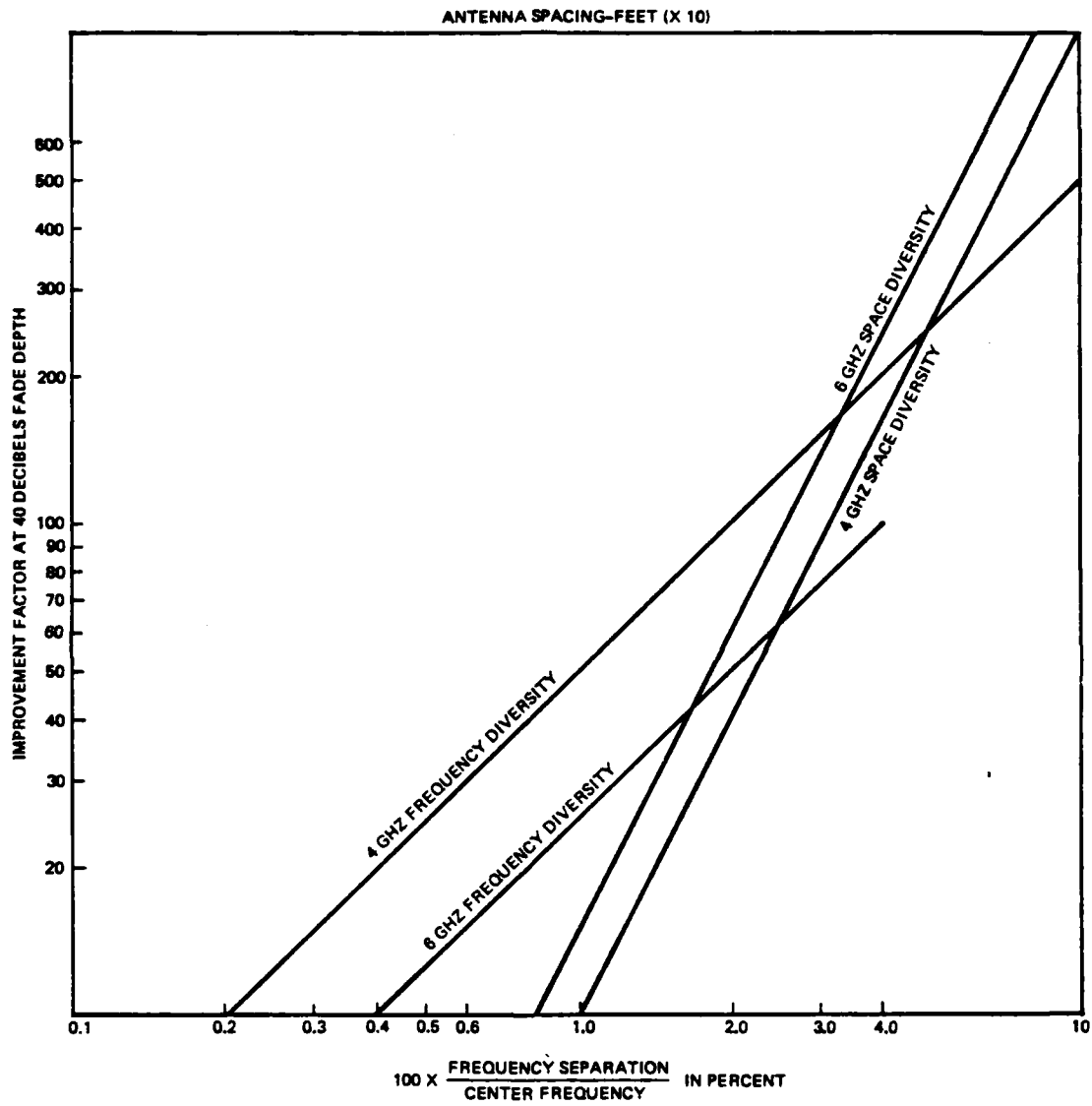


Figure A.4-12. Frequency and Space Diversity Improvements

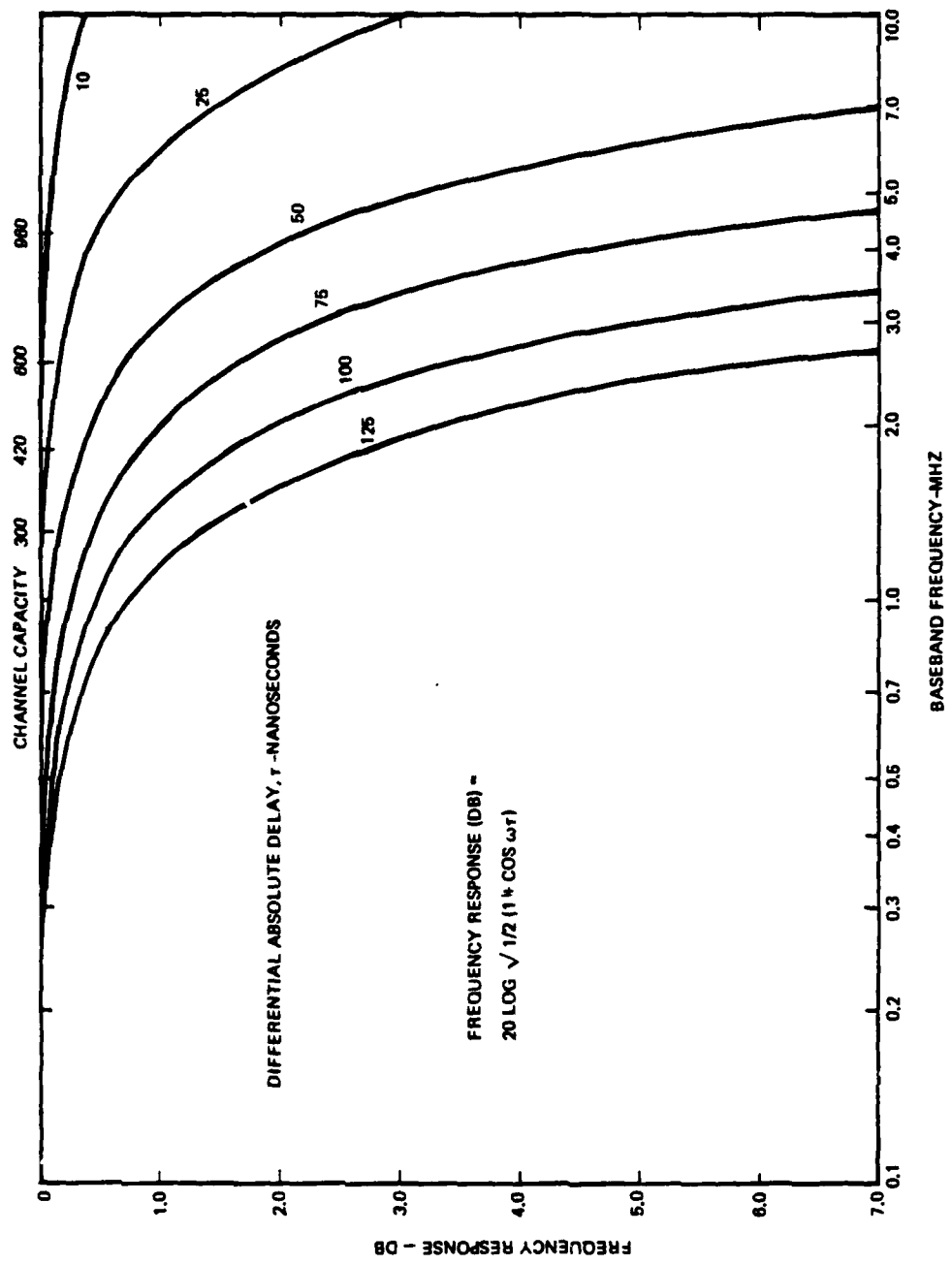


Figure A.4-13. Frequency Response Versus Differential Absolute Delay for Space Diversity

A.4.3 Development Trends

Rapid advance in semiconductor and pulse-circuit technologies gave impetus to research and development of digital radio-relay systems. The market trend now indicates that the telecommunications network is moving toward digital systems.

The advantage of digital over analog systems lies in the technique of signal renewing. The digital signal, consisting of discrete pulses, is regenerated (i.e., a new pulse is created based upon decision that a valid input pulse exists) each time it passes through a repeater, whereas an analog signal must be amplified at each repeater location. However, because the amplification process does not discriminate between the desired signal and unwanted noise, the noise tends to accumulate along the transmission path, thus seriously degrading the quality of the analog signal. The cumulative effect of noise therefore eventually limits the transmission-path distance over which the signal may be transmitted due to reduction in signal-to-noise ratio.

Significant features of digital microwave systems may be summarized as follows:

- Realization of low-cost high-speed PCM terminal equipment will reduce total system cost
- High-quality long-haul transmission is attainable due to almost complete pulse regenerative repeating capability (provided carrier-to-noise power is above the threshold level)
- Flexibility in transmitting various kinds of signals such as voice, data, and video is available without mutual interactions among different signals.

Frequency bands used for commercial digital systems are mainly 2, 6, 11, 12, and 13 GHz at the present time. They also include 4.4 to 5.0 GHz and 7.125 to 8.400 GHz for military systems.

The 2-GHz band is generally applied to small-capacity systems at 10 Mbps and the 11- or 13-GHz bands to medium-capacity systems at 50 or 100 Mbps. These frequencies are generally applied to short-haul radio-relay systems. One example of a long-haul radio-relay digital system is the 6-GHz band system at 4.5 Mbps which has been operational for some years in the U.S. A long-haul digital system using the 20-GHz band at 17.7-21.2 GHz that was placed in service in Japan has a transmission capability of 400 Mbps per radio channel (equivalent to 5760 VF channels) and of about 46,000 voice channels over a route. A digital radio system employing the 18-GHz band by BTL can transmit 274 Mbps per RF channel (equivalent to 4032 voice channels) and about 30,000 voice channels over a route (Ref. A.4-3).

One military all-digital microwave system for DoD is the Washington Area Wideband System (WAWS), which uses transmission at 6 and 11 GHz and can transmit 90-Mbps data. Another military digital microwave system will operate in the 4400-5000 and 7125-8400 MHz bands. This digital radio and multiplex acquisition (DRAMA) program will provide up to 384 VF channels at a maximum data rate of approximately 26 Mbps (Refs. A.4-12 and A.4-13). When different signals are transmitted over digital systems, no restrictions exist because there is no significant difference between signals after being encoded.

A number of simultaneous transmission systems for analog and digital signals have recently been developed. The purpose of these systems is to economically construct digital circuits over analog radio systems. Some systems transmit digital signals in the lower band of frequency-division multiplex (FDM) telephone channels, and other systems in the upper vacant band of FDM telephone channels or on a television signal.

Figure A.4-14 shows the trend of transmission capacity for analog and digital systems between about 1945 and 1980 (Ref. A.4-3), indicating the push towards higher frequencies and larger VF channel capacities whereby digital systems have been growing faster than analog systems. Digital systems probably will become more efficient in frequency utilization than analog systems through application of bandwidth-reduction technology. However, they are currently inferior to analog transmission systems in the case of voice transmission. Further efforts therefore are required for increasing the frequency utilization efficiency of digital systems. Although 2-PSK is employed in some small-capacity systems, 4-PSK is preferred in many current system and some advanced ones employ 8-PSK. Currently available frequency-utilization efficiency is about 2.5-bps/Hz bandwidth, which is equivalent to 35 voice channels per MHz bandwidth (Ref. A.4-5).

To further increase efficiency requires exploiting a technique of higher-level modulation with the modulating clock frequency kept constant. Figure A.4-15 shows the frequency-utilization efficiency and the necessary signal-to-noise ratio of various modulation methods. Increasing the modulation level results in increased susceptibility to interference and needs a greater branching angle at junction stations. Therefore the optimum level of modulation (QAM) and partial response modulation are promising as multi-level modulation techniques (Ref. A.4-3).

Partial response to modulation permits efficient frequency utilization, and is being actively studied in Canada and other countries. Research on QAM also is being emphasized in Japan with an aim of establishing a 16-level QAM technique. If successful, the efficiency of frequency utilization will become about 5 bps/Hz, which is equivalent to 72 voice channels per MHz and is twice as high as that of 4-PSK. It is such a sophisticated modulation technique that further research is necessary to understand effects of signals of multipath fading, rainfall attenuation, and cross-polarization discrimination degradation on signals. More work also is required for improving space diversity techniques, which are believed to be effective against multipath fading. Table A.4-5 lists some of the latest radio-relay systems, including topical analog systems, that either are operational or under development (Ref. A.4-3).

Table A.4-5. Efficient Spectrum Utilization

modulation	frequency (GHz)	RF channel separation (MHz)	capacity		RF channel arrangement	spectrum use efficiency ((bit/s)/Hz)	(ch MHz)	present state
			bit rate (Mbit/s)	number of telephone channels				
digital system								
QPR *	8	41	91	1344	interleave	2.2	3.3	BNR (Canada) under development
8-PSK	11	41	91	1344	interleave	2.2	3.3	Collins (United States)
4-PSK	11	67	140	1920	interleave	2.1	2.9	Post Office (United Kingdom) under development
4-PSK	11	60	140	1920	interleave	2.3	3.2	CNET (France) under development
4-PSK	18	220.2	274	4032	co-channel	2.5	3.6	BLI (United States) field test finished
4-PSK	20	160	400	5760	interleave	2.5	3.6	NTT (Japan)
16-QAM**	5	40	200	2880	interleave	5.0	7.2	NTT (Japan) under development
analogue system								
F.M	4	20	—	1500	interstitial	—	7.5	BTI (United States)
F.M	6	40	—	2700	interleave	—	67.5	GII (Italy)
F.M	5	40	—	3600	interleave	—	90	NTT (Japan) under development
SSB-AM	6	30	—	6000	interleave	—	200	BTI (United States) under development

* QPR : quadrature partial response.

** QAM: quadrature amplitude modulation.

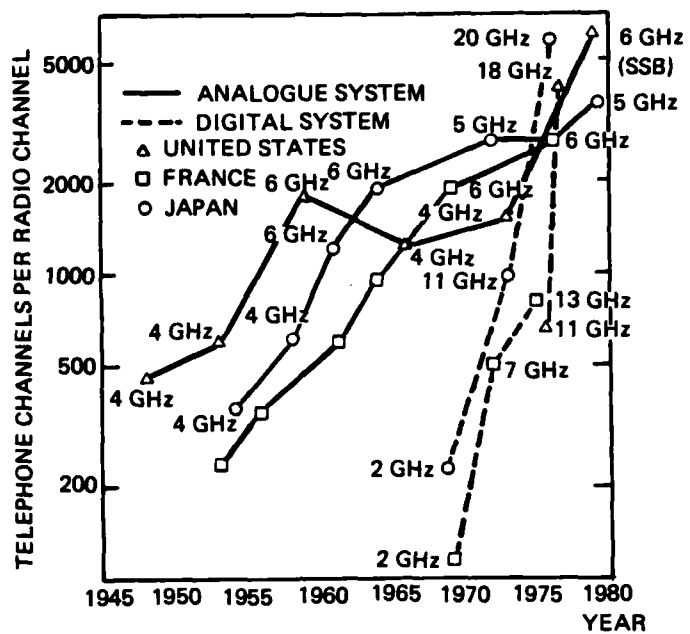


Figure A.4-14. Trends of Transmission Capacity

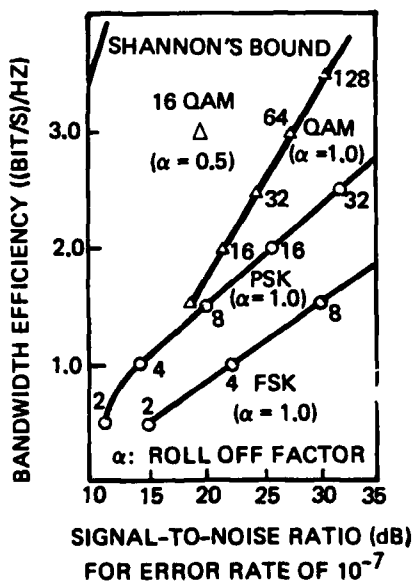


Figure A.4-15. Frequency Utilization Efficiency

At the initial stage of development the 2-, 4-, 6-, and 8-GHz frequency bands were used for radio-relay systems. However, used frequencies gradually entered higher bands, to the point where now the 11-, 13-, 15-, and even 20-GHz bands are actually utilized. Transmission characteristics of the bands in the range of 4-8 GHz are comparatively uniform and therefore these bands are generally used for long-haul high-capacity systems. At frequencies above about 10 GHz the influence of rainfall on propagation becomes significant, so that rainfall attenuation is one of the controlling factors in radio-relay system design. In particular, at frequencies above about 15 GHz, radio-wave attenuation and degradation due to rainfall are the most crucial factors in determining circuit performance. A digital radio-relay system in the 20-GHz band which has recently been developed in Japan employs a repeater spacing of about 3 km and each radio channel transmits a 400-Mbps signal by means of 4-PSK (Ref. A.4-3).

The increase in attenuation becomes comparatively slow at frequencies above about 50 GHz, and required repeater spacing is in the order of 1 km, as shown in Figure A.4-16. Dips at about 60 and 120 GHz show that the necessary repeater spacing becomes shorter because of the additional loss due to oxygen absorption.

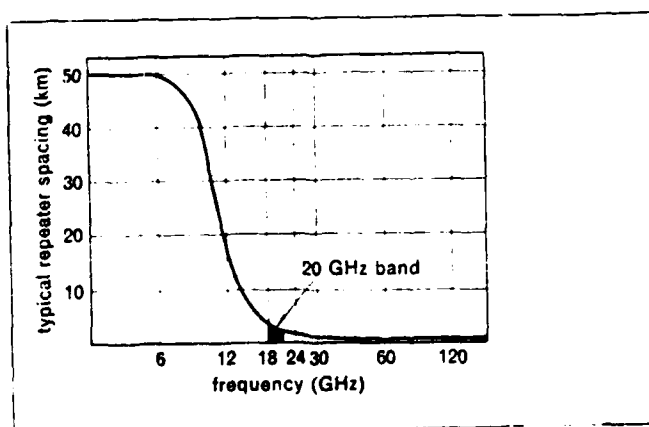


Figure A.4-16. Repeater Spacing

A closer look at the characteristics in the 60-GHz band reveals that there is a frequency band about 6 GHz wide in which the attenuation due to oxygen absorption exceeds 10 dB/km. This fact indicates that there is a possibility of establishing a radio-relay system network of high density free from interference using this frequency band (Ref. A.4-3).

There is a marked tendency that the future telecommunications network will gradually evolve into the integrated digital network. The remaining target in future development of the digital technique is more efficient use of the frequency spectrum. In particular, efforts should be continued for better use of the 1-10 GHz frequency band, which constitutes the most valuable frequency resource (Ref. A.4-3).

A versatile new digital microwave radio developed for the U.S. Government under the Digital Radio and Multiplexer Acquisition (DRAMA) program will convert transmission facilities of the Defense Communication System from analog to digital signal format. This radio can be configured for either space or frequency diversity in either the 4- or 8-GHz military bands. A choice of quadriphase shift keying or quadrature partial response signaling provides bandwidth efficiencies of 1.0- and 1.9 bps/Hz of occupied RF bandwidth.

The AN/FRC-170 (V), -171 (V), and -173 (V) digital microwave radio equipment now being procured by the U.S. Government as part of the DRAMA program initiates the Government changeover from analog to digital telephone by enabling digitization of strategic facilities of the Defense Communication System and of other related facilities of the three U.S. military services. The first application of the DRAMA equipment is the Digital European Backbone intended to interconnect Italy, Germany, Belgium, and the United Kingdom with a digital telephone network for use by the U.S. military.

Advantages of digital telephone transmission to the U.S. Government include attractiveness of this signal format to commercial telephony, ease of switching and multiplexing, virtual immunity to transmission impairments over multiple repeater hops, decreased sensitivity to co- and adjacent-channel interference, increased reliability, improved maintainability, and improved fault isolation for remote monitoring of unattended operation. An additional advantage for the U.S. military is that digital traffic can be readily encrypted to provide communication security throughout the telephone network. Table A.4-6 summarizes DRAMA radio equipment configurations (Ref. A.4-14).

Table A.4-6. DRAMA Radio Configurations

Nomenclature	Frequency Band (GHz)	Diversity
AN/FRC-170(V)	4	Space
AN/FRC-171(V)	8	Space
AN/FRC-172(V)	4	Frequency
AN/FRC-173(V)	8	Frequency

A.5 TROPOSPHERIC SCATTER COMMUNICATIONS

A.5.1 Description of Medium

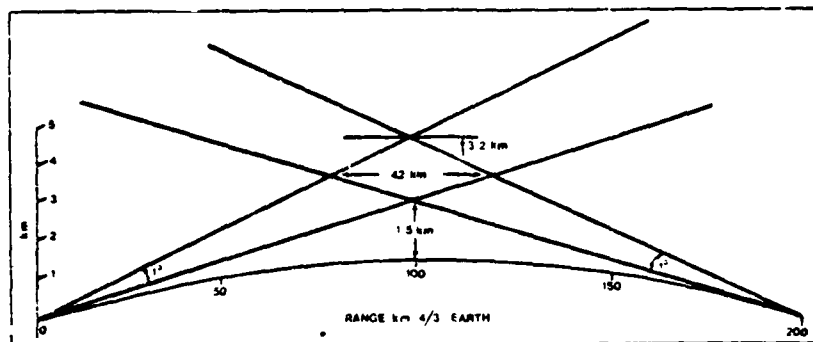
Tropospheric scatter (over-the-horizon), or troposcatter, communication is used when the distance between point-to-point radio relay stations exceed the line-of-sight (LOS) transmission path, and one span or hop must bridge distances up to several hundred miles (e.g., across large bodies of water or foreign countries).

Troposcatter communication may be defined as a method or system of transmitting within the troposphere in the UHF and SHF bands in order to effect radio communication between two points on the surface of the earth that are separated by moderate distances of from 50 to 600 miles. Such a span or hop may be augmented by other spans in tandem to permit end-to-end through circuits up to many thousands of miles.

Systems of multiple spans in tandem composed of tropo links and extending even to thousands of miles are now in operation in many areas of the world, providing reliable multichannel communications. Troposcatter communication is also used in military applications. Capability of troposcatter communication to span hundreds of miles of inhospitable terrain with circuits of relatively high traffic density insures a continuing need for this type of transmission. Troposcatter propagation allows transmission of up to 120 voice frequency channels in the 100 MHz to 5 GHz transmission frequency range over large distances (up to 600 miles or 1000 km) without relay stations. Typical tropo stations now in existence operate in the preferred frequency bands of 100, 400, 450, 750, 800, and 900 MHz and 1.8, 2, 4, and 5 GHz. Typical transmitter powers are from 5 W to 50 KW, and receiver noise figures (NF) range from 2 dB at 900 MHz to 9 dB at 5 GHz. Typical antenna diameters are 10 to 120 feet maximum (Ref. A.5-1).

The source, E, shown in Figure A.5-1 is equipped with a highly directive antenna that emits a high power density into a narrow cone. The receiver, R, is also equipped with a high-gain, highly directive antenna which collects the energy scattered by the volume common to the beams of both antennas. Transmission is better when the altitude, h, of the common

scatter volume as well as the scatter angle, , between both beams are smaller (Ref. A.5-2). For a given distance, this will be realized if the horizons of both antenna are completely clear and their beams are tangential to the ground.



This typical path geometry curve shows the effect of diffraction efficiency on range. Scatter volume is the diamond-shaped area measuring 42 x 3.2 km.

Figure A.5-1. Typical Troposcatter Path Geometry

Available bandwidth is related to the antenna reradiation pattern. If the pattern is very broad the paths of the various rays will be very different in length and therefore in transit time. In this case it is only possible to transmit signals varying so slowly that the difference in transit time becomes irrelevant, which means narrowband signals. To transmit wideband signals it is necessary to use antennas having such a narrow beam that the difference in transit time for the various points of the common volume remains small in relation to the reciprocal of the desired bandwidth.

Obviously, tropospheric scattering exists even when antennas are in line-of-sight, in which case the scattered field is generally weak with respect to the main field and thus causes only a small scintillation of the latter. However, during periods of strong fading the received field can have characteristics similar to those of the troposcatter field (Ref.

In troposcatter, the energy will be scattered by nonhomogenous temperature and humidity conditions of the troposphere within the so-called "scatter volume" shown in Figure A.5-1. A small part of this scattered energy reaches over the horizon because the path attenuation is inversely proportional to the scatter volume and large path attenuations may result with strong variations in time during the day or the year (season). Hence, troposcatter stations usually operate with high transmitter power. The scatter angle influences the achievable bandwidth of the tropo link. (Ref. A.5-3)

Troposcatter links operate with an availability exceeding 99.9 percent. This requires very high gain antennas (large diameters) as well as use of frequency and space diversity. However, increasing antenna size beyond a certain limit has been found to limit antenna gain, whose theoretical increase is diminished by a factor related to the ratio of the scatter angle to the antenna beamwidth called "aperture-to-medium coupling loss" (Ref. A.5-4). Significant quantitative data on various parameters of tropospheric-scatter communications are presented in Figures A.5-2 through A.5-10.

The long-term median (50-percent value) calculated propagation loss for tropospheric modes over a smooth spherical earth is compared to corresponding ground propagation loss in Figure A.5-2, wherein it is apparent that the propagation loss is at a minimum around 100 MHz and falls off sharply above 10 GHz (Ref. A.5-5).

Figure A.5-3 indicates transmitter power requirements vs. carrier frequency for 24 voice channels with respect to parameters of path distance and antenna diameter, transmitter power generally increasing above and below an optimum frequency almost independent of antenna diameter or path distance. Expected maximum ranges vs. frequency for various types of service and different antenna diameters are shown in Figure A.5-4, using 10-kw transmitters and quadruple diversity. Link availability is 99 percent of the hour (Ref. A.5-5).

OVER LAND $\sigma = 0.005$ mhos/meter $\epsilon = 15$
 POLARIZATION: HORIZONTAL
 TRANSMITTING AND RECEIVING ANTENNAS BOTH
 30 FEET ABOVE THE SURFACE

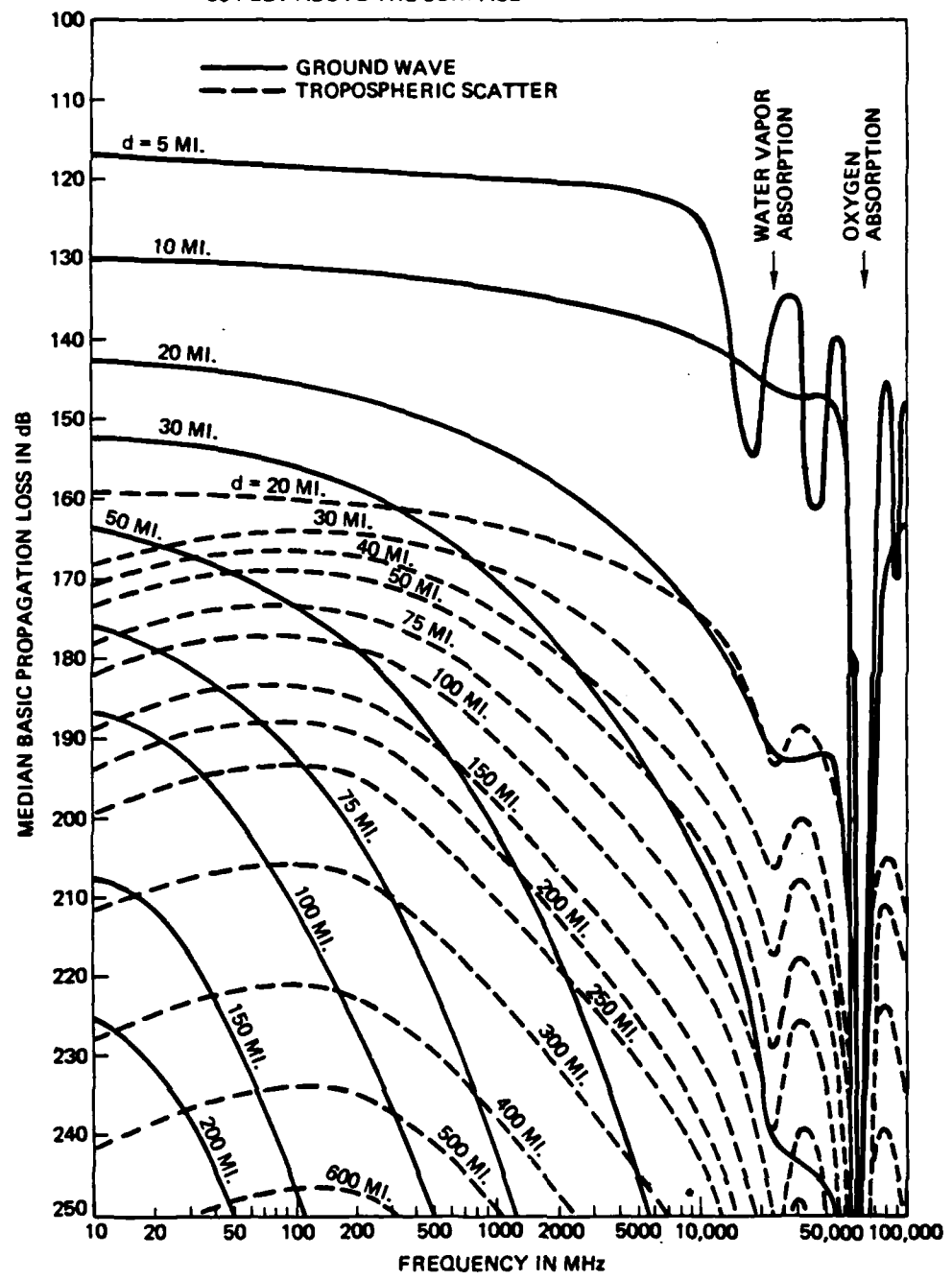


Figure A.5-2. Median Basic Propagation Loss for Groundwave Tropospheric-Scatter Mode of Propagation Over a Smooth Spheric Earth

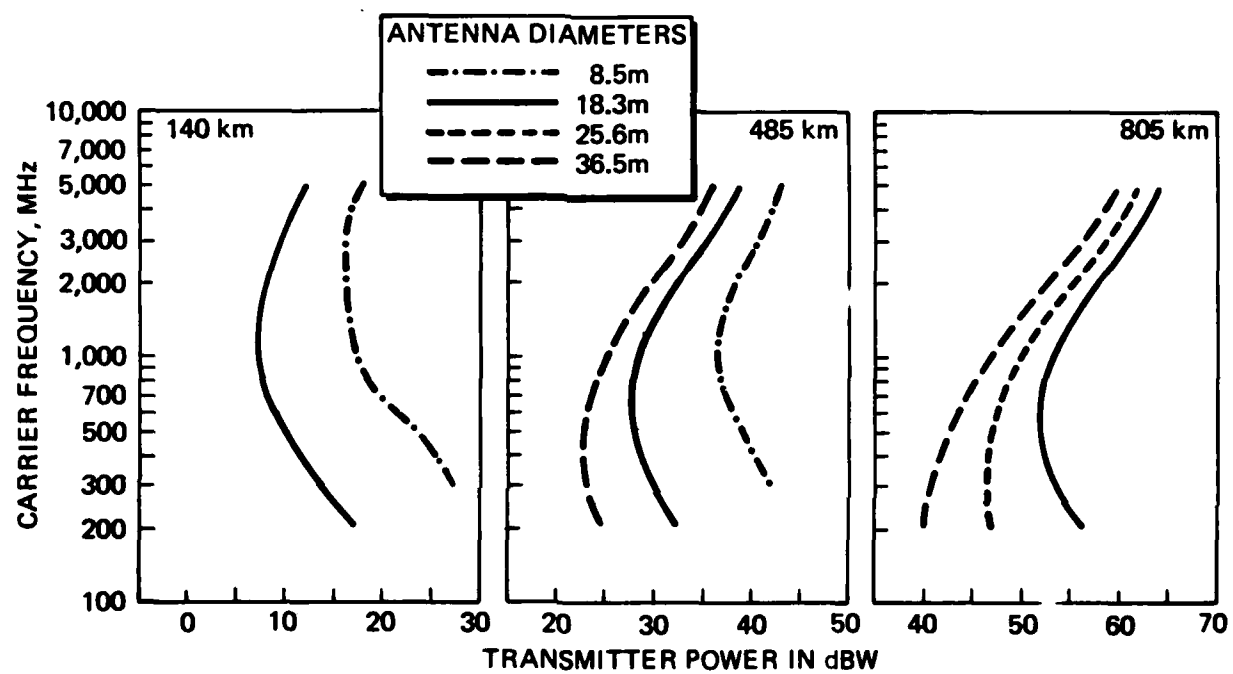
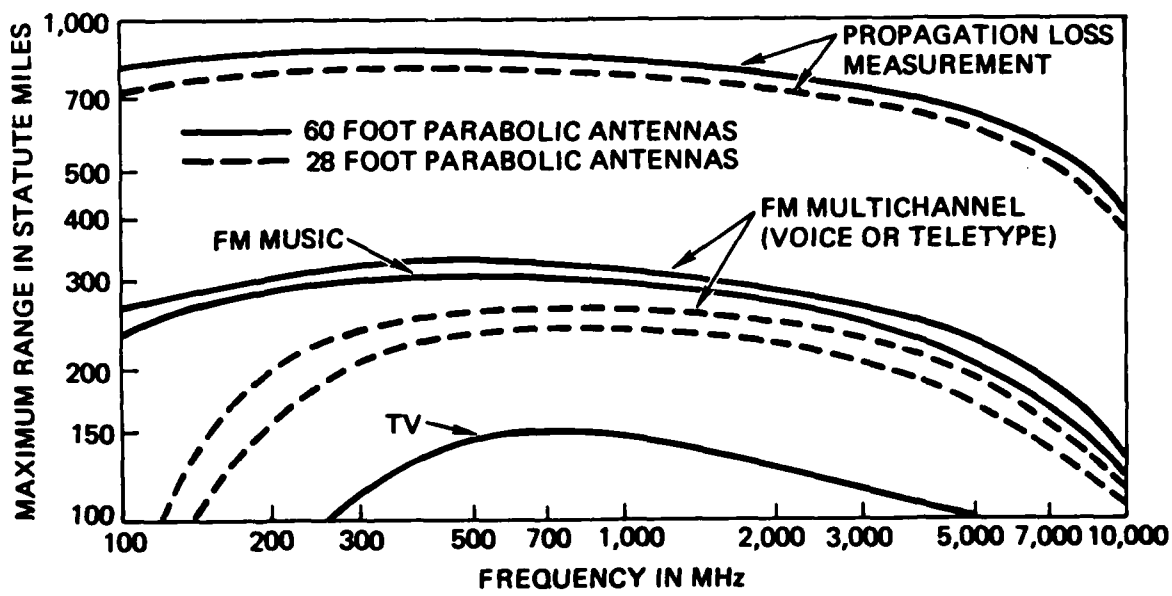


Figure A.5-3. Transmitter Power Requirement for 24-Voice-Channel Tropospheric Scatter Circuit over Smooth Earth



Note: 10 kW transmitter, quadruple diversity, 30 ft antenna Height, atmospheric absorption and rain attenuation type of Washington D.C. area, 99 percent availability.

Figure A.5-4. Expected Maximum Ranges vs Frequency for Various Types of Service and Antenna Diameters

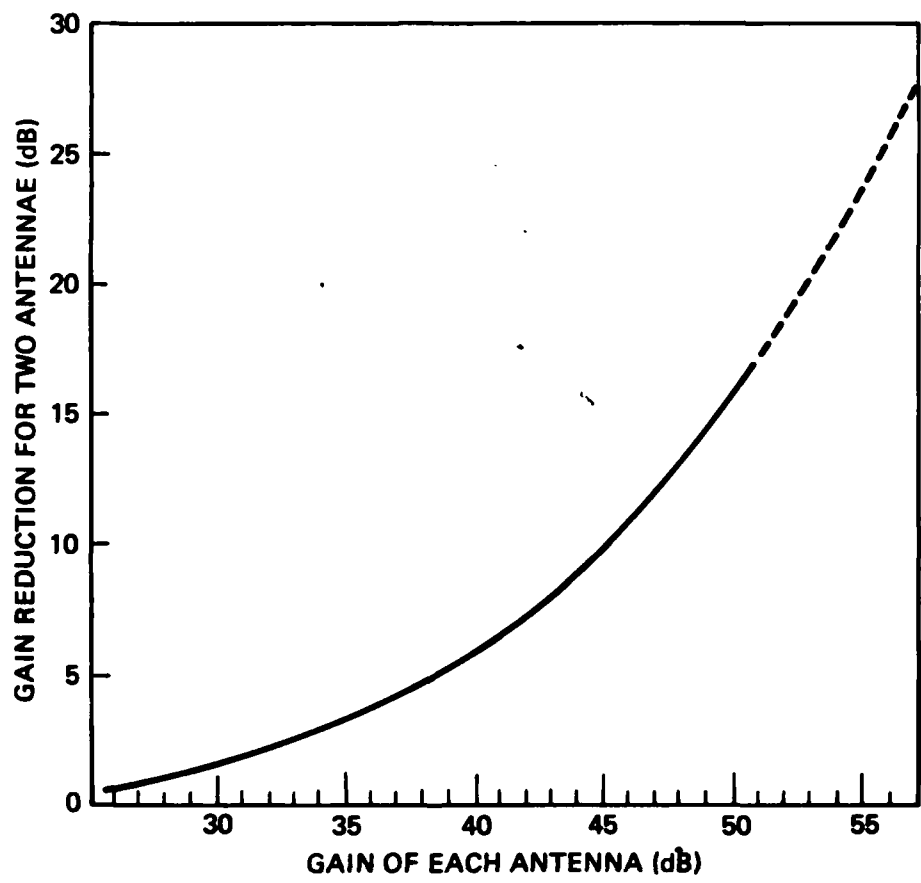


Figure A.5-5. Aperture-to-Medium Coupling Loss

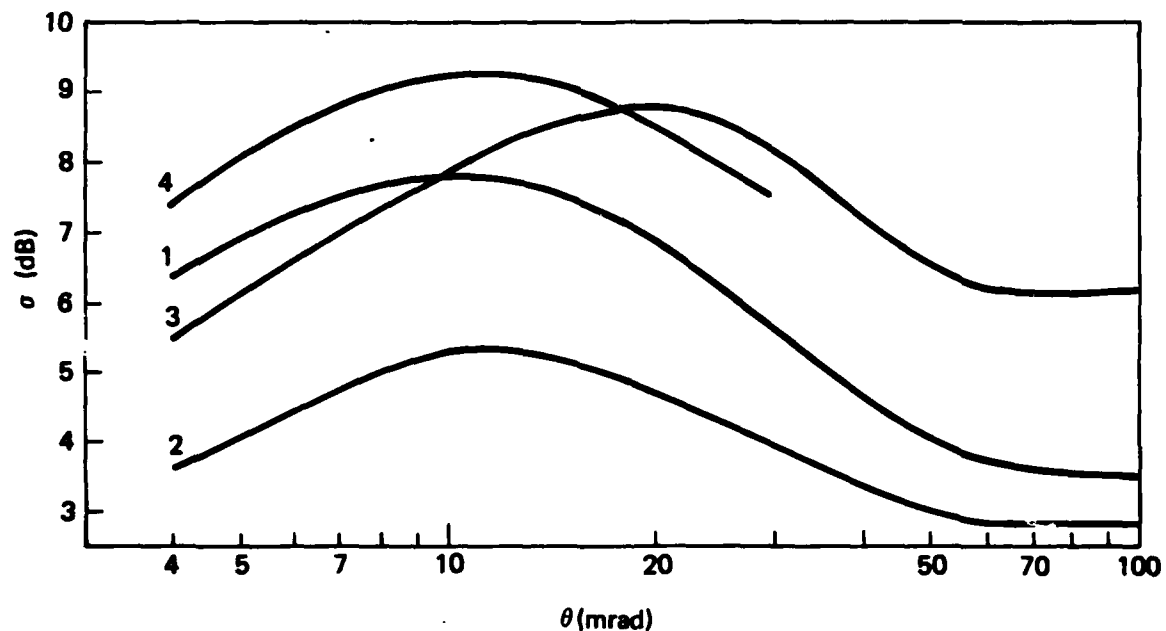


Figure A.5-6. Standard Deviation of Scattered Field for Various Climates

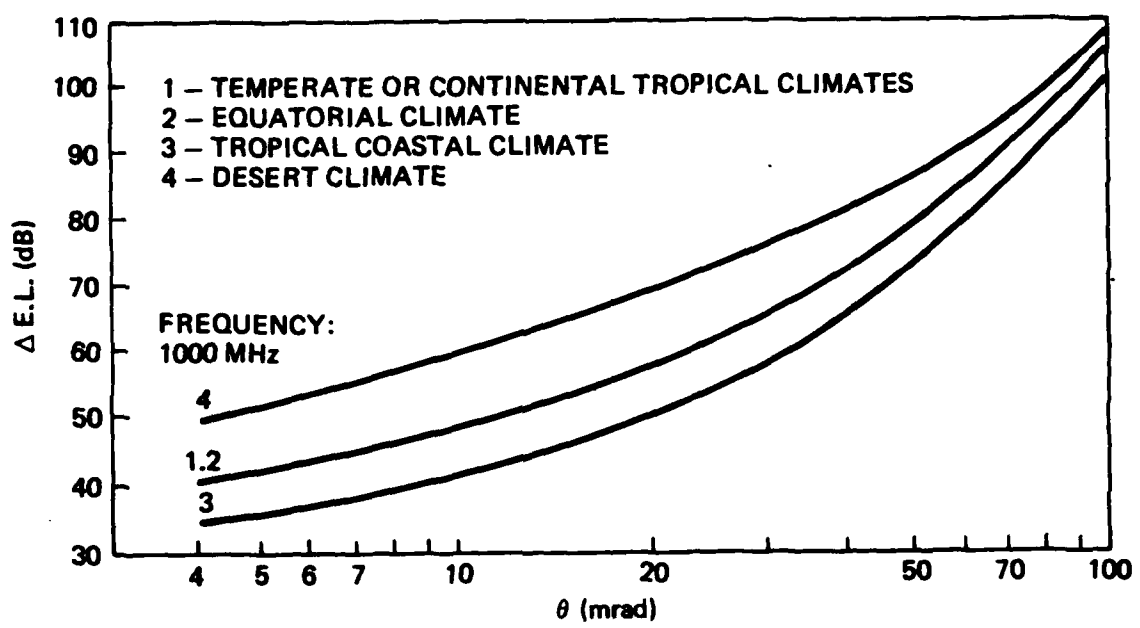


Figure A.5-7. Median Attenuation by Scattering

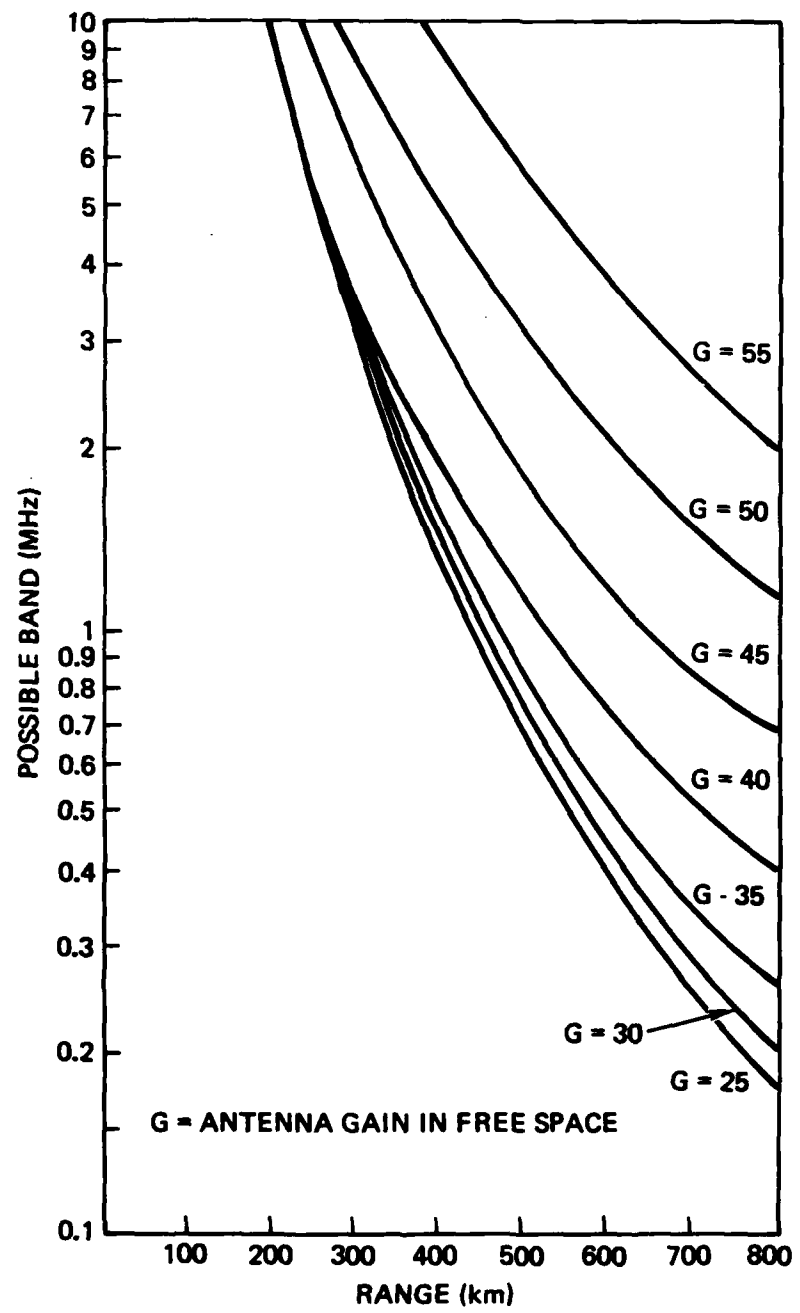


Figure A.5-8. Plots of Bandwidth versus Range with Antenna Gain as Parameters

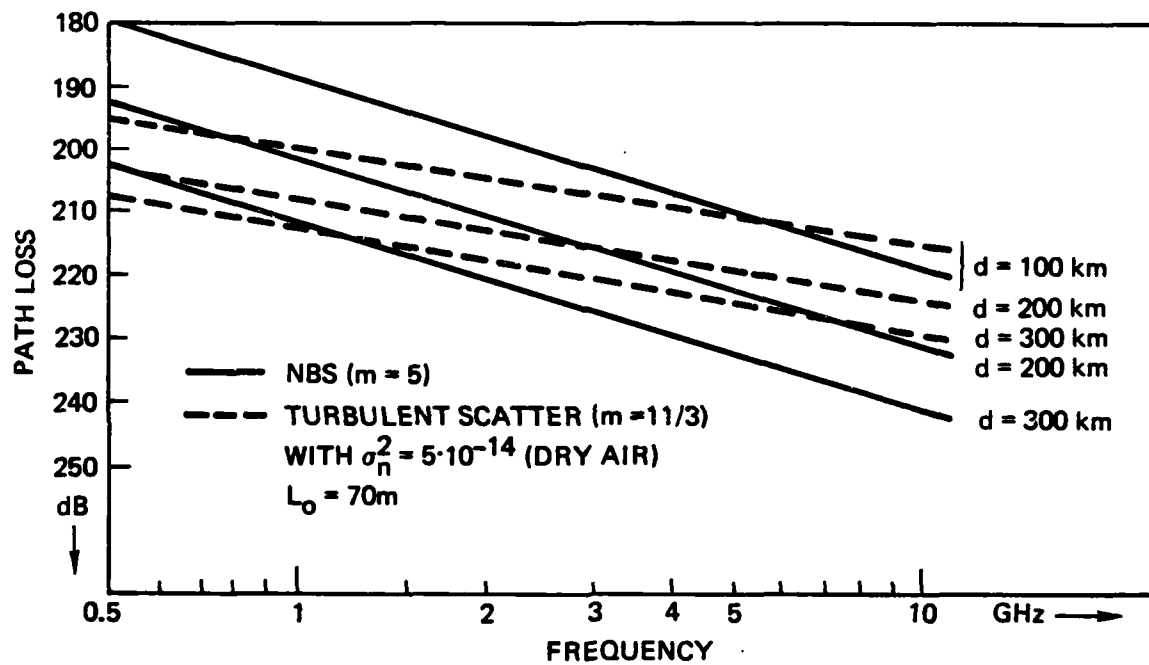


Figure A.5-9. Path Loss vs Frequency from the NMS Model and from the Turbulent Scatter Theory with Type Parameter

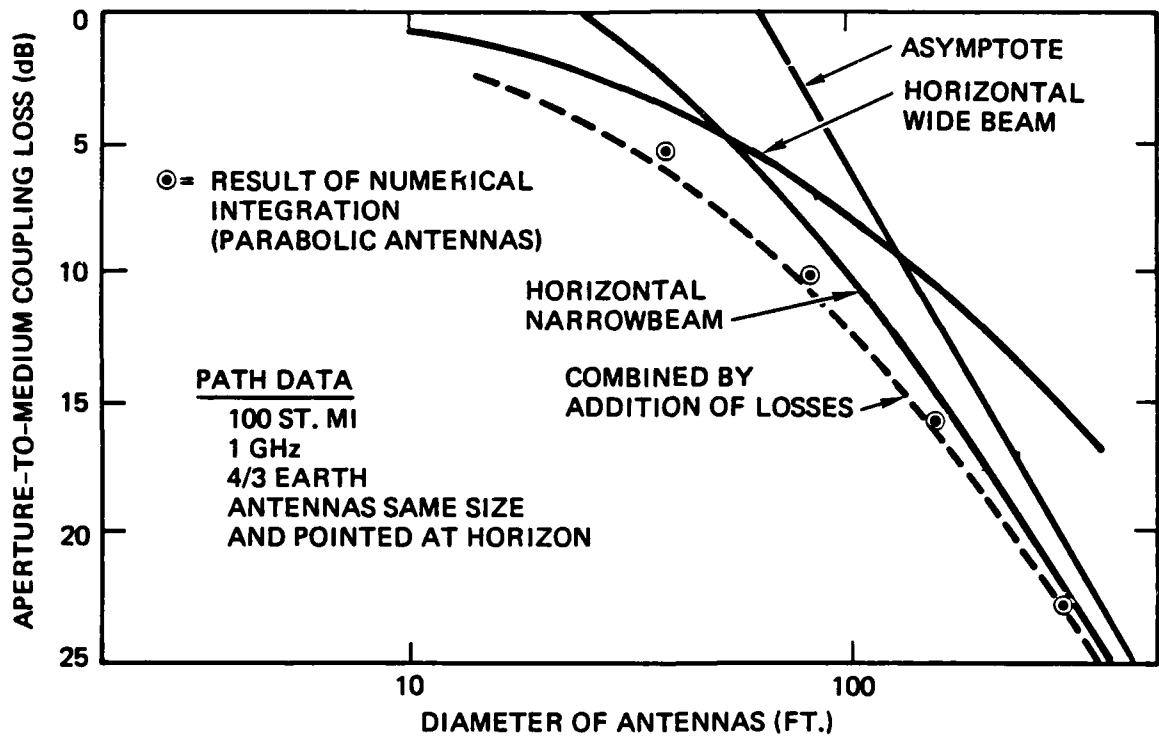


Figure A.5-10. Aperture-to-Medium Coupling Loss vs Antenna Diameter

Aperture-to-medium coupling loss (Ref. A.5-4) with respect to antenna gain is shown in Figure A.5-5, and the standard deviation of the scattered field vs. the scatter angle, θ , in mrad is shown in Figure A.5-6 for various climates (i.e., (1) temperature, (2) equatorial, (3) tropical, and (4) desert) (Ref. A.5-5). Figure A.5-7 indicates median attenuation by scattering (attenuation vs. scatter angle) for 1 GHz and also for the above-noted climates (Ref. A.5-5), and Figure A.5-8 for various antenna gains (Ref. A.5-5). Figure A.5-9 shows path loss vs. frequency for different path lengths as based on the National Bureau of Standards (NBS) model (Ref. A.5-6) and on a newly derived Turbulent-Scatter model (Ref. A.5-7), which are characterized by a parameter m called the spectrum slope. In the NBS model $m = 5$ and in the Turbulent-Scatter model $m = 11/3$. Most tropospheric scatter models use the (short distance) NBS formula. The Turbulent Scatter model provides the dominant transmission at higher frequencies (Ref. A.5-7).

If the antenna beam is narrow, then the path loss calculated from the NBS or the Turbulent-Scatter model is no longer valid because not all potential scatterers are illuminated by the beam. It is customary to account for this by introducing the aperture-to-medium coupling loss, which is defined by the relation, Aperture-to-Medium Coupling Loss (dB) = Total Path Loss (dB) + Antenna Gains (dB) - Basic Path Loss (dB), with use of omnidirectional antennas. The coupling loss and the basic path loss are complimentary and must relate to the total path loss for one specific model. The aperture-to-medium coupling loss vs. antenna diameter for 1 GHz and 100 statute miles is shown in Figure A.5-10 for a symmetric path (Ref. A.5-7).

A.5.2 Fading and Diversity Reception

Variations in the received signal are comprised of the two major components of long-term changes and of short-term (within-the-minute) fading caused by movement of individual scatterers. The former obeys a log-normal distribution with a standard deviation varying between 6 and 20 dB depending upon climate and range, and the latter follows Rayleigh distribution.

Long-term fading depends on frequency range, climatic conditions, and characteristic scatter distance. To overcome long-term variations, for which the path loss may approach 120 dB between 0.020- and 99.98-percent levels, high-power amplifiers and large antennas are employed together with low-noise receivers (Ref. A.5-8).

The median of the path short-term loss depends on frequency range, climatic conditions, actual path length, obstructions as expressed by the scatter angle, θ , and antenna gains reflecting consideration of gain degradation encountered in forward-scatter propagation. Short-term Rayleigh fading, which can be considerably reduced by diversity reception, customarily is considered separately, with the 1-hour medians (50-percent values) of the path loss examined first. Because dependence of the 1-hour medians of the path loss varies with respect to weather, time of day, and season, the slow fading thus induced is usually stated in terms of Gaussian distribution of the 1-hour medians, whereas values attained by long-term fading depend upon the "effective distances" defined by NBS data (Ref. A.5-6).

Diversity circuits are needed to reduce or eliminate the strong noise peaks produced by fast interference fading. Disregarding usage of diversity, the amplitude of residual noise peaks present during small percentages of time depends on such factors as the extent to which diversity circuits are employed, the way in which diversity reception signals are combined, and also on the statistical distribution of slow fading (Ref. A.5-9).

Fast Rayleigh fading is controlled by use of uncorrelated diversity channels and combining techniques. Considerable improvements can be obtained by diversity reception (i.e., either by selecting the strongest available signal (switching diversity) or, better, by combining received signals in such a manner that the strongest signal received determines the signal-to-noise ratio (combination diversity).

Average improvements of the signal-to-noise ratio that are attainable by use of diversity are identified in Table A.5-1 (Ref. A.5-9).

Table A.5-1. S/N-Ratio Improvement Using Diversity

Number of Diversity Paths	Switching Diversity (dB)	Diversity Combination (dB)
2	1.76	2.52
3	2.63	4.10
4	3.19	5.26

It should be noted that during an hour of constant long-term fading the S/N ratios on the average are higher by the amounts indicated in Table A.5-1 than the S/N ratios calculated from the one-hour median-path loss. It also is important to realize that the values given in Table A.5-2 apply only to fast noise fluctuations occurring during a typical hour (Ref. A.5-9) and reflect assumption that constant slow fading continues during that hour.

Table A.5-2. S/N-Ratio Improvement Induced by Diversity System

Number of Combination-Diversity Paths	S/N-Ratio Values for Various Percentages of 1-Hour Fading Period (dB)			
	80%	95%	99%	99.9%
2	<0		<7.4	<12.9
3		<0	<2.4	<6.9
4			<0	<3.4

AD-A101 360

TRW DEFENSE AND SPACE SYSTEMS GROUP REDONDO BEACH CA
EVALUATION OF DCS III TRANSMISSION ALTERNATIVES, PHASE 1A REPORT-ETC(U)
MAY 80 T M CHU
TRW-35142-APP-A

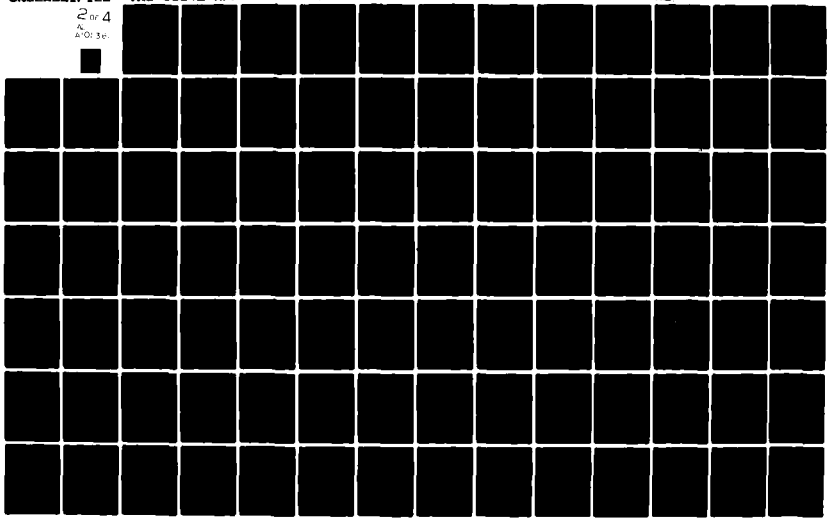
F/0 17-2.1

DCA100-79-C-0064

NL

UNCLASSIFIED

2 of 4
A
AD-101 360



Although space and frequency diversity may be utilized independently (dual diversity), both may also be used simultaneously to afford quadruple diversity. For high-reliability-circuit requirements and in applications where the span length otherwise might produce a marginal circuit, quadruple diversity is the preferred solution despite the additional equipment that is necessary. It therefore is used in the vast majority of fixed-station systems installed to the present time. Other types of diversity in use include polarization diversity and angle diversity (vertically- and horizontally-offset antenna beams).

Earlier links usually employed space/frequency diversity because such a system with two antennas at each terminal then represented the best compromise between cost of antennas and equipment complexity. More recently quadruple space diversity has been implemented by polarization separation of paths, which usually, but not quite accurately, is termed space polarization diversity (Ref. A.5-10). On the other hand, time diversity has never gained favor largely due to the long (approximately 1 sec) time delays involved in transmission. However, more recently, as pressure on the radio spectrum has increased, alternative configurations including angle diversity have been explored.

Under certain conditions angle diversity offers the considerable attraction of requiring only one antenna at each terminal of a long-haul link, for which usage antennas are very costly. However, with angle diversity it also is inherently impossible for all of a group of diversity beams to have optimum signal alignment. Because equipment and cost advantages of angle diversity therefore must be paid for in terms of a small system loss in dB it is of prime importance to ensure the best tradeoff for each particular link in order to minimize such loss.

A typical test configuration for a troposcatter path using dual angle diversity is shown in Figure A.5-11. The purpose of this test was to compare behavior of two optimized dual angle diversity systems against a reference dual diversity system of known performance. The link involved a conventional FM/FDM multi-channel telephone system. Relevant topographical and equipment parameters characterizing this adaptation of an existing troposcatter terminal linking the U.K. with the German Federal Republic are as follows (Ref. A.5-10):

- Path Length - 352 km
- Scatter Angle - 1.41° - 24.5 mrad
- Operating Frequencies - 2 GHz band
- Frequency Diversity Separation - 42 MHz
- Diversity System before Modification - Quadruple space/frequency
- Diversity Systems after Modification - Dual space/frequency and dual angle
- Diameter of Billboard Antennas - 18.3 m
- Antenna Spacing between Centers - 21.3 m.
- Antenna Plane-Wave Beamwidth at Half-Power Points - Approximately 0.5° (Applicable to splayed angle diversity beams as well as to unmodified antenna beams)

Conventional troposcatter systems use two antennas per terminal and two bandwidth allocations per direction to achieve dual space/dual frequency (2S/2F) diversity. Angle diversity provides redundant paths by collecting different angle-of-arrival signals at the receiver. For example, a dual angle diversity system would employ a 2-horn primary feed at the parabolic reflector focus instead of the conventional 1-horn primary feed. In the frequency diversity system, a power amplifier is required at each of the two RF carriers. To convert from dual frequency to dual angle, the second power amplifier is tuned to the same frequency as the first and a new feed structure is provided. The resulting dual space/dual angle (2S/2A) system then requires only one bandwidth allocation in both directions, thereby halving the frequency requirements of present 2S/2F quadruple diversity systems.

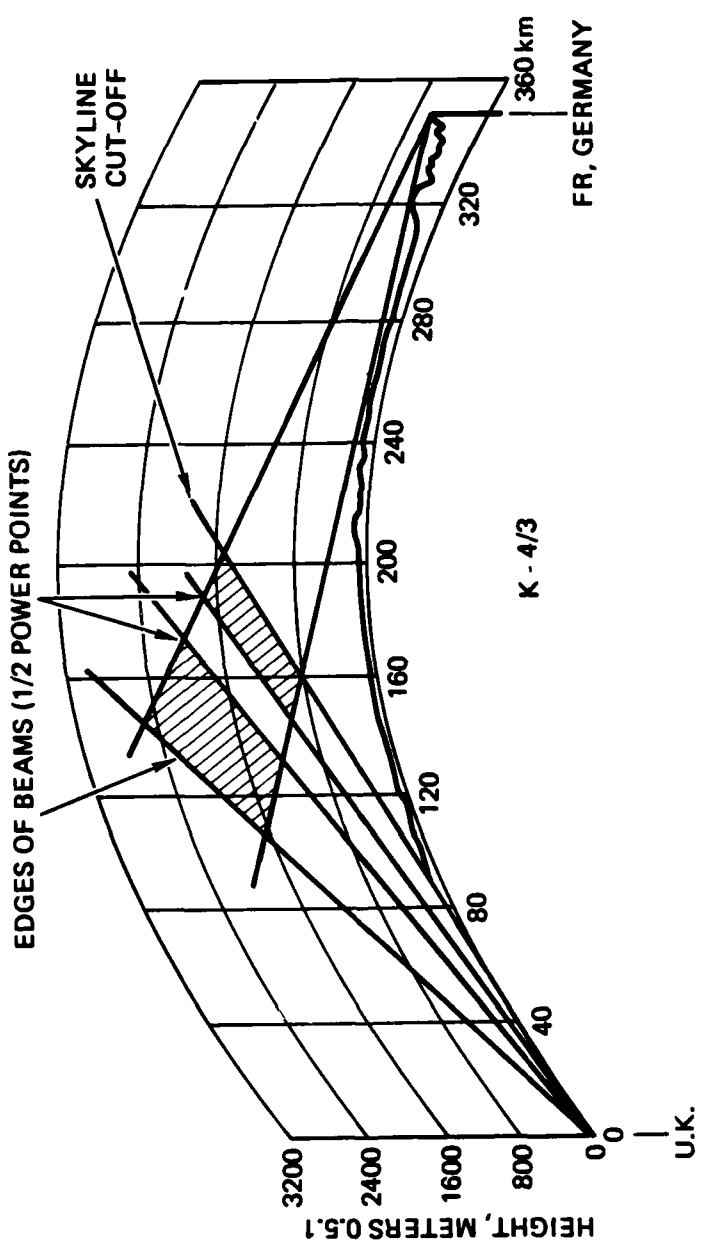


Figure A.5-11. Path Profile with Optimized Vertically Offset Beams

A.5.3 Digital Troposcatter

Although most existing troposcatter links employ FDM/FM modulation, development of high-speed digital transmission techniques for LOS and satellite communications has recently led to interest in considering similar techniques for troposcatter channels. This interest is heightened by need for encryption as well as by desire to integrate troposcatter systems into larger digital nets. However, due to fading and the dispersive nature of the troposcatter channel, high-speed digital transmission over such channels is more difficult than for LOS or satellite and generally requires use of adaptive receiver techniques.

The conversion of existing troposcatter systems from analog FDM/FM to digital TDM/PSK will provide improved network communications quality along with link encryption capability. However, 64-kbps pulse-code modulation digitalization of voice signals expands bandwidth requirements at the voice-channel transmission level. Because FM also expands the baseband multiplex signal relative to PSK modulation, the net increase in RF bandwidth requirement for a digitally-converted system is significantly less than the voice-channel expansion factor but is still greater than unity. This requirement for additional bandwidth and/or frequencies in digital systems can be eliminated with use of (1) spectrally efficient modulation techniques of better than 1-bps/Hz and (2) angle diversity (Ref. A.5-11). Spectrally efficient modulation techniques can be achieved in troposcatter applications through use of adaptive equalizers which compensate for both the troposcatter medium effects and the required transmitter filtering.

Angle diversity in most applications can be used to save a transmission frequency in both directions. Most strategic troposcatter systems currently using frequency diversity can be converted to angle diversity with approximately the same system margin but with half the bandwidth requirement. Angle diversity also provides a means of realizing additional bandwidth for coding applications to improve system margin (Ref. A.5-11). Present strategic troposcatter systems also use a frequency-

division multiplex (FDM) of 4-kHz voice channels as the baseband input to a frequency modulator (FM). However, this FDM/FM system approach has the following serious limitations:

- Encryption of the entire baseband signal is not easily accomplished
- Channel noise accumulates on a link-by-link basis
- Channel multipath causes intermodulation noise and limits channel capacity.

Digital systems which employ a time-division multiplex (TDM) of digitized voice signals as the baseband input to a digital data modulator are planned to replace the FDM/FM systems in order to overcome these limitations. The TDM signal is a serial stream of binary digits which can be conveniently encrypted. The detection process at the digital data demodulator regenerates the transmitted binary digits with some probability of error in transmission on a link-by-link basis is much less serious than the accumulation of noise in the FDM/FM network. This result is due to the fact that short-term signal-quality measures such a bit error rate improve exponentially with signal-to-noise ratio. On the other hand, noise-power addition in analog systems leads to an exponential increase in signal quality degradation. Finally, the channel multipath which degrades FDM/FM systems can be used in digital data systems with adaptive processor structures as a form of path diversity to improve performance because the TDM systems are not limited in capacity by channel multipath but by channel noise. Larger traffic capacities therefore are achievable in digital systems, with additional gains realizable through coding in TDM digital systems (Ref. A.5-11).

A disadvantage of the TDM system that arose in the past resulted from need to use a large number of bits to achieve good quality digitalization of the voice signal. However, a number of narrowband voice digitizers that subsequently have become available and that are especially suitable for military applications provide good voice quality at a 2400-bps data rate.

A 96-channel digital troposcatter system consists of four 24-channel TI systems with a data rate of approximately 6.3 Mbps. Conventional Quadrature Phase-Shift-Keyed (QPSK) systems realize about 1-bps/Hz bit-packing density in the RF channel. Thus, in this example a 7-MHz allocation would be required to accommodate the 96-channel system with conventional QPSK, and to reduce spectrum requirements to 3.5 MHz the digital modem would need to achieve a bit-packing capability of 1.3 bps/Hz. Alternatively, although the frequency diversity used in the conventional dual-space/dual-frequency configuration could be replaced by either angle or space polarization, and in the FM system with 3.5-MHz allocations, a 7-MHz total bandwidth in each direction would be required. Thus, in the digital system with either a dual-space/dual-angle (2S/2A) configuration or a quadruple-space (4S) configuration with polarization marking, a 7-MHz allocation leads to a 7-MHz total bandwidth in each direction (Ref. A.5-11).

A typical dual-space/dual-angle (2S/2A) quadruple diversity troposcatter terminal is shown in Figure A.5-12.

A.5.4 Summary

Troposcatter communications have been developed into a highly successful method of radio communication which provides the following advantages not offered by other modes:

- High-grade multichannel service over 50- to 600-mile distances in a single span
- High propagational reliability on a year-round basis with a properly designed system
- Capability for use in rugged or otherwise inhospitable terrain where other means of communication are impractical or impossible
- Relatively high degree of security compared with other communication methods

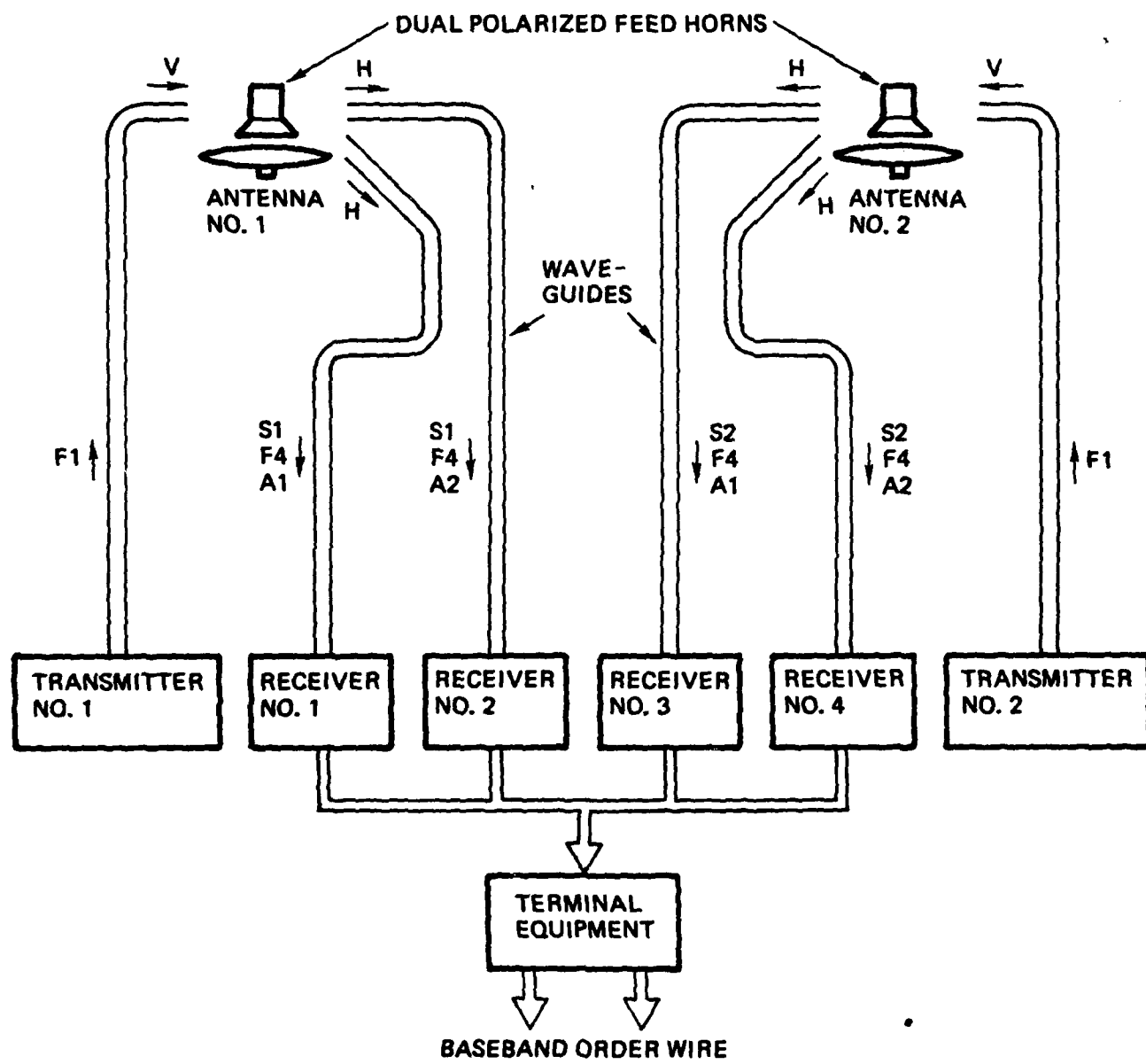


Figure A.5-12. 2S/2A Configurations

- Minimal deliberate or unintentional radio interference unless interfering transmission is within beam and range of any one troposystem station.

Present FDM/FM analog troposcatter links in strategic networks can be converted to time-division multiplexed (TDM) digital systems with only modest increase in total required bandwidth through use of spectrally efficient modem techniques. Angle diversity as a replacement for frequency diversity results in reduction in bandwidth requirements by one-half with approximately the same performance. Analog-to-digital conversion with angle diversity produces a net decrease in occupied bandwidth for a fixed performance. Coding concepts once believed to be impractical on fading troposcatter circuits exploit the extra bandwidth provided by angle diversity, thus realizing significant improvement in link outage availability.

The two most stringent limitations encountered in troposcatter transmission are large path attenuation and bandwidth of the medium. Bandwidth restrictions observed over troposcatter paths are considered to be the result of frequency-selective fading caused by multipath propagation of the signal, and it also has been noted that multipath effects increase with increasing path length and that they are inversely proportional to the RF carrier.

Factors that limit troposcatter-system performance thus may be summarized as path attenuation, bandwidth, frequency allocation, number of tandem links, physical size, weight, and cost.

Undeniably, and under certain conditions, tropo offers certain overriding advantages. When the cost of a tropo system is considered, these advantages must be weighed against the cost of other systems that may lack the advantages peculiar to tropo.

A.6 MM-WAVE TECHNOLOGY

The considerable attention that has been given to the millimeter (mm) waveband between 30 GHz and 300 GHz (and above) in the last few years has produced significant technology advancements. On the other hand, applications involving line-of-sight (LOS) propagation through the earth's atmosphere remain limited to relatively short distances because of well known atmospheric effects. However, despite the range of limitations imposed by weather, the ever-increasing demand for new spectral space, coupled with oncoming technology advancements promise to ultimately result in development of mm-wave LOS communications systems. Technology for deployment of high-performance LOS communication systems operating in the mm-waveband already is sufficiently developed to provide assurance that capability of available mm-wave components is well beyond present requirements and also that any deployment promises to satisfy needs well into the future.

The view that projection of actual usage will depend more on need than on feasibility is substantiated by the history of the GRC-1-173 high-performance mm-wave communication set which was developed by the Air Force in the early 1970s. The GR3-173 equipment, which was intended for operation near the 10-mm wavelength, used bi-phase modulation at data rates up to 250 Mbps and performed as expected, although it was never placed in permanent service for lack of a requirement. The set is powered by a 200-mW semiconductor, uses a 6-ft parabolic antenna, and the receiver has an 11-dB noise figure (Schottky barrier detector).

A.6.1 Transmitters

Sources of mm-wave radiation are currently available in one form or another with power capability ranging from milliwatts up to several hundred kilowatts. For present purposes availability is defined as reflecting repeated laboratory demonstration but not necessarily penetration of the commercial market. This criterion is used to project options available in the 1990 time period.

A.6.1.1 MM Traveling Wave Tubes. Alternative mm-wave sources that currently are available include traveling wave tubes (TWTs) and various other solid-state devices described subsequently. The wide bandwidth commonly identified with TWTs is available at mm wavelengths. The typical sample of TWTs as listed by Hughes Electron Dynamics Division is given in Table A.6-1. All but the first TWT cited are still under development.

Table A.6-1. Current Developmental TWTs

Frequency (GHz)	Minimum Power Output (W)	Gain (dB)	Efficiency (%)	Length (in)
29-31	2	42	5.25	10
49.5-58	150	12	6.25	15
54.5-55.5	1000	25	10.0	18
54.5-55.5	5000	20	37.0	25
54.5-55.5	100	25	3.9	18
91.0-96.0				

A.6.1.2 Gyrotrons. Several hundred kilowatts at mm wavelengths have been obtained from the gyrotron, which perhaps is the most outstanding new development and uses a magnetic field to constrain the electrons to follow helical paths as shown in Figure A.6-1. Relativistic monoenergetic electrons are caused to interact with a traveling wave in a manner analogous to that of a traveling wave tube. Because of the relativistic mass change with small random velocity differences, phase bunching of electrons occurs. Those electrons that lose energy to the surrounding wave become lighter and accumulate phase lead, whereas those that gain energy become heavier and accumulate phase lag relative to the traveling field. This results in bunching, which causes the electrons to radiate coherently.

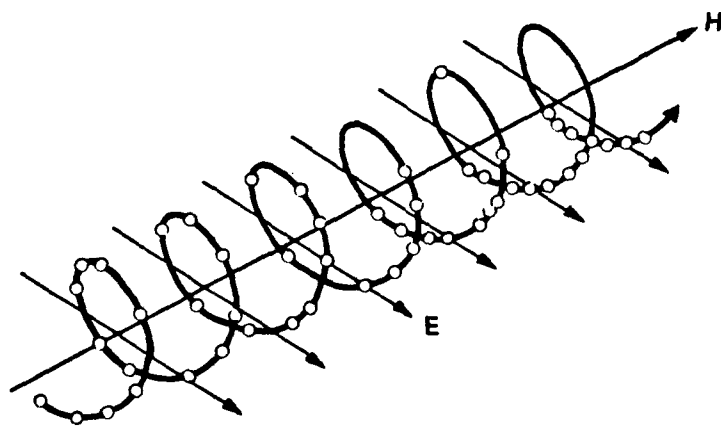
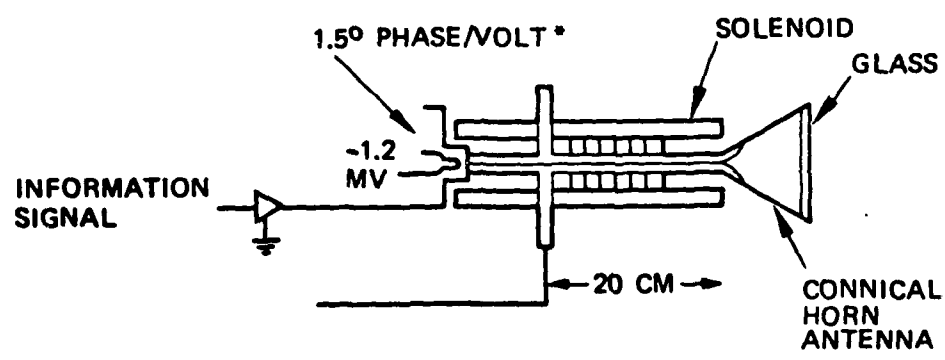


Figure A.6-1. Distributed Interaction Gyrotron

Energy transfer from electrons to the wave is optimized when the operating frequency is slightly higher than the cyclotron frequency of the electrons as determined by the axial magnetic field. The first experimental units exhibited a bandwidth of much less than 1 percent. However, combination of TWT structure with the gyrotron provides an instantaneous bandwidth of 5 to 10 percent. A 40 percent bandwidth is projected as possible based on a theoretical study by the Jacor Company under Naval Research Laboratory (NRL) sponsorship (Ref. A.6-1). This concept uses dielectric loading over an interaction part of the TWT portion of the gyrotron/TWT amplifier to achieve theoretical projection of a 40-percent instantaneous bandwidth. The state-of-the-art and the projected capabilities of gyrotron-type devices for mm-wave generation are summarized in Figure A.6-2. First experimental results are given in Table A.6-2.

Table A.6-2 Reported Gyrotron CW Results

Parameter	Experimental Results			
Wavelength (mm)	2.8	1.9	2.0	0.9
Harmonic Number	1.0	2.0	2.0	2.0
B-Field (T)	4.0	2.9	2.9	6.1
Voltage (kV)	27.0	18.0	16.0	27.0
Output (kW)	12.0	2.4	7.8*	1.5
Experimental Efficiency (%)	31.0	10.0	15.0	6.0
Theoretical Efficiency (%)	36.0	15.0	20.0	5.0

*Pulsed

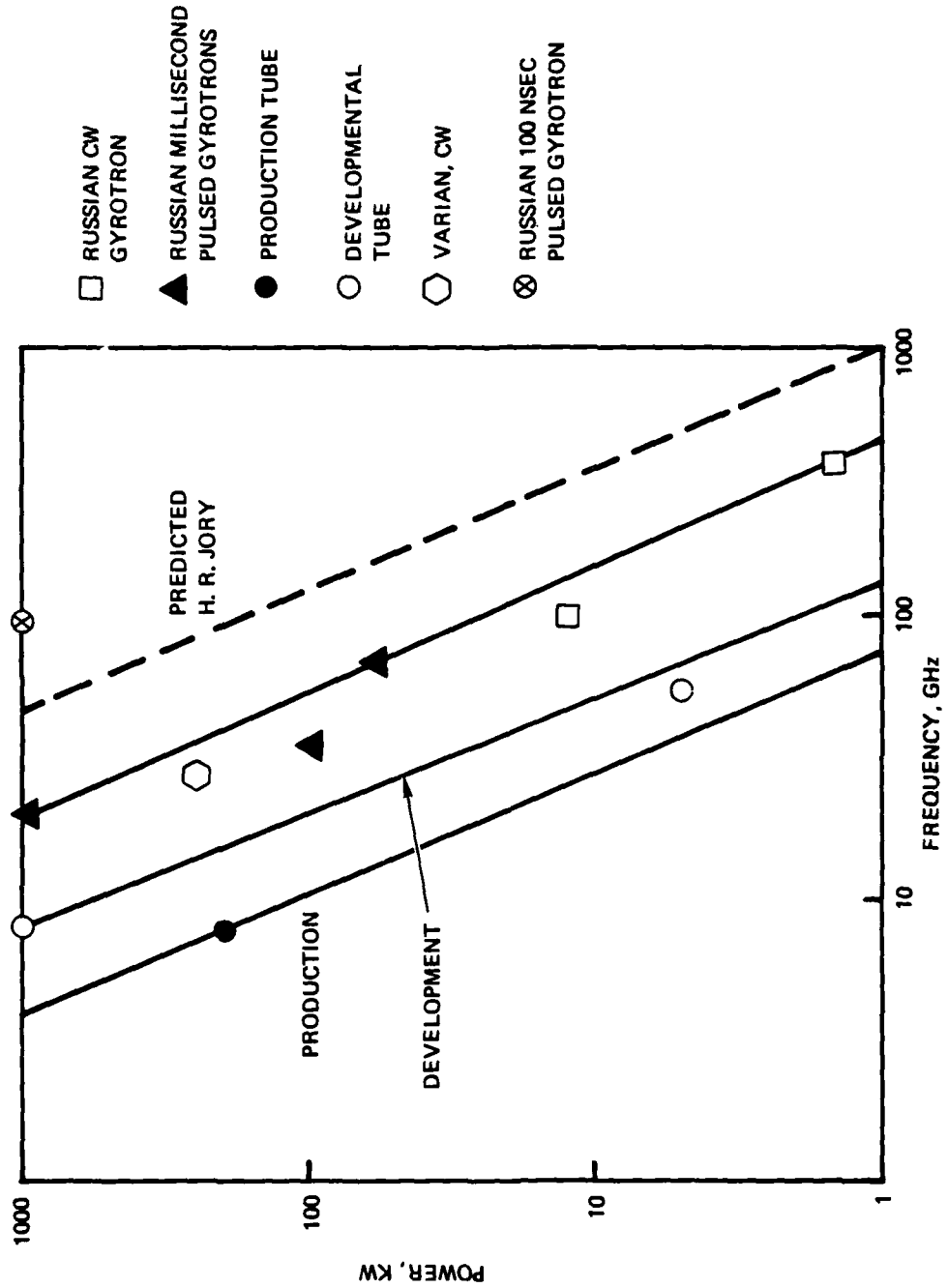


Figure A.6-2. Gyrotron Power Tube State-of-the-Art

Gyrotron development is primarily funded by the U.S. Department of Energy for the plasma heating required in certain fusion systems, but little attention has been given to techniques for impressing modulation on the gyrotron output. Also, no program has been identified which includes development of efficient techniques for modulating the mm-wave output from a gyrotron-type tube. However, modulation could be impressed on the RF drive for the amplifier forms of the gyrotron.

One suggested approach for direct modulation is based on observation that the phase of the output RF varied by 1.5 electrical degrees per volt of cathode acceleration voltage in a tube that used 75,000 volts for acceleration. An amplifier form of this tube produced 35 kW at 35 GHz (Ref. A.6-2).

A schematic of one approach to impressing phase modulation on the output from a gyrotron amplifier has previously been illustrated in Figure A.6-1, wherein the information signal develops a voltage that is added to the acceleration potential shown as 1.2 megavolts. This results in a change in the time of arrival of electrons near the output, which causes the phase of the output to be modulated by a small drive voltage. A circularly-polarized resonant mode drive voltage would be used in the distributed interaction region within the tube shown in Figure A.6-1. Consequently, the axial location where the electrons give up mm-band radiation will vary with the modulation voltage in such a manner that the signal observed at a fixed distance from the output aperture will vary in phase. Because the power requirements for modulation signals are quite modest, this scheme should be directly applicable to FM and phase-modulation formats.

An alternative and also a quite standard modulation technique is to modulate the current which is admitted into the acceleration field. This latter method would be directly applicable to pulse-position and pulse-duration modulation formats.

A.6.1.3 Low-Power Sources. The best mm-wave sources for applications which require no more than a few Watts are solid-state devices. These include the field-effect transistor (FET), avalanche diodes (such as the IMPATT device), and transferred-electron devices such as the Gunn diode.

A.6.1.3.1 FETs. The state-of-the-art for GaAs FETs is summarized in Figure A.6-3 (Ref. A.6-3).

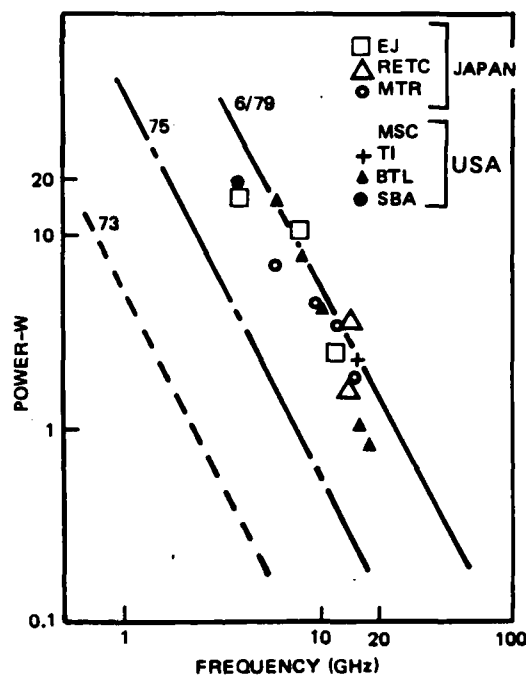


Figure A.6-3. GaAs FET State-of-the-Art

Because higher output power is anticipated each year, if the trend indicated for the 1973-1978 time period were to continue until 1990 FETs would be capable of 1-Watt output at a frequency in excess of 100 GHz.

A.6.1.3.2 IMPATT Unit. The Impact-Avalanche Transit Time (IMPATT) device (and related semiconductors) has proven to be the most efficient low-power mm-wave source that is available. This device, which is a variation on the Read diode (named after the inventor) is composed of a semiconductor with a very special doping profile that causes it to behave similarly to a negative resistance when connected to a DC voltage of 10 to 50 volts. The

active material is either silicon, GaAs, or InP. IMPATT devices designed to operate at mm wavelengths are quite small, the active semiconductor material being on the order of 1 mm in dimension.

State-of-the-art for the IMPATT diode CW oscillator is summarized in Figures A.6-4 and A.6-5, together with that for a competing device, the GUNN diode, which also is a 2-terminal semiconductor that behaves like a negative resistance. Power and efficiency for a single IMPATT device operating in the pulse mode is given in Figure A.6-6. The relative FM noise characteristics of an InP IMPATT oscillator is about one-third that for GaAs units, as shown in Figure A.6-7.

Current manufacturers of IMPATT devices operating at mm wavelengths include Hughes, Raytheon, and RCA. Typical minimum output specifications for a single device are given in Table A.6-3.

Table A.6-3. Current Power Outputs Available from Off-the-Shelf Single-Device IMPATT Source

Frequency (GHz)	Band	CW Power (mW)	Pulsed Power (W)
26.5-40	Ka	300	5
33-50	Q	200	-
40-60	U	200	-
50-75	V	200	1.0
69-90	E	100	-
75-100	W	50	3.0

The primary mechanism limiting the available power in a single device is allowable cross-sectional area, which is inversely proportional to frequency raised to some power that may lie between 1/2 and 3/4. Techniques already have been developed to obtain power by combining the outputs of many small-area elements that are capable of generating mm-waves.

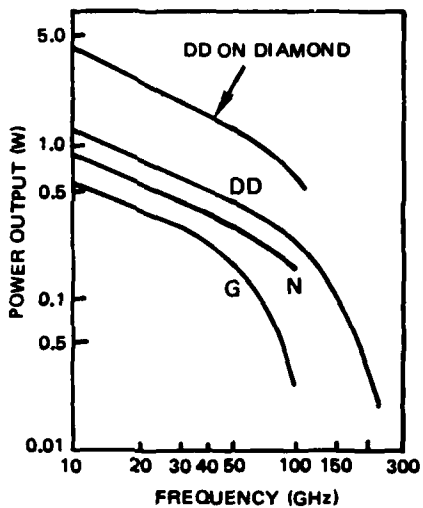


Figure A.6-4. CW Power Output of Negative Resistance Diodes:
G = GaAs Gunn, N = N-Type Silicon IMPATT,
DD = Double Drift Silicon IMPATT

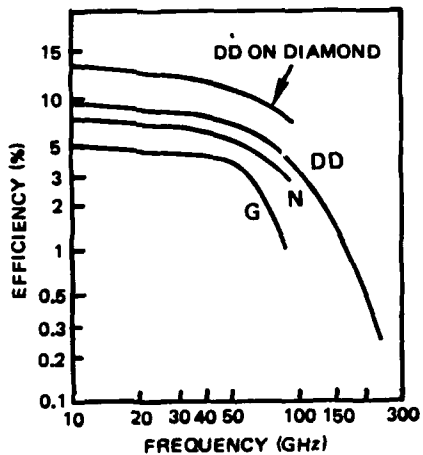


Figure A.6-5. Efficiency of CW Negative Resistance Diodes

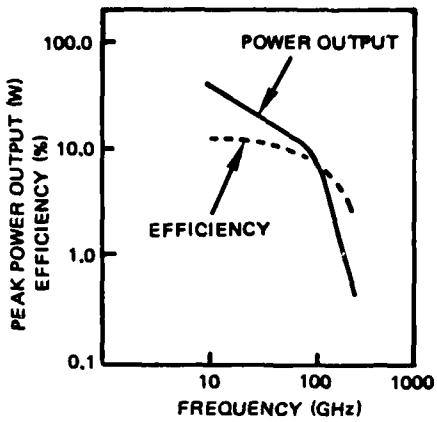


Figure A.6-6. Pulsed Power and Efficiency of Double Drift Silicon IMPATT Diodes Pulse Width = 100ns

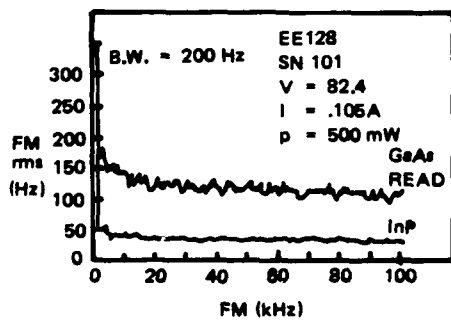


Figure A.6-7. FM Noise of CW InP IMPATT Oscillator QX 130

An example of power combination by multichips in parallel is the increase in output power noted as the number of chips are increased without decreasing efficiency (Ref. A.6-4). Power combiners with 5- to 10-percent bandwidth also have been constructed using 3-dB short-slot combiners (Ref. A.6-5), and TRW has developed a conical line combiner with similar bandwidth. Table A.6-4 summarizes this work.

Table A.6-4. TRW MM-Wave IMPATT-Circuit Developments

Frequency	Demonstrated in a Single Device	Demonstrated or Planned Using up to 12 Devices*
20 GHz	*	10 Watts
40 GHz	1.25 Watts, CW	10 Watts
60 GHz	1.0 Watt	50 Watts
94 GHz	100 mW, CW 7.12-W peak, 100 nsec 1-percent duty cycle	*

Where only 1-percent bandwidth is required, a resonant-cavity approach (Ref. A.6-6) that works well with CW diodes in an injection-locking amplifier mode can be used. It is believed that output of several hundred Watts at 94 GHz will be possible before 1985 by using combiners of several diodes.

The IMPATT diode can be used either as an amplifier or as an oscillator. Because it is a negative-resistance device, the difference between these two forms is only the magnitude of the real part of the load impedance. Injection locking could be used in a repeater configured in an IMPATT-device oscillator form due to the fact that locking causes the output RF to track the phase and frequency of the signal injected into the oscillator, resulting in a much higher effective gain than would be possible for its use as an amplifier. However, circuit failure is abrupt

when locking fails, and occurs when the injection signal falls below the required level for locking. A requirement for locking is that the input signal must be at a frequency within the bandwidth for locking (Ref. A.6-7), as given by

$$B_L = \frac{f_0}{Q_e} \sqrt{\frac{P_s}{P_o}} \quad (A.6-1)$$

where

f_0 = operating frequency

Q_e = external Q of circuit

P_o = output power of oscillator typical capability with locking as noted in Figure A.6-8.

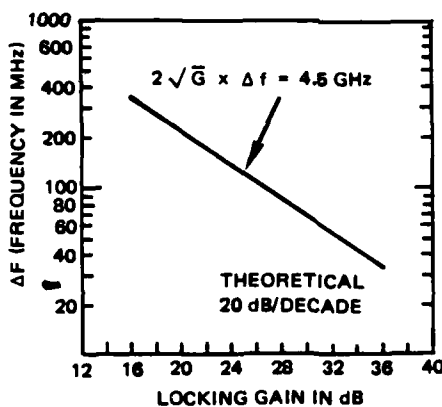


Figure A.6-8. Injection Locking Gain-Bandwidth Characteristics of a Millimeter-Wave IMPATT Oscillator

One limitation on use of the IMPATT-type device is that it has a noise temperature of at least 1000 times room temperature, which renders FM noise in a locked oscillator not negligible. Where the locking signal has negligible noise, the rms frequency fluctuation (Ref. A.6-8) is given by

$$\Delta f_{\text{rms}} = f_m \sqrt{\frac{kT_0}{P_s} M_{\text{fm}} B} \quad (\text{A.6-2})$$

where

$$T_0 = 290^{\circ}\text{K}$$

K = Boltzmann constant

M_{fm} = FM noise measure (for present IMPATT devices $M_{\text{fm}} = 1000$)

B = noise bandwidth of circuit

P_s = Locking-signal power

f_m = frequency separation from carrier

Considering the worst case with FM modulation, wherein the deviation is equal to half the width of the repeater, an angle demodulator will weight the noise power spectrum in proportion to the square of the frequency difference from band center. Accordingly, Eq. (A.6-2) shows that the injection-locked sources introduce noise that is additionally emphasized by the square of frequency (when expressed as power spectral density), which follows from the fact that the magnitude of the rms frequency fluctuation is proportional to the frequency difference from the carrier. If the carrier is at band center, noise will increase at the rate of the square of the frequency difference from band center and has the effect of quieting the spectrum near the carrier due to injection of a signal stronger than the thermal noise (of magnitude given by $kT_0 M_{\text{fm}} B$) if the oscillator is locked. In order to provide for locking over the entire channel bandwidth the locking bandwidth is set equal to the noise bandwidth. Therefore, from Eqs. (A.6-1) and (A.6-2),

where

$$BW = f_0/Q_e = \text{a lower bound on circuit bandwidth}$$

As previously noted, the FM noise measure characterizing presently available IMPATT diodes is at least 1000. Using this value, and assuming that $P_0 = 200 \text{ MW}$, $P_s = 20 \text{ MW}$, and $BW = 10^9 \text{ Hz}$, Eq. (A.6-3) then reduces to

$$\left(\frac{Z\Delta f_{\text{rms}}}{BW} \right)^2 \approx 6 \times 10^{-16} \quad (\text{A.6-4})$$

and the rms fluctuation in output frequency is about 4×10^7 smaller than the bandwidth of the external circuit. Using the rule of thumb that

$$BW = (2\beta + 1) f_m,$$

where β = modulation index and f_m = modulation frequency it follows that

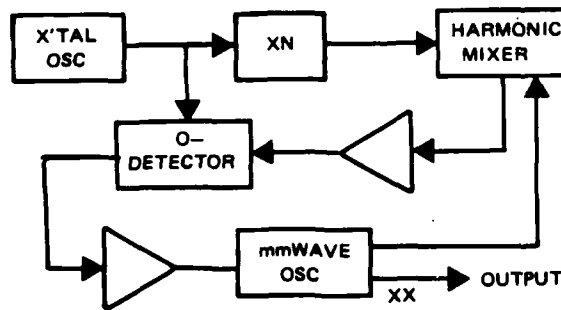
$$\frac{f_m}{\Delta f} \approx \frac{8 \times 10^7}{(2\beta + 1)}$$

A definite limit on the channel capacity that is available therefore exists because $f_m/\Delta f$ is a measure of signal-to-noise ratio at the output of a discriminator, although that limit does not appear to be very restrictive. For example, assuming a 600-voice-channel repeater is to use injection locked oscillators, $f_m/\Delta f$ must be on the order of $600 \times 3000 = 1.8 \times 10^6$ -Hz tone control, so that

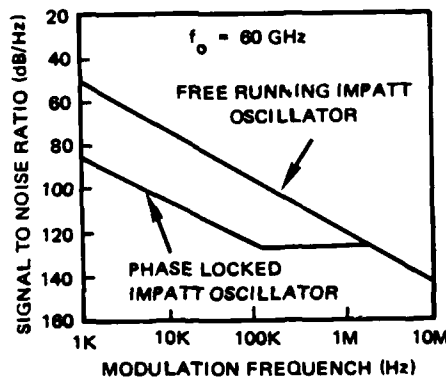
$$2\beta + 1 < \frac{8 \times 10^7}{1.8 \times 10^6} \approx 44$$

The maximum modulation index then must be less than about 22.

Because other modulation formats such as PCM are not as sensitive to FM noise, it is concluded that the IMPATT-type device in an injection-locked configuration can be used in narrow-band repeaters. The relationship between signal-to-noise ratio and modulation frequency for a typical phase-locked system is shown in Figure A.6-9.



(a) Block Diagram



(b) Spectrum

Figure A.6-9. Millimeter-Wave Phase Locking Technique

Another sometimes undesirable characteristic of IMPATT devices is that the output amplitude and frequency (when not injection-locked) varies with the bias current. Behavior of this frequency characteristic, which has been used to impress frequency modulation on device output, is shown in Figure A.6-10 for a typical 94-GHz IMPATT oscillator.

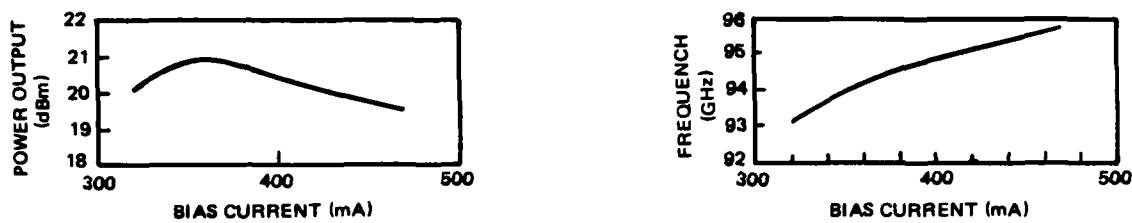


Figure A.6-10. Frequency Tuning Characteristics of an IMPATT Oscillator

When an IMPATT diode is operated in the pulse mode a transient temperature change causes the frequency to change (chirp), which in turn causes the peak power that is produced by pulse-mode operation to decrease with increasing pulse width. However, this effect can be controlled by shaping the bias-current waveform. Typical pulsed-operation capability at 94 GHz is indicated in Figure A.6-11.

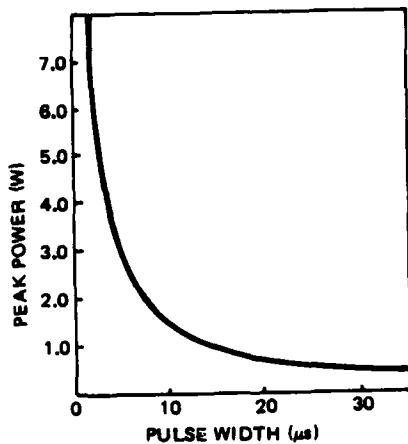


Figure A.6-11. Peak Power Capability Decreases with Increasing Pulse Width Due to Heating During the Pulse

Of several forms of IMPATT-type devices some operate on a significantly different principle, although all may be packaged to present a similar physical appearance. Most significant in this class for mm-wave use are the Tunnel-Effect Transient Time (TUNNETT) and the GUNN-effect devices. The TUNNETT uses quantum mechanical tunneling to inject the working current pulse into the device rather than the avalanching mechanism used in the IMPATT diode. The TUNNETT is a newer development with high-operating-frequency capability.

The Mixed Tunneling and Avalanche Transit Time (MITATT) unit is a similar device that uses a combination of tunneling and the avalanche effect for injection of the working pulse. It has been reported that 6-percent efficiency was obtained at 100 GHz from a quiet TUNNETT mode (Ref. A.6-9), and also that the maximum fundamental oscillation frequency of this mode is at least 1000 GHz (Ref. A.6-10). Because the TUNNETT is a new development that theoretically has been shown to be superior for higher frequencies, rapid and continuing advancements are anticipated for this device. Primary current applications to the TUNNETT and MITATT units include low-noise amplifiers comprised of an amplifying component and a parametric pump (source), local oscillators, and self-oscillating mixers.

A.6.1.3.3 TED Unit. The GUNN device (named after the inventor), also commonly called a Transferred Electron Device (TED), operates on an entirely different principle than the IMPATT-type device although these units are rather similar in external characteristics in that a low-voltage DC power source (or bias supply) is the only power input required to produce an output in the mm-wavelength band. The active part of either device in configurations capable of less than 1 Watt of output is about 1 millimeter in maximum dimension. The TED nomenclature refers to the basic operating mechanism, whereby electrons that take on the proper momentum in the conduction band of certain materials are transferred to a state in which the effective mass of an affected electron is increased and its mobility reduced, causing the TED to act like a negative resistance. This bulk process is very fast, rendering generation of mm-waves possible in a material subjected to a DC electric field. Comparative efficiencies of various IMPATT and TED devices are shown in Figures A.6-12 and A.6-13 as a function of frequency (Ref. A.6-11).

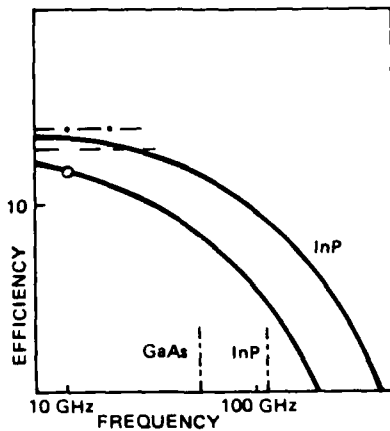


Figure A.6-12. Predicted Transferred Electron Device Efficiency Versus Frequency

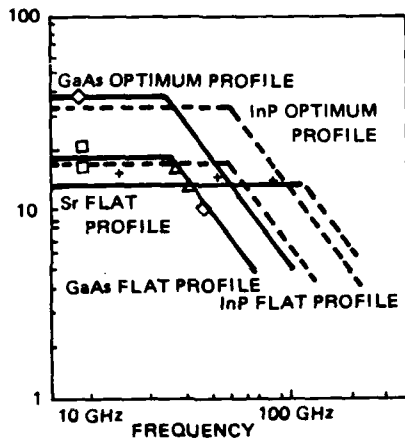


Figure A.6-13. IMPATT Device Efficiency Versus Frequency

The active materials in currently available TED units are either GaAs or InP, which also are the active materials used in IMPATT-type devices. In the TED application the performance of GaAs at 94 GHz predicts similar performance of InP at 188 GHz because the InP device can be larger with the same matching structures due to the fact that InP impedance is significantly higher than that of GaAs.

Output and gain characteristics representative of InP TED devices are shown in Figures A.6-14 and A.6-15. The gain variation with frequency shown in Figure A.6-15 is due to the circuit structure, and similar variation is expected almost universally with more rapid variation in the ripple as more stages are placed in tandem.

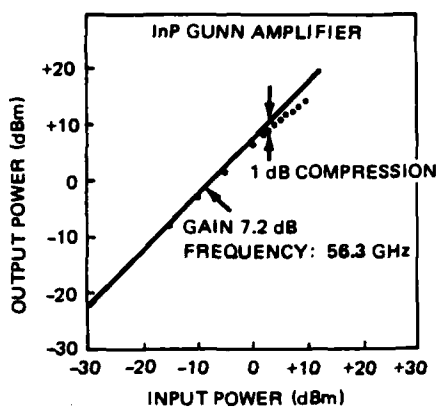


Figure A.6-14. Output Power Versus Input Power for InP Notch Device Biased for Low Noise

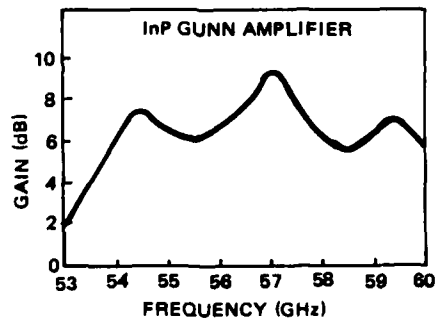


Figure A.6-15. Gain Vs Frequency for InP Notch Diode. Maximum Measured Noise Figure Across Band is 10.9 dB

A.6.2 Modulation of Semiconductor Sources

The IMPATT, FET, GUNN, and related semiconductor devices can be modulated directly by varying the supply voltage or bias. As previously noted, both amplitude and frequency variations occur when these devices are operated as oscillators. This dependence of frequency upon the bias of IMPATT and GUNN oscillators is used in voltage-controlled oscillators (VCOs), which operate at frequencies in the mm-band and can be used to implement frequency modulation without upconversion. However, feedback circuitry is required to achieve good stability and linearity.

State-of-the-art for these devices is summarized in Figures A.6-16, through A.6-18.

The highest data rate demonstrated was attained with phase modulation using PIN diodes designed for 40- to 119-GHz operation, Bell Laboratories reporting 300-Mbps operations with these diodes in a 2-phase path-length modulator (Ref. A.6-12). In this modulator the diode terminates a coaxial line that couples into the waveguide transmitting radiation in the mm-band to be modulated. In one bias state the mm-wave signal is reflected by the switch, whereas in the other bias state the signal passes through the switch and is reflected by an adjustable short to provide equal amplitude but 180-degree phase difference between the bias states. A dual-gate FET modulator to switch a carrier at 70 psec, making possible a data rate up to 2 Gbps and higher, has been developed and could be used assuming logic circuits of similar speeds also can be developed to operate the modulator (Ref. A.6-13). This work, which applied to K band, shows that data rates to 2 Gbps should be feasible at frequencies as high as FETs operate. If advancements continue, 2 Gbps should be feasible at frequencies up to at least 100 GHz (3 mm) by 1990.

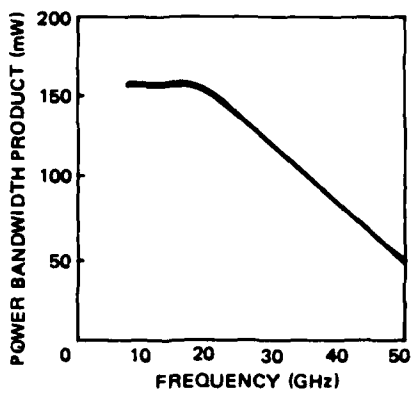


Figure A.6-16. Performance of Hughe's Gunn VCOs

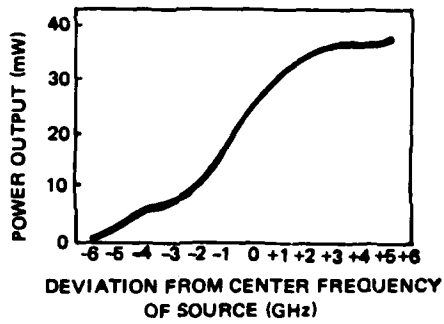


Figure A.6-17. Typical Performance of Millimeter IMPATT Sweeper with 10 GHz Sweep Bandwidth

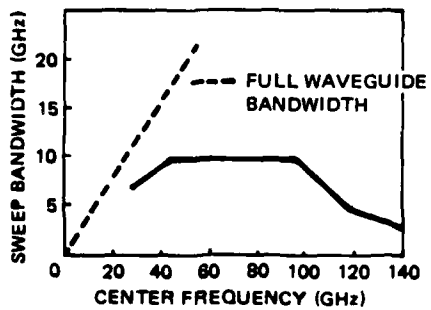


Figure A.6-18. Sweep Bandwidth Capability for Hughe's IMPATT Sweepers

A.6.3 Receiver Technology

The noise figures and instantaneous bandwidths possible in mm-band receivers built in 1990 are expected to be similar to those of 1973 receiver technology at frequencies a full decade lower in frequency. In 1973 transistor amplifiers were available with 3-dB noise figures at frequencies up to about 8 GHz, whereas by 1990 it should be possible to obtain narrow-band transistor amplifiers with 3-dB noise figures at 40 GHz. Current "off-the-shelf" Schottky diodes can be used as a mixer with a 6.9-dB single-sideband noise figure at 50 GHz (Ref. A.6-13), and field-effect transistors (FET) and tunnel-diode amplifier devices commercially available in 1978 are characterized by the noise figures indicated in Figure A.6-19, which shows that the low-noise FET is of limited value in the mm-band from 30 GHz to 300 GHz (Ref. A.6-14). However, recent advancements noted in Figure A.6-20, such as use of InP materials and new FET fabrication technology, provide good performance at the low-frequency end. Figure A.6-21 shows performance similar to current microwave operation at frequencies anticipated in the mm-band (Ref. A.6-15). The FET amplifier is expected to totally replace tunnel-diode amplifiers by 1985 for all but special applications such as those where a limiting amplifier or similar special function is required.

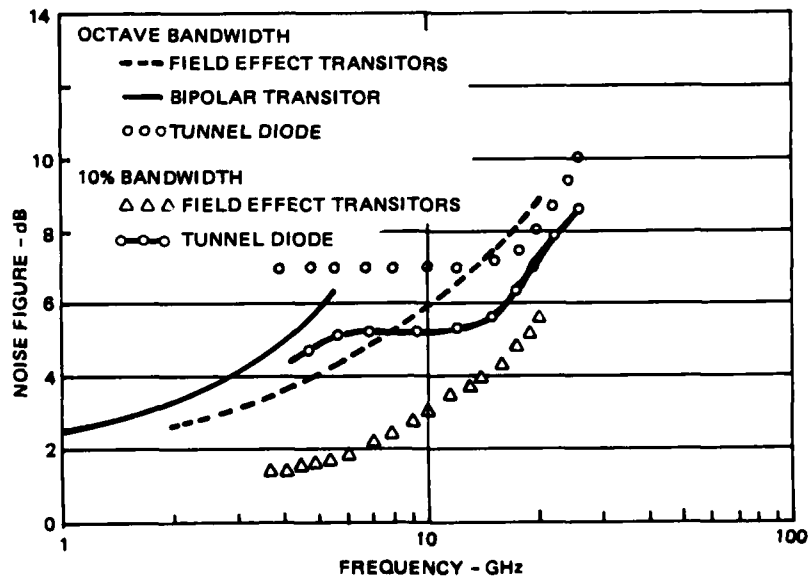


Figure A.6-19. Transistor and Tunnel Diode Amplifier Noise Figures for 1978 Commercially Available Devices

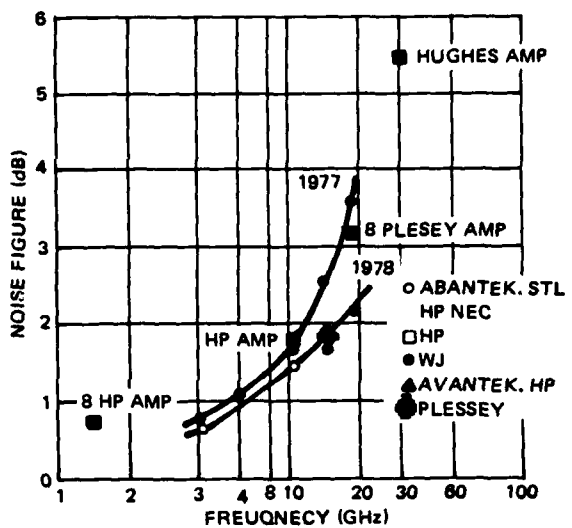


Figure A.6-20. Noise Figures of $0.5 \mu\text{m}$ Gate GaAs FETs

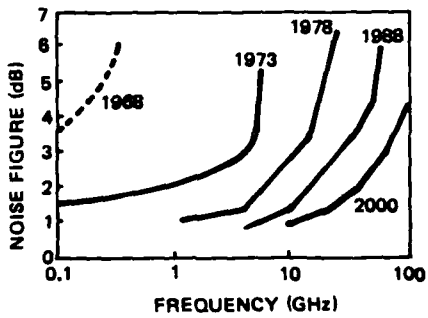


Figure A.6-21. Noise Figure of Narrow Band Transistor Amplifiers as a Function of Frequency and Time

A number of high-performance receiving devices which require cryogenic temperatures may not have much application to LOS communication on the earth's surface because the antenna temperature is on the order of 300°K and thus limits maximum improvement to a few dB, as indicated in Figure A.6-20. However, by 1990 advancements in cooling technique could reduce the complication of cryogenic refrigeration systems sufficiently to render cooled, high-performance receiving devices of general interest, the superconductor-insulator-superconductor (SIS) device and the Josephson junction being of dominant concern are in this class. The cooled parametric amplifier and the maser technology available in 1971 provided amplifiers with noise temperatures on the order of 100°K at frequencies up to 100 GHz (Ref. A.6-16).

The above-noted SIS device has been found to respond at 36 GHz within a factor of 2 of the quantum limit when cooled to 1.4⁰K (Ref. A.6-17). If this device could be used with a local oscillator near-quantum limited performance could be anticipated, so that the equivalent input noise at 100 GHz would be

$$2hf = 2 \times 6.652 \times 10^{-34} \times 10^{11} = 1.3 \times 10^{-22} \text{ Joules.}$$

If this value is equated to Boltzmann's constant times an effective receiver noise temperature, T_R, then,

$$T_R = 9.4^0\text{K}$$

With the SIS first being reported in the fall of 1979 as a laboratory observation, it is reasonable to project commercial availability of cooled mm-band detectors with 100⁰K noise temperatures by the year 1990.

The highest-performance receivers use the superheterodyne configuration with preselector amplifiers having noise figures cited above, followed by a mixer for downconversion to a first amplifier. Such receivers require a low-noise local oscillator source, which often may be obtained from a stabilized low-frequency oscillator using either a modern Surface Acoustic Wave (SAW) resonator or a quartz resonator. The SAW resonator will oscillate at frequencies in excess of 1 GHz, but the quartz crystal resonator is limited to the much lower frequencies that are required to obtain a harmonic of the stabilized source in the frequency of the receiving band. Table A.6-5 presents observed performance of doubler and tripler operations using GaAs Schottky barrier diodes (Ref. A.6-18), as well as design data of an image-enhanced mixer for a 34-GHz signal frequency. The noise figure for the mixer and IF combination was observed to be 5.9 dB.

Table A.6-5. Diode Performance

Operation Type	Frequency (GHz)	Varactor Cutoff Frequency (GHz)	P_{out} (mW)	Efficiency (%)
Doubler	50-100	650	10	>25
	100-200	650	10	>9
	100-200	1000	18	12
Tripler	35-105	650	18	>25
	100-300	1000	2	2

A.6.4 Circuit Fabrication Technology

All the standard components commonly employed in microwave systems also are functionally available for use in the mm band. In addition, new capabilities using quasi-optical configurations are possible (Ref. A.6-19), but these may require oversized waveguides. However, the physical size of oversize waveguides is quite acceptable for most applications, as indicated in Figure A.6-22, and the loss per unit of waveguide running length is reduced. MM-waveband feasibility for almost any well-known function (i.e., isolators, circulators, filters, etc.) also can be assumed due to the fact that feasibility issues such as cooling and size are primarily associated with efficiency.

On the other hand, generalizations concerning size and tolerance requirements can be misleading in that in connection with mm-wavelength practice sizes of elements are quite small by common standards, the total length of a quarter-wave feed for a waveguide for operations at 1 mm, for example, being 0.01 inch.

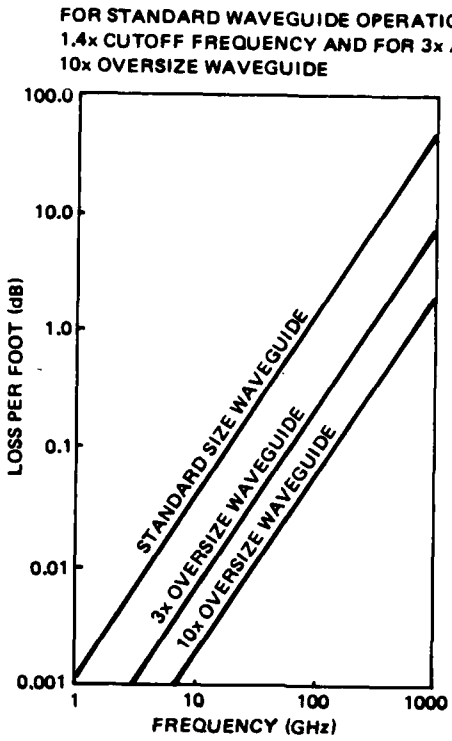


Figure A.6-22. Loss Comparison for Various Waveguide Sizes

Some concern also has been expressed that mm-wave components appear to be subject to extreme tolerance requirements. Conversely, just the opposite would seem true to an optician accustomed to working with 3-orders-of-magnitude smaller tolerances than those required for mm-wave components. The difficulties probably arise from realization that only ordinary fabrication tolerances are required at lower frequencies, whereas at mm-wavelengths material shapes and sizes define the circuit. Nevertheless, tolerances required are actually quite loose compared to standard integrated-circuit (IC) practice.

Microwave integrated circuit (MIC) technology currently is quite adequate for fabricating small assemblies of complex systems built around mm-wave semiconductor devices, hybrid designs consisting of IMPATT devices coupled to metal resonator cavities and to microstrip (finline) transmission lines having been used by TRW to construct an entire 10-Watt transmitter of 38-dB gain at 40 GHz within a volume of 28 cubic inches.

It is anticipated that by 1990 the same power capability will be obtained at frequencies higher than 100 GHz and in a smaller package.

A.6.5 Antennas

A wide variety of antennas which already are on the market and which cover the mm-band include the following:

- Reflector Types
 - Cassegrain
 - Conical Scan (for active alignment)
 - Standard Parabolic with Prime-Focus Feeds
- Horn Lens Types
 - Collimating Lens, Corrected Conical Horn
 - Spot Focusing Lens, Corrected Conical Horn
 - Collimating Scalar Horn

Figure A.6-23 presents typical performance values for selecting the type of antenna recommended by one major manufacturer (Ref. A.6-20).

A.6.6 Atmospheric Effects

Atmospheric effects on mm-waves are evidenced by the three principal phenomena of wave attenuation, scintillation or rapid fading, and beam refraction in the form of long-term fading.

Wave attenuation can result from energy loss from the main beam due to scatter by rain drops, as shown in Figure A.6-24 (Ref. A.6-21), or from energy loss due to absorption caused by molecular resonances of oxygen and/or water vapor in the atmosphere, as noted in Figures A.6-25 and A.6-26 (Refs. A.6-21 through A.6-24). Scatter due to rain also can cause change in polarization, which is of primary concern in systems that use each of two orthogonal polarizations to double channel capacity (Ref. A.6-25), and attenuation is associated with an increase in antenna temperature to the level of the environment temperature, as indicated in Figure A.6-27.

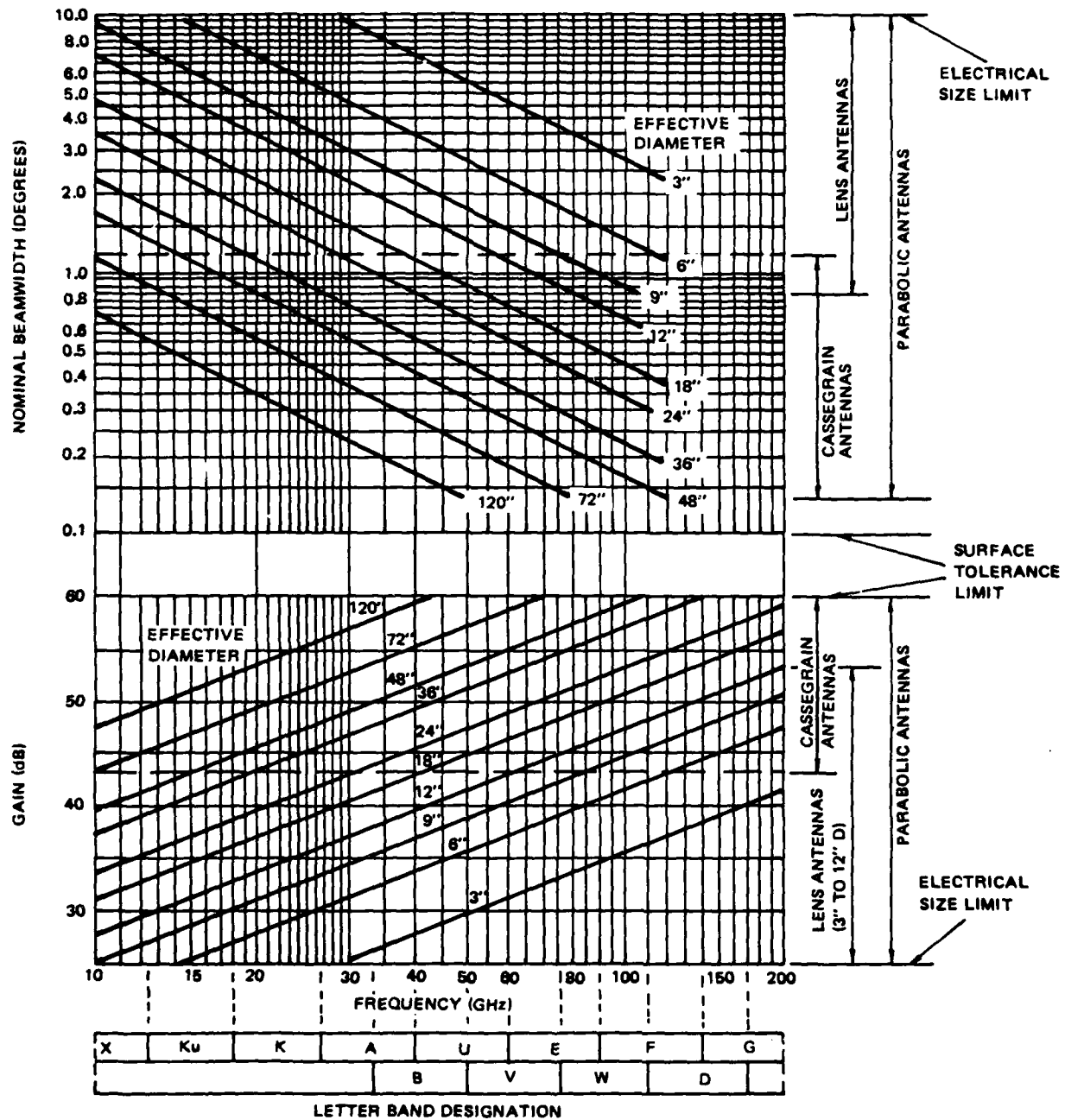


Figure A.6-23. Antenna Selection Requirements

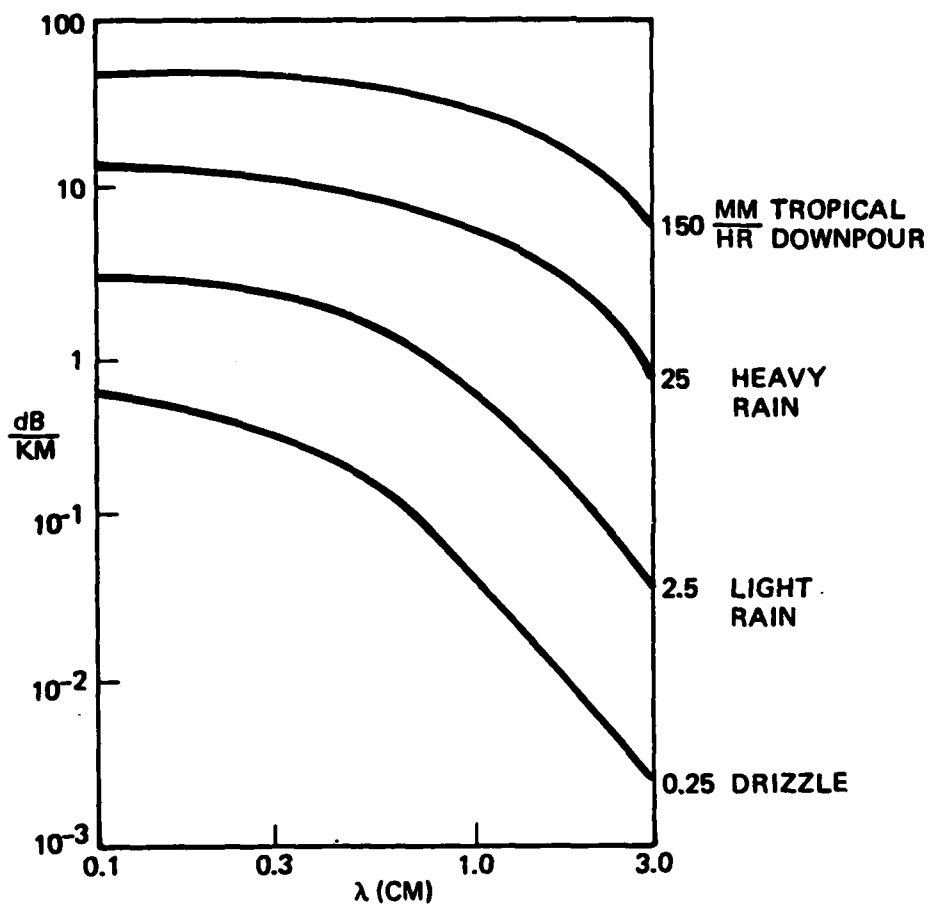


Figure A.6-24. Attenuation Due to Rain

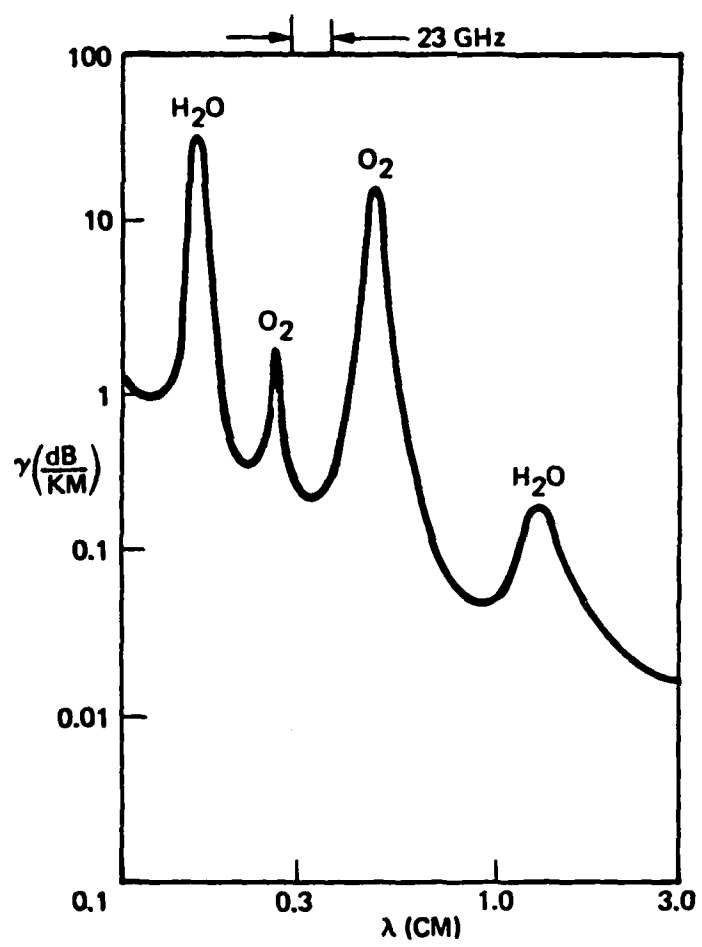


Figure A.6-25. Atmospheric Attenuation

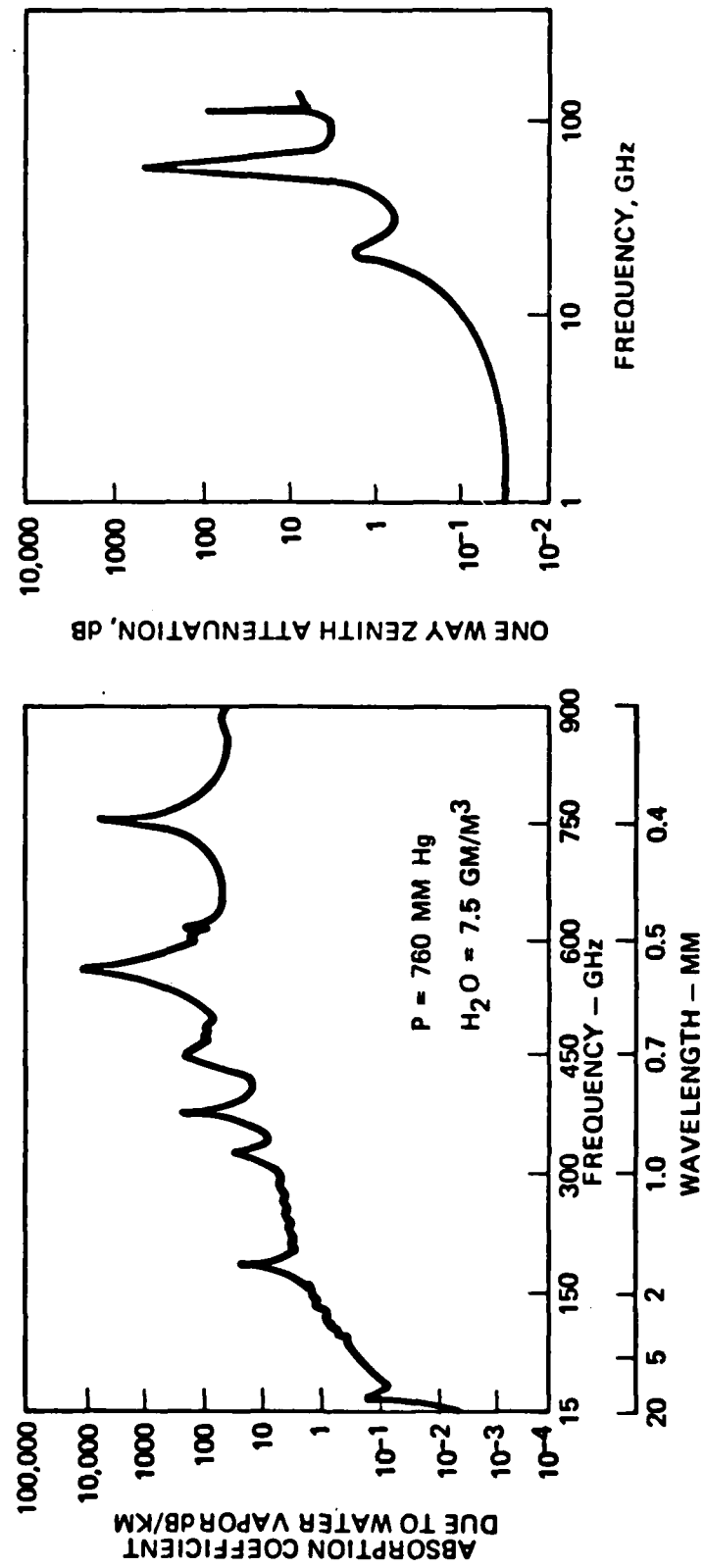


Figure A.6-26. Millimeter Wave Attenuation

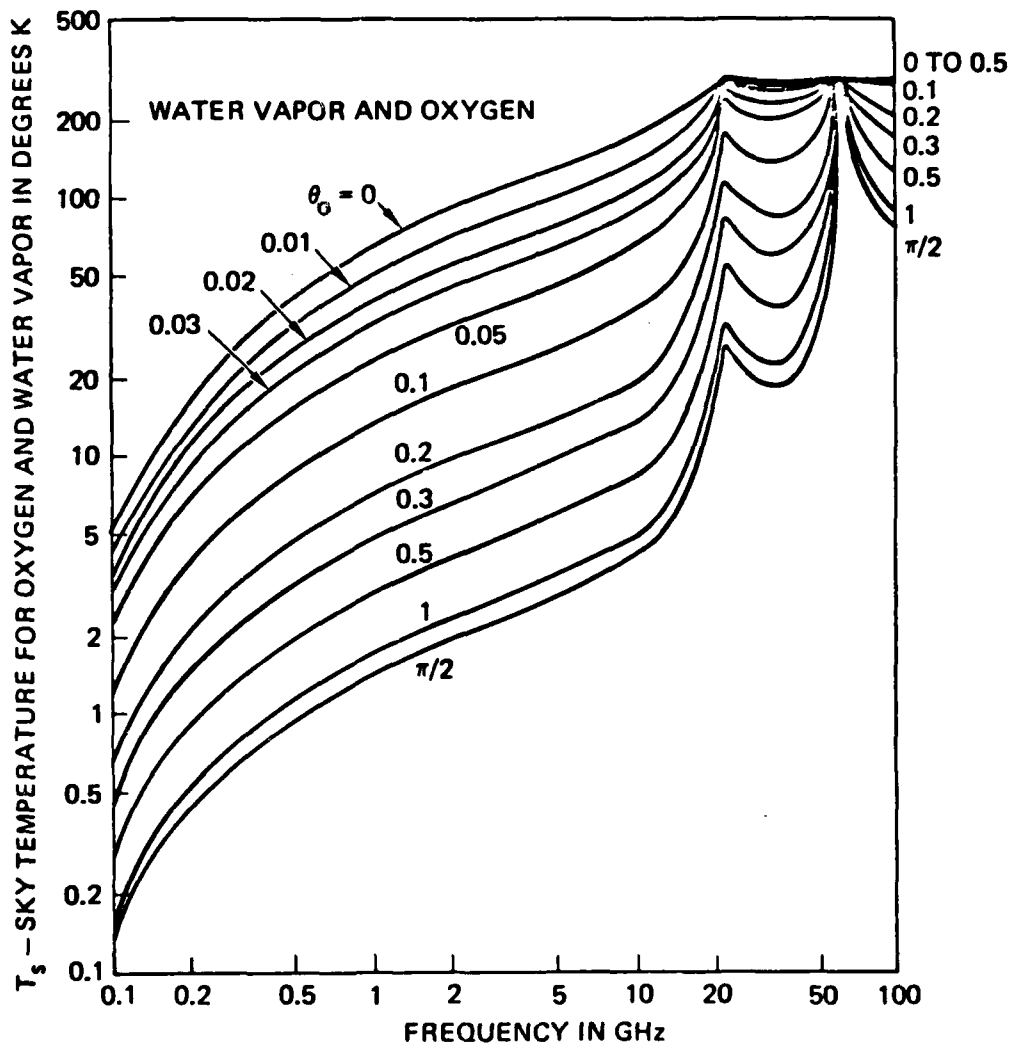


Figure A.6-27. Sky Noise Temperature Due to Reradiation by Oxygen and Water Vapor

Scintillation, or rapid fading, is caused by multipath interference between waves travelling over slightly different paths. Such path difference can be caused by globules of inhomogeneity in the refractive index of the atmosphere, which break up a wave into its components and diffract or refract those components into slightly different directions. These globules of inhomogeneity are caused by turbulence, which is a time-varying random process causing continual change in the relative phase of different waves that contributes to the field arriving at a given point where scintillation is observed. Resulting constructive and destructive interference can produce large random-amplitude modulation of the received signal (Ref. A.6-26).

Beam refraction always exists for horizontal beams due to the transverse gradient in the refractive index of the atmosphere, which is associated with altitude dependence of the refractivity of the atmosphere. Because air refractivity is proportional to air density the effect also varies with barometric pressure and air temperature and causes lateral displacement of the beam (Ref. A.6-27). At certain times the beam also could be displaced above or below the receiving antenna, so that a narrow beam would essentially miss the receiving antenna. The effect would be long-term fading unless an adaptive system were used to correct for this phenomenon.

A.6.7 Point-to-Point Transmission

Transmitter and receiver power in line-of-sight transmission systems are connected by the well-known relation

$$\frac{P_r}{P_t} = \frac{A_t A_r}{\lambda^2 S^2} e^{-2.3LS}$$

where

L = average excess-path loss (dB/kM)

S = distance between receiving and transmitting antennas (km)

λ = wavelength (mm)

A_t, A_r = effective areas of transmitting and receiving antennas (m^2)

The foregoing expression has been evaluated for 2-m diameter antennas using the excess loss from Figure A.6-24 for heavy rain conditions and from Figure A.6-25 for clear weather. The result is presented in Figure A.6-28. This evaluation shows that under heavy rain conditions the transmitter power must be 220 dB greater than the receiver power required for minimum desired performance for a link that is only 20 km in length. Thus, if the 200-kW gyrotron of Figure A.6-2 were used in an attempt to "burn-through" heavy rain, the signal available to the receiver would be 2×10^{-17} Watts. Also, if the noise temperature of the receiver were negligible relative to the temperature of the antenna environment, or 290°K , 2×10^{-17} Watts would be 16 dB greater than receiver input noise if the bandwidth of the receiver were only 125 Hz, and is too narrow to be consistent with the high-data-rate capability expected of mm-wave systems. However, full capability could be obtained by shortening the link by a few kilometers, and because noise is proportional to bandwidth, the bandwidth could be increased to, say, 40 MHz by reducing P_T/P_r by an amount

$$10 \log \frac{4 \times 10^6}{125} \approx 45 \text{ dB}$$

Transmitting loss also would be reduced by 45 dB to a total of 175 dB with antenna separation shortened from 20 to 15 km, which may be verified by noting that with a 200-kW transmitter the received signal would be

$$P_r = 2 \times 10^5 \times 10^{-14} \times \sqrt{10} = 6.3 \times 10^{-12} \text{ watts}$$

For a signal-to-noise ratio of 16 dB the noise level then would be 1.6×10^{-13} Watt, corresponding to the thermal noise for a 290°K temperature in a 40-MHz bandwidth, or

$$KTB = 1.6 \times 10^{-13} \text{ watt}$$

Thus, Figure A.6-28 shows that an additional 3-km reduction in antenna separation to 12 km, which results in a 147-dB transmission loss, will allow use of the full 23-GHz bandwidth of the atmospheric window at 100 GHz (3 mm) for a 16-dB signal-to-noise ratio under heavy rain conditions.

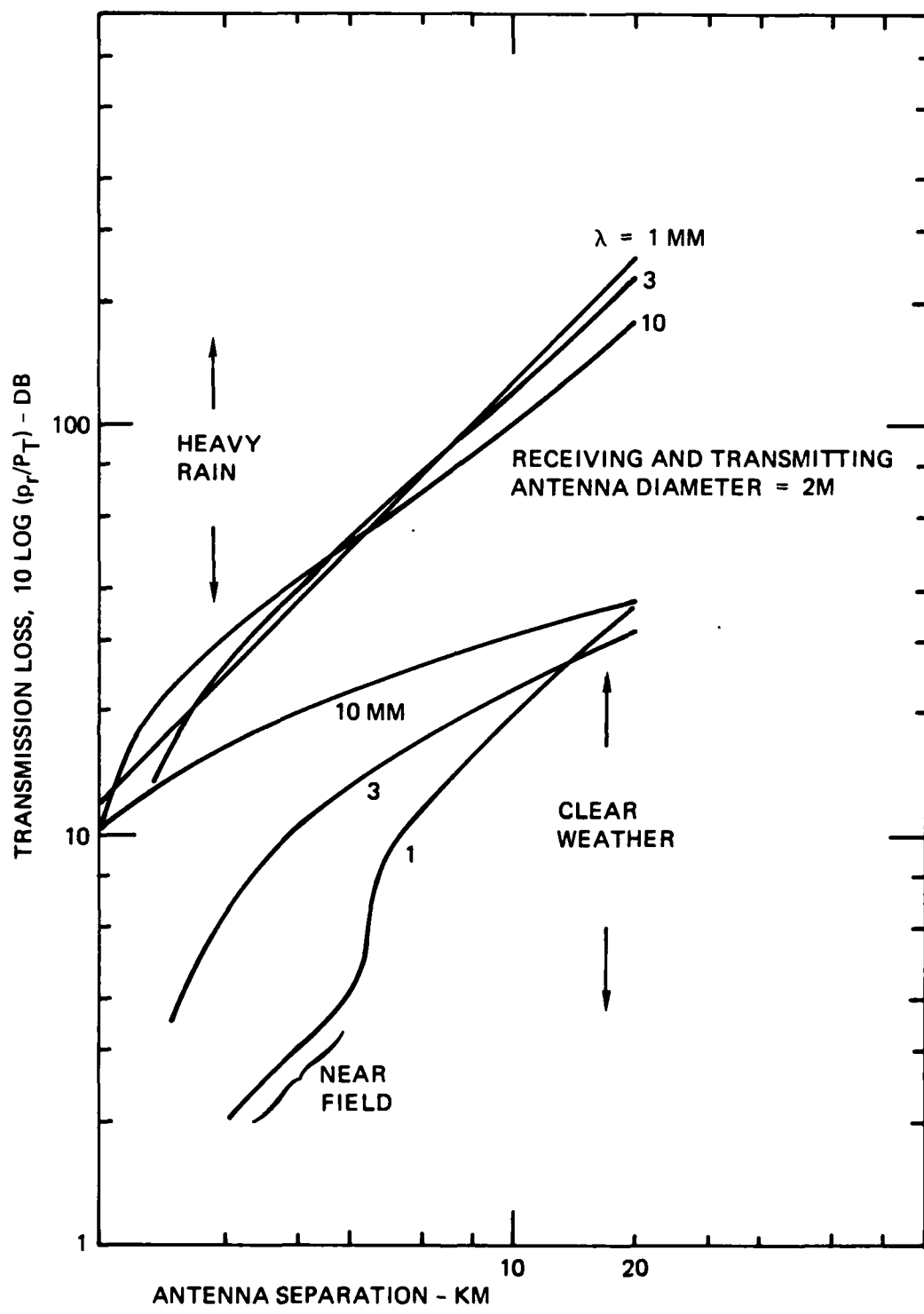


Figure A.6-28. Transmission Loss for a MM Wave LOS Link

However, the suggestion of using 200 kW for a 12-km link seems wasteful even though it would only be used under heavy rain conditions. For example, Figure A.6-28 also shows that the 60-dB reduction from 147 dB to 87 dB in transmission loss that would be experienced with use of a less powerful 200-mW in lieu of a 200-kW transmission power source would correspond to an antenna separation of 7 km (4.35 mi). Consequently, two 0.20-Watt links in tandem can be used to replace one 12-km link for about the same performance under heavy rain conditions, and it therefore appears rather improbable that mm-waves will be used for point-to-point links longer than 7 or 8 km if connectivity must be maintained during heavy rain conditions. As a result, use of gyrotrons for point-to-point communication will probably be limited to multiple-use applications that include other transmission modes in cases where return for investment in a 200-kW device can be justified.

Power required under clear-weather conditions is extremely small, a 20-km link requiring transmitter power that is only 37 dB more than the received-signal level needed for desired performance. For example, for the above case with a 40-MHz bandwidth, required transmitter power is 37 dB more than 1.6×10^{-13} Watt, or

$$P_T = 1.6 \times 10^{-13} \times 10^{3.7} = 8.0 \times 10^{-10} \text{ Watts}$$

Beam width with 2-meter diameter antennas at 100 GHz is about 0.1 degree between nulls, which corresponds to 12.6 meters at a distance of 7 kilometers. However, for the 20-km clear-weather design distance suggested above, beam "whipping" by the atmosphere will cause error-angle fading unless a corrective beam-pointing system is implemented (Ref. A.6-21).

The narrow beams characterizing mm-wave designs introduce other advantages for mm-wave systems, including relative freedom from multipath due to reflections from nearby objects and security from intercept by unwanted listeners. However, one disadvantage of mm-waves is fading, which is more pronounced than at longer wavelengths but which can be mitigated by diversity techniques. Experiments on lateral coherence of mm-waves also show that fields separated by 7 meters are uncorrelated (Ref. A.6-26), so that implementation of diversity reception requires smaller distances than at longer wavelengths.

By 1990 the previously described small solid-state devices generating a few hundred milliwatts are likely to be available at very low cost because of their probable wide use in many high-volume commercial applications. Examples include short distance (range only) radar for automobiles, traffic control signal sensors, camera-focusing sensors, and cable TV distribution. Prices of high-volume large-scale integrated circuits already have been reduced to less than discrete-unit costs, and certainly will continue to prevail for EHF devices such as mm-wave sources and receivers. Other components such as antennas also should experience price reduction because they require only a small amount of material and because tolerance requirements are much less stringent than those for a two-dollar, 2-inch diameter glass lens made for low-cost visual applications. Such a lens (or mirror) would be considered poor quality for optics, but for mm-wave applications it would reflect greater precision than required for diffraction-limited performance because mm-band wavelengths are more than 1000 times longer than visual wavelengths.

It therefore is reasonable to postulate use of many relatively closely-spaced mm-wave relays because of small per-unit cost. Such units very likely could be emplaced on top of existing telephone or power-line poles at, say, 600-ft (0.18-km) intervals without incurring excessive costs. Also, such deployment probably would be more acceptable to a foreign country than placement of new cables (including fiber optics) along existing land-line routes.

As an example of the power requirement for a short-distance relay which is intended to operate at full capacity during a tropical downpour at a wavelength of 3 mm and in which excess loss for a 0.18-km path has been shown to be 12.8 dB (Ref. A.6-1), if the effective antenna area is 6.45 cm^2 (1 in^2) for both the receiver and transmitter power received with a 100-mW 3-mm source, then

$$P_r = 7.86 \times 10^{-9} \text{ Watt},$$

so that for applications requiring a signal-to-noise ratio of 16 dB the noise level must be less than 2×10^{-10} Watt. Presuming a low-cost receiver is used with a 10-dB noise figure, the maximum system bandwidth, B, then can be calculated as

$$kTFB = 1.38 \times 10^{-23} \times 290^\circ\text{K} \times 10 \times B = 2 \times 10^{-10} \text{ Watt}$$

or

$$B = 5.6 \text{ GHz}$$

which is ample to accommodate 100,000 digital voice channels.

Implementation of such a wideband capability in a low-cost repeater remains to be proven feasible, but such a wideband is not required to validate the concept. Figure A.6-29 presents the relation between bandwidth and repeater spacing in greater generality for the case with a 0.20-Watt transmitter, a receiver with a noise temperature of 300°K and an operating signal-to-noise ratio of 16 dB.

Point-to-point surface-based mm-wave systems are generally accepted as a potential alternative for short-distance relay applications. However, their usage probably will not occur until spectrum availability at lower frequencies has been exhausted.

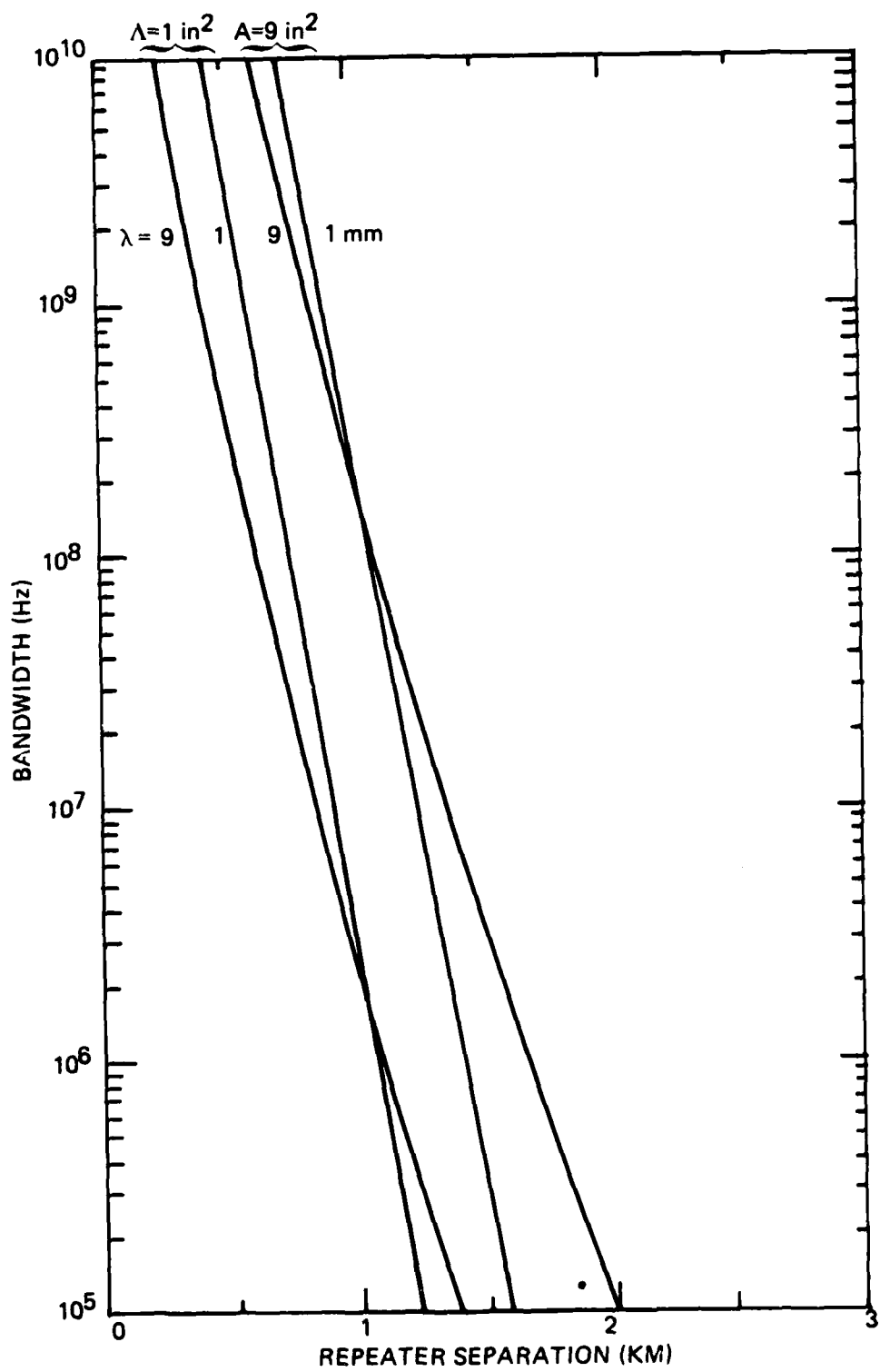


Figure A.6-29. Maximum Repeater Spacing for 16 dB S/N Rain as Heavy Pour (150 mm/Hr) using a 200 Milliwatt Transmitter

A major consideration for deployment of many short relay hops in tandem results from the great change in excess-path loss with weather. This is exemplified in Figure A.6-28, where it is seen that at a transmission loss of about 35 dB the maximum permissible separation of antennas increases from about 3 km to 15 km as conditions change from heavy rain to clear atmosphere. Therefore, if several repeaters are positioned along the same line-of-sight usable signals from several repeaters can be present simultaneously. Although this can seriously degrade performance where simple regenerative repeaters are used, possible degradation can be mitigated by use of spread-spectrum techniques in a manner suggested by multiple-access spread-spectrum modulation, wherein the desired signal is isolated by synchronization. This can be done uniquely if a substantial time delay is incorporated in each repeater, so that the pseudo-random code will only be synchronized with the signal from one repeater. Much simpler repeater circuitry also might be possible which provides self-jamming interference-free operation by using frequency or phase modulation where a limiter is employed, as usually is the case. A discriminator with good capture characteristics then would suppress weaker signals from all but the nearest repeater.

Because the modulation on the signal from all repeaters is the same, the effect of signals from other repeaters can add coherently. Thus, if repeaters are spaced equally the electric fields of signals from each successively more distant repeater are in the ratio of 1/2, 1/3, 1/4.... 1/N relative to the amplitude of the signal received from the nearest repeater if excess-path loss is negligible and all repeaters are the same and are on a single straight-line path. The relative phase can be any value because the effective path length is not controlled to a fraction of a wavelength in the millimeter band. Without any excess-path loss, and noting that $1/2 + 1/3 + 1/4$ is greater than 1, fading could be complete if at least five repeaters are in a straight line.

Figure A.6-24 previously has indicated that at a wavelength of 1 mm excess-path loss is 1 dB/km, which with a 1-km separation is sufficient to reduce the sum representing the relative amplitude of three repeaters to

$$\frac{10^{-0.05}}{2} + \frac{10^{-0.1}}{3} + \frac{10^{-0.15}}{4} = 0.887$$

The peak fade due to self-interference is then approximately

$$20 \log \frac{1}{1-.887} = 19 \text{ dB}$$

at a wavelength of 1 mm. It should not be overlooked that fading with five repeaters in line due to this mechanism could be complete at a wavelength of 9 mm under clear-weather conditions because the excess-path loss is then only 0.06 dB/km at this wavelength.

The nominal system with five repeaters with parameters on which Figure A.6-29 is based clearly should use a wavelength of 1 mm if the desired system bandwidth exceeds 250 MHz and if connectivity is to be unbroken during very heavy rain of 150 mm/hr. Use of a 1-mm wavelength for such a system removes need for enhancement by capture, and such a system would be intrinsically fault-tolerant without special provisions. However, a failure-sensing system would be required to keep every repeater in good repair so that heavy rain can be tolerated, which would be done in the form of telemetry from each repeater.

It is important to realize that the superior quality associated with use of a 1-mm rather than a 9-mm wavelength is not as fundamental as it might appear, in that with regard to fading due to interference from other inband repeaters very similar results can be obtained at 9 mm. For example, in the above case with only five interacting repeaters operating at 1 mm, and wherein 1 dB (negligible) excess-path loss exists under clear-weather conditions, 9-mm wavelength usage with respect to fading would be feasible simply by making the transmitter power of any repeater 1 dB less than the power of the repeater to follow for the four repeaters that are received by the fifth. The first repeater in the string would

deliver a transmitted power of 200 milliwatts, and the remainder 252 mW, 317 mW, and 400 mW respectively. The last repeater has a power level reduced to the original value of 200 mW to match the parameters of the comparative example above because in this instance the last repeater is at most the beginning of a new string in which fading due to self-interference must be controlled. In the case where there are only three or fewer equally-spaced repeaters so located that the third "sees" only the two preceding ones, the depth of a fade in the received electric field cannot be greater than $1 - 1/2 = 1/2$, or 6 dB, due to interference caused by inband repeaters.

Use of short segments of repeaters to provide fault-tolerant behavior in the manner described above cannot by itself provide complete protection because the end repeaters in each segment are critical to connectivity. One way to prevent any given repeater from being a single point of failure under good-weather conditions is to set up the single-hop spacing in such a manner that the excess-path loss is great enough to prevent an acceptable depth of fade with no limit on the number of repeaters along a straight line. Significant deviation from a single straight line of course will introduce critical end points of each straight segment, but these can be covered by adaptively switched redundant circuitry.

The rarely occurring (because of uncontrolled phase) but maximum possible electric field, E_s , that may arise due to a large number of equally-spaced repeaters experiencing excess-path loss (expressed as a fraction) is given by the series,

$$E_s = E_0 \left[1 + \frac{a}{2} 2 + \frac{a^2}{3} 3 + \frac{a^3}{4} 4 + \frac{a^4}{5} 5 + \frac{a^{n-1}}{n} \dots \right] \quad (A.6-6)$$

where

a = excess-path loss

n = number of repeaters

and the minimum electric field (fade peak) possible is given by

$$E_m = E_0 \left[1 - \sum_{m=1}^{n-1} \frac{a^m}{m+1} \right] \quad (A.6-7)$$

The latter relation also can be expressed in the form

$$\frac{E_m}{E_0} = 1 - \frac{1}{a} \int_0^a \sum_{m=1}^{n-1} x^m dx \quad (A.6-8)$$

or, using the sum of an arithmetic progression, as

$$\frac{E_m}{E_0} = 1 - \frac{1}{a} \int_0^a \left[\frac{1}{1-x} - 1 - \frac{x^n}{1-x} \right] dx \quad (A.6-9)$$

It already is apparent that the factor, a , must be significantly less than unity to limit the fade level. Therefore, for large values of n , and with $a < 1$, the last term in Eq. A.6-9 is essentially zero for a large number of repeaters, and the remaining terms then become

$$\frac{E_m}{E_0} = 2 + \frac{1}{a} \ln(1-a) \quad (A.6-10)$$

The condition for infinite fade then arises under the circumstance wherein $E_m = 0$, which occurs when

$$1 - a = e^{-2a} \quad (A.6-11)$$

from which $a = 0.797$, or -2dB .

If the excess-path loss is only 2 dB , a possible fade of signal to zero occurs due to self-interference if a large number of repeaters are in view of an end receiver. It is then evident that about ten repeaters are sufficient to approximate an infinite number of repeaters. Figure A.6-30 indicates depth of possible fading due to mutual interference as a function of excess-path loss per hop in accordance with Eq. A.6-10, and also shows that mutual-interference fading drops precipitously as the excess loss per hop increases to as little as 4 dB , where the peak fade cannot exceed 7 dB due to mutual interference. Also, Figure A.6-25 indicates that at a wavelength of 1 mm clear-weather excess-path loss is 1 dB/km , so that a 7-km hop is suggested.

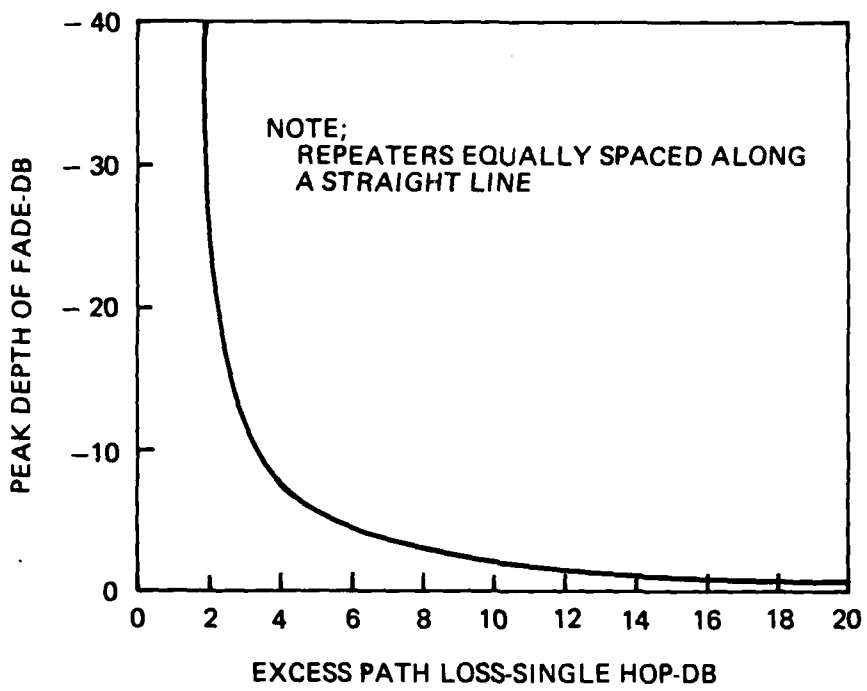


Figure A.6-30. Peak Fade with a Large Number of Repeaters in Line Due To Mutual Interference

Figure A.6-28 shows that the transmitted power, P_T , must be 85 dB more than the receiver power under heavy rain conditions if both the antennas are 2 meters in diameter with 7-km separation. With equal-size transmitting and receiving antennas free-space loss is proportional to the fourth power of antenna diameter, so free-space loss must be increased by 33 dB if 12-inch (30-cm) diameter antennas are used rather than the 2-meter diameter units assumed for Figure A.6-28. Required transmitter power is then 138 dB more than required receiver power under heavy rain (25 mm/hr) conditions. Referring to the case previously discussed at the beginning of this subsection, the required transmitter power with a 40-MHz bandwidth is 138 dB more than the required received signal of 1.6×10^{-13} Watts. Required transmitter power is then about 10 Watts to "burn through" heavy rain over a 7-km path using 1-ft diameter antennas. Under clear weather the required power drops by 75 dB from the requirement under heavy rain, or to about 3 Microwatts.

These parameters are easily feasible with existing technology but not at low cost, as the solid-state technology which promises low cost would have to provide two-orders-of-magnitude increase in power capability by 1990 to make such a system appealing. Only a few installations can use a 70-km-long straight-line path on which repeaters are placed. These considerations show that the above approach is not as promising as the alternative where more complex signal formats such as spread spectrum are used to prevent mutual interference. The continual decrease in cost of complex signal processors also makes the spread-spectrum or other PCM approach with anti-mutual-interference properties a better alternative. The lowest-cost alternative with fault-tolerant properties is likely to incorporate switchable, low-cost, redundant, low-power equipment with single-hop distances on the order of 1 km, using paths that do not follow a straight line and therefore tend to isolate repeater signals by geometry of antenna boresights. Such systems can follow existing rights-of-way along streets and highways, possibly criss-crossing from side to side, whereas a straight street would be followed for appreciable distance.

A.6.8 Fading Due to the Atmosphere

Considerable data have been collected on the statistics of fading caused by turbulence in the atmosphere. For path lengths well over 20 km very significant losses in signal strength occur at mm wavelengths, in which connection it has been shown that the variance defining the log-amplitude of these fluctuations is proportional to path length raised to the 11/6 power (Ref. A.6-27). However, at sufficiently short path length fading due to the atmosphere will be negligible.

In considering the threshold distance where the atmosphere begins to have an effect upon intensity, the probability density function describing intensity fluctuations is given by (Ref. A.6-28).

In considering the threshold distance where the atmosphere begins to have an effect upon intensity, the probability density function describing intensity fluctuations is given by Ref. A.6-28.

$$P(\gamma) = \frac{1}{\sigma\sqrt{2\pi}} e^{-\gamma^2/2\sigma^2} \quad (\text{A.6-12})$$

where

$$\gamma = \log(I/I_0)$$

I = intensity received

I_0 = mean intensity received

$$\sigma^2 = 1.23 C_n^2 k^{7/6} L^{11/6}$$

Consider the threshold distance where the atmosphere begins to have an effect upon intensity. Also, because of the small size of the fluctuations, letting

$$I = I_0 + \Delta I \quad (\text{A.6-13})$$

where $\Delta I \ll I_0$, then

$$\gamma = \log(1 + \frac{\Delta I}{I_0}) \approx \frac{\Delta I}{I_0} \quad (\text{A.6-14})$$

and

$$P(\gamma) = P(\Delta I) \approx \frac{1}{\sigma\sqrt{2\pi}} \exp(-\frac{(\Delta I)^2}{2I_0^2\sigma^2})$$

and the RMS level of intensity fluctuation consequently is

$$(\frac{\Delta I}{I_0})_{\text{rms}} \approx 1.11 C_n k^{7/12} L^{11/12} \quad (\text{A.6-15})$$

To validate the approximation and assess the importance at a range of 1000 meters, the case with maximum turbulence also should be considered, in which instance,

$$\frac{\Delta I}{I_0} \approx 1.11 \times 3.16 \times 10^{-7} \left(\frac{2\pi}{\gamma}\right)^{7/12} (1000)^{11/12}$$

or

$$\frac{\Delta I}{I_0} = 5.77 \times 10^{-4} / (\gamma)^{7/12} \quad (A.6-16)$$

wherein γ is expressed in meters. At $\gamma = 6$ mm, then

$$\frac{\Delta I}{I_0} = 1.14 \times 10^{-2}$$

The above approximation is clearly valid for mm wavelengths at ranges up to several thousand meters under maximum-turbulence conditions and where obstacle-free fading is negligible.

A.7 EHF SATELLITE COMMUNICATIONS

A.7.1 Introduction

Recent significant developments in Extremely High Frequency (EHF) technology and constraints on available performance at lower frequencies lead to the reasonable assumption that the Defense Satellite Communication System (DSCS) will incorporate millimeter-wave capability when DSCS III is upgraded or replaced in the late 1980 time frame. Moreover, within this time frame use of the Shuttle/IUS combination will provide a much greater weight capability permitting inclusion of EHF add-ons to later launches of DSCS III for evaluation of experimental and limited operational packages, and ultimately will lead to a new DSCS design which will probably be an optimally integrated super high frequency (SHF)/EHF satellite communications system. The purpose of this section therefore is to briefly review the advantages and disadvantages of EHF and the current state of EHF technology, as well as to investigate potential performance of small EHF transponders which could provide improved long-haul communications for the DCS of the 1990 time frame.

A.7.2 Major Features of Current EHF Technology

A.7.2.1 Hardware Technology. Table A.7-1 illustrates current technology achievements that are of importance to EHF/SHF SATCOM systems. Although maturity of the X-band components has not yet been reached, EHF components will become available for space qualification in the next few years. At the present time silicon IMPATTs dominate the field of solid-state small microwave power sources, but further major improvements appear less likely. However, GaAs Field Effect Transistor (FET) low-noise amplifiers are approaching the performance of parametric amplifiers without the complexity and instability disadvantages of the latter, and GaAs FET power amplifiers are expected to overtake the silicon IMPATTs in the near future not only because of their higher efficiency and circuit flexibility but also because they are multi-post devices that do not need circulation or hybrid circuits to isolate input from output signals, as in the case of IMPATTs.

Table A.7-1. Current Technology Development Programs

Equipment Type	Characteristics/Performance
Multimode TWTA	<u>Spacecraft</u> Variable power output Prime power savings in fine weather Efficiency: $\eta = 20$ percent at 4 Watt output $\eta = 33$ percent at 30-16 Watt output $\eta = 37$ percent at 8-Watt output
Low-Noise Amplifier	GaAs FET, noise figure 6 dB at 30 GHz, power consumption 0.5 Watt, weight 0.2 lb
Multibeam Antennas	Offset-feed design more efficient than lens design
High-Power Amplifiers	<u>Ground Terminals</u> 250-500 Watt output at 44 GHz (Hughes/Siemons)
Low-Noise Amplifiers	GaAs FET, noise figure 4 dB at 20 GHz
Low-Cost Terminals	NASP program ship terminal, cost goal \$900k, antenna 1 meter or less

As indicated in Table A.7-1, the 950H TWT equipment under active development for spacecraft operation has achieved an efficiency of about 33 percent for 30 Watts output at 20 GHz. High-power amplifiers for SATCOM terminals are being developed at the 250- and 500-Watt levels at 30 and 44 GHz, and multi-beam antennas are becoming more practical for use in spacecraft.

A.7.2.2 Propagation Losses. Propagation losses under bad-weather conditions are much greater at EHF than at 8 GHz and must be considered very carefully in the design of an EHF SATCOM system even though these losses are offset by higher spacecraft antenna gains. Weather models which appear to be adequate for prediction and determination of such losses when combined with good-weather data from a particular location, from a nearby location, or from a location with the same climate, have been developed. In the European Theater the DSCS backbone system traverses the following temperate-climate regions (Refs. A.7-1 and A.7-2):

- Marine West Coast Federal Republic of Germany
(FRG) United Kingdoms (UK)
- Humid Subtropical Northern Italy
- Mediterranean Subtropical Spain, Greece, Southern Italy,
 Coastal Regions of Turkey
- Middle Latitude Steppe Central Turkey (assumed similar
 to Albuquerque, New Mexico)

Because each of the above regions has a different monthly precipitation pattern and also because a weather model as a function of precipitation rate depends on the temperature, humidity, and height of rain storms, which themselves vary by season, reliable monthly rain statistics are required to calculate possible outages due to heavy precipitation at each location. Applicable data have been tabulated by the Illinois State Water Survey Department (Ref. A.7-3) for a number of specific locations around the world in all of the major climatic regions. In some cases such as the GRD and the UK these data can be used directly. In others, data from a similar location within a neighboring country (e.g., Israel for coastal regions of Turkey), or data from other similar locations at about the same latitude which have the same climate, are used even though those locations may be on a different continent.

In some instances, as a check on the validity of this approach, a comparison also is made with the annual weather statistics (which are much more readily available than monthly statistics) for the two locations being considered. Table A.7-2 illustrates the seasonal weather statistics and the number of hours per season a certain attenuation will not be exceeded

at 20 Ghz and at 30 Ghz for an elevation angle of 30° at a particular location. These values are then corrected for the actual elevation line-of-sight angle from the terminal to the spacecraft and are used to adjust the assumed (baseline) bad-weather propagation losses.

Table A.7-3 summarizes estimates of atmospheric attenuation at 20 and 30 Ghz which are not exceeded for 99.5 percent of the year for typical sites representing various climates. The greatest attenuations (10 dB and 6.4 dB) are used in the general uplink and downlink power budgets, and additional performance margins are accredited to various terminal locations of significance. In less severe rain storms and in fine weather the attenuations are considerably smaller, with minimum attenuations of 1.1 dB at 30 Ghz and 1.6 dB at 20 GHz in fine summer continental climates at an elevation of 30° (Ref. A.7-4).

A.7.3 Other EHF SATCOM System Features

Development of EHF/SHF equipment generally is progressing favorably toward the goal of an operational SATCOM system, and previous difficulties appear to be resolved. The problem of comparatively high attenuation under bad-weather conditions may be overcome by the higher antenna gains now achievable and by diversity reception. Thus it appears that as the limited spectrum space and the number of available positions in the synchronous equatorial orbit become saturated the following important advantages of the EHF band will be found irresistible:

- Widened bandwidth (1 Ghz at 20, 30, and 40 GHz)
- Higher-gain, small antennas
- Reduced jamming-threat effectiveness
- Feasibility of smaller spacing between satellites in same orbit.

A.7.4 Applications

The significant performance possible with EHF terminal antennas on the order of 4- to 8-ft diameter emphasizes the potential of many EHF SATCOM uses for mobile terminals. Another very important application would be

Table A.7-2. SATCOM Attenuation at 30° Elevation as Function of Season in Representative Climate Zones

RAIN RATE MM/HR	HOURS	WINTER		SPRING AND FALL		SUMMER	
		ATTENUATION (dB)		ATTENUATION (dB)		ATTENUATION (dB)	
		30GHz	20GHz	30GHz	20GHz	30GHz	20GHz
KOBLENZ, FRG							
1.25	32.8	2.8	1.8	50.6	4.1	3.3	30.7
2.5	9.9	4.5	2.6	25.0	6.3	4.4	19.5
5.0	2.0	6.7	3.7	8.1	9.7	6.0	10.3
10.0	0.28	10.0	5.6	2.4	15.3	8.8	4.2
INCIRLIK, TURKEY							
1.25	47.2	2.8	1.8	69	4.1	3.3	NO SIGNIFICANT PRECIPITATION
2.5	21.0	4.5	2.6	28.3	6.3	4.4	-
5.0	5.6	6.7	3.7	7.8	9.7	6.0	-
10.0	0.5	10.0	5.6	0.89	15.3	8.8	-
AVIANO, ITALY							
1.25	80.1	2.8	1.8	117	4.1	3.3	37.4
2.5	43.0	4.5	2.6	63	6.3	4.4	22.7
5.0	12.5	6.7	3.7	19.4	9.7	6.0	12.5
10.0	3.1	10.0	5.6	6.0	15.3	8.8	5.5
ELMADAS, TURKEY							
1.25	7.8	2.8	1.8	22	4.1	3.3	17
2.5	2.8	4.5	2.6	13.2	6.3	4.4	9.5
5.0	-	6.7	3.7	4.9	9.7	6.0	5.0
10.0	=	10.0	5.6	1.5	15.3	8.8	2.2

Table A.7-3. Beam Pattern and Weather Attenuation for Typical Terminal Locations

Location	Climate (Para 2-2)	Hours Per Year	Percentage Per Year	Elevation Angle Degrees	Attenuation (dB) 30 GHz	Attenuation (dB) 20 GHz	Antenna Pattern Loss (dB)			
							Elliptical (Single)	Uplink	Downlink	Multiple Beam
Reading, England	(a)	28	0.31	30	10.0	6.4	6	3	3	2
Casteau, Belgium	(a)	30	0.34	30	10.0	6.4	4	2	2	1
Koblenz, FRG	(a)	30	0.34	30	10.0	6.4	2	1	1	0
Aviano, Italy ⁽¹⁾	(b)	45	0.51	33	8.8	5.6	1	0	2	1
Naples, Italy ⁽²⁾	(c)	34	0.40	35	5.8	4.0	0	0	2	1
Torrejon AB, Spain ⁽²⁾	(c)	34	0.40	42	5.0	3.3	7	4	2	1
Athens, Greece ⁽²⁾	(c)	34	0.40	34	5.5	3.8	2	1	4	2
Incirlik, Turkey ⁽²⁾	(c)	34	0.40	24	8.0	5.4	6	3	2	2
Elmadaq, Turkey ⁽³⁾	(d)	42	0.48	28	6.7	5.1	4	2	2	1

Notes:

- (1) Assumed same as Island Beach, New Jersey
- (2) Assumed same as Tel Aviv
- (3) Assumed same as Albuquerque, New Mexico

Climates

- (a) Marine West Coast
- (b) Humid Subtropical
- (c) Mediterranean Subtropical
- (d) Middle Latitude Steppes

usage as a replacement for long-haul sections of the European DCS backbone system shown in simplified form in Figure A.7-1. An alternative DCS could deploy EHF SATCOM terminals at important communication nodes which support extensive local networks or specific critical uses (e.g., command posts or logistics centers). This scheme potentially could eliminate need for many terrestrial relay stations and considerably improve reliability of existing single-thread long-haul circuits such as these currently existing between Italy, Greece, Spain, and Turkey. Terminals also could be more mobile than current SHF terminals for given performance, and could be used for direct communications to certain critical users disposed over large areas. In other more compact areas with a much higher density of small users (such as West Germany) a network of small terminals could be deployed, each supporting an area of about 30- to 40-mile radius using either line-of-sight or defraction microwave communication or fiber-optic cables. Figure A.7-2 illustrates a network concept using EHF terminals which could replace the majority of long-haul troposcatter links in Europe.

A.7.5 EHF SATCOM Network Performance Capability

A.7.5.1 Performance Bounds Under Benign Conditions. Performance capability of an EHF SATCOM network which could replace most of the long-haul traffic of the DCS backbone system in Europe has been evaluated, and two spacecraft transponder configurations have been considered. One consists of an angle transponder with a simple elliptical antenna system that may be suitable as an add-on (piggyback) package to a future satellite of DSCS III type. The other uses a single transponder (that also could be expanded to several transponders) in combination with a more sophisticated antenna system, in this case a 3-ft antenna with multiple offset feeds. Typical European backbone terminal locations and associated parameters attributable to climate or position in the postulated antenna-system pattern have been identified previously in Table A.7-3, and the coverage of each of these systems is illustrated in Figures A.7-3 and A.7-4. Figure A.7-3 shows coverage of an antenna with an elliptical beam for the uplink and downlink.

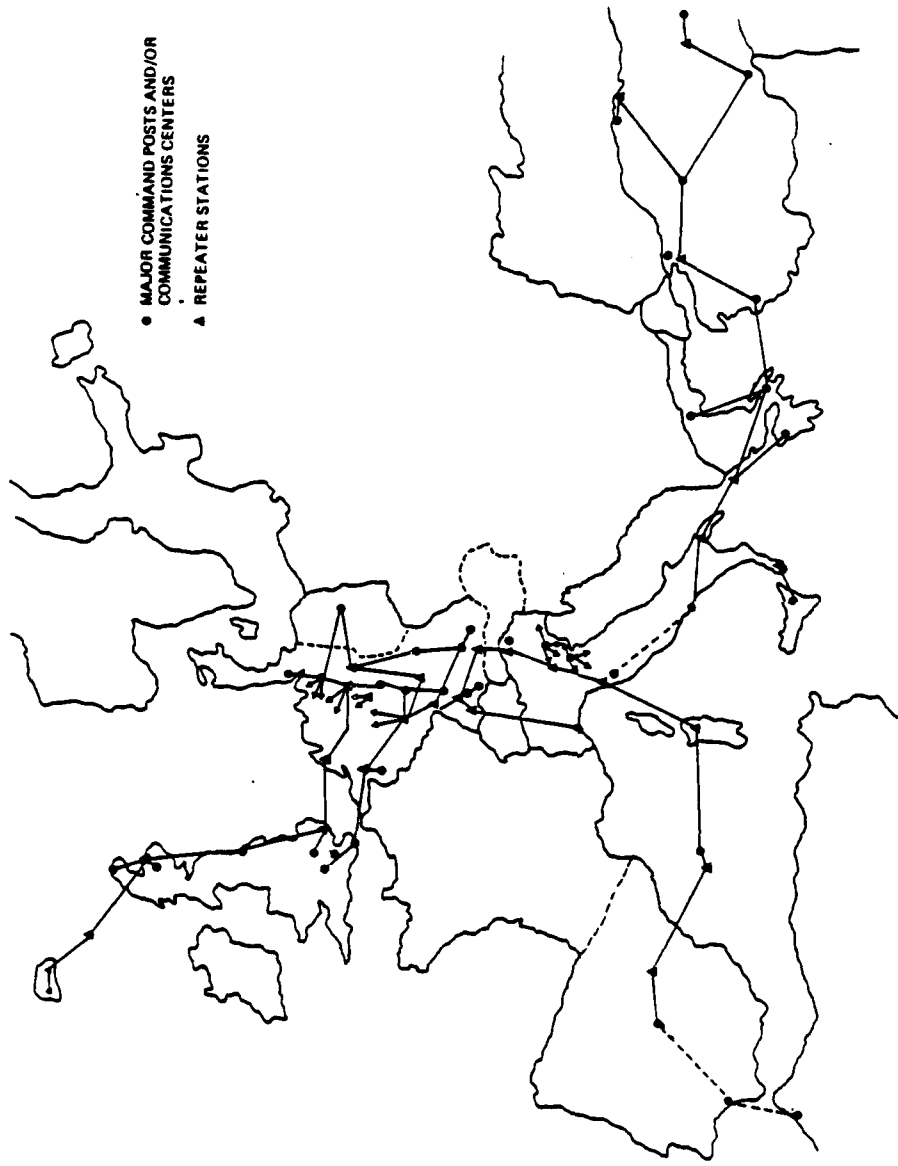


Figure A.7-1. Simplified Diagram of European DCS

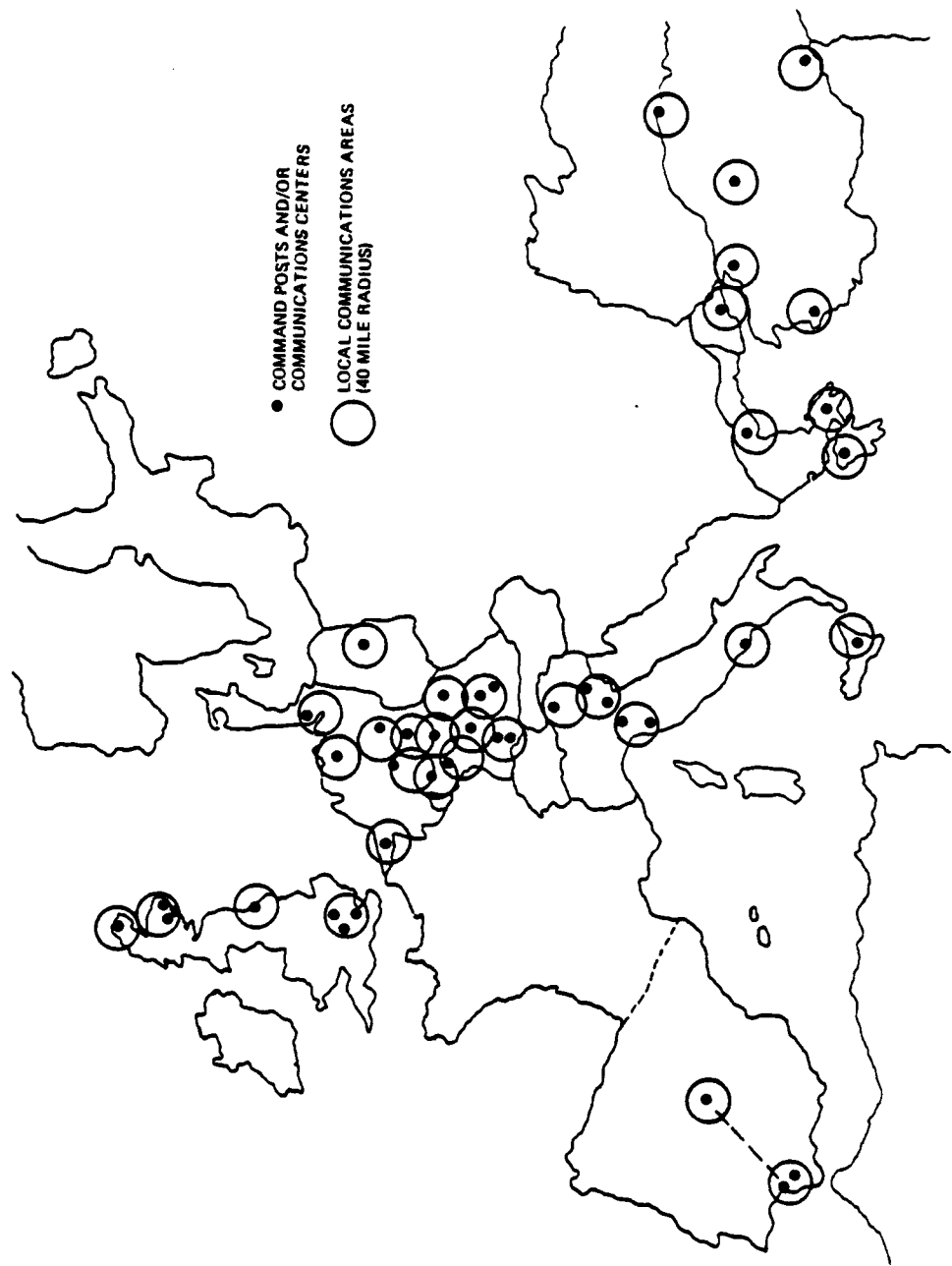


Figure A.7-2. EHF Satellite Network for Replacing European Long Haul DCS Network



A.7-10

Figure A.7-3. Coverage of an Elliptical Satellite Antenna

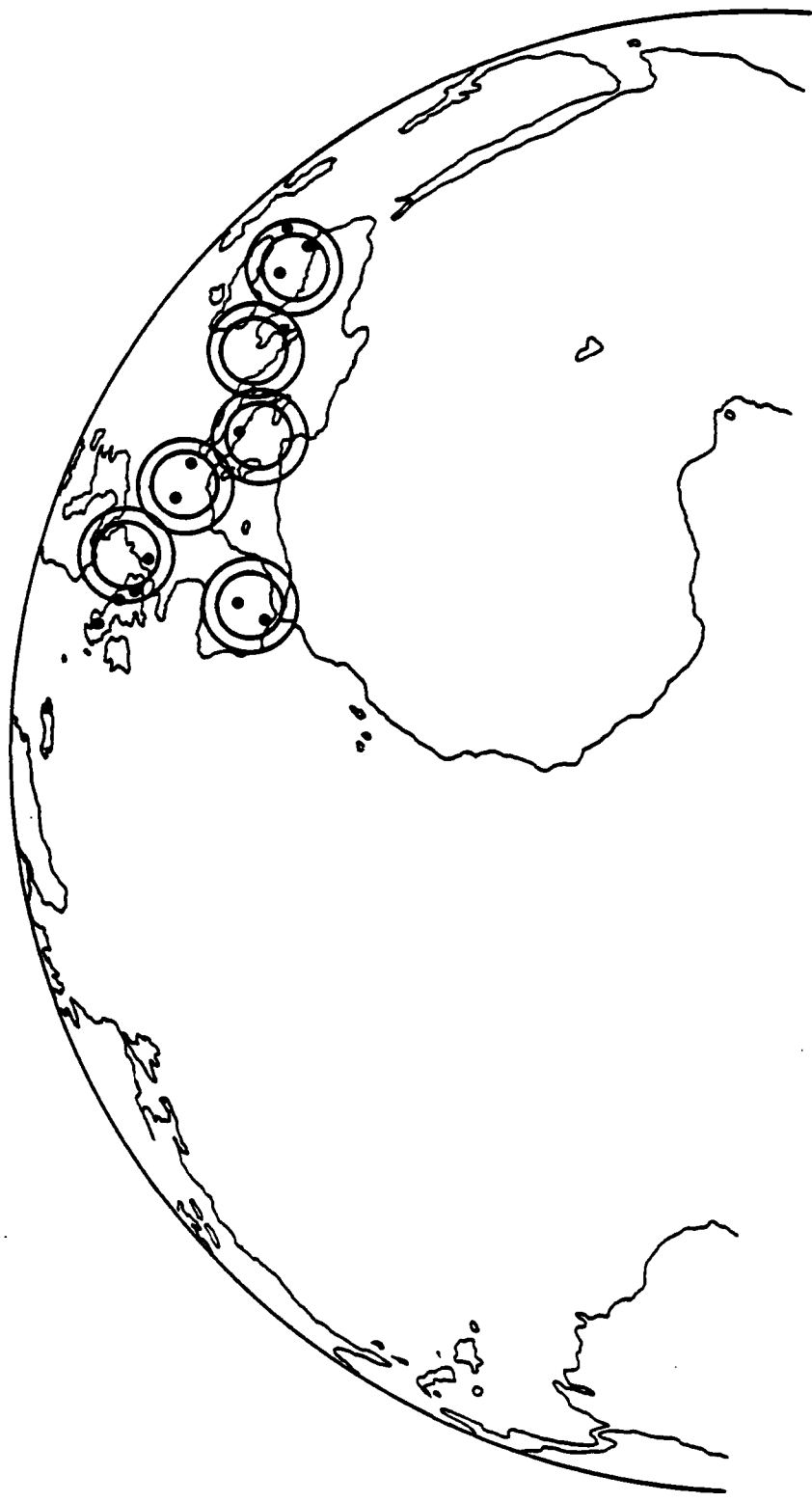


Figure A.7-4. Coverage of a Multiple Feed Antenna with Three Foot Offset Reflector

The same aperture size is assumed for each link, although, depending on antenna type selected, separate antenna apertures may be necessary to ensure truly circular polarization. Use of two small phased arrays, each 15 in x 5 in, also may be required. Coverage illustrated in Figure A.7-4 is possible with a multiple-feed antenna with an offset 3-ft reflector. In each of these systems the outer pattern contour shows the power level 3 dB down from boresight at 20 GHz and 6 dB down from boresight at 30 GHz. The inner contour represents the power level 3 dB from boresight at 30 GHz. Figure A.7-5 illustrates an alternative coverage of the 6-beam MBA providing long-haul circuits from Iceland to Turkey.

Table A.7-4 indicates comparative performance for an 8-ft diameter antenna terminal (500 Watts RF power) near Reading, England that is available for at least 99.7 percent of a typical year. This terminal was chosen as a baseline because its location is the worst both with respect to the weather and to its position in the spacecraft antenna pattern. Maximum performance at other locations can readily be estimated using data from Table A.7-3. It should be noted that in a benign environment the main limiting factor is due to the downlink EIRP of the spacecraft. However, it also is obvious that the uplink parameters may significantly affect performance of the system by 3.8 dB under some conditions. A maximum satellite transmit power of 32 Watts is assumed by comparing the Hughes 950H TWT operated in the backed-off condition (to 16 watts) for the simplest (FDMA) multiple-access system. Using a TDMA downlink, an improvement of nearly 3 dB could be obtained. The improved performance of the multiple-beam antenna is due not only to the increased gain but also to the fact that the downlink power density can be distributed more usefully to match the location of the terminals. Although present multiple-beam antennas have shown higher losses than conventional antennas, thus reducing the actual performance obtained, multiple feeds with an offset reflector appear to have the potential for reduction of these losses. It is apparent that a research and development program in this area could lead to substantial improvements in the support that could be provided to the DCS.

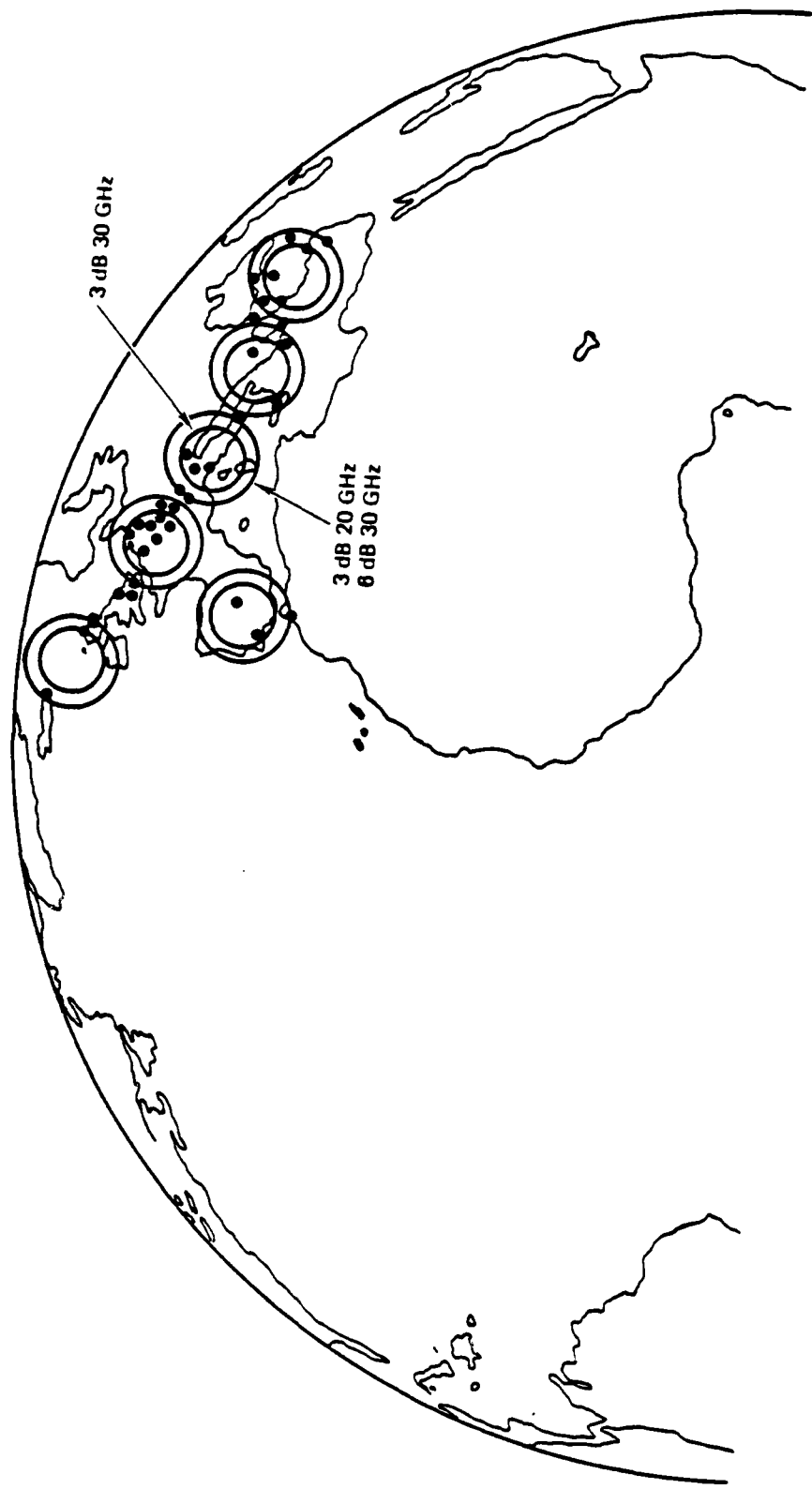


Figure A.7-5. Six Beam MNA Long Haul Coverage

Table A.7-4. Performance Comparison of Two Spacecraft Antenna Systems with a Single Frequency Translation Transponder

	Elliptical Beam Antenna		Multiple Beam Antenna		
	Uplink	Downlink	Uplink	Downlink	Frequency
Spacecraft Antenna Gain (dB)			30.5 GHz	20.7 GHz	30.5 GHz 20.7 GHz
Transmitter Power (16 Watts) in dBW			30.7		35.5
Spacecraft EIRD (Including 1 dB Losses)			12.0		12.0
Terminal EIRD (8 ft, 500 w, 1 dB Losses)			41.7 dBw		46.5 dBw
Maximum Atmospheric Loss					
Spacecraft or Terminal G/T (Boresight)	81.0 dBw	—		81.0 dBw	—
Baseline Location Antenna Pattern Loss (Max)	10.0 dB	6.4 dB		10.0 dB	6.4 dB
Boltzman's Constant (dB)	+4.4 dB	+24.0 dB		+9.0 dB	+24.0 dB
C/No Spacecraft (dB)	6.0 dB	3.0 dB		3.0 dB	2.0 dB
Bandwidth of Spacecraft Transponder (180 MHz)	228.6	228.6		228.6	228.6
S/N ratio in Spacecraft (dB)	83.7	—		91.3	—
C/No Terminal	82.6 dB	—		82.6 dB	—
Uplink Degradation Factor*	1.1	—		8.7 dB	
Required Eb/W ₀ (Coded, 10 ⁻⁵ Error Rate 1.4 dB Loss)	—	73.9 dB		—	79.7
Available Information Rate (dB)	3.8 dB	3.8 dB		0.8 dB	0.8 dB
Max Data Rate (Baseline)	—	—	6.0 dB	6.0 dB	6.0 dB
	—	—	64.1	72.9	
	2.5 Mb/s	2.5 Mb/s		19.5 Mb/s	

* Degradation of Downlink By Uplink Noise = $1 + \frac{C/No_{\text{Terminal}}}{C/No_{\text{Spacecraft}}} + \frac{1}{SNR}$ (Spacecraft)

A.7.5.2 Network Problem. It should be noted that performance figures given in Tables A.7-4 and A.7-5 reflect what could be achieved with use of a dedicated link between two small terminals in some general location. However, DCS requirements call for a number of links often connecting widely spread locations, so that exact characterization of every combination in different weather zones would not be very useful. Also, each terminal operates at much lower data rates and shares the transponder downlink power. Under these conditions (particularly if a number of narrow channels are used in lieu of a wideband channel, or if a 1-kW terminal transmitter were used) the significance of the uplink channel noise could be reduced to negligible proportions and performance of the network would depend primarily on downlink characteristics such as satellite EIRP, downlink coverage pattern, atmospheric losses, and ground-terminal performance.

The single-transponder concept is simple and provides an easy method of arranging conference calls either with the single-beam (elliptical) or multiple-beam concepts. On the other hand, the multiple-beam antenna concept by itself increases the total spacecraft throughput for a given downlink EIRP by better distribution of this power, but loses total message-handling capability because point-to-point traffic is broadcast over the entire serviced area. However, using multiple transponders (for example one transponder per downlink beam), point-to-point traffic would only be transmitted from the satellite in the feed covering the required recipient, thereby saving 83 percent of the power required compared with a single-transponder system. Figure A.7-6 illustrates how this system could be implemented in simple fashion with use of frequency translation transponders by allocating frequency blocks for the uplink corresponding to each downlink beam. The uplink receiving antenna of the satellite then would receive the entire allocated bandwidth and, after pre-amplification to avoid combiner losses, would separate out the signals by frequency band before transmission in the appropriate beam.

Table A.7-5. Performance Capability at Typical Station Location (Single Transponder)

Location	Number of 16 kb/s Voice Channels					
	Single (Elliptical Beam Antenna)			Multiple (6) Beam Antenna		
	Rain	Cloud	Fine	Rain	Cloud	Fine
Reading, England	312	780	934	1,218	3,050	3,700
Casteau, Belgium	294	734	888	1,530	3,824	4,624
Koblenz, FRG	430	1,094	1,300	2,025	5,062	6,112
Aviano, Italy	412	1,424	1,830	1,530	3,062	3,938
Naples, Italy	934	1,406	2,406	4,438	6,624	11,406
Torrejon, Spain	438	656	718	3,688	5,500	5,980
Athens, Greece	780	1,176	1,324	2,324	3,488	3,950
Incirlik, Turkey	394	594	862	1,532	2,250	2,600
Eymdag, Turkey	369	750	923	1,948	2,922	3,304

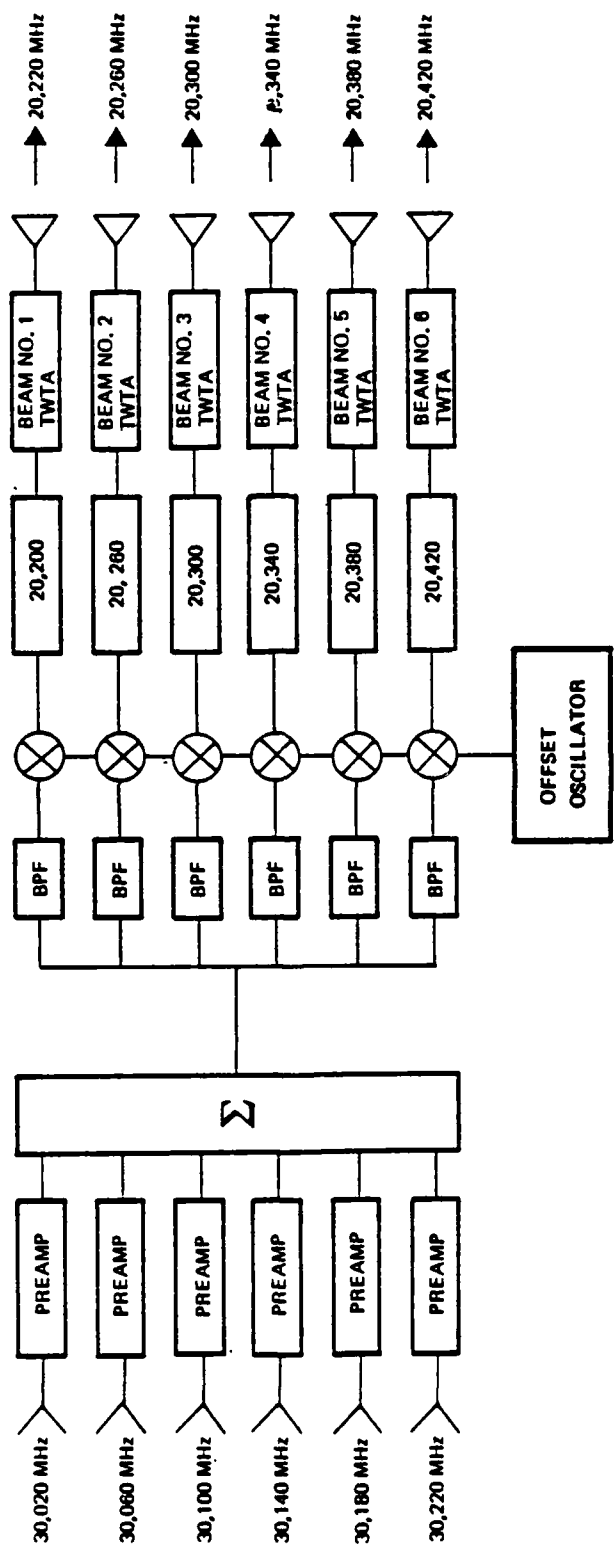


Figure A.7-6. Satellite Translation Transponder

This concept of course is equally applicable to TDMA or CDMA systems, as well as compatible with highly efficient packet switching networks. It could also be used to take maximum advantage of the multipower level capability of the 901H TWTA traveling wave tube, which can be operated at about 4, 8, 16, or 32 Watts output by increasing the spacecraft power output in beams covering areas with heavy rainfall or unusually high traffic rates.

A.7.5.3 Traffic Capability. Table A.7-5 also indicates maximum capabilities that can be expected to be available for 99.5 percent of the time at typical terminal locations, assuming sole use of a single transponder with either a single elliptical antenna or a multiple 6-beam antenna. Minimum total rates are about 5 Mbps and 20 Mbps respectively, corresponding to 321 and 1218 16-Kbps voice channels using SPADE techniques (Ref. A.7-5) with an availability of 99.5 percent or more. Average capabilities would be about 480 and 3050 channels with cloudy weather for the worst location and 1406 and 6624 channels for a terminal located in the Naples area. Using six transponders and an adaptive control system taking into account the weather at each location, this system could gain a capability of over 20,000 voice circuits using a spacecraft of about the same size as DSCS-3.

A.7.5.4 Technology Availability for ECCM Performance and Survivability. Performance in a jamming environment will be discussed in detail in a future report. However, no discussion of EHF SATCOM systems for DCS would be complete without brief consideration of electronic counter counter measures (ECCM), capabilities, and technology. Generally it can be shown that EHF offers much better potential ECCM performance than the lower frequencies, due primarily to the wide bandwidths and the narrow beamwidths that are available. Moreover, design problems of the jammer are increased substantially and greater survivability is possible for the system terminals, which can be much smaller and more mobile.

In the comparatively simple transponders discussed previously, anti-jam performance could be increased considerably over that available in the 7- to 8-GHz frequency bands if full advantage were taken of the total bandwidth that is available for maximum band spreading (i.e., 1 GHz). This is beyond the capability of current anti-jam modems of the frequency-hopping or direct-sequence types exemplified by the TATS type wideband modem and the USC-28 modem respectively, but hybrid modems using a combination of frequency hopping and pseudorandom noise direct-sequence band spreading appear to offer an economical solution.

Multiple-beam antennas (MBAs) with jammer nulling and/or beam steering offer significant improvement in uplink ECCM performance at the higher frequencies because much smaller beamwidths are available for areas such as the European theater without excessive antenna sizes. As an example, an 0.75° beamwidth is available from a 3-ft antenna aperture at 30 GHz. The same beamwidth at 7.5 GHz would require a 12-ft antenna, which is not very practical for use in space particularly because several antennas may be required to cover different areas (e.g., Europe, CONUS, and the Middle East).

Current MBAs such as those designed for DSCS III are inefficient and may not be suitable for use at EHF, where they may be even more lossy. However, recent advances in design of offset-feed antennas appear to be capable of meeting the more stringent requirements of the higher-frequency bands.

Further improvements in anti-jam performance can be obtained by use of on-board processing, which will also provide better control of traffic flow and simplify routing without use of excessive downlink microwave power resulting from broadcasting point-to-point traffic.

A.7.6 Summary and Conclusions. A SATCOM transponder system could play a very important role in long-haul communication for DCS. The 30-GHz (uplink) and 20-GHz (downlink) bands would provide adequate performance with an availability of better than 99 percent. Greater availability, say on the order of 99.99 percent, could be obtained using two terminals spaced about 30 miles apart with an ideal line-of-sight radio or a fiber-optics link. Suitable technology has been demonstrated in the laboratory, and a number of development programs are underway to produce space-qualifiable hardware. Significant performance can be provided by a simple transponder with elliptical-beam antennas. This performance can be greatly improved by use of a beam MBA, and even further improved using six transponders, or one per beam.

A.8 PACKET RADIO

The brief description of technical and operational aspects of a packet radio system given in this section provides the needed background for examining the potential of packet radio with respect to DCS III future requirements.

A.8.1 Packet Radio Technology

Packet radio is a technology that extends application of packet switching, as evolved for networks of point-to-point communication land lines, to the domain of radio. This methodology offers a highly efficient way of using a multiple-access radio channel with a potentially large number of fixed and mobile subscribers to support communication and to provide local distribution of information over a wide geographic area.

A.8.1.1 Packet Switching. The rapid growth in packet communications that has taken place during the last decade following successful development of the ARPANET system is directly related to the increasing demand for effective telecommunication service to handle computer communications (Ref. A.8-1 and A.8-2). This trend became apparent during that period because it previously had not been found cost-effective to utilize minicomputers, and later on, microprocessors, as packet switches in a large-scale network. In a packet-switched network the unit of transmission is called a packet. As shown in Figure A.8-1, a packet consists of a preamble, a header, text, and a checksum. The preamble is used to synchronize the transmitting and receiving units, and to flag the "start" of the message. The message is usually of variable length up to a maximum of a few thousand bits, and includes a variable-length header, text, and checksum. The header contains source and destination identities, routing instructions, package number, and control bits for priority indication, and the checksum provides error detection.

Packet switching was originally designed to provide efficient network communications for "bursty" traffic and to facilitate computer-network-resource sharing. It is well known that the computer traffic generated by a given user is characterized by a very low duty cycle in which a short burst of data is sent or received, followed by a longer quiescent interval after which additional traffic will again be present. Use of dedicated

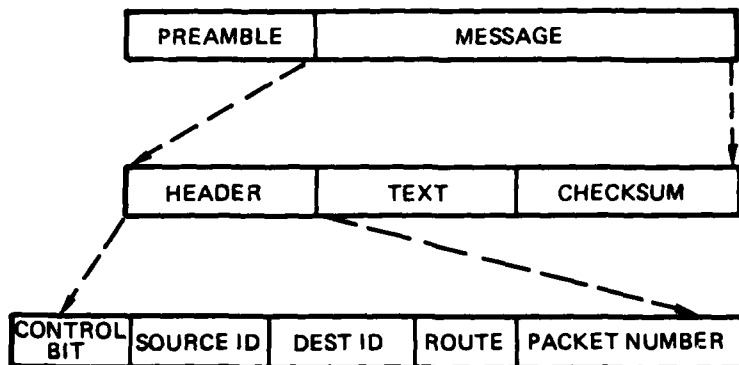


Figure A.8-1. Packet Format

circuits for this traffic therefore would normally result in very inefficient usage of the communication channel. A packet of some appropriate size is also a natural unit of communication for computers, in that processors store, manipulate, and transfer data in finite-length segments as opposed to indefinite-length streams.

A.8.1.2 Packet Radio. Packet radio is a technology that extends the original packet switching concepts which evolved for networks of point-to-point communication land lines to the domain of radio networks (Ref. A.8-3). The rapid development in this area has been greatly stimulated by need to provide computer-network access to fixed and mobile terminals and to computer communications in the mobile environment. Packet radio offers a highly efficient way of using a multiple-access channel, particularly with fixed and mobile subscribers and large numbers of users with bursty traffic. During the early 1970s the ALOHA project at the University of Hawaii demonstrated feasibility of using packet broadcasting in a single-hop system (Ref. A.8-4). The Hawaii work led to development of multihop, multiple-access Packet Radio Network (PRNET) under sponsorship of the Advanced Research Projects Agency (ARPA) (Ref. A.8-5).

PRNET is a fundamental network extension of the basic ALOHA system and broadens the realm of packet communications to permit mobile applications over a wide geographic area. Use of broadcast radio technology for local distribution of information can also provide a degree of flexibility in rapid deployment and reconfiguration not currently possible with most fixed-plant installations.

A.8.1.3 Related Techniques. In addition to the strong ARPANET- and ALOHA-system influences, the following three developments during the early 1970s were largely responsible for evolution of packet switching to the radio environment:

- Microprocessor and associated memory technology permitting incorporation of computer processing at each packet radio network node in a form compatible with mobile usage and portable operation.
- Surface acoustic wave (SAW) technology which can perform matched filtering (to receive wide-band radio signals) on a very small sub-strata of quartz or similar piezo-electric material.
- Conceptual awareness within computer and communications communities of the importance of "protocols" in development of network-management strategies.

A.8.2 Packet Radio System

All users in a packet-radio network are assumed to share a common radio channel, access to which is controlled by microprocessors in the packet radios. In contrast to a CB radio channel in which contention for the channel is directly controlled by the users (who at best can do a poor job of scheduling the channel), the packet-radio system decouples direct access to the channel from user access requests. The microprocessors can dynamically schedule and control the channel within a fraction of a second to minimize or avoid conflict (overlapping transmissions), particularly when the transmissions are very short.

A.8.2.1 Signaling in the Ground Radio Environment. Packet-radio technology is applicable to ground-based, airborne, seaborne, and space environments. Of these, ground-based networks perhaps encounter the most difficult environment in terms of propagation and RF connectivity in that ground radio links, particularly when mobile terminals are involved, are subject to severe variations in received signal strength due to local variation in terrain and man-made structures. In addition, reflections give rise to multiple signal paths leading to distortion and fading, or the differently delayed signals interfere at a receiver. As a result of these phenomena RF connectivity is difficult to predict and may abruptly change in unexpected ways as mobile terminals move about. Spread-spectrum

techniques are applied to the packet radio systems to combat the multipath and jamming environment. Following Subsections A.8.2.1.1 through A.8.2.1.4 briefly discuss radio frequency bands which are most appropriate for ground-base radio networks, multipath effects, man-made noise at these frequencies, and spread-spectrum signaling and its application to ground-based packet radio systems.

A.8.2.1.1 Frequency Band. Operational characteristics of the radio frequency band have a major impact on the packet radio design, rendering it desirable for practical packet-radio systems to use radio frequencies in the upper VHF band, in the UHF band from 300 MHz to 3 GHz, and in the lower portion of the super-high-frequency (SHF) band from 3 GHz to 30 GHz.

An additional factor that must be considered for operational systems is the authorization to radiate packet-radio transmissions due to the fact that VHF and UHF bands are already heavily allocated and that use of spread-spectrum signals potentially could allow coexistence of a packet radio system with existing users of the same frequency band. However, this is a relatively new concept from the regulatory point of view, and significant technical issues would have to be resolved to establish feasibility of coexistence.

A.8.2.1.2 Man-made Interference. Man-made interference in the RF frequency band includes both intentional and unintentional interference. Resistance to intentional interference (jamming) is of utmost importance in strategic and tactical military applications and strongly affects the details of waveform design and system complexity. Unintentional interference results from sources that may be characterized as impulsive in nature, such as automobile ignition, spark discharge, radars, and AC power distribution systems. Packet radios in such environments might therefore experience a few bit errors in almost every packet received and would require error correction in order to maintain system throughput.

A.8.2.1.3 Spread Spectrum Waveform Design Considerations. The packet-radio signaling waveform must be designed to perform well with respect to natural induced environments arising from both intentional and unintentional interference, including system self-interference due to the multiple-access/random-access nature of the packet-radio system. It should be noted that limitations on signaling rate due to multipath can be reduced

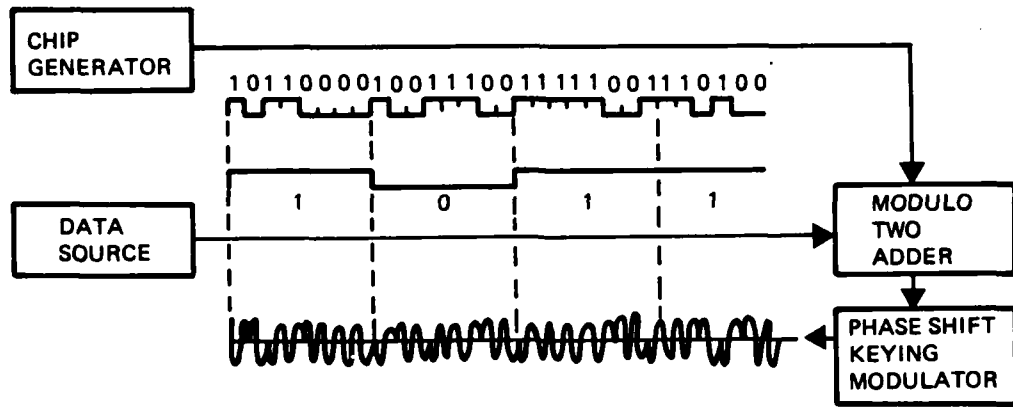
by using spread-spectrum techniques, which also provide rejection of interference and ability to coexist with other systems in the RF band. For these reasons, the forms and associated performance attributes of two major types of spread-spectrum signals that have been found well-suited for packet radio applications are described below.

The most commonly used forms of spread-spectrum waveforms are direct-sequence pseudo-noise (PN) modulation, frequency hopped (FH) modulation, and hybrid combinations of these techniques (Ref. A.8-6 and A.8-7). A typical form of PN modulation is illustrated in Figure A.8-2a. A source produces binary data at a rate of R bits per second. A pseudo-random generator produces a stream of binary "chips" at NR chips per second when N is an integer which is one or more orders of magnitude greater than unity. Each data bit is module-two added to a sequence of N chips to form a PN-modulated data stream which is then input to a modulator in order to convert it to a form suitable for transmission over the radio channel. The phase shift keying (PSK) modulator illustrated in the figure is one way of accomplishing this process.

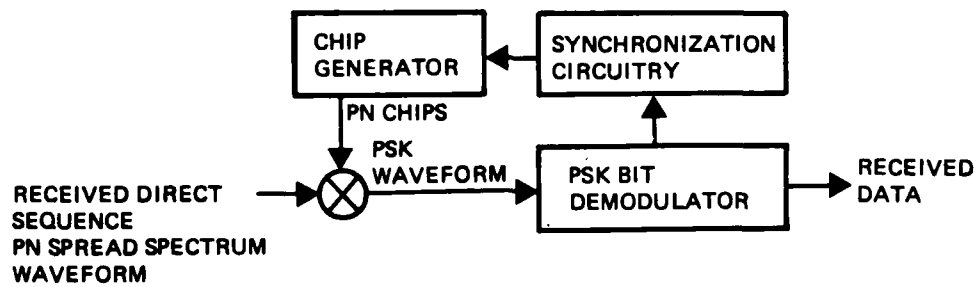
A typical form of demodulation is shown in Figure A.8-2b. The effect of PN-modulating the data stream is to increase the digital rate going into the PSK modulator from R bits per second to NR chips per second. Consequently, the occupied RF bandwidth of the resulting waveform is increased by a factor of N .

Figure A.8-3 illustrates one of many variations of a frequency-hopped system. Data from the source is input directly to a FSK modulator to produce a signal which might ordinarily be converted to a fixed RF frequency for transmission. However, in this case a programmable synthesizer is used as a local oscillator (LO) to dynamically select the RF frequency for transmission. The LO pseudo-randomly hops among N frequencies over time as determined by a suitable algorithm. As with PN modulation, the bandwidth used by the system is N times that used by the system without frequency hopping, and the wider bandwidth of a FH system yields certain advantages in return for expanded bandwidth.

Combinations of FH and PN techniques can result in a waveform with desirable attributes of both techniques. For example, on each RF hop, one of M PN sequences could be transmitted in order to send $\log_2 M$ bits of

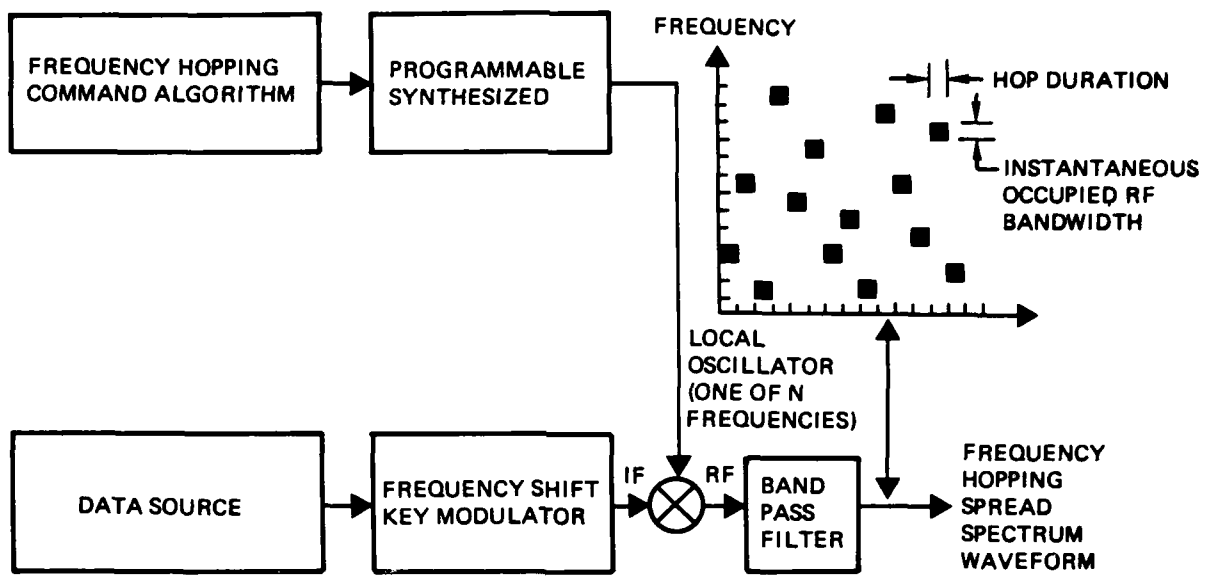


(a) Signal Generation

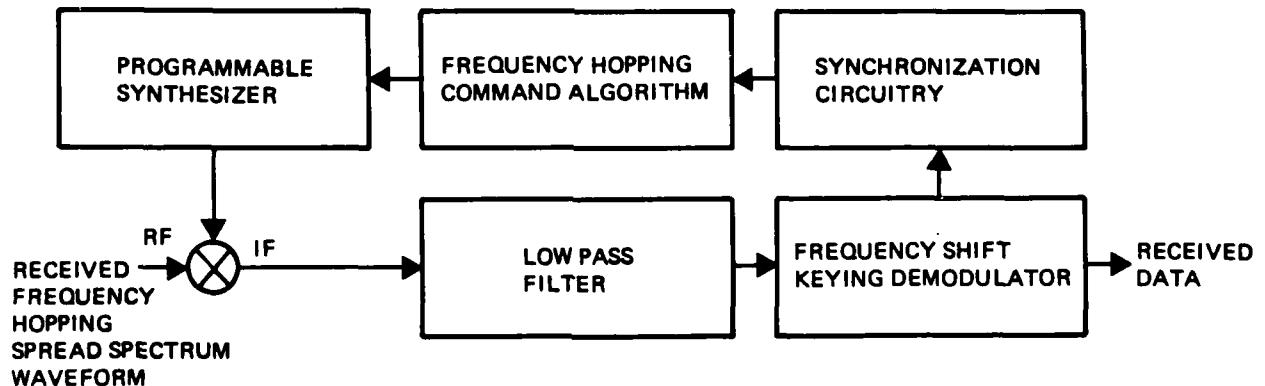


(b) Signal Reception

Figure A.8-2. Pseudonoise Spread Spectrum System



(a) Signal Generation



(b) Signal Perception

Figure A.8-3. Frequency Hopping Spread Spectrum System

information. Such a technique could achieve diversity reception based on components and reduced symbol distortion, but a receiver for this type of system can be complex.

A.8.2.2 Multiple Access and System Performance. A variety of theoretical and experimental studies have been carried out to determine the most effective techniques for sharing a Multiple Access (MA) channel. Classic ALOHA, slotted ALOHA, and carrier sense will be discussed.

A.8.2.2.1 Classic ALOHA. One of the simplest techniques known as classic ALOHA was designed for very-low-duty-cycle applications and involves no control other than the ability to recognize overlapping packet conflicts when they occur and to randomly reschedule these unsuccessful transmissions at a later time. This scheme is normally implemented using a positive acknowledgement and timeout procedure based on packet checksums (Ref. A.8-7).

In considering the channel throughput of a classic ALOHA it should be assumed that the start times of packets in the channel comprise a Poisson point process characterizing the parameter, packets/second. If each packet lasts λ seconds, the normalized channel traffic, G , may be defined as

$$G = \lambda\tau \quad (\text{A.8-1})$$

If it also is assumed that only packets which do not overlap with any other packet are received correctly, the $\lambda' < \tau$ may be defined as the rate of occurrence of those packets which are received correctly, and the normalized channel throughput, S , as

$$S = \lambda' \tau \quad (\text{A.8-2})$$

The probability that a packet will not overlap a given packet is just the probability that no packet starts τ seconds before or τ seconds after start time of the given packet. Then, because the point process formed from the start times of all packets in the channel was assumed Poisson, the probability that a packet will not overlap any other packet is $e^{-2\lambda\tau}$, or
therefore,

$$(A.8-3)$$

versus channel traffic for a classic ALOHA
is shown in figure A.8-4.

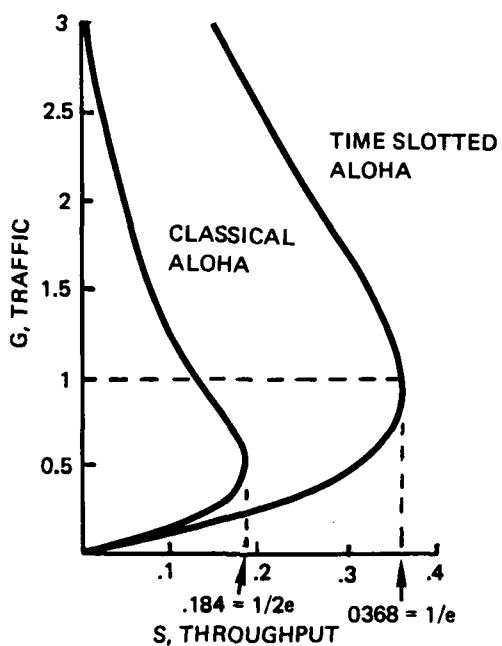


Figure A.8-4. Traffic Versus Throughput for a Bare ALOHA Channel and a Slotted ALOHA Channel

Figure A.8-4 indicates that as channel traffic increases, throughput also increases until it reaches its maximum value of $S = 1/23 = 0.184$, which is known as the capacity of a classic ALOHA channel and occurs for a value of channel traffic equal to 0.5. If the channel traffic is increased to a value above 0.5 the throughput of the channel will decrease.

A.8.2.2.2 Slotted ALOHA. A time-slotted version of random access known as slotted ALOHA also is possible (Ref. A.8-8 and A.8-9). In this process a central clock establishes a time base for a sequence of "slots" of the same duration as a packet transmission. A user with a packet to transmit then synchronizes the start of his transmission with the start of a slot, whereby if two messages conflict they will overlap completely, rather than partially.

The curve for the slotted ALOHA channel with n independent users, and in the limit as $n \rightarrow \infty$, is given by the relation

$$S = Ge^{-G} \quad (\text{A.8-4})$$

which also is plotted in Figure A.8-4 (curve labeled "slotted ALOHA"). It should be noted that the message rate of the slotted ALOHA channel reaches a maximum value of $1/e = 0.368$, or twice the capacity of the pure ALOHA channel.

A.8.2.2.3 Carrier Sense Multiple Access. One of the more efficient control techniques for the ground radio multiple access is Carrier Sense Multiple Access (CSMA) wherein each sender first senses the channel and then transmits a packet only if the channel is idle (Ref. A.8-10 and A.8-11). If the channel is determined to be in use, the transmission is rescheduled at a later time when the same procedure will be invoked. Various elaborations on the CSMA scheme offer the possibility of achieving 70-90 percent utilization of the channel with low end-to-end transmission delay per packet, as indicated in Figure A.8-5.

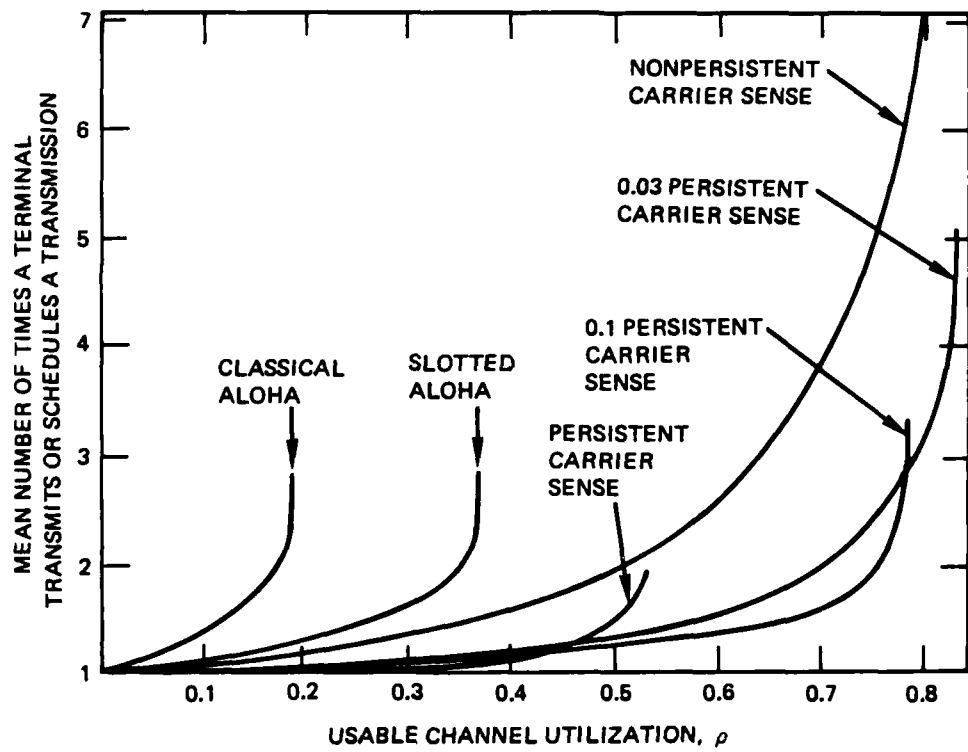


Figure A.8-5. Channel Utilization of Various Multiple Access Methods of Packet Radio

A.8.2.3 Network Elements. The packet-radio system consists of the three primary network elements of terminals, control stations, and repeaters, as illustrated in Figure A.8-6.

A.8.2.3.1 Terminals. A terminal contains the RF and digital processing circuits. Necessary terminal capabilities include the following functions:

- Packet generation, with ability to format header, add parity, and modulate the packet for transmission.

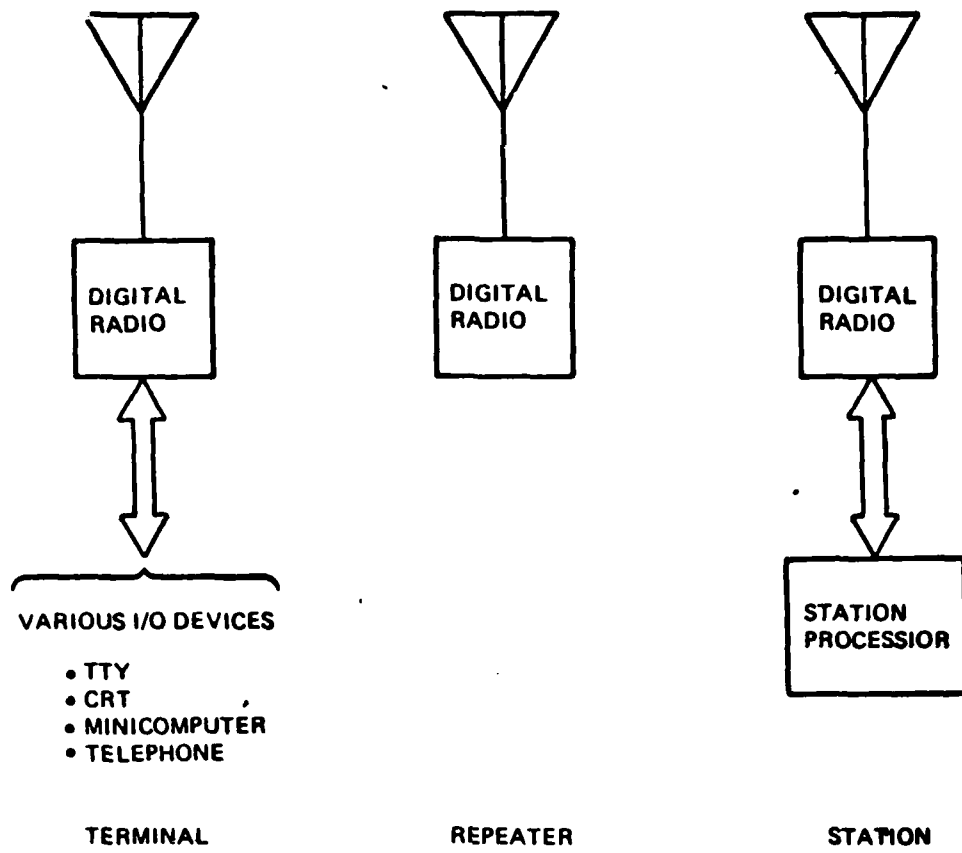


Figure A.8-6. Packet Radio Network Elements

- Packet reception, with ability to check the header and text portion and to route the arriving packet to its destination or local user.
- Packet retransmission, when acknowledgements are not received in a certain time out.
- Efficient routing control between terminal and the control station.

A.8.2.3.2 Control Station. The control station demodulates the incoming packets, stores and switches the information at the digital band, and remodulates the packets onto a broadcasting channel. In addition it has capability to implement network protocols including initialization, routing, flow control, directory, and accounting functions, and it also serves as an interface to other networks. All the above functions are performed by an on-board microcomputer.

A.8.2.3.3 Repeaters. In the event that some of the terminals are too far away from the control station, radio repeaters are used as relay devices which provide network area coverage by extending the range between terminals and stations. A repeater can operate on a single frequency for transmitting and receiving, switching off its receiver momentarily while it transmits a package. Some packages will be lost when this happens, and as in the case of a collision will have to be retransmitted. However, operating at a single frequency saves the expense of frequency-translation equipment. The repeaters use a single frequency for relaying packages to the control location and a different frequency for relaying packets back to the terminals. If two frequencies are used in this way the repeater antennas pointing towards the central station can be highly directional.

In general, repeaters may not require the same degree of mobility as terminals and frequently may be unattended, which means that higher antenna mounts may be feasible and longer-life batteries are desirable. For a highly survivable network each terminal should be within radio range of two or more repeaters, so that this increased network interconnectivity would improve survivability. Controlled routing procedures permit use of preferred routes to minimize delay and prevent propagation of duplicate messages. However, in the event of repeater failure automatic alternate routing procedures will be implemented.

A.8.3 Experimental Packet-Radio Developments

Although significant analytical progress has been achieved, a complete mathematical analysis of a multiple-access multihop radio network is not yet possible. Computer simulations having reasonable detail are being developed and show great promise, but their practicality and degree of realism remain to be validated. Consequently, the Advanced Research Project Agency (ARPA) has sponsored the experimental packet-radio program detailed in following Subsections A.8.3.1 through A.8.3.3.

A.8.3.1 ARPA Packet-Radio Experimental Program. In 1973 (ARPA) initiated a theoretical and experimental packet radio program having the initial objectives of developing a geographically distributed network consisting of an array of packet radios managed by one or more mini-computer-based stations and of experimentally evaluating the performance of that system

(Ref. A.8-3). The first packet radios were delivered to the San Francisco Bay area in mid-1975 for initial testing and a quasi-operational network capability was established for the first time in September 1976.

Approximately 50 radios are currently available for use. The location of the major elements of the packet radio testing during 1977 also is shown in Figure A.8-7.

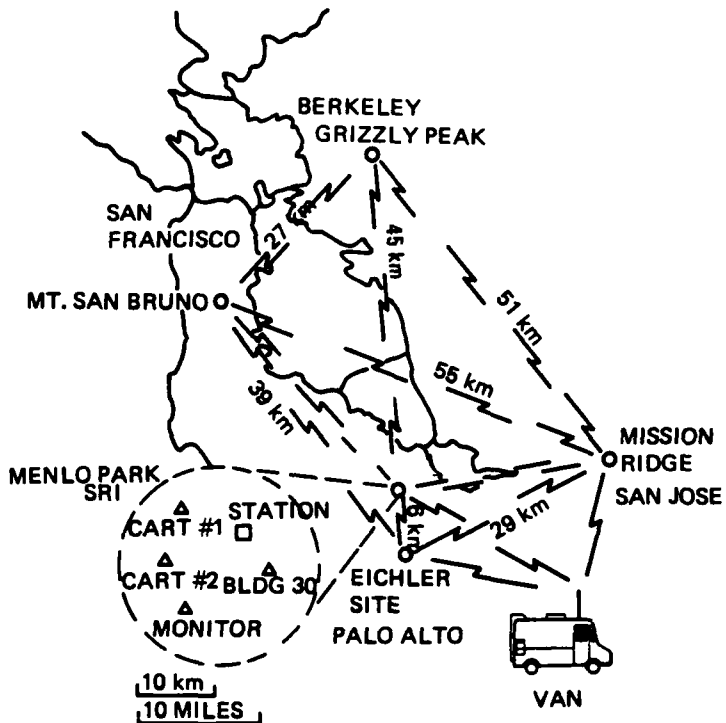


Figure A.8-7. Location of Major Elements of the 1977 Packet Radio Testbed

The packet-radio equipment currently in use in the Bay Area testbed is designed to support development and evaluation of fundamental network concepts and techniques. The initial radio experiment was designated the Experimental Packet Radio (EPR), as described in Subsection A.8.3.2. A major new development in 1978 was completion of an Upgraded Packet Radio (UPR), which is similar in architecture to the EPR but which in addition has the ECCM features necessary to verify viability of packet-radio concepts in tactical military applications.

A.8.3.2 Experimental Packet-Radio Unit. The EPR design which has been implemented for use in the testbed is functionally configured as shown in Figure A.8-8. Each EPR consists of a radio unit which transmits and receives packets and of a microprocessor-based digital unit which controls the radio and provides packet header processing (e.g., for routing of packets between nodes). An EPR may operate as a repeater or may be connected to a user host computer or terminal or to a station. The interface between the user equipment and the EPR digital unit is the portal through which packets enter and leave the network.

The EPR radio unit operates with a fixed PN spread-spectrum pattern which for simplicity in implementation is identical for each transmitted bit. Two transmission data rates of 100 and 400 Kbps are available, with corresponding spread-spectrum patterns of 128 and 32 chips per bit respectively. The 100-bps rate is used for links with potentially large multipath spreads because the fixed-bit-length PN chip pattern does not provide ability to discriminate against intersymbol interference. The radio unit operates in a half-duplex mode. When a packet is transmitted, the preamble header and text are read from microprocessor memory under direct memory access (DMA) control. The radio unit completes the packet format previously shown in Figure A.8-1 by adding a 32-bit cyclic redundancy checksum (CRC), then differentially encodes the data, and adds (mod 2) the appropriate PN chip pattern for the selected data rate. The resulting PN-modulated stream is then applied to a minimum-shift-keying (MSK) modulator, the signal is up-converted to a selected 20-MHz portion of the 1710-1850 MHz band, and power is amplified and transmitted through an azimuthally omnidirectional antenna.

When not transmitting, the EPR remains in the receiver mode, and an arriving packet proceeds through RF-amplification, down-conversion, IF-amplifier, and wideband automatic gain control (AGC) functions. Because the PN chip patterns used for the 100- and 400-Kbps data rates are chosen for low-cross-correlation performance, two parallel receive chains following the IF amplifier/AGC can be simultaneously active. A fixed surface acoustic wave (SAW) device is used to match filter the PN-modulated waveform two bits at a time in a differential detector. The outputs of the differential detector are used to set a narrowband AGC, and after a

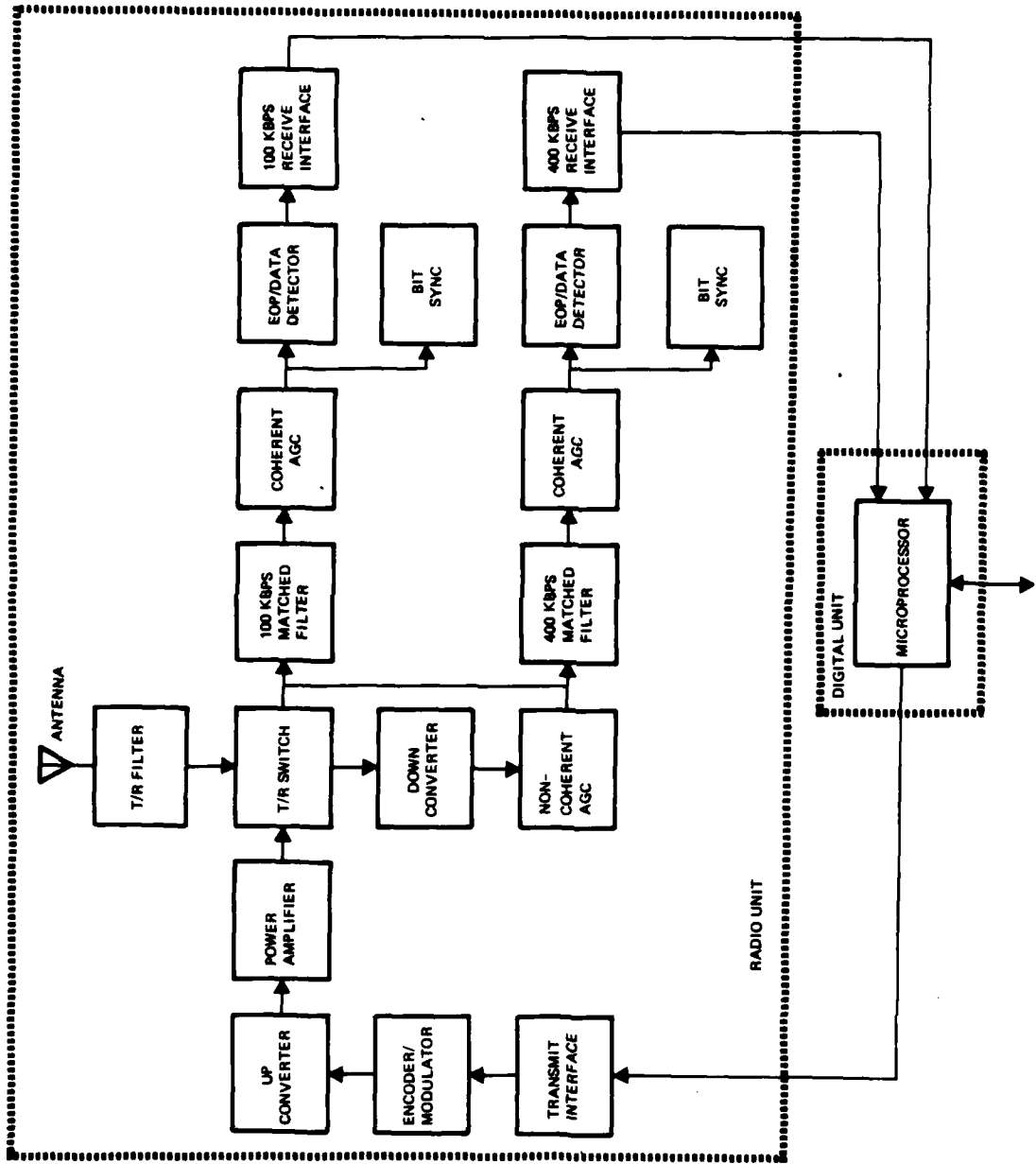


Figure A.8-8. Experimental Packet Radio (EPR) Configuration

phase-locked loop bit sync circuit has settled and the end of preamble (EOP) bit pattern has been detected, the differentially detected data in the active channel are passed to microprocessor memory under DMA control. The microprocessor executes the appropriate protocol software to determine whether the received packet should be relayed, delivered to an attached user or station, or discarded.

A.8.3.3 Upgraded Packet Radio Unit. The upgraded packet-radio (UPR) design which has been developed in response to existing need differs from the EPR design primarily in its enhanced electronic counter countermeasures (ECCM), low probability of intercept, and position-location capabilities.

In the UPR, a PN pattern which varies on a bit-by-bit basis is used to spread-spectrum-modulate each bit. As a result the UPR must have a programmable matched filter to receive the PN-modulated waveform, and the UPR network must maintain a degree of synchronization among network elements to enable the receiver to generate the same PN sequence as the sender. Timing is provided by means of an accurate time-of-day clock maintained by all the UPRs. In addition to varying the PN pattern used, a higher spread factor (or number of chips per bit) is used in the UPR than in the EPR. The data rate in the UPR is approximately the same as in the EPR, but the corresponding bandwidth of the UPR is larger at approximately 140 MHz (i.e., 1710-1850 MHz).

Reliable packet transmission in the EPR system relies on error detection and retransmission strategies. These techniques are inadequate in a tactical environment because they allow very simple jamming strategies to force large numbers of packet retransmissions with a low attendant throughput. The UPR is provided with a forward error correction (FEC) mechanism based on convolutional encoding and sequential decoding which operates in combination with error-detection and packet-retransmission techniques.

The functional organization of the UPR is illustrated in Figure A.8-9. Similarly as in the EPR, the UPR digital unit interfaces with user terminal equipment by means of a direct memory access (DMA) channel and with the radio unit by means of DMA channels under processor control.

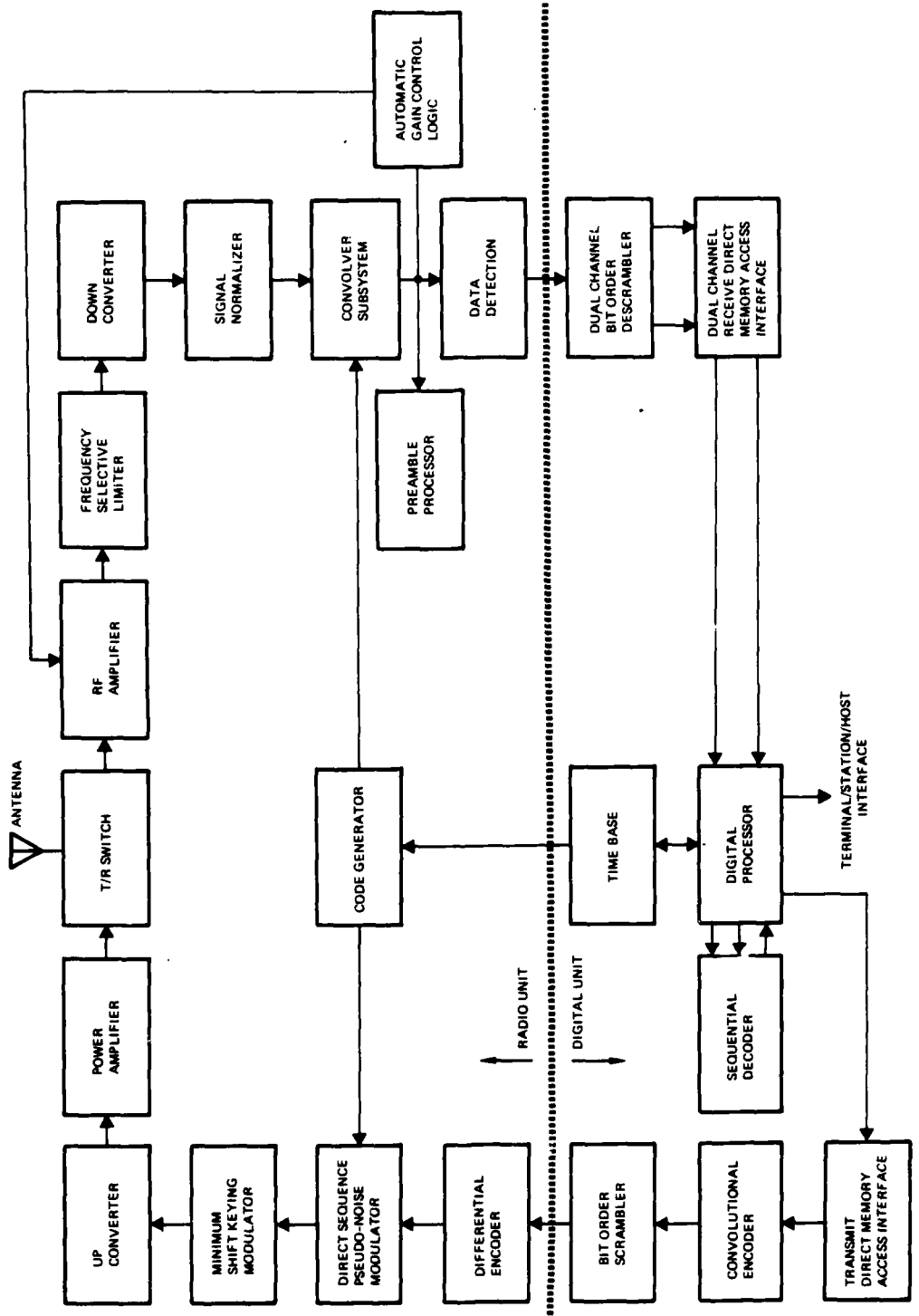


Figure A.8-9. Upgraded Packet Radio (UPR) Configuration

When a packet is to be transmitted the processor activates a DMA channel to control and monitor the transmission. Under DMA control, the packet is read from the processor memory, convolution encoded with a constraint length 24 codes, and loaded into a buffer prior to scrambling (bit order permutation). The packet data are then read from the buffer bit by bit in pseudorandom order, differentially encoded, and passed to the spread-spectrum modulator, where each data bit is module-two added to each chip of the PN chip sequence used to encode that bit. The-PN modulated chip sequence is then passed to a PSK modulator that is implemented with a SAW device having an IF output at 300 MHz. The signal is upconverted to 1780 MHz amplified to 10W and is fed to the azimuthally omnidirectional antenna.

The UPR operates in a half-duplex mode. When the UPR is not transmitting, received packets pass from the antenna through a number of RF amplifier/automatic gain control (AGC) stages. The signal is then processed by two frequency selective limiter (FSL) stages which provide an adaptive notching mechanism for narrowband interference. After downconversion to 300 MHz, the signal is processed by a signal normalizer which tries to normalize any wideband source of interference. The UPR can also be operated with an adaptive antenna array to null wideband jammers.

The convolver subsystem provides the spread-spectrum matched filtering function. During the preamble of the packet the convolver outputs are further processed by a preamble processor, where packet detection and synchronization functions are performed. During the remainder of the packet, the convolver outputs are processed by the data-detection circuitry, which makes hard binary bit decisions and provides a matched filter function for the postamble sequence. Received packets are buffered in one of the receiver's descramblers prior to bit reordering and storage of the packet in processor memory under control of a DMA channel. Two receive descrambler/DMA channels are provided to allow reception of two successive packets with minimum interpacket arrival time. When a packet has been received and stored in memory, the processor initializes DMA transactions with the sequential decoder to decode the packet. The

decoding process thus takes place "off-line" so that additional packets may be received in memory while previous packets are still being decoded. As soon as the packet header is decoded it may be submitted to network protocol processing to determine disposition of the packet.

A.8.4 Packet Satellite Experiment

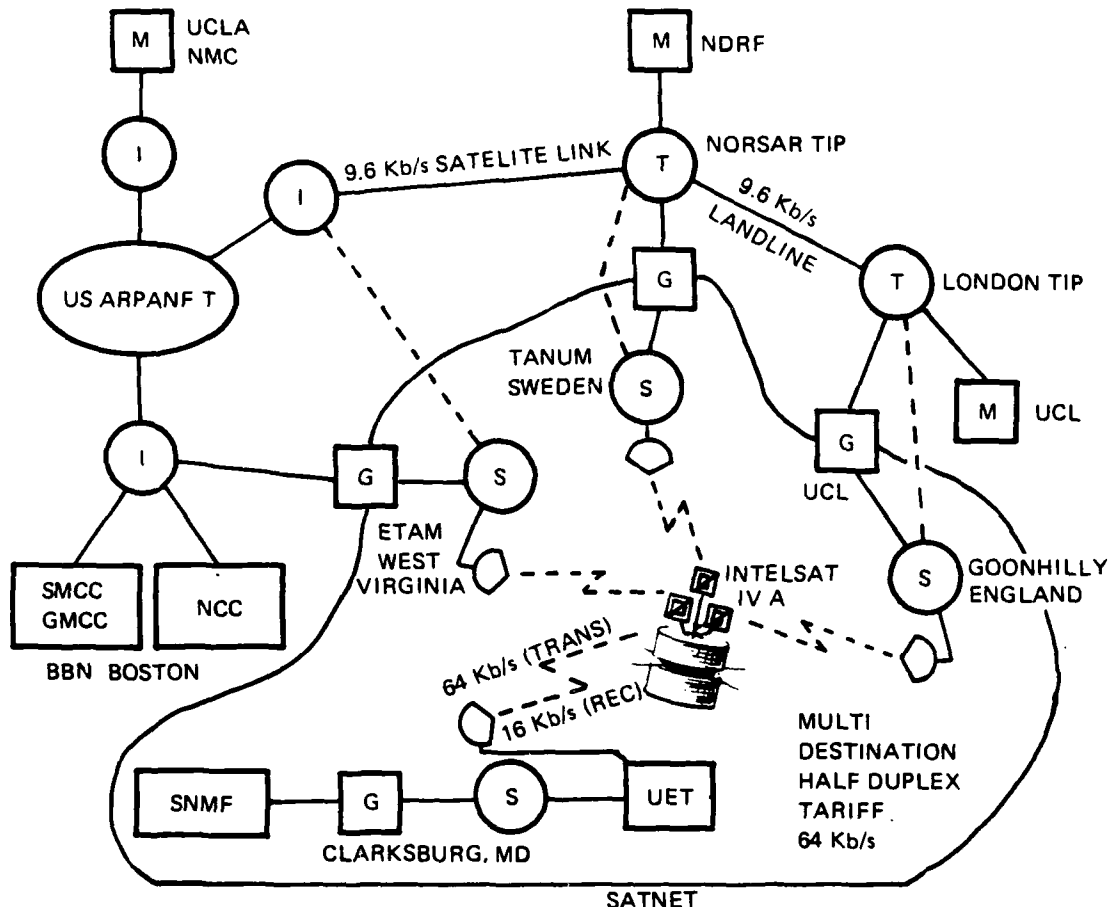
The two packet satellite experiments and efforts now in progress are the Atlantic Packet Satellite experiment and the Wideband Experimental Integrated Switched Network, as discussed in following Subsections A.8.4.1 and A.8.4.2.

A.8.4.1 Atlantic Packet Satellite Experiment. The Atlantic Packet Satellite Experiment serves as the development vehicle and experimental testbed for the overall Packet Satellite Program, and includes both the experimental SATNET satellite network and supporting development and measurement activities and facilities (Ref. A.8-12). A schematic representation of facilities supporting this effort is shown in Figure A.8-10.

Participating organizations include Bolt Beranek and Newman, Inc. (BBN), Communications Satellite Corporation (COMSAT), LINKABIT Corporation, MIT Lincoln Laboratory, and the University of California at Los Angeles (USCA) in the United States, the University College London in England, and the Norwegian Defense Research Establishment in Norway. Technical coordination is the responsibility of LINKABIT. The project is jointly sponsored by the Defense Advanced Research Projects Agency (DARPA), the British Post Office (BPO), and the Norwegian Telecommunications Authority (NTA), with participation of the Defense Communications Agency (DCA) and the USAF Space and Missile Systems Organizations (SAMSO).

A.8.4.1.1 Experimental Facilities. As noted in Figure A.8-9, SATNET is composed of four earth stations which communicate with each other over a shared channel derived from the Atlantic INTELSAT IV-A satellite. These earth stations, located at Etam WV, USA, Goonhilly Downds, England, and Tanum, Sweden, are INTELSAT Standard.

Although SATNET hardware facilities of SATNET are limited to four earth stations at the present time, the cognizant design activities assume that potential future networks might include hundreds of earth stations.



H HOST
 I INTERFACE MESSAGE PROCESSOR (IMP)
 T TERMINAL INTERFACE MESSAGE PROCESSOR (TIP)
 S SATELLITE INTERFACE MESSAGE PROCESSOR
 G GATEWAY COMPUTERS
 M NETWORK MEASUREMENT FACILITY
 UET UNATTENDED EARTH TERMINAL (G-T-29) (G-T-29)
 SNMF SATELLITE NETWORK MEASUREMENT FACILITY
 NCC NETWORK CONTROL CENTER
 SMCC SATELLITE MONITORING AND CONTROL CENTER
 GMCC GATEWAY MONITORING AND CONTROL CENTER
 -- DEBUGGING LINES

Figure A.8-10. Schematic of SATNET Experiment

A.8.4.1.1 Communications Channel. A 38-kHz channel is shared among the earth stations in accordance with demand-assignment multiple-access techniques, this channel being one of the 800 possible frequency-division multiplexed channels in the global SPADE transponder of the Atlantic INTELSAT IV-A satellite. This full-period assigned channel is operated at nominal power levels, supporting 64-kbps data transmission with a bit error probability on the order of 10^{-6} to 10^{-7} to an INTELSAT Standard A earth station.

A.8.4.1.2 Earth Station Equipment. Figure A.8-11 shows the major subsystems located at each of the earth stations in block diagram form. These subsystems implement the various functions identified in Figure A.8-12. The earth-station RF-transmission, RF-reception, and RF/IF-conversion equipment is conventional, and at the large stations is shared with other channels which access the SPADE transponder.

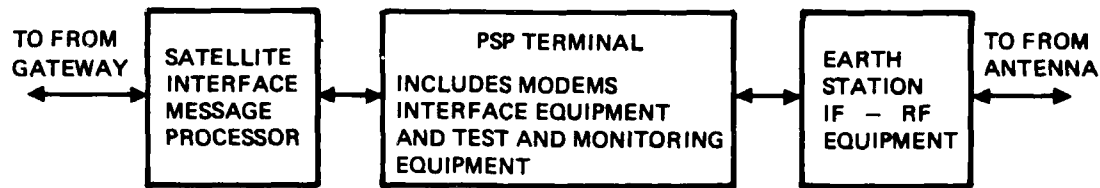


Figure A.8-11. Earth Station Equipment Associated with SATNET Experiment

The PSP terminal consists of redundant-burst modems and associated frequency-selection interface equipment to support a variety of transmission modes, as well appropriate equipment to support both local and remote test and monitoring functions. The digital 32-kilosymbol-per-second microprocessor-based modems used in the PSP terminals are designed to provide very rapid burst acquisition to process both BPSK and QPSK packets with near-optimum error-rate performance, and to automatically acquire certain performance and monitoring information (e.g., signal-to-noise ratio and frequency offset) with each packet reception.

AD-A801 360

TRW DEFENSE AND SPACE SYSTEMS GROUP REDONDO BEACH CA
EVALUATION OF DCS III TRANSMISSION ALTERNATIVES, PHASE 1A REPORT—ETC(U)
MAY 80 T M CHU
TRW-35142-APP-A

F/8 17/2.1

DCA100-79-C-0044

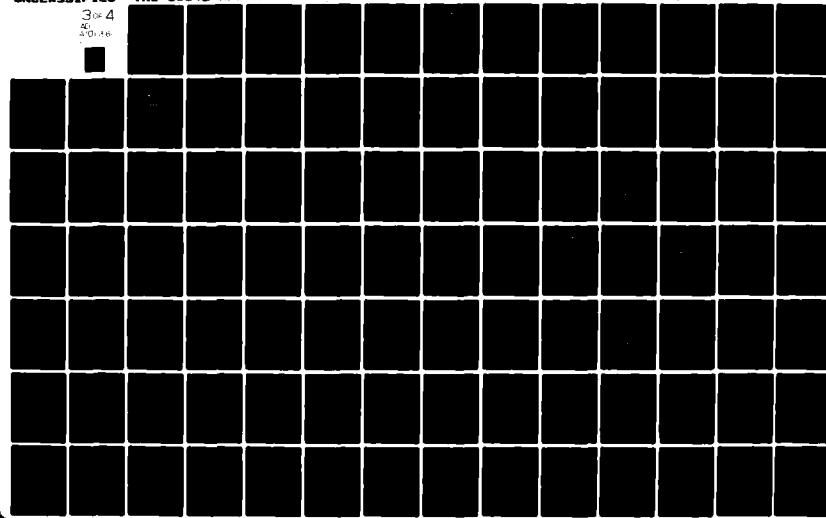
ML

UNCLASSIFIED

30x4

40x6

20x6



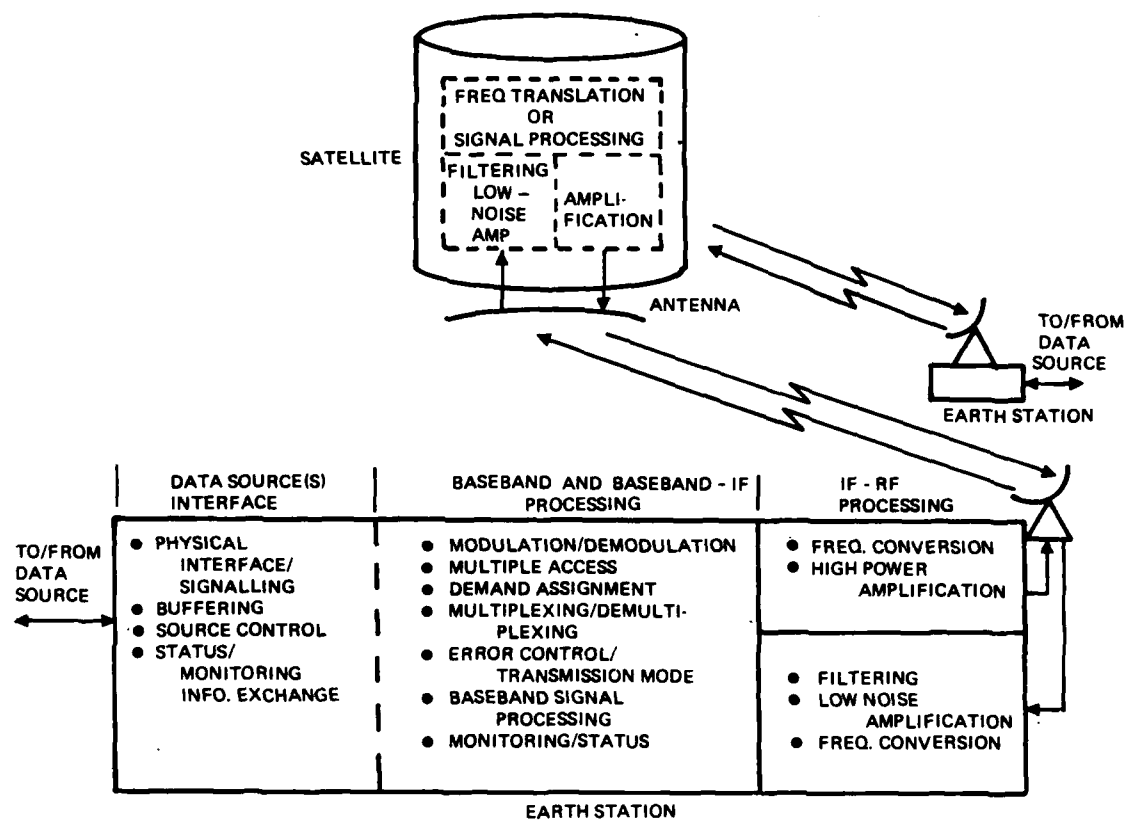


Figure A.8-12. Block Diagram of SATNET System

The interface equipment of the PSP terminal allows control over the bit patterns (preambles) used for acquisition and bit framing, and also provides local and remote capability to control certain system parameters (e.g., preamble lengths) and to support certain monitoring and testing functions.

Network protocols are implemented in the Satellite Interface message Processor (Satellite IMP), a Honeywell 316 minicomputer with 32K words (16 bits) of memory. This equipment is interfaced to the PSP terminal and to the gateway by full-duplex high-speed data paths, as well as to two asynchronous character-oriented paths for interfacing certain test, monitoring, and interface control functions. The Satellite IMP as shown in Figure A.8-13 implements global timing control, demand-access protocols, input and output to the PSP terminal, internal network protocols, the SATNET side of the host access protocol, certain measurement capabilities, software to control and receive data from the PSP terminal test and monitoring functions, and software to allow interaction with the SATNET monitoring and control center.

A.8.4.1.3 Network Interface and Data Source. The gateways interfacing SATNET and ARPANET act as host computers on each of the connected networks. The gateways shown in Figure A.8-14 implement the following several functions:

- Separating the ARPANET and SATNET so that SATNET performance can be separately optimized and measured while still using certain ARPANET facilities for traffic generation and data collecting.
- Providing a realistic environment for inter-network experiments involving traffic flow between ARPANET and SATNET.
- Supporting certain experimental applications (e.g., packet voice conferencing).
- Providing facilities to emulate various traffic sources and sinks and to measure source-to-sink performance.

It should be noted that the gateways are the only external data source to SATNET, with gateway functions being implemented in a PDP 11 minicomputer with 128K words (16 bits) of memory.

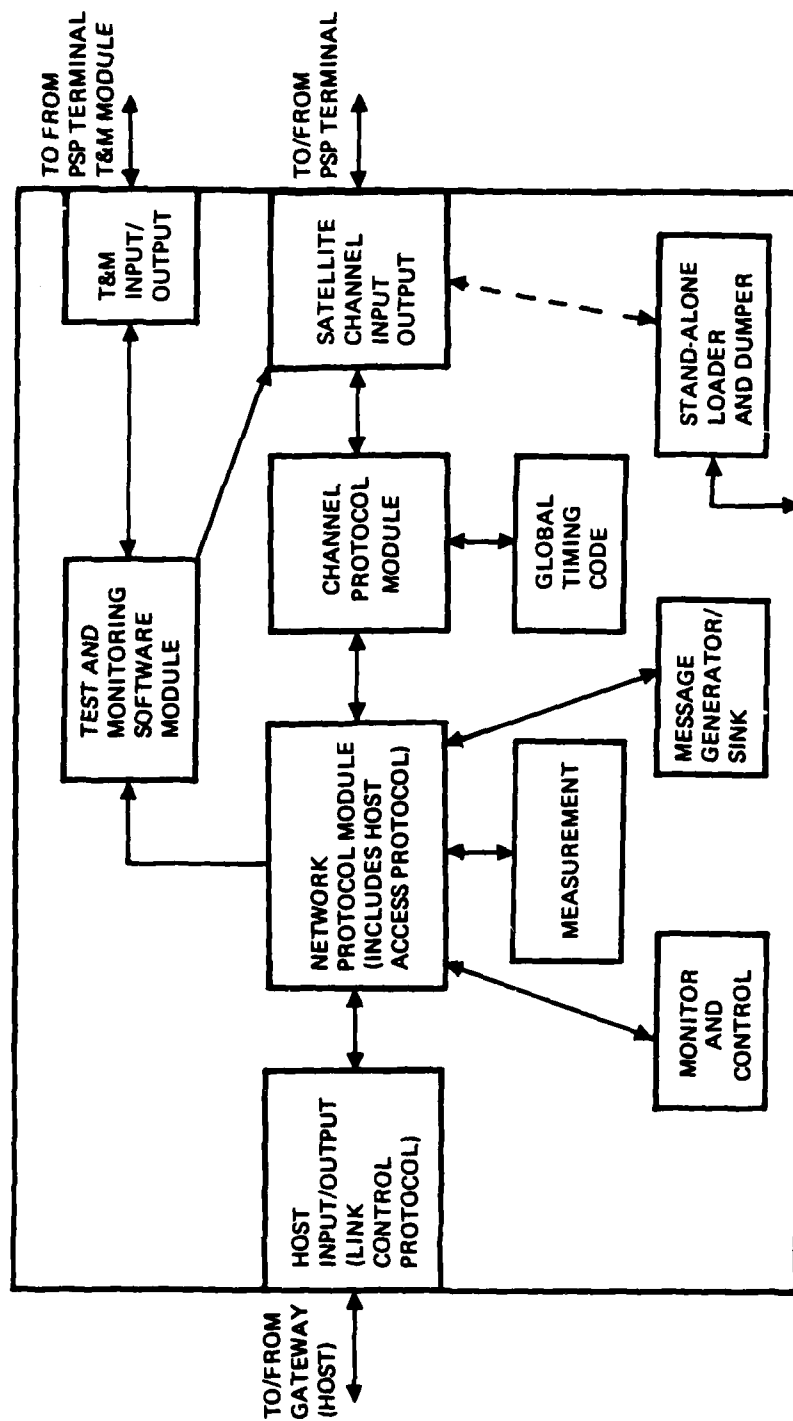
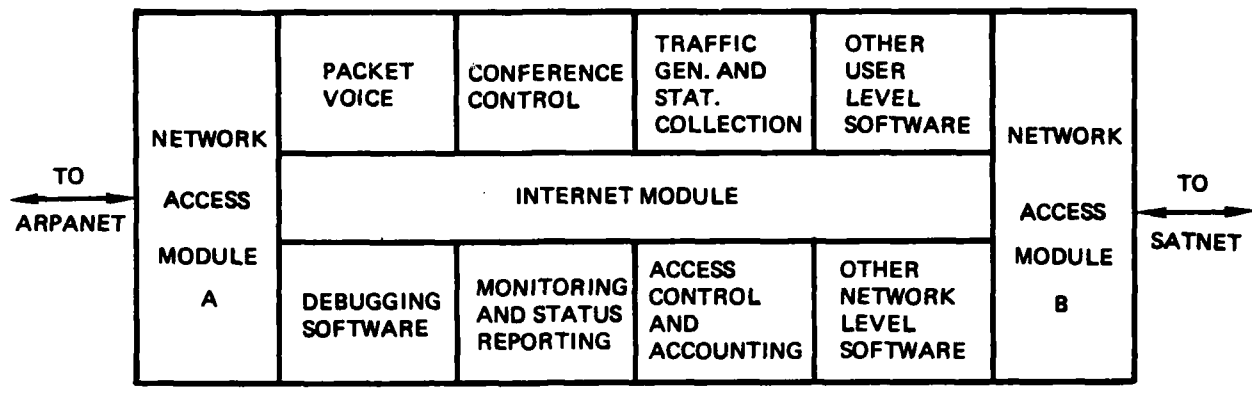


Figure A.8-13. Schematic of Satellite IMP Software



NOTE IN THE CASE OF THE SMALL STATION, TRANSLATION GATEWAY A CONNECTS DIRECTLY TO A MEASUREMENT COMPUTER. (IBM 360/65)

Figure A.8-14. Elements of the Gateway

A.8.4.2 Wideband Experimental Integrated Switched Network. The Wideband Experimental Integrated Switched Network (EISN) is currently being developed under joint sponsorship of the Defense Communications Agency (DCA) and the Defense Advanced Research Projects Agency (DARPA) (Ref. A.8-13). Organizations currently participating in the program include Bolt Beranek and Newman (BBN), Communications Satellite Corporation (COMSAT), Information Science Institute (ISI), LINKABIT Corporation, MIT Lincoln Laboratory, and SRI International. The network provides a unique experimental capability for investigation of systems issues involved in a communications facility which includes wideband satellite and terrestrial links and which carries large volumes of voice and data traffic. Areas for experimental investigation include the following:

- Demand-assignment strategies for efficient broadcast-satellite communications.
- Packet voice communication in a wideband multi-user environment.

- Alternate integrated switching techniques for voice and data.
- Rate-adaptive communication techniques to cope with varying network conditions.
- Routing of voice and data traffic.
- Digital voice conferencing.
- Internetting between satellite and terrestrial subnetworks.

Existing networks such as the ARPANET and the SATNET lack sufficient capability to permit experiments on a scale large enough to realistically represent the multiple and varied user environments that will be typical of future military communications networks. The EISN is intended to provide a more realistic environment for experimental investigation and demonstration of the advanced communication techniques cited above.

A.8.4.2.1 Plan for the Experimental Wideband Network. The experimental network includes a wideband satellite network, a wideband terrestrial network, access facilities including concentrators and terminals, and internet gateways. The satellite net includes four earth stations at Defense Communications Engineering Center (DCEC), Reston, Virginia; ISI, Marina del Rey, California; Lincoln Laboratory, Lexington, Massachusetts; and SRI International, Palo Alto, California. At least one of the terrestrial switching nodes will be collocated with a satellite station, but the locations of all terrestrial nodes have not yet been specified. A topology for the satellite and terresrial node is shown in Figure A.8-15, wherein the DCEC location is depicted as the site of both a satellite and a terrestrial node as well as of a gateway interconnecting the two. Locations of the other three terrestrial nodes are unspecified.

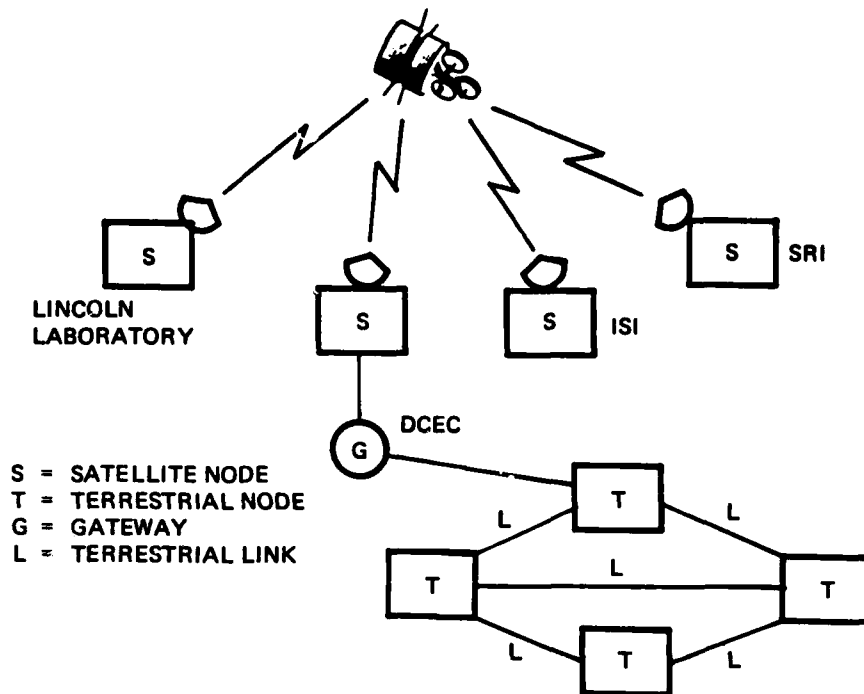


Figure A.8-15. Topology for Experimental Wideband Network

A.8.4.2.2 Configuration of Subsystems. Figure A.8-16 shows a projected configuration for subsystems to be available at a network location which is the site of both satellite and terrestrial nodes. The functions of each subsystem are briefly discussed below.

Subsystems functions such as implementation of satellite network communication protocols, which also include the Demand-Assignment Multiple Access (DAMA) protocols for the broadcast channel, will be performed in the PLURIBUS Satellite Interface Message Processor (PSAT IMP). The Earth Station Interface (ESI) provides an interface between the PSAT IMP and a 70-MHz intermediate frequency (IF) line into the satellite earth station. ESI modules include a packet/burst controller which accepts packets from the PSAT IMP and forms bursts of digital data for transmission, a burst modem, and a command/monitoring unit.

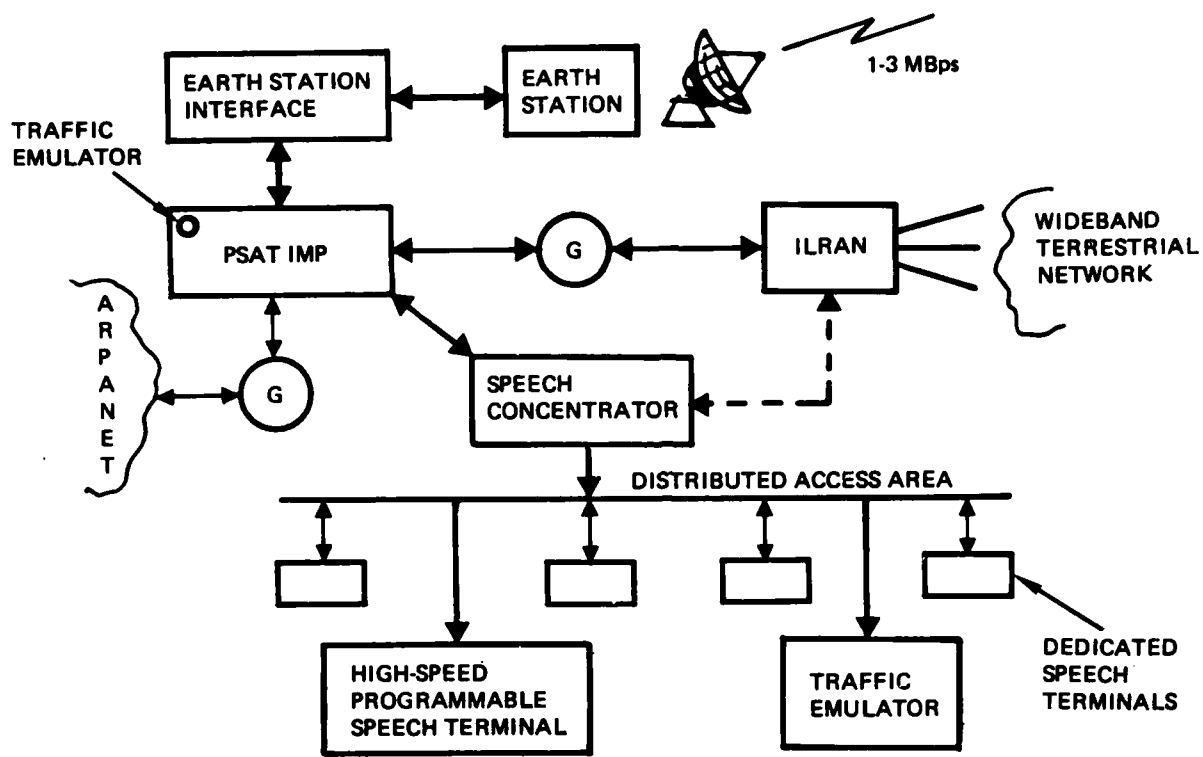


Figure A.8-16. Subsystems for Experimental Network

The earth-station equipment will interface with the ESI at 70 MHz IF, and will include a low-noise receiving amplifier, a high-power transmitting amplifier, and an antenna. To minimize interference and siting problems, operation in either the 12 to 14-GHz or 18 to 30-GHz frequency bands is preferred. The Integrated Local/Regional Access Nodes (ILRAN) are the switching/multiplexing nodes for the wideband terrestrial subsystem.

Access facilities will include speech terminals, host computers, speech concentrators, and traffic emulators. The purpose of the speech concentrator is to collect the digital voice outputs from individual voice terminals and to enter them into one wideband data stream. The concentrator also performs the inverse process of splitting the return stream for transmission to the terminals. The function of the traffic emulator is to simulate the traffic loading effect of many voice terminals in the access area.

A.9 OPTICAL FIBER COMMUNICATION

This section reviews the current state-of-the-art of optical-fiber communication system and its components. Trends in the development of fiber optics are outlined and discussed.

A.9.1 Introduction

Since the laboratory demonstration of the ruby laser in 1960 (Ref. A.9-1) and of the gas laser in 1961 (Ref. A.9-2), the potential usefulness of the laser as a coherent source for optical communications was recognized and experimental work on optical communications initiated. However, the pioneer work done by Kompfer, Miller, and Tillotson (Refs. A.9-2 and A.9-4) and by others was limited to the line-of-sight atmospheric optical systems, with theoretical and experimental research work being carried out on optical devices and components and on optical signal-processing techniques and subsystems. Although experimental communications systems were demonstrated, their reliability and usefulness were shown to be limited by adverse weather conditions (Ref. A.9-4).

Use of optical fiber for communications media was proposed by Kao and Hockham (Ref. A.9-5) in 1966. Although the best existing fiber was characterized by greater than 1000 dB/km at that time, Kao and Hockham speculated that losses as low as 20 dB/km should be available and it was suggested that such fiber would be useful for telecommunication. This anticipated 20-dB/km fiber was realized in 1970 (ref. A.9-6), and from then on progress in the field of optical-fiber transmission has been both rapid and abundant. Two excellent examples are the reduction of loss in optical fibers and the reliability improvement of the semiconductor injection laser, the common transmitter of an optical-fiber communication system.

The solid curve in Figure A.9-1 depicts the continuous decrease of optical-fiber loss in the wavelength region of 0.8 to 0.9 μm . Some recently reported fiber losses in other wavelengths of 0.6 dB/km at 1.3 μm (Ref. A.9-7), 0.47 dB/km at 1.2 μm (Ref. A.908), and 0.2 dB/km at 1.55 μm (Ref. A.9-7) are also indicated.

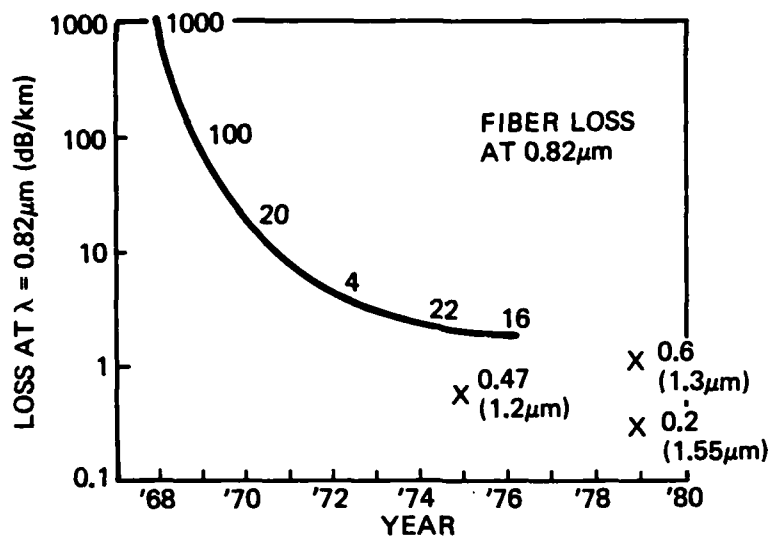


Figure A.9-1. Progress in Reliability Reduction of Optical Fiber Transmission Loss

In this same period the reliability of the AlGaAs injection laser operating continuously at room temperature also has been greatly improved. As shown in Figure A.9-2, projected-room-temperature mean life being in excess of a million hours based on accelerated temperature tests (Ref. A.9-9).

The photodetectors, in particular silicon photodetectors, needed for optical fiber systems had already been developed when fiber communication system studies were initiated in 1971. Additional development in this area accomplished over the past decade has mostly been concerned with optimization of existing technology for use with the anticipated data format.

Some milestones of optical-fiber communication development are identified in Table A.9-1. Due to the rapid component development that has taken place some optical communication systems have been fielded not only for test but also for the actual carrying of commercial traffic. Table A.9-2 lists a few representative systems.

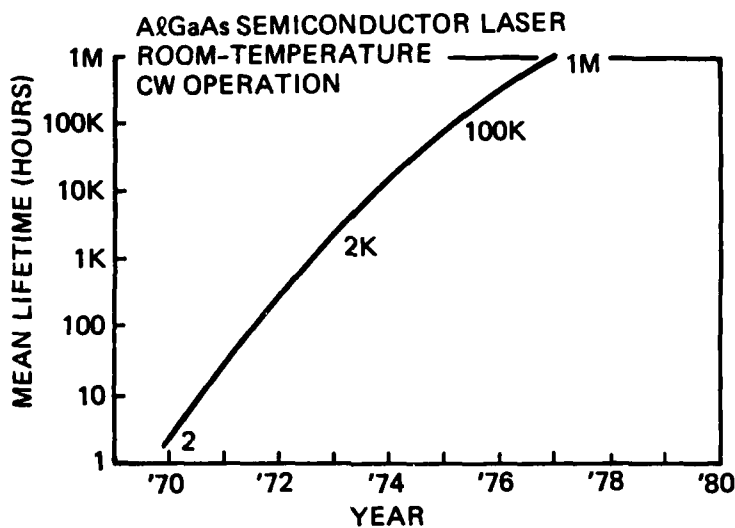


Figure A.9-2. Progress In Reliability Improvement of Semiconductor Injection Laser

Table A.9-1. Milestones of Optical-Fiber Communications Development

Event	Time
Ruby Laser Demonstrated, and Optical Communications Suggested	1960
Fiber Communications Proposed (1000 dB/km)	1966
AlGaAs/GaAs Heterojunction Laser	1969
Low Loss Fiber (20 dBkm) Available	1970
Light Source Reliability (10^6 Hr) Improved	1977
Commercial Field Test System	1977 Present

Table A.9-2. Representative Test and Operational Optical Fiber Systems

Country	Date Rate (Mbps)	Link Length/Repeater Spacing (km)	Month Year	Location	Reference
USA	1.544	9/3.7	April 1977	Long Beach, Ca	A.9-10
USA	44.7	2.8/2.8	June 1979	Phoenix, AR	A.9-11
Canada	6.3	6/1.5	October 1977	Montreal, Canada	A.9-12
Canada	274	42/3.5	November 1979	Alberta, Canada	A.9-13
Japan	32	18/18	September 1978	Tokyo; Japan	A.9-14
Japan	800	7.3/3.2	April 1979	Tokyo, Japan (1.3 μ m)	A.9-15
England	8	13/13.6	December 1976	Suffolk, England	A.9-16, A.9-17
England	140	13/6	December 1976	Suffolk, England	A.9-17, A.9-18
Italy	140	9/9	September 1977	Turin, Italy	A.9-19

A.9.2 Optical Fiber Communication System

An optical-fiber communication system as shown in Figure A.9-3 consists of a transmitter, a receiver, and an optical fiber connecting the transmitter and the receiver.

The transmitter contains a microscopic optical source which is either a light-emitting diode or an injection laser. Both sources emit light power in response to an electrical current. The LED light output is roughly proportional to the applied current which is typically about 10 mA. The injection laser is a threshold device which turns on at an injection current of about 100 mA, and with an additional 20 mA or so emits a peak power of few milliwatts into a fiber.

A good transmission fiber carries power from its input to its output with an attenuation of less than 10 dB/km. In the process of transmission, the modulated power waveform is not only attenuated but also is distorted in shape. This occurs because different portions of the light travel at different speeds within the fiber. The power impinging upon the optical detector is converted to an electrical current which must be amplified and processed electronically. In most cases the current resultant emitted by the detector is very weak and therefore is subject to corruption by amplifier noise and pickup.

Similar to a conventional cable system, repeaters are needed for a long optical-fiber link. A repeater consists of a detector, an amplifier, an equalizer, and a regenerator followed by a driver and light source pair, as shown in Figure A.9-4. Once the signal has been amplified the rest of the processing up to a driver is fairly conventional, and is identical to the processing done in conventional cable system.

In the following section, the major elements of an optical communication system, the optical fiber, the light source, and the photodetector are discussed.

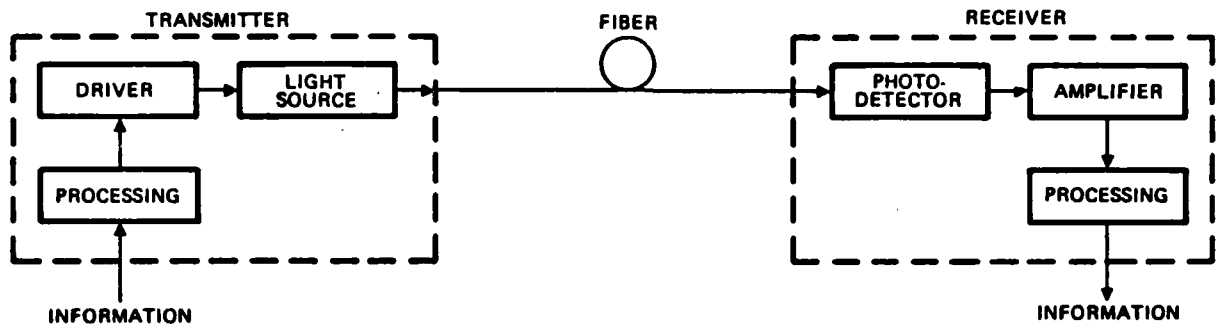


Figure A.9-3. Optical Fiber Communication System

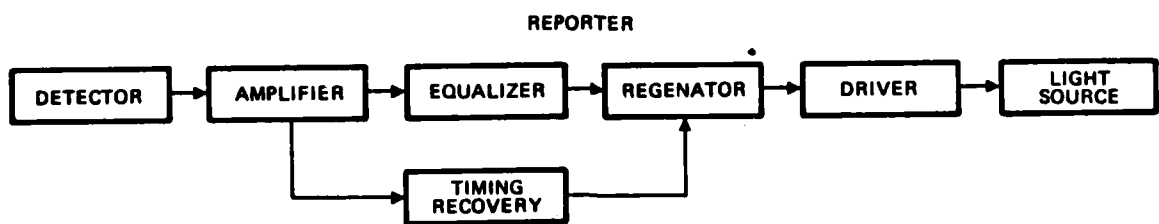


Figure A.9-4. Repeater of an Optical Fiber Communication System

A.9.3 Optical Fiber

Various kinds of optical fibers are available, the major ones being fiber bundle, graded-index fiber, multi-mode step-index fiber, and single-mode step-index fiber. These four kinds of fiber and their corresponding cross-sections in the fiber, and input and output pulses are shown in Figure A.9-5. The fiber bundle was the type of low-loss fiber that was produced in the early 1960s. However, because its losses still remain too high for communication usage the following discussion is limited to description of the other three fiber types.

A.9.3.1 Fiber Propagation Modes. Each of the three major types of optical fiber (graded-index, step-index multiple, and step-index single mode) has a core region of radius a , and a region of lower refractive index cladding the core. Besides providing the desired light confinement, the cladding lends mechanical strength to the fiber, helps reduce the scattering loss due to dielectric discontinuities, and protects the guiding region from absorbing surface contaminants. Depending on how the refractive index varies within the core, the fibers are described as either step-index type or graded-index type.

For a step-index fiber, letting n and n_c denote constant refractive index for core and cladding respectively, their relation may be expressed as

$$n_c = n (1 + \Delta) \quad (A.9-1)$$

where, in general, Δ is index fractional difference and

$$\Delta \ll 1 \quad (A.9-2)$$

In the case of graded-index fibers, the index of refraction varies in a nearly parabolic fashion, proceeding outward from the center of the core, or

$$n_c = n (1 + \Delta (r/a)^a), \quad 0 \leq r \leq a \quad (A.9-3)$$

where a has a value close to 2 for maximum fiber bandwidth. Graded-index fibers act as a continuous lensing medium that continually refocuses the beam as it travels down the fiber length. This refocusing and lensing tends to equalize the optical path lengths of the various modes and is of practical significance in that it results in a higher fiber bandwidth when compared with multimode step-index fibers.

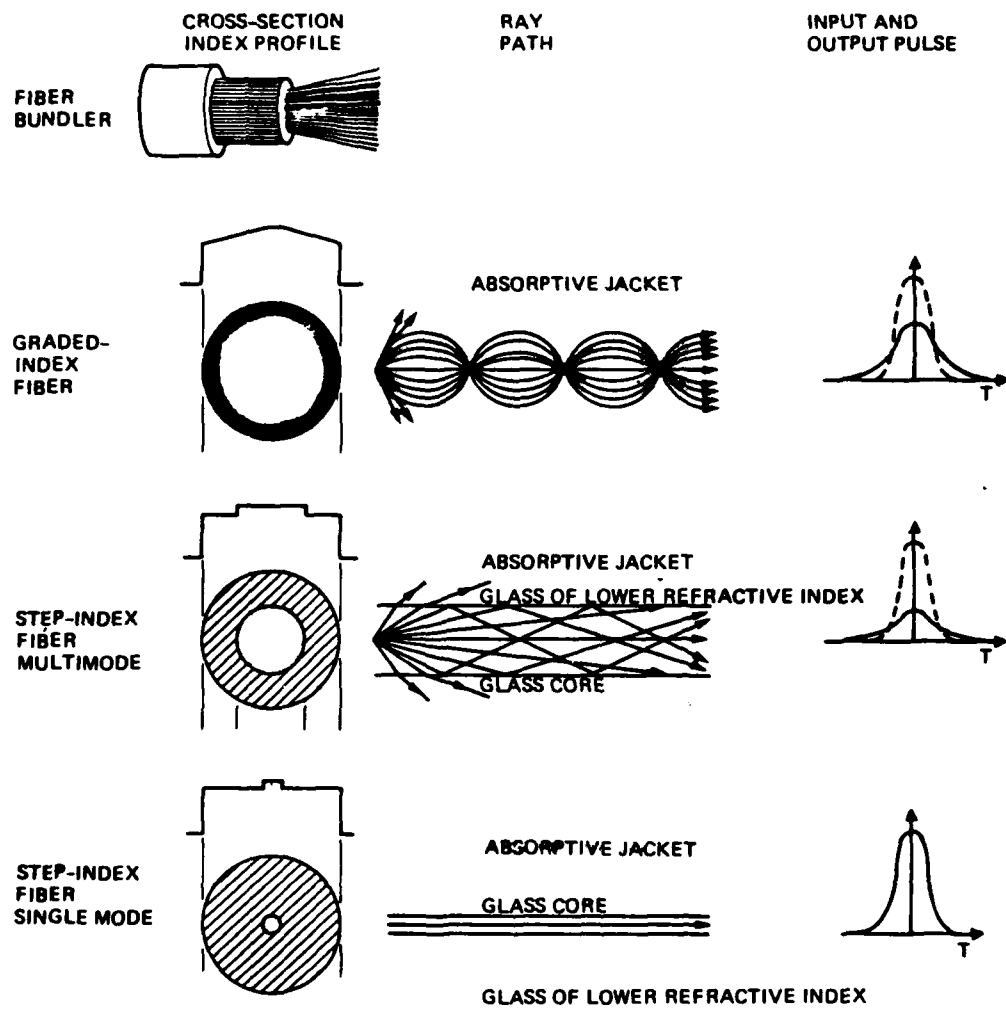


Figure A.9-5. Types of Optical Fibers

By solving the Maxwell equations governing electromagnetic wave propagation along a step-index fiber it can be shown that the fiber supports many different guided modes of propagation (Ref. A.9-20). Each mode has its own phase velocity and its own field distribution on a cross-section plane. A parameter, V , that can be used to denote the number of modes in a guide also can be approximately related to the fiber acceptance angle and to the dispersion of a fiber as induced by modal path differences. This parameter is called the normalized frequency as a consequence of the relation,

$$V = (2\pi a/\lambda) (n_c^2 - n^2)^{1/2} \quad (A.9-4)$$

$$\approx (2\pi a/\lambda) n_c (2\Delta)^{1/2}$$

where λ = wavelength in a vacuum.

Figure A.9-6 presents a plot of effective modal index (k_{mn}/k_0) for step profile fibers as a function of the characteristic modal parameter, V , where k_{mn} is the wave number of the mn -th mode. Each of the modes shown are doubly degenerate (i.e., HE_{11} is doubly degenerate in polarization), which results from the fact that in circular waveguides all orientations are equivalent, thus permitting two orthogonal polarization modes to exist with the same wave number. However, core ellipticities can lift this degeneracy. Below 2.405, a single mode, designated HE_{11} exists, whereas for $V > 2.405$ other modes are possible.

As the value of the parameter, V , increases above a critical value of 2.405 the number of propagating modes increases rapidly, and the approximate number of guide modes in a step index fiber (Ref. A.9-21) is then given by

$$N \sim V^2/2 \sim (kan_c)^2 \Delta \quad . \quad (A.9-5)$$

Ray theory can describe propagation accurately for a large number of modes. A few are shown in Figure A.9-5 for the three major types of fibers.

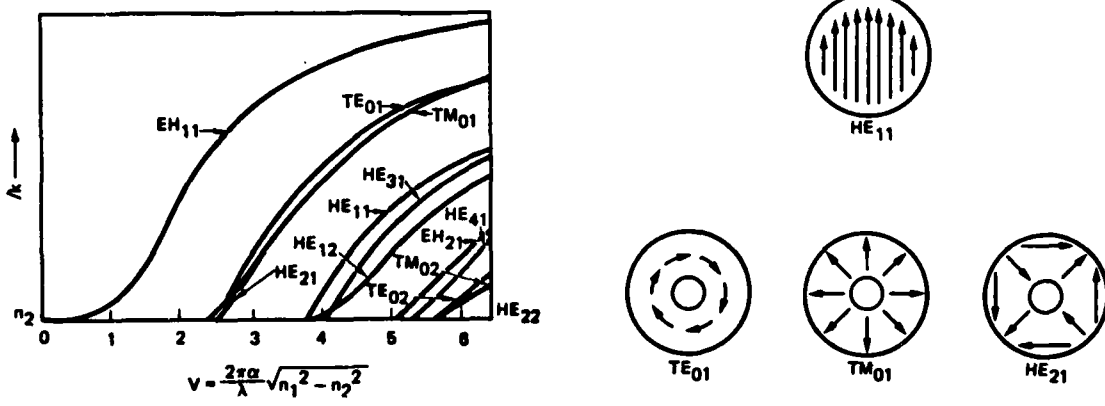


Figure A.9-6. Normalized Modal Propagation Constant Versus Modal Parameter V and Field Distribution Patterns

An important factor in the use of fibers is their light-gathering capability. For step-index multimode fibers, in which large numbers of modes can propagate, ray theory can be applied. The maximum off-axis angle at which a ray will be accepted, θ_{\max} , is determined by the total-internal-reflection angle in the fiber, θ_c , by the relation, $\theta_{\max} = n_c$. The quantity $\sin \theta_{\max}$ is defined as the fiber numerical aperture (NA). Thus,

$$NA = \sin \theta_{\max} = n_c^2 - n^2 \approx n_c (2\Delta)^{1/2} . \quad (A.9-6)$$

For example, a fiber of NA = 0.14 will accept rays at off-axis angle values up to 8° .

Another feature of single-mode fibers is the dependence of propagation loss on wavelength (Ref. A.9-22). For a fiber designed to have a V number ~ 2.3 at $0.85 \mu m$ is plotted in Figure A.9-7. The loss dependence on wavelength also holds for a multimode fiber. It should be noted that for single-mode fibers, loss is a strong function of wavelength, λ , through the dependence of V on λ . Single-mode propagation is realized by designing core sizes to be a few wavelengths in cross-sectional dimension and by having small index differences between the core and cladding. Because $2.505 > V = (2\pi a/\lambda) n_c (2\Delta)^{1/2}$, it is seen that the physical core size a and the core-cladding index difference, Δn , may be varied over a considerable range.

By making either Δn or a small, it is possible to cause the guided fields to extend significantly into the cladding and increase the physical extent of the mode. This feature is of interest in fiber splicing in that it affords a means of relaxing the translational dimensional tolerances. However, as V becomes small, the wave in the fiber becomes loosely guided and thus susceptible to bending losses. Reducing the V number of the fiber only in the region of the splice by elongating the fiber should reduce the accuracy with which the ends of the fiber must be aligned on-center and not significantly increase the propagation losses (Ref. A.9-22).

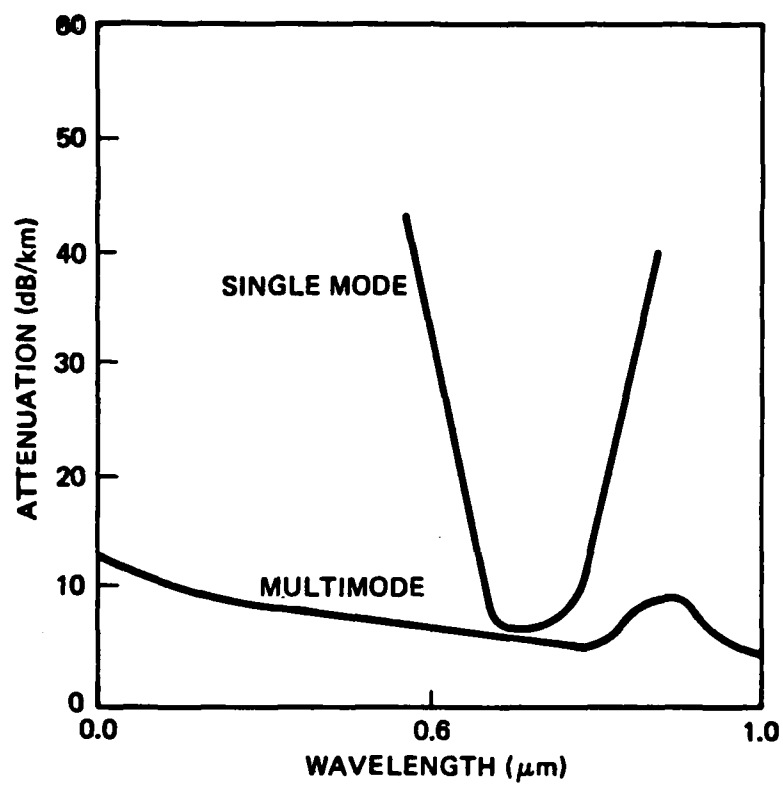


Figure A.9-7. Fiber Attenuation Versus Wavelength

In the case of graded-index fiber, the refractive index of the core may vary radically in a power law manner in accordance with the relation,

$$n_c = n [H\Delta(r/a)^\alpha] \quad , \quad 0 > r > a \quad (A.9-7)$$

where α is chosen to be in the vicinity of 2 (i.e., parabolic index variation) for maximum fiber bandwidth (Ref. A.9-23). Although the varying refractive index of the core makes exact solution of the Maxwell equations 1 of the fiber impossible, these equations can be solved in terms of the Hermite-Gaussian function (Ref. A.9-24). Model considerations, while more complex, remain essentially the same as those for the step-index fiber.

Excitation of a graded-index fiber is more difficult, and higher-order modes are hard to avoid. This arises because the NA of graded-index fibers is a function of position along the core and is not a constant across the core as is the case with step-index fibers. From geometric optics one finds that light incident on the fiber core at position r will propagate as a guided mode only if it is within the local numerical aperture, $NA(r)$, at that point. The local $NA(r)$ is defined as

$$NA(r) = NA(0) (1 - r/a)^\alpha \quad r < a \quad (A.9-8)$$

where a is the core radius, α is the graded-index power law coefficient, and

$$NA(0) = n_c (2\Delta)^{1/2} \quad (A.9-9)$$

The graded-index fiber NA thus decreases with increase of distance away from the fiber axis. Also, the expression for the number of modes in a graded-index fiber has been shown to be (Ref. A.9-21)

$$N = (kan_c)^2 \Delta\alpha / (2+d) \quad (A.9-10)$$

from this it follows that a step-index fiber with a given radius will have twice as many modes as a graded index fiber ($\alpha = 2$) with the same peak and radius.

Index grading has the effect of equalizing the optical path lengths of the various propagating modes and thus drastically reducing pulse distortion due to intermodal dispersion. Much higher bandwidths than for step-index multimode fibers are thereby achieved. However, the value of a must be controlled very accurately (within 1 percent) for maximum bandwidth (Ref. A.9-23). Also, the optimum value of a depends on wavelength (Refs. A.9-23 through A.9-25).

Fiber loss dependence on wavelength for a graded-index, multiple mode fiber is much less when compared to that of a step-index, single-mode fiber. This is because in a multimode fiber, the presence of hundreds of modes leads to an averaging over wavelength of loss from each mode, with the higher order modes (i.e., those close to cutoff) being most sensitive to loss-inducing perturbations. This averaging results in a very weak dependence of loss on wavelength. Single-mode fibers must, therefore, be designed for a wavelength of interest, and large deviations from the design wavelength will lead to excessive losses.

A.9.3.2 Optical Fiber Attenuation. The most important fiber characteristic is its attenuation, particularly for optical fiber that is to be used for long-range communication. Major mechanisms which contribute attenuation for waves propagating along the fiber are absorption losses, scattering losses, and radiation losses.

A.9.3.2.1 Fiber Absorption Loss. Absorption loss in a fiber can be grouped in three categories, intrinsic absorption of basic material, extrinsic absorption due to impurity, and atomic defect (color center) absorption.

Intrinsic absorpiton originates due to charge transfer in the ultraviolet region and vibration modes in the near infrared. If these modes are sufficiently strong their tails will extend into the spectral region of interest for fiber communications, 0.7-1.1 μm . For most glasses considered for optical fibers, the vibration modes in the near infrared are both far enough removed, occurring in the 8-12 μm wavelength region, and not sufficiently strong to cause a problem. The ultraviolet modes are far stronger and potentially more troublesome. For the case of germanium doped silica, however, Urbach's rule has been applied to the band edge (Ref. A.9-26) and it was shown that for wavelengths greater than about 0.6 μm , less than 1 dB/km absorption resulted.

Extrinsic absorption implies that the absorption is caused by some impurity material in a fiber such as metal ions in a fiber and other traditional sources of impurity absorption. Initially these were most concerned and many studies on bulk fiber material showed that the allowed levels for such impurities as Fe, Cu, V and Cr could not exceed 8, 9, 18 and 8 parts per billion respectively in order to obtain sub-20 dB/km loss at band center. High silica fibers are regularly made, however, such as the one whose spectrum is shown in Figure A.9-8 in which these impurities do not contribute significantly to the loss. The only impurity for which a direct correlation has been shown is the OH radical, whose bands at 0.725, 0.825, 0.875, and 0.950 μm are clearly visible in Figure A.9-8. These are overtones and combination bands of the fundamental OH at 2.73 μm and of silica matrix. The strength of the 0.950 μm band has been shown to be approximately 1 dB/km/ppm. All absorption in the spectrum shown can be accounted for by OH absorption.

Atomic defect absorption is induced by a stimulus such as the thermal history or by intense radiation of the fiber. The magnitude of such induced losses can be quite large as, for example, in the case of titanium doped silica where a reduction; $\text{Ti}^{4+} \rightarrow \text{Ti}^{3+}$, occurs during fiberization to produce losses of several thousand dB/km (Ref. A.9-27). Similarly, radiation induced losses of $\sim 20,000$ dB/km are possible for conventional fiber optic glasses from gamma radiation levels of 3000 rads. Generally, however, one can choose glasses which are less susceptible to these effects. For example, germanium doped silica has been shown to exhibit an attenuation at 0.82 μm of only ~ 16 dB/km for a radiation level of 4300 rads (Ref. A.9-28). Such things as background cosmic radition for example would have a small long term effect on such a waveguide.

A.9.3.2.2 Fiber Scattering Loss. Scattering losses are caused by density and refractive index variations within the fiber material; these variations are due to frozen-in thermal fluctuations of constituent atoms. The intrinsic scattering sets the fundamental attenuation limit in fibers.

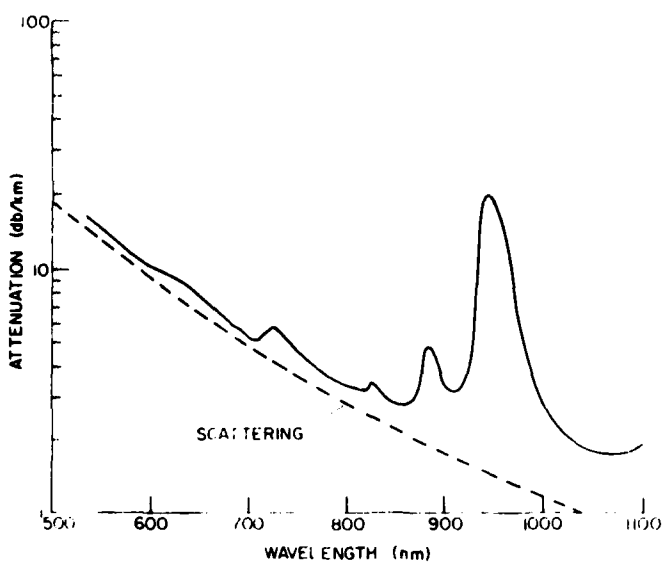


Figure A.9-8. Attenuation Spectrum for a High Silica Waveguide

The scattering loss can be calculated by subdividing the sample into small volumes which act as dipoles. One then sums all the dipoles integrated over all angles and can relate the scattering loss to the isothermal compressibility β ,

$$\alpha_s = \frac{8\pi^3}{3\lambda} (n^2 - 1) k T \beta, \quad (A.9-11)$$

where T is the transition temperature at which the fluctuations are frozen into the fiber, and k is Boltzmann constant. For equation A.9-11, it is seen that the intrinsic scattering loss is inversely proportional to the fourth power of wavelength. For fused silica using a transition temperature of 1500°C one calculates a loss of 1.7 dB/km at $0.82 \mu\text{m}$ which is in good agreement with experiment. A tradeoff between the transition temperature and the compressibility, for a given material has been shown to exist (Ref. A.9-29). In fact Li-Al-SiO₂ glasses have been measured to have losses due to density fluctuations several times less than that of fused silica.

For fibers with more than one kind of oxide, another scattering occurs. This is due to concentration fluctuation in the constituent oxides and also causes a loss.

Non-linear effects, such as stimulated Raman and Brillouin scattering, can induce further scattering loss. However, the power level, required for telecommunication use, is not high enough to cause any non-linear attenuation (Ref. A.9-30).

A.9.3.2.3 Fiber Radiation Loss. In addition to the discussed absorption and scattering losses, radiation is another loss usually associated with optical fibers caused by the microbands.

Bend-induced radiation can significantly increase the loss of fibers. Generally, a radius of curvature of $R_{\min}^2 = a/(NA)^2$ will result in a very high transmission loss. Thus fiber should have a curvature significantly greater than r_c . For large radii of curvature, R , the effect will decrease exponentially according to $\exp(-R/R_{\min})$.

A.9.3.3 Dispersion and Pulse Broading. Communication transmission capacity of an optical fiber depends on fiber dispersion characteristics. Three major components of dispersion in fibers are waveguide dispersion, modal dispersion (multimode effects) and material dispersion. Dispersion effect is shown by broadening the light pulses propagating along an optical fiber. Figure A.9-5 indicates qualitatively the dispersion effect of various kinds of fibers.

A.9.3.3.1 Waveguide Dispersion. Considering a single mode propagating along a fiber made of dispersionless material, the phase constant, β , is not linear with wavelength, λ , i.e.,

$$\frac{d^2 \beta}{d\lambda^2} \neq 0, \quad (A.9-12)$$

then, the group velocity varies with wavelength. This kind of fiber is dispersive and broadens a transmitted pulse.

In the geometric optic approach, equivalently, if the angle between the ray representing the mode and the fiber's axis varies with wavelength, the ray trajectory and its flight time also varies. However, the waveguide dispersion is in general negligible compared with other dispersions. Particularly, for a multimode fiber, this waveguide dispersion can be neglected because it only affects higher order lossy modes which are of little relevance for long fiber of interest for communications.

Consider a light pulse transmitted through a fiber of length, L , the travel time, t , is given by

$$t = L \frac{d\beta}{d\omega} ,$$

or

(A.9-13)

$$t = L \frac{\lambda}{\omega} \frac{d\beta}{d\beta} ,$$

where ω is angular frequency of the light pulse. Assume that the carrier light has a spectral width $\Delta\lambda$ which is centered at λ and is broad compared to the detected pulse envelope, then the pulse spread, Δt , can be computed by (Ref. A.9-31)

$$\frac{\Delta t}{\Delta\lambda} = \frac{dt}{d\lambda} = \frac{L}{2\pi c} \left(2\lambda \frac{d\beta}{d\lambda} + \lambda^2 \frac{d^2\beta}{d\lambda^2} \right) \quad (A.9-14)$$

where c is the vacuum in a velocity of light. Therefore spread is caused by the change of $d\beta/d\lambda$.

The propagation constant β is a function of λ not only because the index changes with wavelength (material dispersion), but because β is a function of a/λ also, where a is the core radius (waveguide dispersion). In a single mode fiber material and waveguide dispersion are inter-related in a complicated way. By computing one in the basence of the other, it can be shown that the material dispersion usually dominates.

A.9.3.3.2 Material Dispersion. The fiber material is dispersive if its index, n , does not vary linearly with wavelength, i.e.,

$$\frac{d^2 n}{d\lambda^2} \neq 0$$

(A.9-15)

Physically, this implies that the phase velocity of a plane wave propagating in this dielectric varies non-linearly with frequency and consequently, a light pulse will broaden as it propagates through it. The pulse broadening due to material dispersion is given by

$$\frac{\Delta t}{L} = \frac{1}{c} \frac{\Delta\lambda}{\lambda} \lambda^2 \frac{\frac{d^2 n}{d\lambda^2}}{} \quad (A.9-16)$$

where c is speed of light, $\Delta\lambda$ the relative spectral width between $1/e = 0.368$ points, and L the fiber length.

Pure silica exhibits zero material dispersion near the wavelength of $1.27 \mu\text{m}$ (Ref. A.9-32). Dispersion in borosilicate ($\text{B}_2\text{O}_3 \cdot \text{SiO}_2$) and germanium borosilicate ($\text{GeO}_2 \cdot \text{B}_2\text{O}_3 \cdot \text{SiO}_2$) glasses used for low-loss fibers has been measured in the bulk and found to be not too different from that of pure silica, as shown in Figure A.9-9 (Ref. A.9-33 and A.9-34). Zero material dispersion near $2.3 \mu\text{m}$ has been verified experimentally in several doped-silica fibers by pulse-delay measurements using Raman radiation from a single-mode silica fiber pumped by a Nd:YAG laser (Ref. A.9-35). It is indeed fortunate that these fibers also exhibit their lowest attenuation in the vicinity of $1.3 \mu\text{m}$. Naturally, intense research interest is presently focused on optical sources and detectors that will work efficiently near this wavelength. This point will be discussed later.

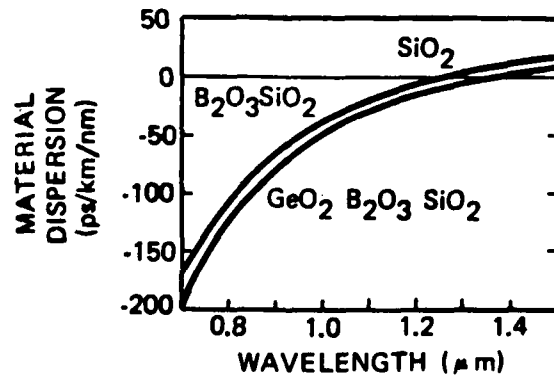


Figure A.9-9. Fiber Material Dispersion

A.9.3.3.3 Modal Dispersion. In a multimode fiber, the modes have different group velocities. Neglecting waveguide and material dispersion, a light pulse with energy distributed among various modes at the input end evolves into a number of debunched pulses as they propagate along the fiber. At output end a broad single pulse appears; the duration of the output pulse is equal to the difference between the flight times of the slowest mode and the fastest mode.

A ray analysis yields a time difference between the fastest and slowest modes in a fiber of length L

$$\frac{\Delta t}{L} \approx \frac{n_c \Delta}{c} = \frac{(NA)^2}{2n_c c}, \quad (A.9-17)$$

For example, with an $NA = 0.14$ and $n_c = 1.5$, a relatively large pulse dispersion value is obtained: 20 ns/km. For fibers where mode mixing is substantial, it is found that the pulse spreading dependence on the fiber length is closer to \sqrt{L} rather than L (Ref. A.9-36). Another factor which accounts for pulse spreading values lower than the ones deduced from equation (A.9-17) is that in long lengths of fiber the actual number of modes is lower than the theoretical one given by Equation (A.9-5), due to heavy differential attenuation of the high-order modes (Ref. A.9-37).

A dramatic improvement in multimode fiber bandwidth is achieved by grading the fiber index in a parabolic fashion. The reason is that a nearly parabolic index tends to equalize the modes' group velocities thus it theoretically reduces the pulse dispersion to (Ref. A.9-38 and A.9-39)

$$\Delta t/L \approx n_c^2/(2c) = (NA)^4/(8n_c^3 c) . \quad (A.9-18)$$

for the previous example (i.e., $NA = 0.14$ and $n_c = 1.5$) this gives $\Delta t/L = 47$ ps/km and thus provides an improvement factor of 425 over step-index fibers. An accurate analysis provides an improvement factor of 1000 when $\Delta = 0.01$, $\alpha = 1.98$, and $\lambda = 0.85 \mu\text{m}$ (Ref. A.9-25). Actually, due to technological difficulties in controlling the index profile radially and/or over long lengths of fibers, the improvement factor is at best 100 (Ref.

A.9-24). Thus the practical pulse broadening values for graded-index fibers lie in the 0.2-1.0ns/km range. In turn, one can achieve transmission bandwidths (i.e., data-rate-length product values) between 1 and 4 Gbit·km/s when using lasers and fibers with an optimum graded-index profile (i.e., optimum α as a function of wavelength) (Ref. A.9-23). Experimental results have confirmed these figures at $\lambda = 0.8 \mu\text{m}$ and $1.27 \mu\text{m}$. If wide-spectrum sources, such as LED's, are used with graded-index fibers, then in addition to multimode dispersion effects material dispersion must also be considered.

For single-mode fibers, dispersion is caused by chromatic effects, i.e., the combined effects of material and waveguide dispersion. The cause of chromatic dispersion is the wavelength dependence of the mode group velocity V_g . The pulse spreading Δt over a fiber of length L is

$$\frac{\Delta t}{L} = \frac{1}{V_g} = \frac{\Delta^2}{c} \quad \frac{\Delta \lambda}{\lambda} \quad \frac{d^2 n}{d \lambda^2} \quad (\text{A.9-19})$$

where $\Delta\lambda$ is the maximum spectral width produced by either the source or the signal modulation bandwidth (Ref. A.9-40). The second derivative of the refractive index n with respect to λ is characteristic of the index dispersion of the dielectric. In Figure A.9-10, the dispersion of a single mode waveguide fabricated of fused silica is presented (Ref. A.9-41). As can be seen, the material dispersion is a function of wavelength and vanishes at $1.27 \mu\text{m}$. Above $1.27 \mu\text{m}$, material dispersion changes sign (not shown) relative to its values below $1.27 \mu\text{m}$. This sign change is significant in that at some value, the material dispersion exactly cancels the waveguide dispersion ($1.32 \mu\text{m}$ in Figure A.9-10). At this wavelength, the bandwidth of a single mode fiber is enormous, ($>100 \text{ GHz/km}$) for single mode injection laser sources with narrow linewidths of ten picometers. It is fortuitous that the minimum propagation loss also occurs in this spectral region. As shown in the figure, the influence of waveguide dispersion is to shift the dispersion minimum toward the long wavelength.

SINGLE MODE FIBER DISPERSION

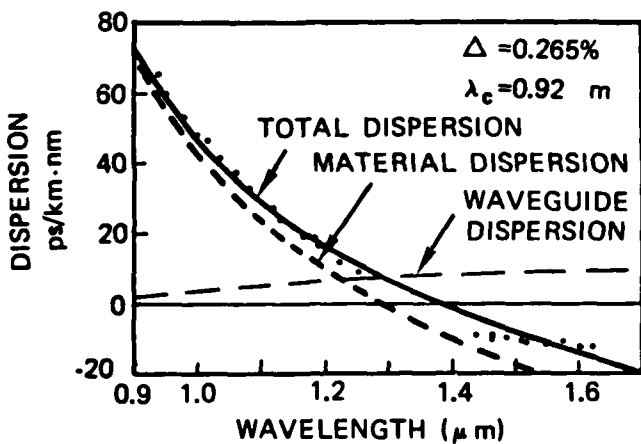


Figure A.9-10. Dispersion of a Single Mode Optical Fiber

A.9.3.3.4 Pulse Spreading and Data Rate-Length Product. To illustrate the differences in pulse spreading between step-index multi-mode, graded-index multi-mode and single-mode fibers, pulse spreads are plotted in Figure A.9-11 (Ref. A.9-42). The plots are for the typical cases; multi-mode fiber with $\Delta = 0.01$; graded-index fiber with a bandwidth improvement factor of 100; and single-mode fiber with $\Delta = 0.001$. Multimode dispersion effects control the bandwidth for step-index fibers (lasers and LED's) and for graded-index fibers, when lasers are used (i.e., spectral widths $< 2\text{nm}$). Chromatic dispersion, which by its nature is dependent on the source or modulation spectral width, controls pulse spreading for single-mode fibers as well as for graded-index fibers in conjunction with wide-spectrum sources (e.g., typical AlGaAs and InGaAsP LED's are marked in the figure). The advantages of using long wavelength sources, LED's with graded-index fiber and lasers with single-mode fibers are obvious. The data-rate-time-length product is given as right hand side ordinate in Figure A.9-11. This figure shows that material dispersion limits the product of a multimode graded-index fiber to about 140 Mbit·km/s. If an AlGaAs LED (At $\lambda = 0.85 \mu\text{m}$) is used, and to about 600 Mbit·km/s if an InGaAsP LED (At $\lambda = 1.25 \mu\text{m}$) is used. This improvement of bandwidth has been confirmed in an experimental data link operating with AlGaAs and InGaAsP LEDs at 137 Mbps (Ref. A.9-43). Figure A.9-11 also shows that a single-mode fiber operating with a laser at wavelength of $1.25 \mu\text{m}$ has a potential bandwidth of 2.5 Gbps with a repeater spacing of 100 km.

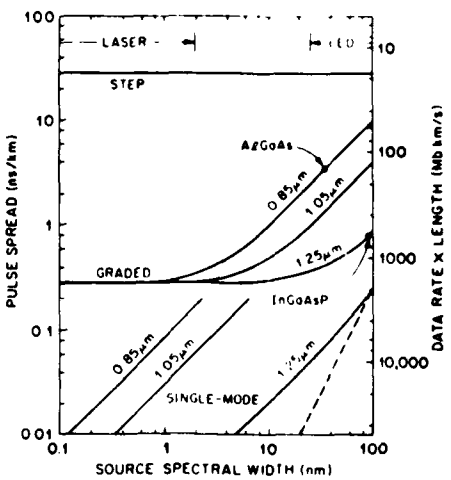


Figure A.9-11. Comparison of Pulse Spread of Various Types of Optical Fiber

A.9.4 Optical Sources

Optical sources for communications should be capable of stable, continuous (CW) operation at room temperature for long times they should be of size and configuration compatible with the transmission media. The sources should operate at wavelengths for which the transmission fiber has both low loss and low dispersion, as discussed in the last section. The sources also should operate with reasonable efficiency and at wavelengths where detectors are sensitive. Although the power output of these sources are not the most important consideration, the sources must be capable of coupling at least microwatts, and preferable a milliwatt or more optical power, into the transmission fiber.

Currently, light-emitting-diodes (LEDs) and solid state lasers are generally in use either for laboratory experiments or fielded test systems. In general, lasers offer the advantage of narrow spectral bandwidth, about 20 Å or less, which is also a very useful characteristic for minimizing the effect of fiber dispersion. Lasers also can be modulated up to a rate of a few hundred megahertz and can be coupled to a fiber because of relatively directional emission. Lasers are now considered primarily of use in single mode fiber systems. In contrast, incoherent LEDs offer inherent advantages of simplicity of construction and operation, and thus the expectation of long trouble-free operational life. It is seen from the dispersion discussion in the last section that wideband incoherent sources must operate at 1.2 to 1.4 μm wavelength where fiber dispersion is low.

Other than injection devices mentioned above, optically pumped lasers with neodymium (Nd) as the active element seem quite attractive for fiber communications use. The Nd-doped materials are stable, oscillate at the favorable wavelengths of 1.06 or 1.3 μm , and have a strong pumping band conveniently located at wavelength of 0.8 μm .

These sources and other related considerations are reviewed in this section.

A.9.4.1 Light-Emitting Diodes. Holes and electrons injected into a forward biased PN junction can combine and emit spontaneous radiation in the visible or infrared regions of the spectrum. Such devices are called Light Emitting Diodes (LEDs). In operation, the normally empty conduction band of the semiconductor is populated with electrons injected into it by a forward current through the junction. Light is generated when these electrons combine with holes in the valance band.

The light is emitted at a wavelength, λ , given by

$$\lambda = \frac{ch}{E} \quad (\text{A.9-20})$$

where c is the speed of light in free space, h is Planck's constant, and E is the junction bandgap energy. The energy of the emitted photon is equal to E . When holes and electrons recombine in a semiconductor, the resulting energy can be released by a photon of light or can be reabsorbed into the material. A pair of electrons and holes that combines without emitting a photon is called a nonradiative process. Because of nonradiative processes, the internal quantum efficiency of an LED is not 100 percent. In practice the quantum efficiency can be quite high, usually exceeding 50 percent in simple homostructure LEDs and falling in the range of 60 to 80 percent in double-heterostructure (DH) LEDs.

To design an LED, one of the major goals is to maximize the quantum efficiency, i.e., to choose a material in which radiative process dominates. Such a material falls into the family of direct "bandgap" material, of which GaAs is a member. In a direct bandgap material, holes and electrons can combine without the intervention of a third particle.

The second design goal is to produce the radiation in a geometry from which it can be collected or coupled into a fiber, thus to maximize the external efficiency. Two different diode geometries are in general use; edge emitters and surface emitters.

Another design goal is to produce a diode in which the light out can be directly current-modulated at a high rate.

Because the light output of an LED drops by 2 to 3 dB if the junction temperature rises 100°C, the device geometry is so chosen such that heat can be removed efficiently.

The spectral bandwidth of an LED is in the range of 1 to 2 kT or 300 to 400 Å at room temperature. This is at least one order of magnitude broader than the inject laser emission. This broad radiation spectrum limits the bandwidths for long haul communication because of the dispersion characteristics of optical fiber as discussed in the previous section. Comparing with the injection laser, the coupling efficiency into low numerical aperture fiber is much lower. However, the LED has the advantage of a simpler construction and a smaller temperature dependence of the emitter power.

A.9.4.1.1 Edge Emitting LEDs. A typical heterojunction edge emitter LED is shown in Figure A.9-12 (Ref. A.9-44, and A.9-445). This kind of LED emits part of its radiation in a relatively directed beam as illustrated in the figure, and hence has the advantage of improved efficiency in coupling radiated light into a fiber. The edge emitting structure uses the partial internal waveguiding of the radiation source to obtain improved directivity of the emitter power in the direction perpendicular to the junction plane. This is particularly important in coupling to an optical fiber with a small acceptance angle. In the structure shown in Figure A.9-12, the active layer region is extremely thin, about 500 Å, so that the light generated there is not completely contained but leaks into the surrounding waveguide layer and is coupled strongly to the lowest order guided mode perpendicular to the junction. Absorption in the active layer is high but the absorption in the surrounding layers is low, so that most of the light propagating in this mode is transmitted to the end faces and emitted with a beamwidth determined by the waveguide parameters. Providing a reflective coating at

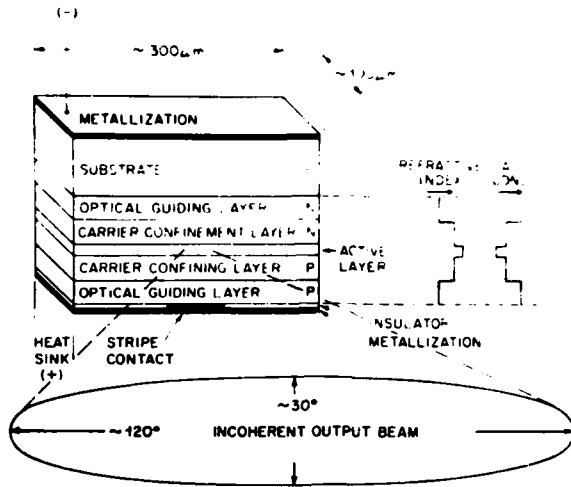


Figure A.9-12. Edge Emitter DH LED

one end and an antireflecting coating at the other causes most of the light to be emitted at one end. A typical emitted beam is sketched in Figure A.9-12 and is Lambertian with a half-power width of 120° in the plane of the junction and of 20 to 35° in the plane perpendicular to the junction due to the waveguiding effect of the structure.

This structure provides another advantage which as a result of the channeling of emitted light to a very small end face by the waveguide, causes the effective radiance at the end face to be very high. The value of 1000 - 1500 $\text{W}/\text{cm}^2\text{-sr}$ in an emitting area of 2 - $4 \times 10^{-6} \text{ cm}^2$ has been achieved (Ref. A.9-46). The same reference reported that 0.8 mW of optical power has been coupled into a 0.14 NA, $90 \mu\text{m}$ core fiber from one of these edge-emitters operating near diode saturation at $5.1 \text{ kA}/\text{cm}^2$.

The width of the emitting region in the junction plane is adjusted for the fiber dimension, but is typically 50 to $80 \mu\text{m}$. If the source is Lambertian, and the source diameter is smaller than the fiber core diameters, the coupling efficiency into a step-index fiber is (Ref. A.9-47)

$$n_c \approx \sin^2 \theta_{\max} = (\text{NA})^2 . \quad (\text{A.9-21})$$

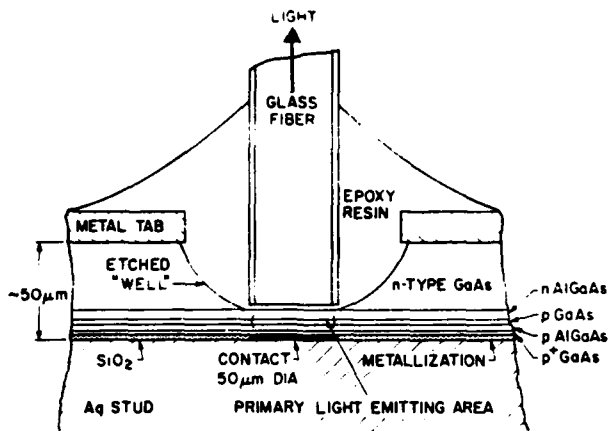


Figure A.9-13. Surface Emitting LED

Hence, for a fiber with a NA of 0.14, $n_c \approx 2$ percent. For edge emitters, the coupling efficiencies to low NA fibers (i.e., NA < 0.2) are 5 to 7 dB (About four times) higher than for surface emitters (Ref. A.9-48).

Typically, when coupling to 0.14 NA step-index flat-ended fibers, the coupling loss is 16 to 20 dB for surface emitters and 10 to 14 dB for edge emitters. The Lambertian coupling efficiency into graded-index fibers with the same NA (i.e., same Δ) and of a ≈ 2 is around a half of that into step-index fibers (Ref. A.9-49).

A.9.4.1.2 Surface Emitting LEDs. Figure A.9-13 illustrates a high-brightness Barris-type surface emitting LED (Ref. A.9-50). The output of this type of source is approximately Lambertian. The expected coupling of the output to the fiber depends on the exact geometry and condition, such as LED radiation pattern and radiance, fiber size and refraction index grading, fiber effective NA, relative area of the fiber core and LED emitting area, distance and alignment of the two and the medium between them. Coupling in an individual case can probably be determined measurements. However, it can be estimated for step-index fiber by

$$P = RA\Omega$$

(A.9-22)

where P is the power coupled into the fiber, R the radiance into free space of the source, Ω solid acceptance angle of the fiber, and A is the smaller of the fiber cross-section area or the emitter area.

It has been possible to couple about 1 mW of optical power at 0.8 μm wavelength into a graded-core fiber of 0.36 NA butted directly against the diode surface (Ref. A.9-51). The double heterostructure LED had a contact area of 75 μm diameter and without antireflection coatings delivered 15 mW of optical power into free space in the 130° cone. The diode was operated at about one-half of its saturated value, 3.4 kA/cm^2 .

A.9.4.1.3 Power Output, Coupling and Other Characteristics. Surface-emitting and edge-emitting structures provide several milliwatts of power output in the 0.8 to 0.9 μm spectral range, when operated at drive currents of 100 to 200 mA. Surface emitters generally radiate more power into air than edge emitters (\approx a factor of 3), since the emitted light in surface LEDs is affected much less by reabsorption in interfacial recombination. A recent comparison (Ref A.9-52) between high-radiance surface emitters of moderate bandwidth and high-radiance high-speed edge emitters, when coupled to fibers of various NA, has revealed that edge LEDs couple more absolute power than surface LEDs for $\text{NA} < 0.3$ and that the opposite is true for $\text{NA} > 0.3$.

Coupling to fibers can be improved by using index-matching epoxies or various types of lenses: hemispherical lens on the emitting facet, spherical lens between LED and fiber, spherical-shaped fiber receiving end, or tapered fiber end. For instance, the coupling efficiency of a surface-emitting LED (35- μm -dot contact diameter) to a 0.14 NA step-index fiber (85- μm core diameter) has been increased from 2.3 to 10 percent, by forming a sphere on the end of the fiber. In the case of graded-index fibers, however, lensing the fiber end brings about only a minor improvement. By using self-aligned spherical lenses, a monolithic circular array of surface LEDs has been used to couple 600 μW into a 0.39 NA ten-core flat fiber cable at a drive current level of 100 mA. Very high efficiencies (30 to 50 percent) can be obtained by LED coupling to large NA fibers ($\text{NA} = 0.6-0.6$) for use in short optical data links. Figure A.9-14 shows LED power coupled into various type of optical fiber.

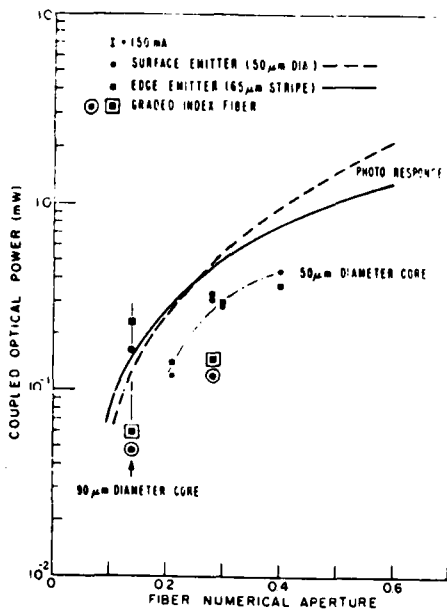


Figure A.9-14. Couples Power Versus NA for LEDs

The spectral width of the output of an LED operating at room temperature in the 0.8 to 0.9 μm region is usually 250 to 400 Å at the 3 dB points, and 500 to 1000 Å for material with smaller energy gap operating in the 1.1 to 1.3 μm wavelength region. The output spectrum of an LED broadens as the temperature rises. This effect may be very pronounced in diodes heated up due to internal dissipation. The peak emission wavelength from a surface emitter and from an edge emitter made from the same material can differ significantly, sometimes by 200 to 300 Å. This difference is caused by internal radiative recombination spectrum and absorption characteristics of the semiconductor window through which the radiation must pass or the waveguide and/or gain region in which it must propagate.

A.9.4.2 Injection Laser. An LED becomes a laser at high current densities by adding a cavity to provide feedback. The optical feedback in a laser diode can be obtained by cleaving two parallel facets to form the mirrors of the Fabry-Perot cavity. The lateral sides of the lasers are either formed by roughing the device edges by wire sawing to form a broad-area diode as shown in Figure A.9-15, or combining the ohmic contact to selected areas to produce a strip conduct diode, illustrated in Figure A.9-16.

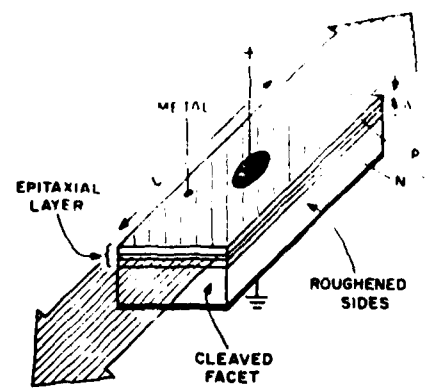


Figure A.9-15. Board Area Injection Laser

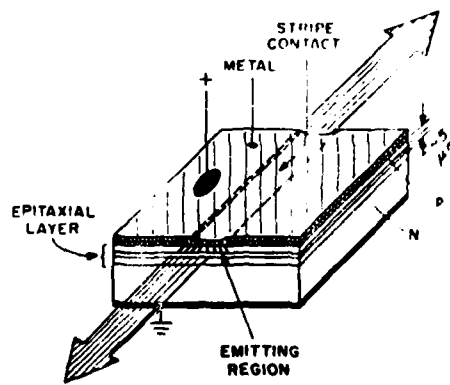


Figure A.9-16. Stripe Injection Laser

Many different laser diode structures have been fabricated and tested. The most common types of heterostructure lasers are:

- Single heterojunction
- Double heterojunction with full carrier and radiation confinement
- Double heterojunction with full carrier confinement but partial radiation confinement
- Four-heterojunction diode
- Large optical cavity diode.

The double heterojunction (DH) laser diode is the most widely used continuous wave (CW) source for optical communications. The following discussion is limited to the DH structure.

A.9.4.2.1 DH Injection Laser. A broad area laser diode is one formed by sawing the edges perpendicular to the cleared facets forming the mirror cavity. This type of laser has been widely used for pulsed operation and in early double heterojunction laser studies. Continuous wave diode lasers now use a stripe contact geometry. The advantages of stripe geometry are the followng.

- The radiation is emitted from a small region which simplifies coupling of the radiation into fibers with low numerical aperture.
- The operational current density amperes/m² can be made to be under 0.5 A because it is relatively simple to form a small active area.
- The small active area makes it simple to obtain a reasonably defect-free area.
- The active region is isolated from an open surface along its two major dimensions, a factor believed to be important for reliable long life operation.
- The thermal dissipation is made easy because the heat-generating action region is imbedded in an inactive semiconductor medium.

Figure A.9-17 illustrates a typical cross-section of a stripe geometry laser diode. The light generating region, which is called the active layer is the P-AlGaAs layer. The layer shown is $0.1 \mu\text{m}$ thick. The adjacent N- and P-regions are AlGaAs to combine the injected carriers and provide the waveguide. The P^+ -GaAs layer aids in making the ohmic contact. Continuous operation at room temperature and up to 100°C is possible.

The far-field radiation pattern of the stripe geometry DH lasers is shown in Figure A.9-18. Because the radiation is from such a small area, it is not well confined, but diverges strongly. Typical beam divergences at one-half the peak intensity are 45° perpendicular to the junction plane and 9° parallel to the junction plane. This wide beam must be considered for coupling the laser radiation to an optical fiber.

9.4.2.2 Modes of Operation of DH Laser. As previously indicated, a DH injection laser is actually a Fabry-Perot cavity. The cavity supports many modes of electromagnetic oscillation which are separable into two independent sets, with transverse-electric and transverse-magnetic polarization. The mode numbers m , s , and q define the number of sinusoidal half-wave variations along the three axes of the cavity, transverse, lateral and longitudinal, respectively.

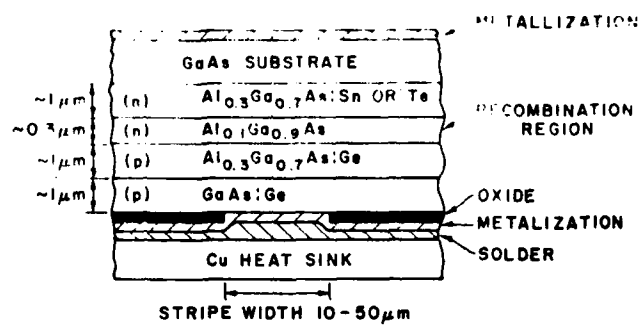


Figure A.9-17. Geometry of a Stripe Injection Laser

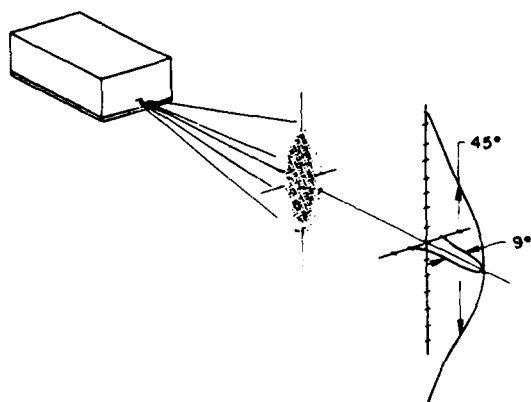


Figure A.9-18. Far-Field Pattern of a Edge Emitter Laser

The allowed longitudinal modes are determined from the average index of refraction and dispersion seen by the propagating wave. The Fabry-Perot mode spacing is several angstrom units in typical laser diodes. The lateral modes depend on the method used to define the two edges of the diode. In stripe-geometry lasers generally only low-order modes are excited; their mode spacings are 0.1 to 0.2 Å and they appear as satellites to each longitudinal mode. The transverse modes depend on the dielectric variation perpendicular to the junction plane. In the devices discussed here, only the fundamental mode is excited, a condition achieved by restricting the width of the waveguiding region (the heterojunction spacing) to values well under one micron. Therefore, the far-field radiation pattern consists of a single lobe in the direction perpendicular to the junction. (High-order transverse modes would give rise to "rabbit-ear" lobes, undesirable for fiber coupling.)

For a laser operating in the fundamental transverse mode, the full angular beam width at half power perpendicular to the junction plane is a function of the near-field radiation distribution. The narrower the emitting region in the direction perpendicular to the junction plane, the larger the beam width. In practical cw laser diodes the beam width is about 30° to 50°. The beam width in the plane of the junction (lateral direction) is typically 5° to 10° and varies only slightly with diode topology and internal geometry. At least one half of the power emitted from one facet can be coupled into a multimode step-index fiber with a numerical aperture of 0.14 and a core diameter of 80 microns.

While operation in the fundamental transverse mode is easily achieved, most narrow-stripe laser diodes operate with several longitudinal modes, and therefore emit over a 10 to 30 Å spectral width, although some units can emit several milliwatts in a single mode. Figure A.9-19 shows the emission spectrum from such a device operating in the fundamental lateral and transverse mode and a single longitudinal mode. The line width is 0.15 Å and the power emitted is 3 mW.

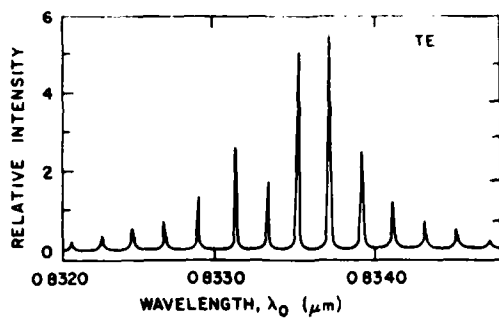


Figure A.9-19. Modes of An Injection Laser

A.9.5 Modulation Techniques

To convey information on a lightwave, it is necessary to modulate a property of the wave according to a signal. The properties of the wave which may be varied are intensity, phase, frequency, and polarization. At present, the intensity modulation appears to be the most practical approach.

Both analog and digital modulation are suitable for a fiber optic communication system, analog modulation has the advantage of simplicity but the large signal-to-noise ratios required limits its use to relatively narrow-bandwidth short-distance application. Digital modulation trades noise immunity for bandwidth, therefore digital modulation is ideally suited for fiber optic transmission where available bandwidth is large.

Intensity modulation is simple to implement, especially with currently available light sources such as light emitting diodes and injection lasers. These sources can be modulated directly by varying their driving current at rates up to a few hundred megahertz. However, an external modulator may be needed for future systems employing wide bandwidth or other light sources. An external modulator can also be used for multiplexing and switching of optical signals.

The phase or frequency of an optic wave can be easily modulated externally. Once phase modulation of a wave is realized, then, intensity and polarization modulation can be derived from a phase modulated wave with passive components. The physical effects commonly employed for external

modulation are electrooptic, magnetooptic, and acoustooptic effects whereby the refractive index, n , of a medium is varied by Δn in proportion to an applied electric field, E , magnetization, M , or strain s , respectively. Each of these effects serve to vary the phase of an optic wave propagating through the medium with a varying Δn . Intensity modulation can be derived by combining a phase modulated wave and an unmodulated wave in phase opposition. Phase grating created acoustooptically or electrooptically may be used to deflect a light beam and produce intensity modulation. Recently some effort has been devoted to develop a modulator in waveguides in various forms rather than bulk configuration. These various modulation methods are presented in this subsection.

A.9.5.1 Direct Modulated Light Emitting Diodes (LEDs). The output of a LED can be modulated by varying the driving current. The output is linear with the current over a wide range of the current as shown in Figure A.9-19. If the driving current consists of a small AC component of signal frequency, ω , superimposed on a DC bias, the light output contains a modulated part, $P(\omega)$, superimposed on a quiescent part, $P(0)$. The modulated power is given by Ref. A.9-55.

$$P(\omega) = P(0)/[1 + (P\tau)^2]^{1/2} \quad (\text{A.9-3})$$

where $P(0)$ is the modulated power extrapolated to zero frequency. The 3-dB modulation bandwidth, $\Delta\omega$, is defined as the frequency band over which $P(\omega) > P(0)/z$, that is

$$\Delta\omega = 1/2 \quad \text{or} \quad \Delta\omega = 1/\tau \quad (\text{A.9-4})$$

where τ is the carrier combination time in the active region. As the modulation frequency increases and approaches the carrier combination time, the modulation depth decreases.

When both radiative and non-radiative recombinations are present, the carrier lifetime

$$\frac{1}{\tau} = \frac{1}{\tau_r} + \frac{1}{\tau_{nr}} \quad (\text{A.9-5})$$

where τ_r and τ_{nr} and is the radiation and non-radiation lifetime respectively. The quantum efficiency is τ/τ_r for high frequency operation. It is required that the radiative combination process dominates the non-radiative process occurring at impurity and defect centers in the bulk, and in the heterojunction. In general, the carrier lifetime can be reduced either by decreasing the thickness of the active layer at low doping levels by increasing the active layer doping level (Ref. A.9-56). For surface emitting diode, increasing in bandwidth is commonly achieved by heavy Ge doping of the active layer and/or high carrier confinement. Nevertheless, both methods decrease the diode external efficiency. Hence, for active layer doping levels greater than 10^{18} per cm^3 , the power-bandwidth product is almost constant for most surface emitting diodes reported to date. This fact is clearly shown in Figure A.9-2. Contrary to the surface emitting diodes, the active layer of edge emitting diodes is virtually undoped, and the carrier lifetime is controlled by the injected carrier density.

The linearity between light output and driving current is important if the modulation format is analog. Nonlinear distortion of a directly modulated LED depends on diode structure, active layer thickness, carrier concentration and operating frequency. The limit on the tolerable level of nonlinear distortion in an analog system is determined by the particular application.

Nonlinearity is much less important in a digital system. In an intensity modulated multiple level digital system, nonlinear importance decreases as the number of levels diminishes. When binary signals are used, the LED is driven between the off-state of zero output, and the on-state near saturation. In order to operate at a high bit rate, a small DC bias current is necessary to keep the effect of junction capacity small.

The relatively large optical spectral bandwidth of LEDs has been pointed out in the previous section, and this characteristic influences LED's usefulness as a modulated source. Material dispersion of an optic fiber limits link capacity for non-zero spectral bandwidth. The spectral bandwidth of typical Ge-doped LEDs ranges from $250 \text{ } \text{\AA}$ for lightly-doped material to over $500 \text{ } \text{\AA}$ for heavily doped material (Ref. A.9-57).

Because minimum material dispersion occurs at wavelength range 1.25 to $1.35 \text{ } \mu\text{m}$ for a high-silien fiber, there is considerable interest in LEDs operating in that region. Experimental DH InGaAs/InP LEDs have been fabricated.

A.9.5.2 Direct Modulated Injection Lasers. Semiconductor injection lasers can be directly modulated by varying the drive current. Because the laser output is proportional to the drive current over a broad current range above the threshold level as illustrated in Figure A.9-20 for a typical stripe geometry DH laser, both analog and digital modulation can be used. Because of the short recombination lifetime of the carrier, less than 10^{-8} second, the modulation bandwidth is expected to be up to a few gigahertz.

Wideband analog signal with frequency up to several hundred MHz can be directly modulated on diode injection lasers (Ref. A.9-58). However, at a sufficiently high frequency a strong resonance occurs due to the interaction between the carrier population inversion and the photon in the optical cavity. Oscillations of both the light ouput and the electron density occur at this point. Above this resonance, the modulation depth decreases rapidly with frequency. Without compensation, the useful analog bandwidth is limited to less than the resonant frequency by severe amplitude and phase distortions. The resonant frequency is a function of drive current and increases as the current operating point is increased. The resonant frequency ω_r can be approximated by the equation:

$$\omega_r^2 \approx \frac{1}{\tau_s \tau_p} \quad \frac{I}{I_{th}} - 1 \quad (\text{A.9-6})$$

where τ_s and τ_p are the electron spontaneous recombination lifetime ($\sim 1 \text{ ns}$) and photon lifetime ($\sim 1 - \text{ps}$) in the cavity, respectively. I is the drive current and I_{th} is the threshold current. Recently, thin

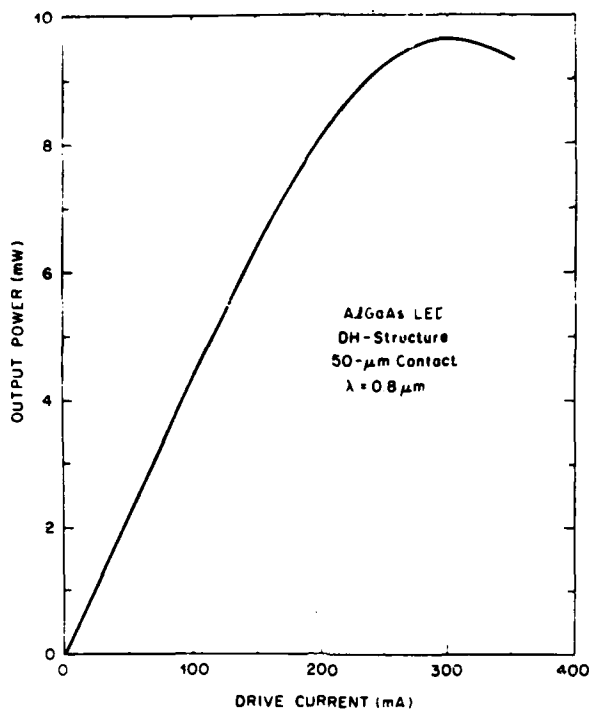


Figure A.9-20. Output Characteristics of ADP LED

junction lasers ($7 \mu\text{m}$ stripes) have been modulated with flat (within 5 dB) frequency response up to 2 GHz at low drive currents ($I/I_{th} \sim 1.15$) without a resonant peak (Ref. A.9-59). The observed flat response was attributed to the narrow stripe width and the proper impurity dopant. When the stripe width becomes narrow, the effective photon lifetime shortens, and the effects of spontaneous emission and lateral carrier diffusion increase. The effect of changing τ_s and τ_p in Eq. A.9-6 thus moved ω_r above 2 GHz. Direct modulation speeds up to 4 GHz have been also reported (Ref. A.9-60).

Digital modulation of diode injection lasers may be accomplished to very high pulse rates about 1 Gbps. However, the following problems arise when a diode injection laser is modulated with a fast digital signal:

- Turn-on delay-time between current and light pulses (a few nano-seconds)
- Ringing transient
- Intersymbol interference and pulse patterning
- Spectral boarding effects.

The impacts of the first three effects may be minimized by proper choice of current waveforms and prebiasing level. Direct current biasing at or above threshold suppresses the oscillation but only at the expense of on/off ratio.

Work on injection laser modulation is currently underway to minimize the above-listed problem discussed and to improve above performance. Other studies are concentrating on obtaining single mode operation. The output wavelength of diode lasers is strongly influenced by temperature, changing up to a few angstroms for each degree $4\text{ \AA}/^{\circ}\text{C}$) diode temperature shift. Through the use of grating reflectors, the operating wavelength is set by the grating periodicity. This results in an order of magnitude less thermal sensitivity of the lasing wavelength ($\sim 0.5 \text{ \AA}/^{\circ}\text{C}$).

The AlGaAs lasers are the near term light sources for optical communications offering tens of milliwatts of CW power. The current interest in developing lasers operating at long wavelength is because of zero dispersion of optical fibers as discussed in Section A.9-3.

A.9.6 Optical Detector

At the receiving end of an optical communications system, an optical detector or photodetector is employed to convert optical signals to electronic signals which are subsequently amplified and processed. Detector design and characteristics which are important to the transmission system are presented in this subsection.

A.9.6.1 Detection Process and Detector Requirements. The fundamental detector process is to generate an electron-hole pair while a photon hits a region of the detector. The region is usually within a high electric field as the depletion layer of a PN junction. The carrier-pairs, being generated by incident photons, are separated by the high field and collected across the reverse-biased junction. The ratio of carrier pairs generated to the incident photon is usually referred to as quantum efficiency. In order to have high quantum efficiency, the depletion layer must be sufficiently thick to allow a large portion of incident photon to be absorbed.

On the other hand, because long carrier drift times limit the speed of operation, a thin depletion layer is preferred for high speed operation. Hence there is a tradeoff between quantum efficiency and speed of response.

The quantum efficiency for all photodetectors is less than a unit except, for the avalanche photodetector (APD) which provides internal amplification.

A photodetector of a fiber communications systems should meet the following performance requirements:

- High sensitivity at the operating frequency
- Sufficient bandwidth or response speed to accommodate the anticipated traffic
- Minimum background noise and noise free internal gain
- Characteristics independent of environment and operational conditions.

A.9.6.2 PN Photodiode. A PN photodiode, in essence, consists of a reverse-biased semiconductor diode whose reverse current is modulated by the electron-hole pair produced in or near the depletion layer by the absorption of incident photons. For the photodiode, the applied reverse bias voltage is not large enough to cause avalanche breakdown. This is in contrast to the avalanche photodiode to be discussed in Section A.9.6.4 in which an internal current gain is obtained as a result of the impact ionization under avalanche breakdown condition.

The basic structure of a PN photodiode is shown in Figure A.9-21. Regarding the operation of this diode, there are two important features. First, there is a relatively high field electric in the depletion region, and second, only the depletion region is allowed to be hit by incident photons. The depletion region is formed by immobile positively charged donor atoms on the N side of the junction and immobile negatively charged acceptor atoms on the P side. The width of the depletion region depends upon the doping concentrations. The lower the doping level, the wider the depletion layer. The absorption region position and width depends upon the wavelength of the incident light and the material used to make the diode. The more strongly light is absorbed the shorter the absorption region. The

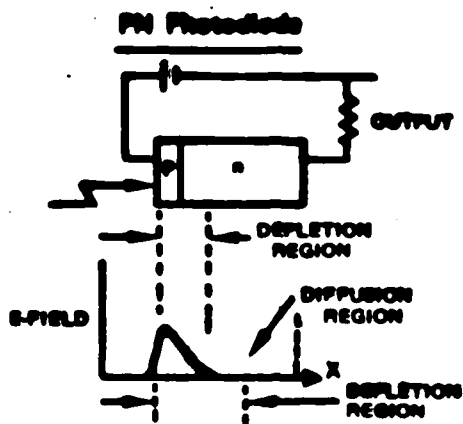


Figure A.9-21. PN Photodiode

absorption region may extend completely through the diode if light is only weakly absorbed. When photons are absorbed, electrons are excited from the valence band into the conduction band. Thus, an electron hole pair is created. If the pair is created in the depletion region, then these carriers will separate (drift) under the influence of the field in the depletion region. This will produce a displacement current in the biasing circuit. If a hole-electron pair is created outside of the depletion region, then the hole will diffuse toward the depletion region and then be collected. Since diffusion is very slow compared to drift, it is desirable that most of the light be absorbed in the depletion region. Thus, the diode designer tries to make the depletion region long by decreasing the doping in the N layer. This leads to such a lightly doped n layer that it can be considered intrinsic. This results in a PI junction. If for the practical purpose of making a low resistance ohmic contact, a highly N doped region is added as shown in Figure A.9.22, and it forms the familiar PIN structure. It should be pointed out that any light absorbed in this added N region will not result in delayed carriers diffusing into the depletion region since in the highly doped N region, carrier lifetime is short. That is, carriers produced there are likely to combine with electrons before they can reach the depletion region.

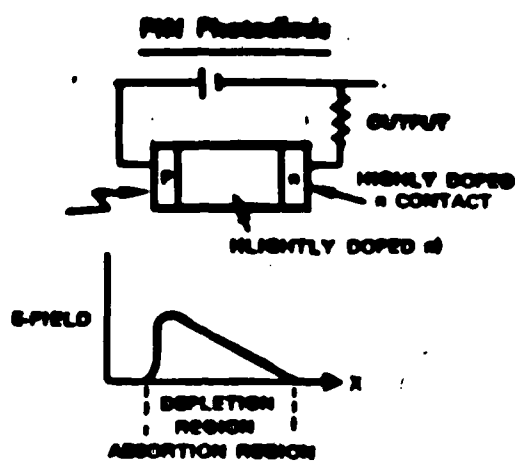


Figure A.9-22. PIN Photodiode

A.9.6.3 PIN Photodiode. As seen in the last section, a PIN photodiode is a logical extension of a PN photodiode. Figure A.9-22 depicts a PIN photodiode. The PIN photodiode is the most common depletion layer photodetector. This is because the depletion region thickness can be tailored to optimize both the sensitivity range and the frequency response. In the PIN diode there is often a tradeoff between quantum efficiency (fraction of light absorbed) and speed of response. For high quantum efficiency, we desire a long absorption region. For fast response we require short drift times; thus, a short absorption region with high carrier velocities.

At the long wavelength where light penetrates more deeply into the device, front-illuminated PIN photodiodes with wide depletion layers are preferred. Silicon PIN detectors for operation in the wavelength range of 0.8 to 0.9 μm to obtain high quantum efficiency; response times as short as 1 nsec have been achieved (Ref. A.9-?). Various silicon PIN photodiodes with quantum efficiency greater than 85 percent and response of a few nanosecond are now available commercially. A front illuminated PIN photodiode is shown in Figure A.9-23.

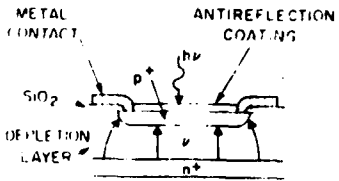


Figure A.9-23. Front Illuminated PIN Diode

At wavelengths of $1.0 \mu\text{m}$, the required depletion layer in silicon is about $500 \mu\text{m}$ or more, which severely limits the bandwidth of a front illuminated device. A compromise between quantum efficiency and bandwidth is achieved by using side illumination in which the light is incident on the edge of and injected parallel to the plane of the junction, as shown in Figure A.9-24 (Ref. A.9-61).

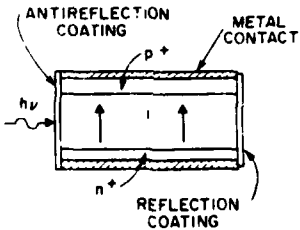


Figure A.9-24. Side Illuminated PIN Diode

The response of Ge photodiodes spans the entire frequency range of interest for fiber optic communication, however the relatively high dark current remains a problem. Experimental PIN diodes with good response and large bandwidth have been built and are now commercially available.

For a PIN detector, the best obtainable is one electron per one incident photon or about 0.5A/W of optical power at $1 \mu\text{m}$ wavelength. Since the optical power level of interest in detecting can be as low as 1nW , it is desirable to have a mechanism to increase the detector responsivity beyond 0.5A/W in order to overcome the thermal noise introduced by the following amplifier. The avalanche photodiode (APD) described in the next section provides such an amplification function internally.

A.9.6.4 Avalanche Photodiode. An avalanche photodiode is shown in Figure A.9-25. The doping profile of an APD is adjusted to result in a narrow region to the left of the "i" region where very high electric fields exist. Carriers which drift into this region can be accelerated to velocities of sufficient magnitude to generate new hole-electron pairs through the process of collision ionization. These new carriers can in turn generate additional pairs. The multiplication of carriers is random with average carrier multiplications of tens or hundreds being possible. Thus average responsivities of avalanche photodiodes can be 50 A/W, or more. It is limited by the statistics of the multiplication process (which generates noise), and by imperfections in the detector that can cause premature breakdown at localized points in the detector.

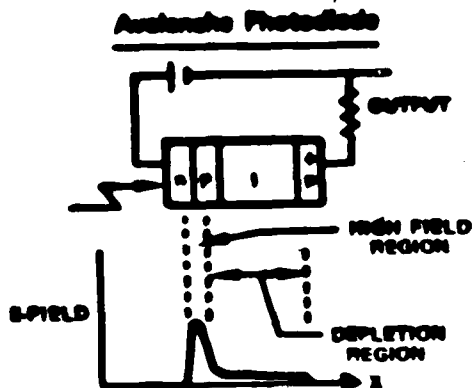


Figure A.9-25. Avalanche Photodiode

A variety of silicon avalanche photodiode (APD) structures are now commercially available. They increase receiver sensitivity by multiplying primary signal photocurrent internally before it encounters the thermal noise associated with input circuit of the following amplifier. In general, all APDs are operated at elevated voltage to obtain high internal gain. Since the noise increases with the gain, there is an optimum value of gain that maximizes sensitivity.

Generally the fabrication technologies can be grouped into five classes:

- Mesa planar
- N+PP+ Structure
- Reach-through APD (RAPD)

- Epitaxial RAPD
- Novel approaches (but unproved).

A mesa APD is sketched in Figure A.9-26, and is of the P+NN+ form with illumination entering from the P+ face. The P+ layer is driven in deeply (~3 mils) to achieve the correct field profile and for good overall quantum efficiency. The heavy doping, however, produces a wide dead layer at the surface that results in rapid recombination of the photocarriers generated by short wavelength illumination. To reduce this effect, the P-layer back is etched to remove the more heavily doped portion.

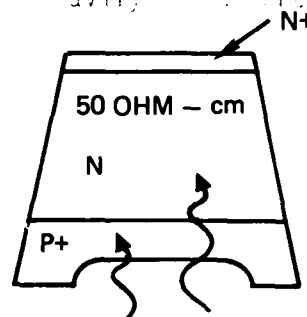


Figure A.9-26. Mesa APD

Electrically, this structure suffers from low gain of the deep generated minority photocarriers, which are holes, and not as readily multiplied as electrons. The structure does show high gain for the photoelectrons in the P-region, and the wavelength region from 500 to 800 nm suits this device.

Figure A.9-27 shows a N+PP+ structure (Ref. A.9-62). This APD is purely planar in design and relies on a guard ring to circumvent the field curvature problem. The guard ring is more lightly doped than the active region. Also, it is diffused deeper, is graded and covered with metal. This is to ensure that there will not be premature breakdown or rise of microplasmas.

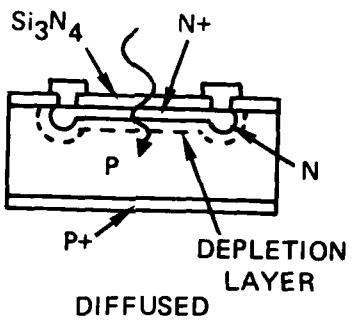


Figure A.9-27. N+PP+ Guard APD (GAPD)

The device structure has a good response in the 600 to 850 nm range because the electrons are generated and multiplied in the depletion region. Photocarriers from longer wavelengths must diffuse to the edge of the depletion region and lengthen the response time. The dead region absorbs wavelengths below 600 nm.

A so-called "reach-through" structure is sketched in Figure A.9-28. This kind of device takes full advantage of the possibility offered by silicon for carrier multiplication with very little excess noise, (Ref. A.9-63. The reach-through structure is composed of $P+\pi P+$ layers as shown. The high field PN^+ junction, where electron initiated avalanche multiplication takes place, is formed by diffusion or ion implantation with precise doping concentration. Under low reverse bias, most of the voltage is dropped across the PN^+ junction. As the bias is increased, the depletion layer widens predominantly into the P region and, at a certain voltage V_{rt} below the breakdown voltage of the PN^+ junction, reaches through to the nearly intrinsic π region. The applied voltage in excess of V_{rt} is dropped across the entire π region. Since the π region is much wider than the p region, the field in the multiplication region, and therefore the multiplication factor, will increase relatively slowly with increasing voltage above V_{rt} . In the operating range the field in the π region is substantially lower than that in the PN^+ junction, but is high enough to maintain limiting carrier velocities, thus assuring a fast speed of response.

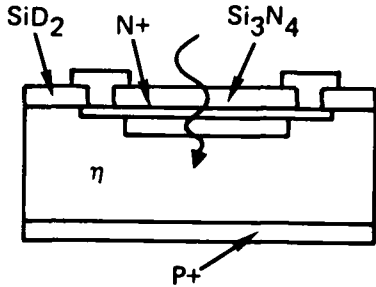


Figure A.9-28. Reach-Through APD

Because of the light incident on the P+ surface is almost completely absorbed in the n region, a relatively pure electron current is injected into the high field PN+ junction where carrier multiplication takes place. Thus a nearly ideal situation is obtained where the carrier type with the higher ionization rate initiates the multiplication process, resulting in a current gain with very little noise. An excess noise factor of 4 at a gain of 100 has been observed in a silicon reach-through avalanche photodiode (RAPD) produced for operation in the 0.8 to 0.9 μm wavelength range (Ref. A.9-63).

The three kinds of structures of APD discussed so far have P-regions with thicknesses that call for relatively high operating voltage. A solution to this problem is to use high resistivity, thin epitaxial layers. The configuration shown in Figure A.9-29 was developed for fiber optic communications that use a GaAlAs heterojunction laser, and it is based on a moderate resistivity ($\sim 50 \mu\text{m}$) epitaxial layer grown in a P+ substrate (Ref. A.9-64).

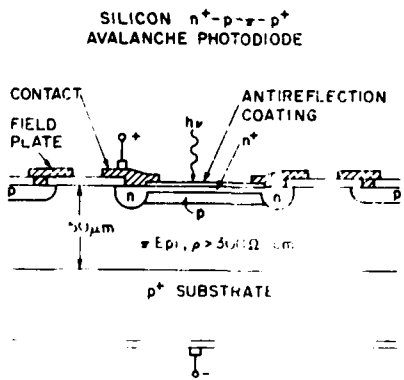


Figure A.9-29. Epitaxial Reach-Through APD

Quantum efficiency of epitaxial RAPDs is high. The field profile is so tailored that electron in the P region meet a low field while being injected through the junction, and holes in the N+ meet a high field to reduce the multiplication noise. Capacitance is low and response is fast.

In addition to the APD structures described above, there are a variety of alternatives under development, for example, new APD approaches and APDs employing mixed III-V compounds. The double mesa thin film RAPD consists of N+PnP+ layers (Ref. A.9-64). The double mesa reduces the fringing electric fields of this thin device, the small diameter (~3 mil) yields low capacitance and small dark current; the small thickness permits good quantum efficiency (at 600 nm) with rear gold reflector contact layer and a low, fully depleted operating voltage (20-50V) range. The device was measured to have a 300 GHz gain bandwidth product.

The double epitaxial structure is of the form of P+nPnN. The structure is designed for low multiplication noise, high speed of response and a relatively low avalanche breakdown. Its gain bandwidth product is also 300 GHz (Ref. A.9-64). There are two low loss infrared windows in optical fibers (1300 and 1550 nm) and industry has been pressured to provide fast APDs for these windows. To obtain the right energy gaps for these wavelengths, intermixed III-V semiconductor compounds have been investigated because the intermixed compound can provide the correct energy gap and be sensitive to any desired wavelengths. Three promising ADPs have been fabricated using the following intermixed III-V compounds:

1. $(Ga_{.17}Al_{.83})$ as on GaAs
2. $(Ga_{.24}In_{.76})(As_{.58}P_{.42})$ on InP
3. $(Ga_{.84}Al_{.16})Sb$ on GaSb.

All of these developed APDs are still in the laboratory development stage.

A.9.7 Research Trends and Systems Capability

The current state-of-the-art of fiber optics including aspects of components and systems has been briefly summarized and discussed in the previous subsections. It is seen that major breakthroughs and tremendous

growth have been occurring in the fiber optics fields in the last two decades. It can be concluded that fiber optic systems have already passed their prototype and field trial evaluation in the late 1970s, and now are phasing into widespread use. The universal availability of the virtually unlimited bandwidths at low cost through fiber optics will lead to rapidly increasing production of wideband communications system including videophone and high speed facsimile.

The advantage of utilizing fiber optics, as previously discussed, which will drive changeover from cable and microwave relay system to the fiber optic system can be summarized as follows:

- Very high bandwidth; billion-bit-per-fiber capability available at low cost by the late 1980s
- Greater bandwidth/volume; orders of magnitude more bandwidth in one-tenth the space
- Rapidly declining unit costs, in contrast to strongly increasing copper cable prices
- Extremely low loss; a few tenths of a dB per kilometer with low dispersion, virtually eliminating repeaters
- Freedom from electrical interference
- Greater security.

This subsection discusses predicted future development trends and system capability.

A.9.7.1 Fiber Optics Research Areas. Although fiber optics has been developed to a state where many experiment systems have been fielded over the world, and a few systems actually carry commercial traffic. Further research and development efforts are essential.

- Continuous improvement in the reliability of optical sources (both 0.8 to 0.9 μm and 1 to 1.7 μm)
- The realization of low loss reliable connectors and splices
- The development of efficient sources and detectors in the 1.0 to 1.7 μm wavelength region; in particular, 1.3 to 1.35 μm LEDs and 1.5 to 1.7 μm lasers

- Continuous progress in laser mode stabilization (spatial and in frequency) under system operation conditions (i.e., temperature variations; feedback from the fiber)
- High bit rate modulation
- The development of more efficient single mode and multimode modulators and switches as well as efficient techniques for coupling single mode fibers to I/O devices (sources and/or modulator/switches).

A.9.7.2 Fiber Optics Components

In a series of recently published articles, (Ref. A.9-64) the potential for fiber optics has been forecasted for the year 2000. Much of the following material is taken from these articles.

The optical graded-index fiber currently available can transmit data at 2 Gbps for one kilometer, within the error tolerance typically specified for data transmission. Figure A.9-30 shows the projected progress of graded index fiber data capacity toward 10 Gbps/kM. This improvement will result from continuing reduction of light dispersion in the fiber, due to improved material and more precise manufacturing controls, as well as a shift to longer wavelengths.

The continuing decrease in fiber attenuation and dispersion promises to drive a proportional increase in spacing between repeaters for a given data transmission rate. Repeater spacing by the year 2000 can be increased to 50 kilometers for one Gbps transmission in single mode fiber and 200 Gbps transmission in the lower cost graded index fiber. This will eliminate repeaters in virtually all except transcontinental and intercontinental links;

Single mode fiber will be used for long haul, high data rate links. This will greatly reduce the number of repeaters required, compared to wire links, and thereby increase reliability and reduce costs. Graded index multimode fiber will be used for interchange links and step index multimode fiber will meet nearly all subscriber service needs.

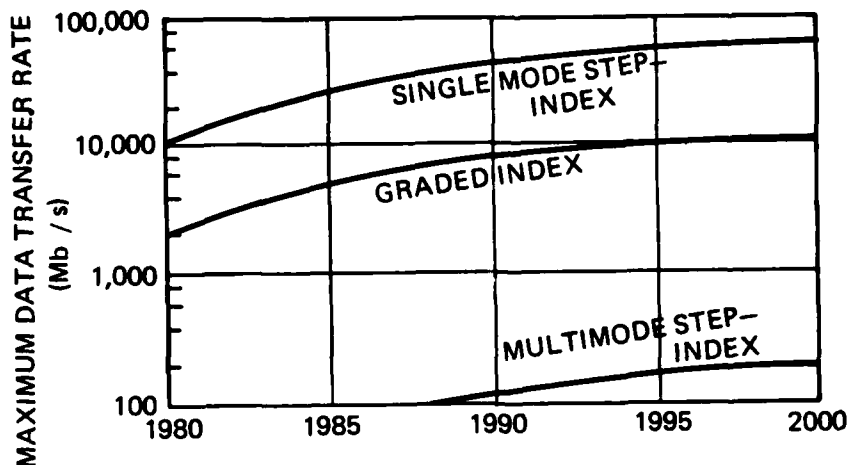


Figure A.9-30. Project Progress of Optical Fiber Transmission Capacity

It is anticipated that by the year 1990, over a dozen different fiber designs will become established industry standards. There will also continue to be special fibers specified by some users. Optical fibers will be used in hundreds of different cable configurations. Over 85 percent of optical cable, dominated by telecommunications use, will consist of standard cataloged designs. However, it is also expected that some special cable of custom design will be produced for special applications for example, those required by computer manufacturers.

Cable designs can vary in many ways, including:

- Varying numbers of one fiber type
- Varying numbers of several fiber types
- Combined fibers and various copper lines
- Choice of outer constructions, for different installation environments, including: flexible pull in; aerial; buried; submarine; harness etc.
- Internal construction details.

With the trend to much stronger fibers, less jacketing material will be used in the design. This will significantly reduce size, weight and cost.

High performance fiber optic cable prices have dropped by a 10:1 factor over the 1975-1980 span, as production transitioned from laboratories to pilot plants. With increased efficiency of high volume production, prices will drop by another order of magnitude by 2000, as noted in Figure A.9-31. High performance cable will be available at less than ten cents per fiber meter. Lower performance cable for subscriber connection will cost much less. Likewise transmitter and receiver modules, connectors and other components will also experience drastic price reductions. Displacement of copper cables will approach 10 percent by 1990; it will be much higher in certain applications. By 2000, virtually all new installations will use fiber. Also, many copper cables will be pulled out, scrapped, and replaced by fiber.

Regarding solid state light sources, there has been rapid advancement over the last few years in areas such as increased lifetime, power output, linearity, radiation pattern, and efficiency. These improvements will likely continue over the next two decades. The power output from the stripe double heterostructure laser diode will rise to several watts by 2000, and the power of the low cost hemisphere LED will climb to several tenths of a watt, as shown in Figure A.9-32.

Over the same period, lifetime will increase so that it no longer is a constraint in overall system planning. Some laser diodes already carry life guarantees of over 10,000 hours. This is an order of magnitude improvement over the past five years. High temperature accelerated life tests show that these same currently produced devices have a projected life of over 100,000 hours. Beyond 1990, lifetime exceeding 100,000 hours (11 years) will be routinely available in production devices, as depicted in Figure A.9-33. Also, longer wavelength devices promise to enhance useful life.

A.9.7.3 Predicted System Capability. In the interest of the current study, a prediction of fiber optic communications systems capability has been made for the period of the 1990s. Because of the dynamic growth and development of the optical field, reassessing the prediction may be needed at two to three year intervals.

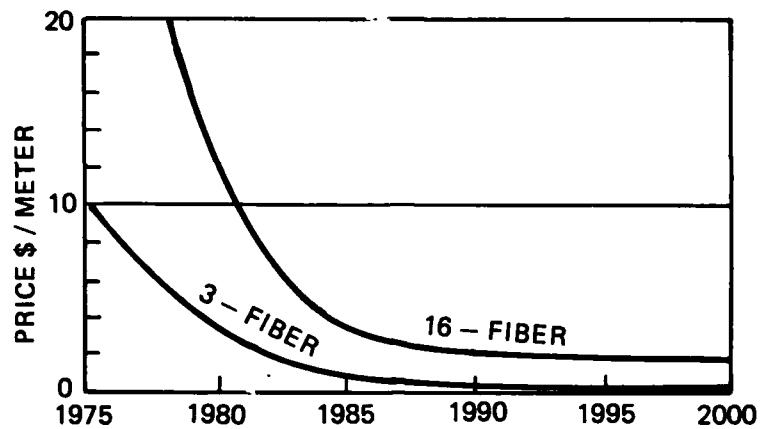


Figure A.9-31. Projected Optical Fiber Price

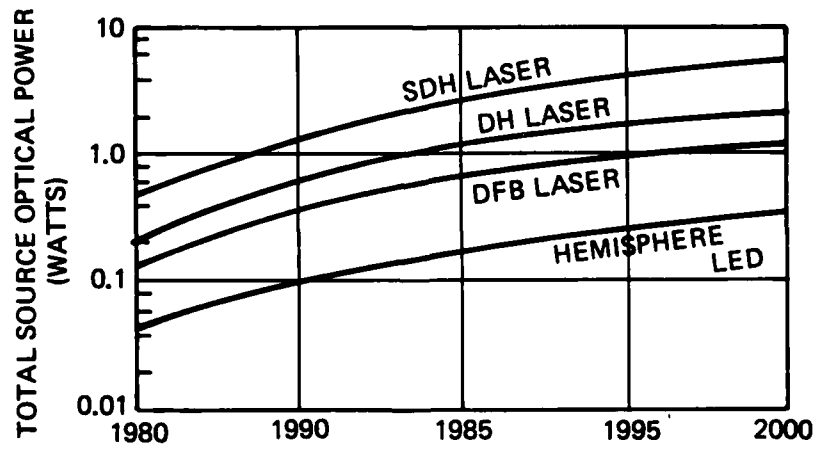


Figure A.9-32. Projected Power Output of Optical Sources

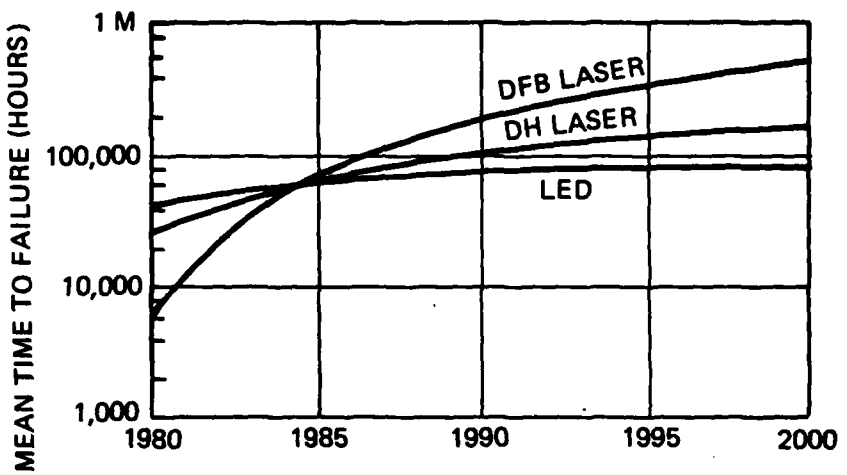


Figure A.9-33. Projected Mean Time to Failure of Optical Sources

Table A.9-3. Predicted Capability of Fiber Optic Communications System

	Bit Rate	Repeater Spacing (km)	Circuit Length (km)	Fiber	Source	Detector
Large Capacity Long Haul System	1.2~1.6 Gbps	15~30	2,500~4,000	Single Mode	LD	APD
Medium Capacity Short Haul System	300~400 nbps, PCM	20~40	200~300	Single Mode or multimode, graded index	LD or LED	APD
Small Capacity, Local System	10~30 Mbps PCM or Analog	50	10f50	Multimode, step index or graded	LD or LED	APD or PIN

A.10 SUBMARINE CABLES

The principal transoceanic transmission media are HF, submarine cable, and satellite. These media have been developed and implemented for use in that order.

The first transatlantic HF circuit was established in 1927 and from then to the 1950s many advances have been realized. However, one radio carrier frequency at most can carry only two voice channels by employing independent single-sideband (ISB) techniques. A number of frequencies also must be allocated for each circuit to maintain continuous operation due to diurnal and seasonal changes of the ionosphere. Nevertheless, a large volume of digital data cannot be handled by a HF circuit owing to the low received signal-to-noise ratio, frequency-selective fading characteristics, multipath, and Doppler spread.

Beginning at about 1950, multiple-circuit submarine cables began to provide transoceanic telephone service. The number of circuit miles of submarine cable systems has increased from less than one million in 1956 to about 70 million in 1978. Since 1960, the ever-increasing satellite service provided by INTELSAT shares transatlantic and transpacific traffic with the submarine cable systems. There is now considerable competition between high-capacity submarine cables and satellites for future international telecommunications.

Use of diversified telecommunications comprised of submarine cables and satellites nevertheless is justified and beneficial because the advantages and disadvantages of cable and satellite systems are supplementary to each other. For example, the communications backbone network of the British Commonwealth, as shown in Figure A.10-1 (Ref. A.10-1), clearly demonstrates the supplementary nature of these two long-haul transmission media.

A.10.1 Development of Submarine Cable

Following Subsections A.10.1.1 through A.10.1.3 present a brief description and discussion of the development of submarine cable communication systems.

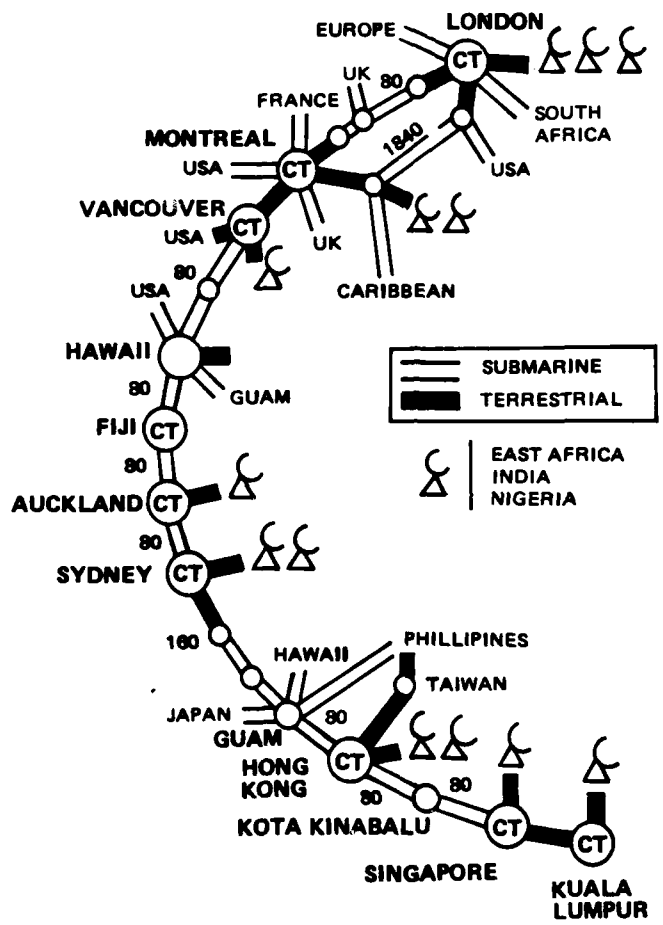


Figure A.10-1. Commonwealth Backbone Network

A.10.1.1 Development of Submarine Telegraphic Cable. The first successful armored submarine cable was laid in the English Channel between England and France in 1850. England was first linked to Ireland in 1853 by submarine cable, and two more cables were laid in the same year. In 1854, cables were laid in the Mediterranean Sea for the French and Italian governments, and an unarmored cable was laid from Varna in Bulgaria to Balaklava, now part of the Ukrainian USSR. This cable remained serviceable for about one year. Attempts were also made to lay cables between La Spezia and Corsica and between Bone and Sardinia that were intended to connect France to its colony of Algeria via Italy. With the Sardinia-Benz link telegraph engineers tackled deep water of 2926 meters (1600 fathoms) for the first time.

Two attempts at laying transatlantic cables occurred in the years 1857 and 1858. The first failed completely and the second provided satisfactory signal for only half a year. In the summer of 1866 a successful transatlantic lay operation resulted, as even then it had become possible owing to development of deep-sea grappling techniques to splice the two ends of the 1865 cable which had parted. Consequently, the Atlantic Ocean was spanned by two working telegraph cables. From that time onward, submarine cables proliferated until by the end of the century there were few points of strategic or commercial importance that could not communicate telegraphically.

A.10.1.2 Development of Submarine Telephone Cables. Although first Anglo-French telephone cable was laid in 1891, the first submarine telephone cable across the Atlantic, which provided 37 voice circuits, was not laid until as recently as 1956. It also should be noted that the first radio telephone service across the Atlantic was established in 1937. By 1966 the total number of cable circuits across the Atlantic had risen to about 500, and now in a normal day over 5000 telephone calls are made between North America and the UK. Cables TAT-2 and TAT-4 are installed between USA and France, cables TAT-1 and TAT-3 carry calls between America and Britain, and cables CANTAT-1 and CANTAT-2 carry calls between Canada and Britain.

The first submarine telephone cable between Canada and UK (CANTAT-2) was put into service in 1961, providing 80 voice circuits. CANTAT-2, inaugurated in 1974, based on greatly improved technology, is capable of carrying 1840 voice circuits.

An alternative indirect route for transatlantic traffic is through TAT-5 submarine cable between Spain and the USA, which has a direct connection with the cable constructed for the UK post office between the UK and Portugal in 1969. It is the sixth submarine telephone cable that has been laid on the bed of the Atlantic.

An order for an undersea telephone cable system between Europe and South America was awarded in 1975 jointly by the telecommunications administrations of Spain and Venezuela. This contract is for a 6,000-km cable capable of carrying 1840 simultaneous telephone conversations between the Canary Islands and Venezuela, and it will also be used for data and telex transmission.

Across the Pacific, the transpacific telephone cable runs from the United States through Hawaii and Guam to Japan and the Philippines, and the Commonwealth COMPAC/SEACOM link runs from Canada to New Zealand, Australia, Hong Kong, and Singapore. Mixed cable systems serve the Caribbean.

In 1975 the largest undersea telephone cable contained only 1840 circuits. However, in 1977 a new-generation system linking the UK with Belgium and Providing 3900 circuits (Europe's biggest-ever undersea telephone cable) was installed. At the present time one of the world's largest-capacity undersea cables known as the NS-1 system is being laid in the Mediterranean Sea. This Italian PTT cable system connects Palermo in Sicily with Rome and provides from 3600 to 5000 circuits utilizing 45-MHz bandwidths.

A.10.1.3 Major Submarine Cable Routes. The major submarine cable telephone routes in the Atlantic Ocean, Pacific Ocean, and Mediterranean Sea are shown in Figure A.10-2. Important cable parameters of these cable routes are listed in Table A.10-1.

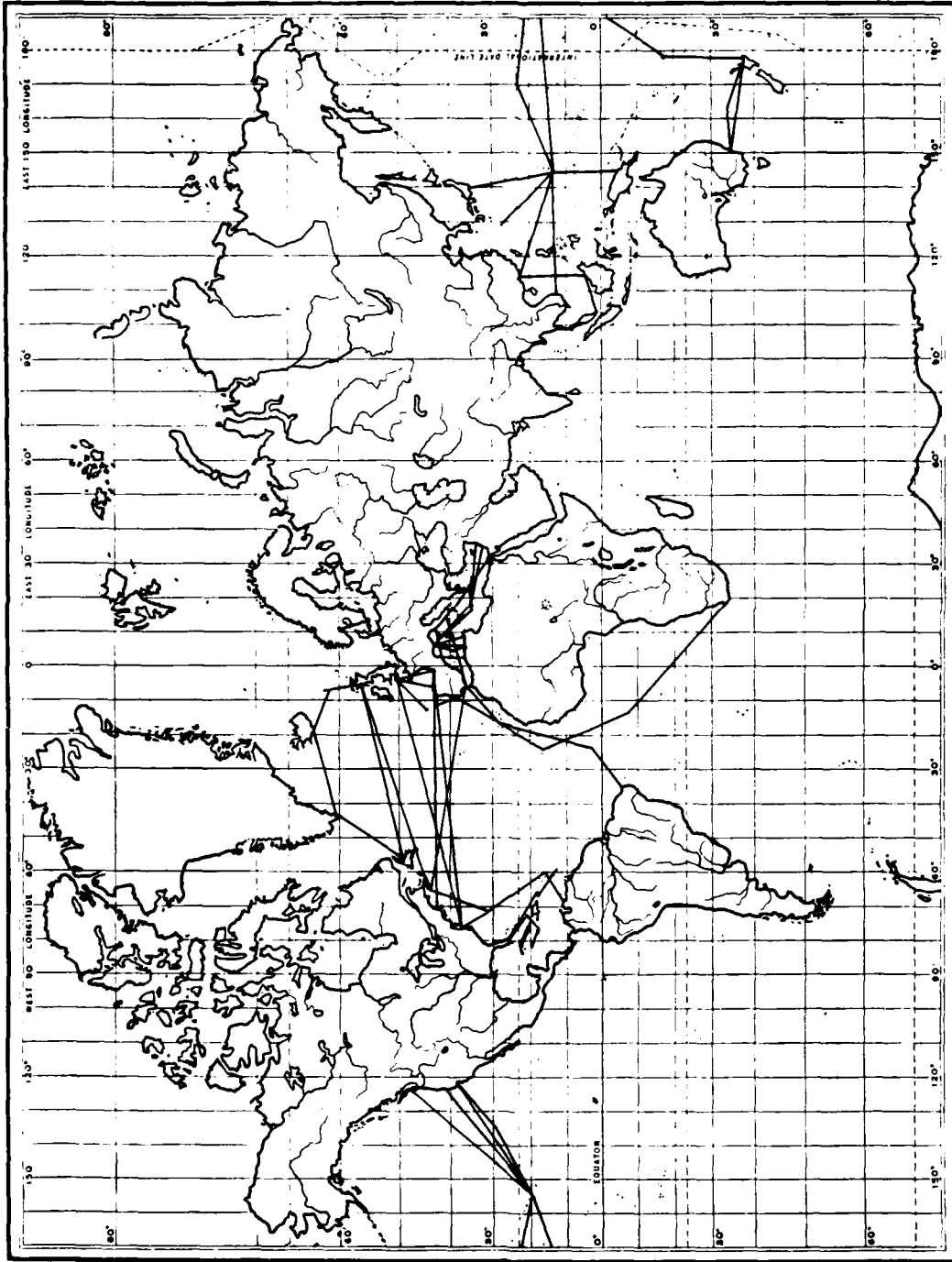


Figure A.10-2. Major Transoceanic Submarine Cable Route

A.10-5

Table A.10-1. Some Typical Transoceanic Submarine Telephone Cables

Designation	Laying Date	Terminals	Number of Circuits	Length and Repeater	Remarks
TAT-1	1956	Obon-British Terminal Clarenville-Newfoundland Western Terminal	29 London to New York 6 London to Montreal 1 Split between London to New York and London to Montreal for Tele- graph and other narrow band users.	7210 km, 51 flexible one-way repeater in each cable	Armored cable; 4 kHz speech channel, 3 sections with cable length, carrier frequency band 20-164 kHz. 37, 2319, 930 km; extension from Clarenville to Sidney mines, Nova Scotia using a single 503 km cable with 14 rigid repeater.
TAT-2	1959	Pennarach-France Clarenville-Newfoundland	36 USA to Europe	8354 km, 51 flexible one-way repeater in each cable	Armored cable (same as TAT-1). 642 km cable used for clarenville to Sidney mines.
CANTAT-1	1961	CANTAT A: Scotland and Newfoundland CANTAT B: Corner Brook, Newfoundland and Grosses Roches on Canadian mainland	80	CANTAT A; 3710 km, 90 rigid two-way repeater Cantat B: 743 km, 20 repeater	Lightweight unarmored cable; 3 kHz speech channel with quality slightly inferior to standard 4 kHz channels carrier frequency bands, 60-310 kHz and 360-618 kHz.
TAT-3	1963	Widemouth Bay, Cornwall Tuckerton, NJ	128	6683 km, 183 rigid two-way repeater	CANTAT-1 cable, 3 kHz bandwidth.
TAT-4	1965	St. Hilaire, France Tuckerton, JF	128	6683 km, rigid two-way repeater	CANTAT-1 cable, 3 kHz bandwidth
SAT-1	1968	Lisbon, Canary Islands, Cape Verde Island, Ascension Island, Cape Town	360	11,000 km, 643 repeaters and 51 equalizers	Lightweight cable, high quality channel, Ascension Island to Cape Town is the world's longest deep water link.
UK-Portugal	1969	Lizard, Cornwall Lisbon	480	1600 km, 133 transistorized repeaters, 10 equalizers	CANTAT-1 cable with armored cable at the shore ends, high quality 4 kHz channel. First deep water long haul transistorized cable.
TAT-5	1970	Rode Island, USA San Fernando, Spain	845	6500 km, 332 repeater	CANTAT-1 cable, 3 kHz bandwidth. cable buried in the seabed at both ends.
CANTAT-2	1974	Widemouth Bay, Cornwall Halifax, Nova Scotia	1840	5012 km, 490 repeater	CANTAT-1 cable, 3 kHz bandwidth. external armored cable used in shallow water of depths less than 300 fathoms. Cable and repeater are buried.
TAT-6	1976	Green Hill, USA St. Hilaire France	4200	6100 km, 990 repeater, 30 block equalizer and 5 shore con- trolled equalizers	Armorless deep-sea cable, 3 kHz speech channel, carrier frequency bands 0.5-13.9 MHz and 16.1-29.5 MHz.

A.10.2 Submarine Cable Technology Development

Ever since the first submarine cable design (Bell SB system) was installed in 1955-1956, voice-communications traffic growth has continued at a rapid rate. To fulfill these escalating requirements, improved intercontinental submarine cable systems have been designed, installed, and put into service. The great increases in bandwidth and channel capacity that have been achieved are the result of a massive evolution in the physical and electrical configurations of submarine cable systems, which in turn has required new laying and testing techniques. Systems of today have little similarity with their predecessors.

Three new designs have been adopted after the Bell SB system was completed in 1956, each one having channel capacity many times greater than that of its predecessors. Table A.10-2 summarizes the major parameters of the Bell System submarine cable system (Ref. A.10-3), and clearly indicates the technology developments occurring over the last two decades. The last few years particularly have witnessed an unprecedented development of submarine cable system technology, with systems having bandwidths of 25, 28, 36, and 48 MHz progressively introduced into service by various administrations. These systems offer varying circuit capacities of between 3000 and 5500 circuits, as noted in Table A.10-3.

The progression of technology in terms of the system bandwidth with time is indicated graphically in Figure A.10-3, systems of 45 MHz bandwidth now offering some 4000-5500 circuits capable of spanning Atlantic distances. As indicated, during the last 20 years bandwidth and system capacity have increased more than one-hundred-fold. Advanced laboratory research and development work has confirmed the technical feasibility of even larger-bandwidth systems that are capable of providing 10,000 to 15,000-circuit capacity when the demand for such systems arises. Thus as in many other areas of technological developments, submarine systems currently are ahead of traffic requirements and hence abreast with market demand, and this condition is likely to prevail for several years. In the meantime most research and development work is directed toward improvements in system performance and in the economics of current designs. These

Table A.10-2. Bell System Submarine Cable

System Parameters	System				
	SB	SD	SF	SG	C*
Service Date of First Installation	1956	1968	1968	1963	1980s
Top Transmission Frequency (MHz)	0.164	1.05	6	30	125
Coaxial Cable Diameter (mm/in)	15.9/0.625	26.7/105	38.1/1.5	43.2/1.7	57.2/2.25
Maximum Length (km/nmi)	3704/2000	7408/4000	7408/4000	7408/4000	7408/4000
Length Between Ocean Block (spacing between block equalizer) (km/nmi)	370.4/200	35.6/192	355.6/192	277.8/150	138.9/75
Repeater Spacing (km/nmi)	70.4/38	37.4/20	18.5/10	9.3/5.0	4.6/2.5
Repeater Gain at Top Frequency (dB)	60	50	40	41	38
Repeater Type	Physical, 4-wire, 2 cables	Equivalent, 4-wire 1 cable	Equivalent, 4-wire, 1 cable	Equivalent, 4-wire, 1 cable	Equivalent 4-wire 1 cable
Repeater Active Device	Tube	Tube	Germanium Transistor	Silicon Transistor	Silicon Transistor
Repeater Housing	Flexible	Rigid	Rigid	Rigid	Rigid
Type of Deep-Sea Cable	Armored	Armorless	Armorless	Armorless	Armorless
Maximum Terminal Voltage (V)	1600	6000	4200	7000	?
Relative Cost**	1	1/4	1/10	1/30	1/60

* Planning Estimates

** Cost Relative to First (SB) System

Table A.10-3. Varying Cable Bandwidth and System Capacity

Parameter	System Capacity			
System Bandwidth (MHz)	25	28	36	45
System Designation	S.25	SG	CS-36M	NG
Circuit Capacity (3 kHz)	3440	4000	3600	5520
Repeater Gain (dB)	40	41	33	35
Repeater Spacing (nmi)	4.4	5.1	3.2	2.8
Cable Size (mm)	38.1 (A1)	43.2 (Cu)	38.1 (Cu)	37.3 (A1)
Country of Manufacture	France	USA	Japan	UK
Year of First Installation	1976	1976	1974	1977
System Miles in Service	1492	3396	743	1273

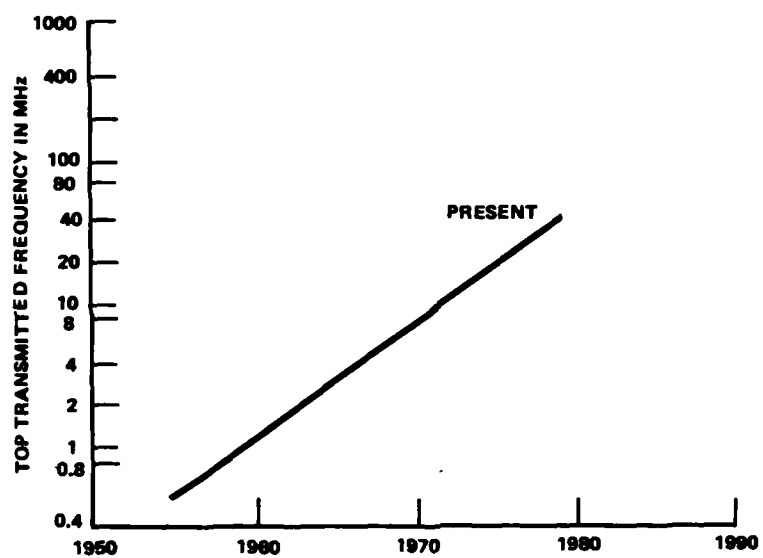


Figure A.10-3. Growth of Submarine Cable System Bandwidth

present designs conveniently service all ranges of traffic requirements, and costs have been greatly reduced by the new technology and the ever-increasing bandwidth and system capacity. Figure A.10-4 illustrates progressive cost reduction in the past two decades.

A.10.3 Recent Growth of Submarine Cable

The satellite system is the only competitor which can provide about the same capacity as a submarine cable system, the INTELSAT-4 satellite, for example, providing capacity of 6000 voice channels with an average operational life of five years. In contrast, the US/UK/France TAT-6 cable system has a capacity of 4000, and the NG-I system in the Mediterranean Sea has a capacity of 5520 voice channels. The cable system usually has a life span of twenty years or more. For example, the first transatlantic TAT-1 submarine cable system was phased out in November 1978 after providing service for 22 years, and at the time of retirement was still in operating condition.

Although much has been said on the subject of satellite communications in the last two decades. The submarine cable system has also advanced and expanded at comparable speed. However, submarine cable systems remain relatively unknown and unrecognized. Due to the fact that since initiation of INTELSAT-4 service in 1974 a massive expansion of the INTELSAT-4 network has occurred, this discussion will outline the little-known growth of submarine cable systems over the same period.

By the end of 1973 the global submarine network consisted of some 140 individual point-to-point links with an overall total of 41.5 million circuit kilometers. The term circuit miles is a very useful indicator, in that in addition to providing a product of distance and system capacity, it also reflects an indirect relationship with associated investment costs.

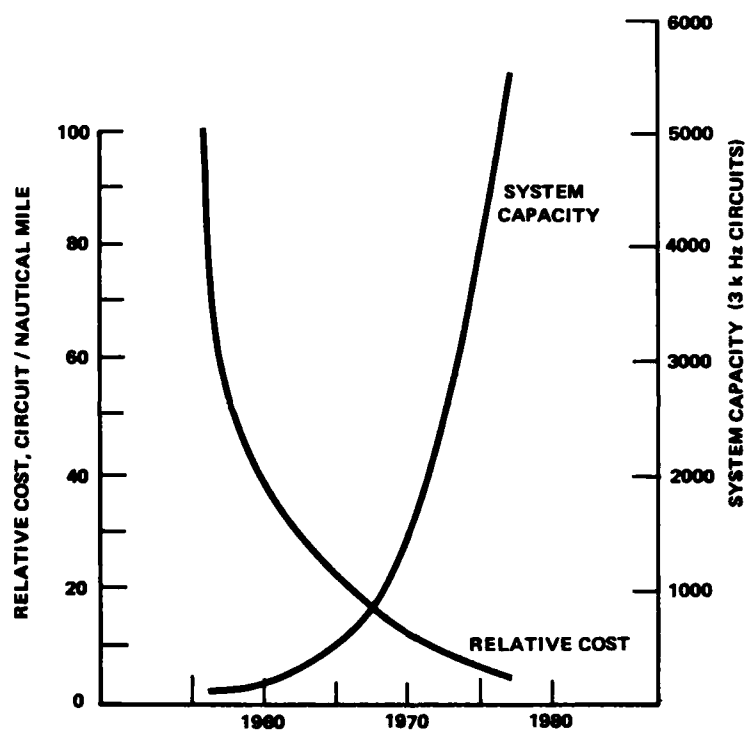


Figure A.10-4. Submarine Capacity and Relative Cost Progress

The distribution of these 140 links by broad geographical area is shown in Table A.10-4 (Ref. A.10-4). It should be noted that although the majority of systems operating in 1973 were deployed on the short sea crossings in Europe and North Africa, there also were 20 cable links crossing the Atlantic Ocean and 14 links crossing the Pacific.

In the five-year period from 1974-1978 the submarine cable network grew from 41.5 circuit kilometers to 144.5 million circuit kilometers. Table A.10-5 indicates cable network growth by year over this span. It is interesting to note that in all of these years except 1978 a major transoceanic cable system had been inaugurated (i.e., CANTAT-2 in 1974; TRANPAC-2 in 1975; TAT-6 in 1976; and COLUMBUS (Canary Islands to Venezuela) in 1977).

According to a 1979 statistic there are 8 submarine cables for a total length of 6863 kilometers, and 12.0 million circuit kilometers were scheduled to be completed by 1979 and 7 cables with a total length of 7126 kilometers and 10.5 million circuit kilometers in 1980 (Ref. A.10-4). Based on the same source, there also are the 14 known planned submarine cable systems that are listed in Table A.10-6.

Table A.10-4. Distribution of Submarine Cables

Area	Number of Submarine Systems	System Circuit Kilometers (Mkm)
North Sea and Northern Europe	37	5.4
Mediterranean Sea	29	10.0
Atlantic, Including Caribbean	39	18.3
Pacific, Including Southeast Asia	35	7.8
Indian Ocean	None	None

Table A.10-5. Cable-Network Growth in 1974-1978 Period

Year	Number of Cables	Route Length (km)	Circuit Kilometers (Mkm)
1974	6	13,610	17.1
1975	11	16,462	15.2
1976	9	14,284	32.8
1978	7	9,426	21.7
1978	7	9,426	16.3
Five Year Total	42	56,053	103.1

Table A.10-6. Planned Submarine Cable Systems

Interconnected Countries	Tentative Capacity (Circuits)	Length (km)	Minimum Expected Circuit km (Mkm)
France-Greece	2,580	2,222	5.7
Brazil-Senegal	1,200	3,334	4.0
Senegal-Portugal	2,580	3,056	7.9
CONUS-Hawaii No. 4	3,000	4,445	13.3
Bahrain-Qatar-UAEWE	1,380	685	6.9
Greece-Cyprus	900	1,167	1.0
Egypt-Greece	900	740	0.7
US/Canada-Europe (TAT-7)	4,200	6,197	26.5
Thailand-Malaysia-Singapore	480	1,556	0.7
Bahrain-Kuwait	900	556	0.5
Australia-Hawaii	1,380	8,890	12.3
Hawaii-Canada	1,380	4,815	6.6
Japan-Hawaii	1,600	6,852	11.0
India-Gulf	900	1,296	1.2

A.11 METEOR-BUST COMMUNICATIONS SYSTEM

A Meteor-Burst Communications System (MBCS) is a medium-range system operating at VHF (30-300 MHz) band that can provide a rapid, secure, two-way digital communications service. Other types of services such as voice and facsimile, although they have been tested, have not as yet been implemented. MBCS operation is based on use of the meteoric forward-scattered wave phenomenon induced by the ionized trails left behind by meteors penetrating the lower ionosphere.

A.11.1 Introduction

It is estimated that the earth's ionosphere and atmosphere are bombarded by about 10 billion meteors a day, most being burned or vaporized upon entry to the ionosphere due to collision with air molecules. The collision process produces trails of free electrons in the meteoric wakes, and resulting ionized trails are capable of reflecting or scattering electromagnetic waves in the VHF band. These forward-scattered signals reach a distance far beyond the usual line-of-sight range because of the high altitude of these trails (80-110 km).

A MBCS which utilizes meteor-scattered waves is an intermittent system because of the short duration of each trail and the randomness of trail occurrence. A meteor-scattered signal in general is much stronger than an ionospheric and/or tropospheric scattered signal which is a varying-amplitude but continuous signal produced by scattering within inhomogeneities of the ionosphere or troposphere. A MBCS consequently is a lower-power and a low-transmitting-rate system in contrast with the scatter systems, which employ large directional antennas and high-power transmitters. Initial investigation of the feasibility of using meteor-scattered waves for communications, design and development, system evaluation, and testing was conducted in the U.S. and Canada in the years immediately after World War II, and this pioneer work was declassified in 1957. A special issue of IRE (Ref. A.11-1) describes efforts undertaken during this classified time period.

The well-known Canadian JANET System (Ref. A.11-2) was developed in this period and put into use in 1954. Several experimental-data (TTY), voice, facsimile, and air-ground data (TTY) systems have been successfully

demonstrated in the U.S., but no further developmental work to put them into practical use has been performed. Recently the Supreme Headquarters Allied Powers in Europe (SHAPE) Technical Center (STC) has developed a meteor-burst system called Communications by Meteor Trail (COMET), which incorporates both diversity reception and automated request for repeat card features, and this system has been intensively tested in the past several years. In addition, there is an ongoing DCA/MEECS program to investigate and evaluate potential applicability of a MBCS-to-MEECN system for the purpose of EAM dissemination.

The following subsections briefly review the operational principle of a MBCS, describe developed systems features and their capability, and evaluate the utility of such systems for DCS III.

A.11.2 System Concept

The intermittent communications capability of a MBCS depends on high-altitude scattering meteor trails. Information on meteors, their ionized trails, and scattering characteristics is presented below to facilitate understanding of the operation of a meteor communications system and to evaluate the utility of such a system.

A.11.2.1 Physical Properties of Meteors

The two classes of meteors are shower meteors and sporadic meteors. A shower meteor is a collection of a large number of meteor particles all moving at the same velocity in a fairly well-defined orbit around the sun. Orbit of these particles intersect the orbit of the sun at a specific time each year, at which times spectacular meteor showers are observed and the resulting signals are enhanced. However, it is the non-shower, or sporadic, meteors which provide all of the ionized trails of interest causing wave scattering.

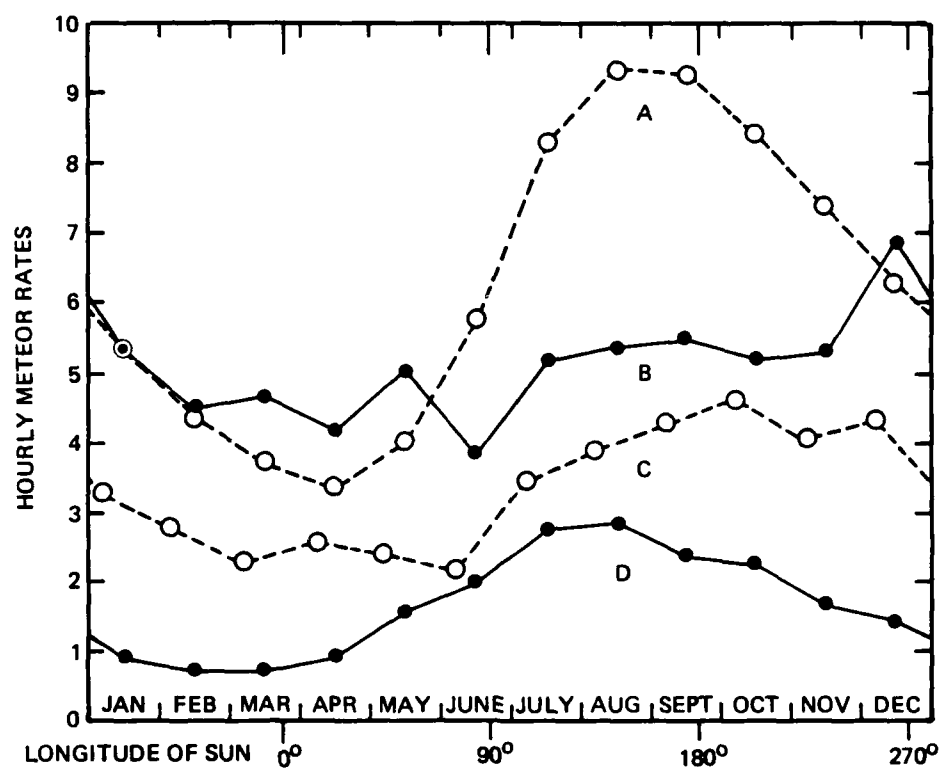
Sporadic meteors are classified according to their order of magnitude of weight, as shown in Table A.11-1 (Reference A.11-3). The total number of meteors of mass magnitude of order N or greater swept by the earth in a day is 10^N , the meteors of interest for a MBCS being those of between an order of 2 and an order of 12. The total number of meteors of interest are 10^{11} per day.

Table A.11-1. Characteristics of Sporadic Meteors

Mass (g)	Radius (cm or μm)	Number of Meteors of This or Greater Mass Swept by Earth Per Day	Electron Density of Trail (electrons/m)
10^4	8 (cm)	10	--
10^3	4	10^2	--
10^2	2	10^3	--
10^1	0.8	10^4	10^{18}
10^0	0.4	10^5	10^{17}
10^{-1}	0.2	10^6	10^{16}
10^{-2}	0.08	10^7	10^{15}
10^{-3}	0.04	10^8	10^{14}
10^{-4}	0.02	10^9	10^{13}
10^{-5}	80 (μm)	10^{10}	10^{12}
10^{-6}	40	10^{11}	10^{11}
10^{-7}	20	10^{12}	10^{10}
10^{-8}	8 (μm)	?	?

Such a large number of meteors is not uniformly distributed either temporarily or spatially. As shown in Figure A.11-1, the rate of meteor incidence not only has a strong diurnal variation, with a maximum rate at 6 am and a minimum of 6 pm, but also a superimposed annual variation. Observed velocities of meteors approaching the earth lie between the limits of 11.3 and 72 km/sec and significantly impact characteristics of resulting ionized trails such as their heights and electron densities.

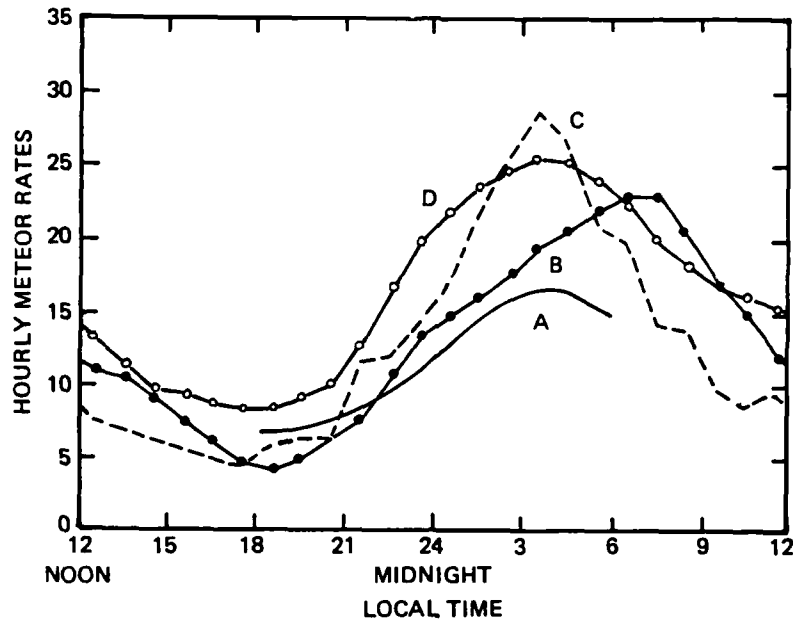
The height at which a meteor trail appears depends upon mass, velocity, and path geometry of the meteor, the density of the ionosphere or atmosphere, and the method of observation used. Figure A.11-2 shows meteor heights as observed by the photographic radio method.



(a) MEAN ANNUAL VARIATION OF METEOR RATE

- A. NAKED-EYE VISUAL OBSERVATION
- B. TELESCOPIC VISUAL OBSERVATION
- C. FORWARD-SCATTER RADIO OBSERVATION (MULTIPLE ORDINATE SCALE BY 20)
- D. BACKSCATTER RADIO OBSERVATION (MULTIPLE ORDINATE SCALE BY 2)

Figure A.11-1. Temporal Variation of Meteor Rates



(b) MEAN DAILY VARIATION OF METEOR RATE

- A. NAKED-EYE VISUAL OBSERVATION
- B. BACKSCATTER RADAR OBSERVATION (MULTIPLE ORDINATE SCALE BY 50)
- C. BACKSCATTER CW OBSERVATION
- D. FORWARD-SCATTER CW OBSERVATION (MULTIPLE ORDINATE SCALE BY 2)

Fig. 1. Mean Daily Variation of Meteor Rates

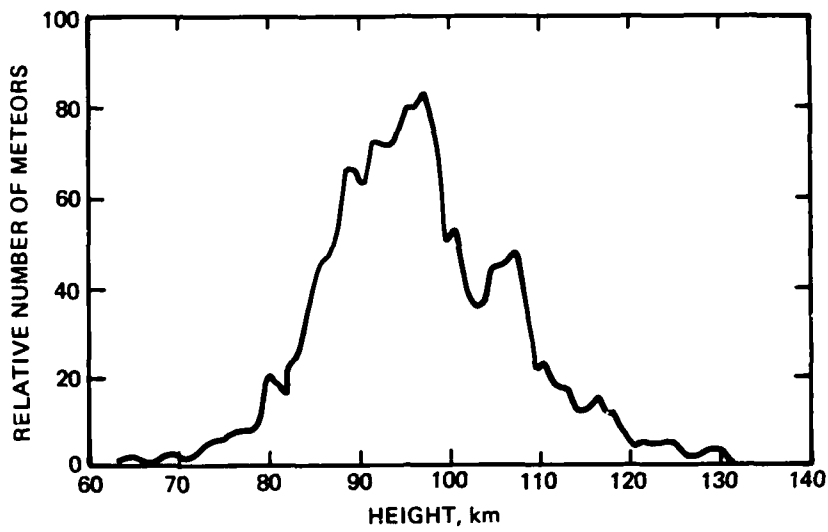


Figure A.11-2. Frequency-Height Distributions of Long Enduring Meteor Trails

A.11.2.2 Meteor Trails

The meteor trails formed when meteors impinge the ionosphere consist in part of highly ionized gases. The electron density of these trails, which are of more or less cylindrical form, often is high enough to scatter incident radio waves.

A study has shown that the region of ionized gas formed near the meteor path expands almost instantaneously to about 2 meters at 15-km altitude and to 3 meters at 85 km altitude, after which it continuously expands at a much slower rate by normal diffusion (Ref. A.11-4). The radius of the thin ionization column of diffusion, r , is given by

$$r^2 = 4 Dt + r_0^2 \quad (\text{A.11-1})$$

where

r_0 = initial radius

t = time measured from the instant the meteor passes the point under consideration

D = diffusion coefficient ($1 \text{ m}^2/\text{sec}$ at 85 km and $140 \text{ m}^2/\text{sec}$ at 115 km)

It should be noted that both D and r_0 vary rapidly with height.

A.11.2.3 Scattered Signal of an Idealized Trail

An idealized trail is defined as an ionized column of zero radius with an electron line density, γ , in number of electrons per meter. The pertinent geometry of the forward-scattering case under consideration is shown in Figure A.11-3, wherein the plane containing the transmitter, T , the receiver, R , and the scattering trail center, S , is the propagation plane and the plane containing the meteor trail, which is perpendicular to the propagation plane, is the tangent plane. The incident and scattered rays make an equal angle, ϕ , with the trail, and the meteor trail may assume any orientation in the tangent plane, the angle between the trail and the intersection of these planes being denoted by β . The major contribution to the forward-scattered wave is from electrons located along the trail inside the first Fresnel zone, the half length of which is denoted by ℓ . From the definition of the Fresnel zone, then,

$$R'_t + R'_r = R''_t + R''_r = R_t + R_r + \frac{\ell}{2} \quad (\text{A.11-2})$$

where R'_t and R''_t or R'_r and R''_r are distances from one end or the other end of the zone to the transmitter and receiver respectively. It follows that

$$\ell^2 = \frac{R_t R_r}{(R_t + R_r) (1 - \sin^2 \phi \cos^2 \beta)} \quad (\text{A.11-3})$$

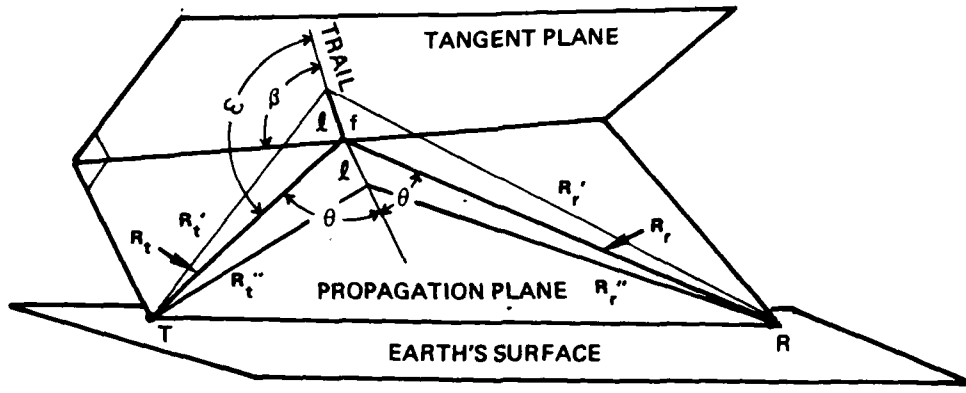


Figure A.11-3. Geometry of Forward-Scattering

and therefore the received scattered signal power from an idealized trail is

$$P_r = P_t \frac{G_t G_r \lambda^3}{(4\pi)^2} \times \frac{r_e^2 q^2 \sin^2 \gamma}{R_t R_r (R_t + R_r) (1 - \sin \phi \cos \beta)} \quad (A.11-4)$$

where

P_t = transmitted power

G_t, G_r = power gains of transmitting and receiving antennas respectively

R_t, R_r = distances from the electron to transmitter and receiver respectively (m)

λ = wave length (m)

T_c = effective electron cross-section area (m^2)

and the effective cross-section area of a free electron is

$$\sigma = 1.5 \left(\frac{8}{3}\right) \left(\frac{e^2}{M_c^2}\right) \sin^2 \gamma = 4\pi r_e^2 \sin^2 \gamma \quad (\text{A.11-5})$$

where

e = electron charge (C)

M = electron mass (kg)

C = velocity of light (m/sec)

γ = angle between electric field vector of incident wave and line-of-sight from scattering electron to receiver.

r_e = classic electron radius

1.5 = numerical coefficient representing dipole-type scattering by a free electron

It is important to note that the scattered power from an idealized trail as given by Equation (A.11-4) will subsequently be referred to as $P_r(0)$, or received power from various kinds of meteor trails, in the following discussion.

A.11.2.4 Scattered Signal from Meteor Trails

To model the meteor trails for scattered-signal analysis, the trails are classified as high-density (overdense) and low-density (underdense) trails. However, the density of importance in meteor-trail analysis is line density rather than volume density. Also, the division between high or low density is not a well-defined quantity but usually is taken as 10^{14} electrons per meter. For low-density trails, the approximated analysis is based on summing scattered waves from each ionized electron, with assumption that the incident wave passes through the trail without change. On the other hand, in the case of high-density trails ray tracking through the ionized trail is used.

Due to the fact the scattered signal from a trail not only depends on the density but also on the frequency of incident waves, division in frequency is also needed for analysis because at higher-frequency modeling a trail by a cylinder longer remains accurate. The division between high and low frequency is commonly taken to be about 100 MHz. However, with present interest limited to the low-frequency case, only low-frequency underdense trails and low-frequency overdense trails are addressed in the following discussion.

a. Low-Frequency Underdense Trails

Eq. (A.11-4) yields received scattered signal power after the zero-radius underdense trail is formed. For a trail with a non-zero initial radius, r_0 , the effect of a finite radius then is a reduction of scattered power by an attenuation factor of

$$\exp [-8 (\pi r_0 \sin \phi / \lambda)^2] .$$

Furthermore, a trail of zero or non-zero initial radius, once it is formed, immediately begins to expand by diffusion. Therefore, the scattered signal power also decays with time according to an exponential law

$$\exp [-2Dt (4\pi \sin \phi / \lambda)^2] .$$

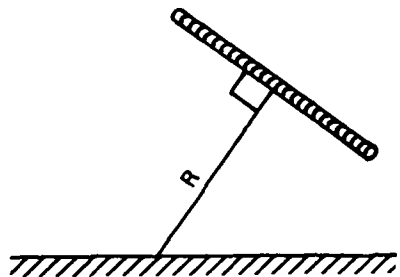
Hence, the time-varying scattered signal power for a low-frequency underdense trail is given by

$$P_r(t) = P_r(0) \exp \left[-2 \left(\frac{\pi r_0}{\lambda \sec \phi} \right)^2 \right] \exp \left[-2Dt \left(\frac{4\pi}{\lambda \sec \phi} \right)^2 \right] \quad (A.11-6)$$

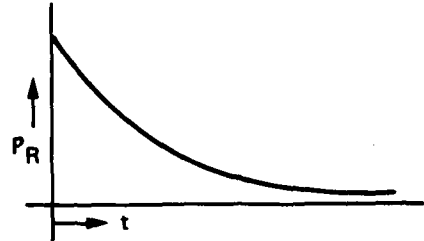
It should be noted that the maximum scattered signal power occurs at $t = 0$ (i.e., the instant of trail formation), after which the power decays exponentially with a time constant, τ , as given by

$$P_\tau = \left(\frac{\lambda \sec \phi}{4\pi} \right)^2 / (2D) \quad (A.11-7)$$

Figure A.11-4 shows a model and a theoretical scattered signal from a low-frequency underdense trail.



(a) TRAIL MODEL



(b) RECEIVED SCATTERED SIGNAL

Figure A.11-4. Low Frequency Underdense Meteor Trail

b. Low-Frequency Overdense Trail

For an overdense trail it is appropriate to assume that an incident wave with sufficiently low frequency penetrates the trail until it reaches a cylindrical surface of radius, r_c , of sufficiently high electron density that the incident wave is reflected at the cylindrical surface. This model assumes an expanding metallic cylinder, the radius of which is given by

$$r_c^2 = (4Dt^2 + r_0)^2 \ln \left[\frac{r_e q \gamma^2 \sin^2 \phi}{4\pi Dt + r_0^2} \right] \quad (\text{A.11-8})$$

For this model the received scattered signal power is

$$P_r(t) = P_r(0) \frac{\lambda r_c}{2r_e^2 q^2 \sec^2 \phi} \quad (\text{A.11-9})$$

until approximately at a time

$$T = \frac{r_e q \lambda^2 \sec^2 \phi}{4\pi^2 D} \quad (\text{A.11-10})$$

after which the electron density inside the trail is less than the critical value for a valid metallic reflecting cylinder model. After $T = T_c$, the received scattered signal power is given by Eq. (A.11-6) for the low-frequency underdense case. Figure A.11-5 indicates the model used for this case and the variation of the received signal with time.

A.11.3 Meteor Communications Systems

Currently no meteor communications are in practical use. However, to facilitate evaluation of the potential utility of a meteor communications system for the DCS in the years beyond 2000, essential features and capabilities that either have been used or have been developed and tested in the past for the Canadian JANET, STC COMET, and Boeing Data-Acquisition systems are briefly summarized in this section, and results of certain other related experiments and tests also are described.

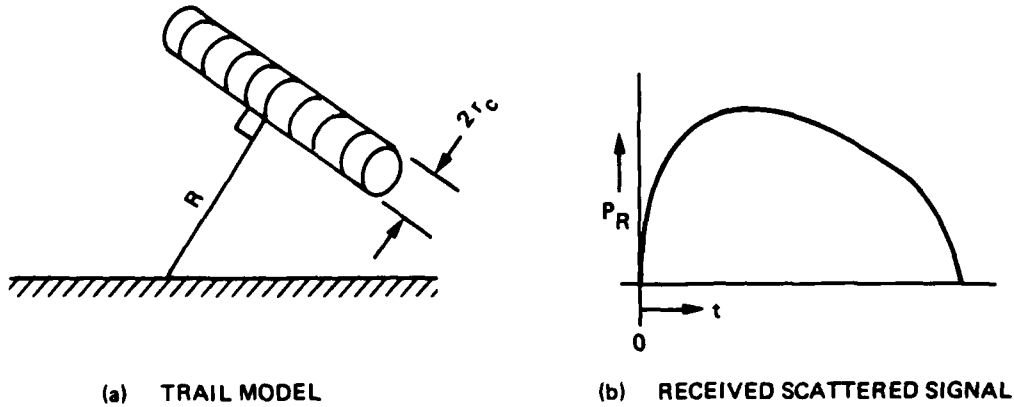


Figure A.11-5. Long Frequency Overdense Meteor Trail

A.11.3.1 Canadian JANET Buffer-Burst System

JANET is the first practical communications system utilizing meteor burst. The code name JANET is after the Roman God of doorway, JANUS, who looks both ways at once. This system was developed, designed, and manufactured by the Ferranti Electric Company of Canada under sponsorship of the Canadian Defense Research Board, and was based on numerous earlier experiments conducted and sponsored by the board (Refs. A.11-2 thru A.11-5). The permanent link between Edmonton and Yellowknife, Canada, became fully operational in 1958 (Ref. A.11-5). A similar set, designated as JANET B and manufactured by the same company for the Supreme Headquarters Allied Power Europe (SHAPE) Technical Center (STC), was used for test purposes.

Figure A.11-6 shows a simplified block diagram of a JANET system. Transmitters at both ends transmit carriers continuously on different frequencies spaced typically 1 MHz apart within the range of 30 to 50 MHz. When a meteor trail is formed, each receiver detects the carrier from the distant transmitter, the received carrier level is monitored by the control unit, and when the signal-to-noise ratio has risen to a predetermined value the transmitting gate is opened. This process permits transmitting stored information by modulating the transmitter, and the transmission continues until the signal-to-noise ratio falls below the gating value. The received signal then is demodulated and inserted into the receiving store, which in turn is discharged into a conventional terminal at a lower rate. Double-sideband amplitude modulation is used, and the carrier is monitored for gating purposes after it has passed a narrow filter.

The JANET used separate antenna arrays for transmitting and receiving, each array consisting of four 5-element Yagis spaced and driven in such a manner as to form a horizontal split-beam pattern with a null pointing along the greater-circle bearing and with two major lobes pointing 7.5 degrees to each side of the path. The elevation angle of the main lobe is 8 degrees and the transmitter carrier output is 500 Watts.

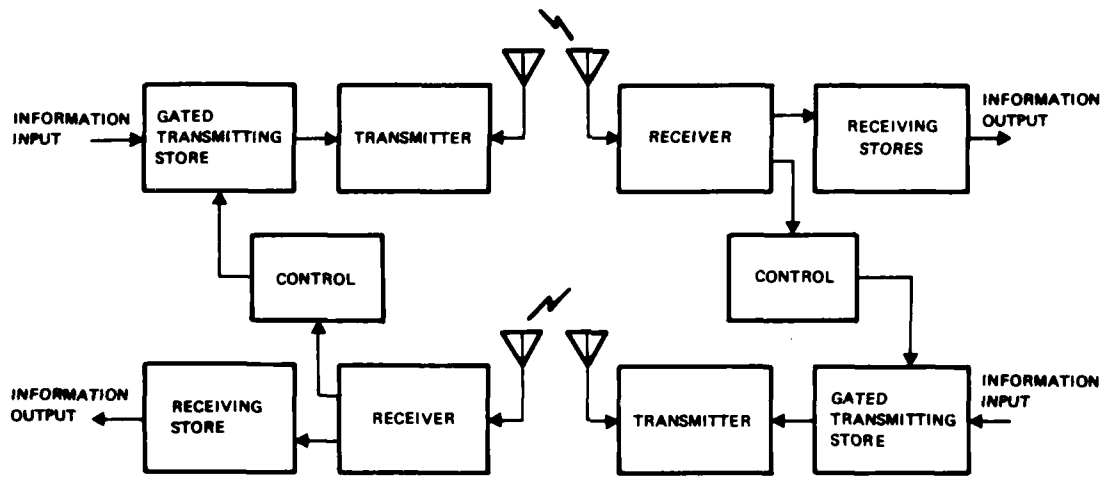


Figure A.11-6. Simplified Block Diagram of JANET System

Operating experience is available from several Canadian JANET circuits. The average information rate over the Toronto-Port Arthur circuit during the test period was 34 words per minute and the individual hourly means of the rate varied widely. Distribution of the mean hourly rate is displayed in Figure A.11-7, wherein the number of hours shown as percentage of the total time for which the rate exceeded a given value is plotted as function of that value. Diurnal variation of hourly mean rate, whose maximum rate occurs near 4 am and whose minimum rate occurs near 5 pm with a slight enhancement near noon, is shown in Figure A.11-8.

The average character error rate as obtained during continuous tests in summer 1956 was approximately 1.5 percent, most of the errors occurring near the end of individual transmissions. As a result, a refinement was incorporated into the gate-off procedure and the system has been operated subsequently with an error rate less than 0.1 percent.

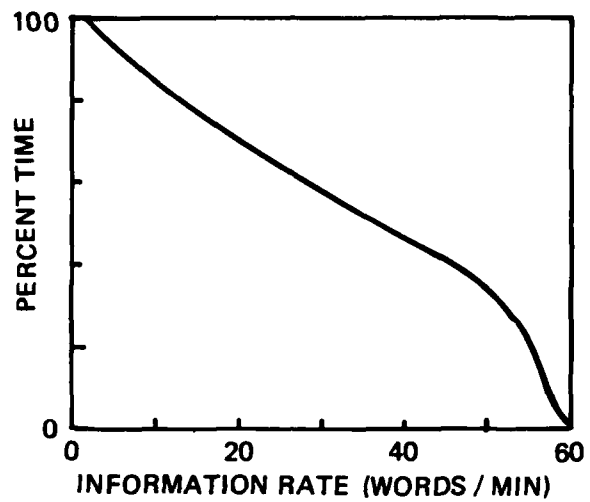


Figure A.11-7. Distribution Information Rate - Percentage of Time the Information Rate Exceeded a Given Value

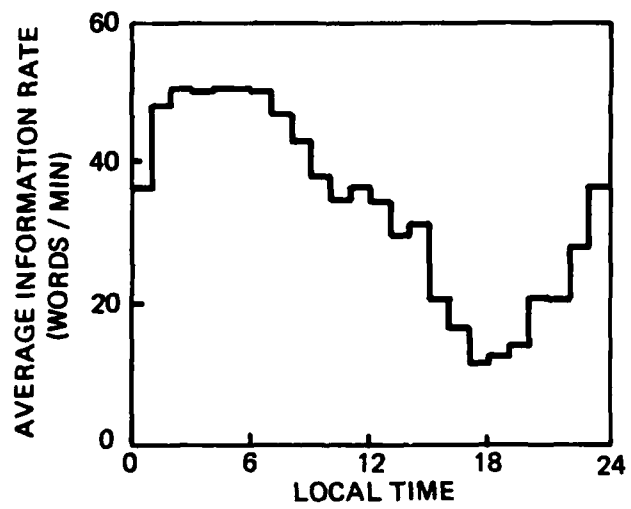


Figure A.11-8. Diurnal Variation of Average Mean Information Rate

A similar system fabricated for SHAPE/STC was used for demonstration and evaluation purposes in Europe over a 1000-km path. Obtained results indicated that the channel capacity or transmission rate often was below 50 bands and that the error rate usually was between 0.1 and 1.0 percent. The STC then started their own development program, which resulted in the COMET system described in Subsection A.11.3.2 and which demonstrated much better performance.

A.11.3.2 STC COMET System

The COMET system developed and tested by SHAPE/STC in 1955 and 1956 is an operational and test link between headquarters of the Allied Command Europe. A block diagram of a COMET terminal is shown in Figure A.11-9 (Ref. A.11-6).

The COMET system is designed to provide two-way TTY and data transmission between two ground stations at a maximum spacing of 2000 km. The information is transmitted in frequency shift keying (FSK), with a total frequency deviation of 6 kHz at a signaling rate of 2000 bauds. The receiving terminal uses a combination of frequency, space, and/or height diversity. Space and height diversity are obtained by using four receiving antennas mounted on two masters erected side by side at a spacing of four wavelengths apart. The lower antennas are single Yagis and the upper ones are twin Yagis at a height of 2.6 wavelengths above the ground. The transmitting antenna consists of two Yagis mounted on a separated master at a height of two wavelengths. Information is fed into the system through a high-speed (285 characters per second) tape reader. The 5-element character code is converted into the 7-element automatic request for repeat (ARQ) code, which consists of three marks and four spaces for each character. The message received is first checked character-by-character for the correct number of marks and spaces. If a character is found in error, then a "request for repeat" signal is transmitted in the reverse direction. The accepted and presumed corrected information is converted back to 5-element code.

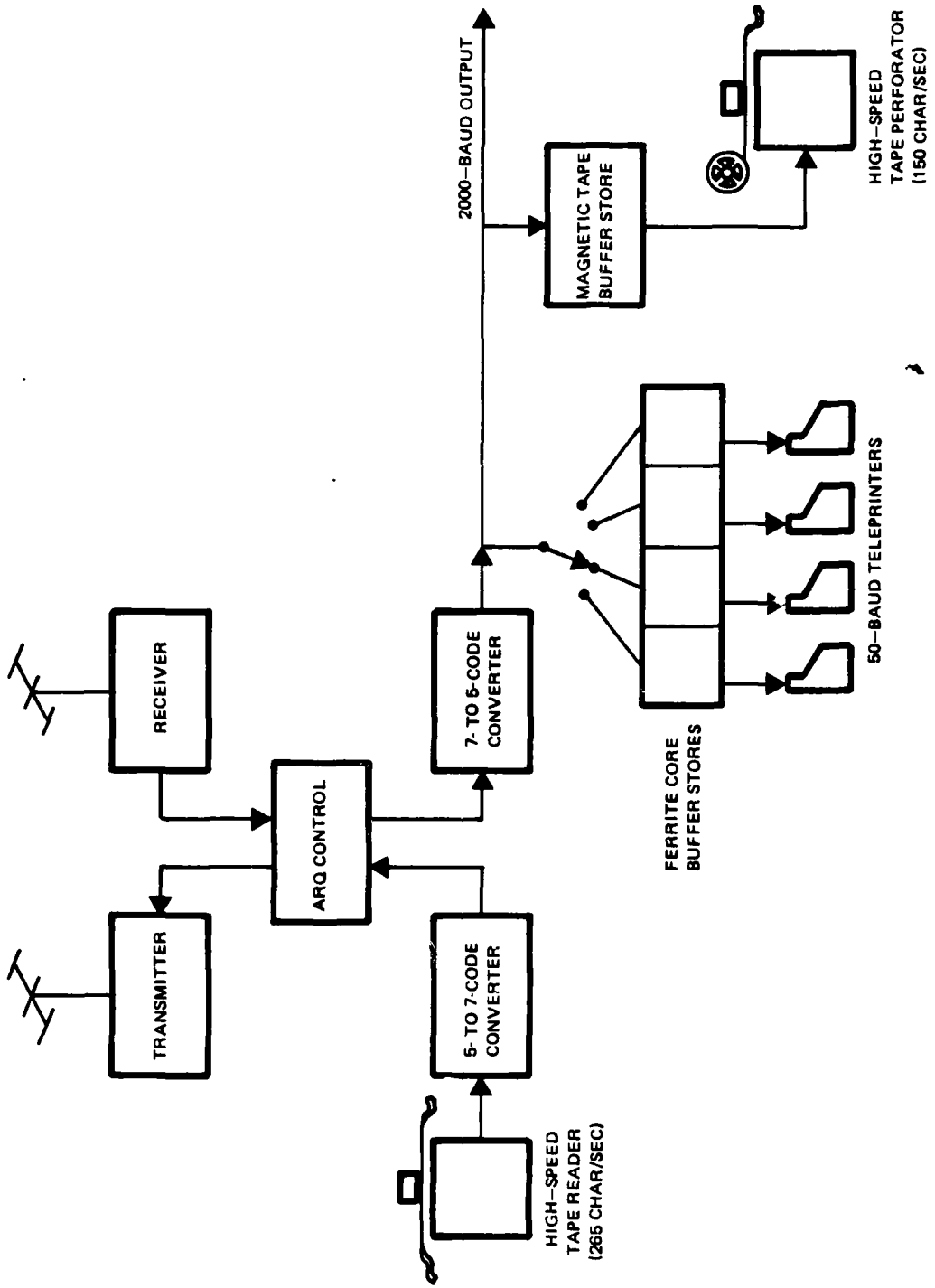


Figure A.11-9. Block Diagram of Terminal Equipment of STC COMET System

Of the two kinds of storage that are available, the first uses magnetic tape which has a storage capacity of 10,000 characters and can be used in conjunction with a 150-character-per-second tape perforator. The second storage type uses ferrite core as the memory element and is divided into four compartments each with a storage capacity of 2,000 characters from which messages can be printed out by four teleprinters simultaneously. It therefore is capable of handling a traffic of up to four 50-band TTY channels on a message-switching basis.

The COMET system was extensively tested over a 1000-km path between the Netherlands and Southern France over a 1-year period during 1955 and 1956. Transmitter power was 200 Watts, and the frequencies used were 56 and 39 MHz, one for each direction. Some statistical data of link capacity, trail scattered signal, transmission delay, character error rate, and diversity gain that are available are noted below.

- a. Link Capacity. Link capacity varies diurnally and annually, the hourly average link capacity roughly following a sinusoidal curve with a maximum in the morning and a minimum in the evening. For the unfavorable period of less meteor activity from October to May, the hourly average data rate or link duty cycle varied from 40 to 320 bands, or 2 to 16 percent, and the 24-hour average data rate or link duty cycle was 115 bands or 5.8 percent. During the favorable period from June to September, the hour average data rate or link duty cycle varied from 50 to 660 bands, or 2.5 to 33 percent, and the 24-hour average rate or link duty cycle was 310 bands, or 15.5 percent.
- b. Scattered Signal Statistics. The statistical date of meteor scattered signal, commonly referred to as burst, is available only for the month of October 1966, so that associated data at best are pessimistic. The distribution of burst count per 7.5 minutes carrying at least 10 characters, as noted in Figure A.11-10, shows that the number of meteor trails varied from 40 to 120 in the early morning, with the most probable value of 80, and varied from 2 to 70 in the evening, with the most probable value of 20. It is seen from this figure that the average burst length is 140 characters (i.e., 980 bits), or about half a second. The burst duration statistics is shown in Figure A.11-11. The interval between bursts varied with the time of the day, the distribution of intervals between bursts being shown for the early morning and late afternoon in Figure A.11-12. It should be noted that the ratio of average burst length to average burst interval is 12.5 percent in the morning and 2.5 percent in the afternoon.

AD-A101 360

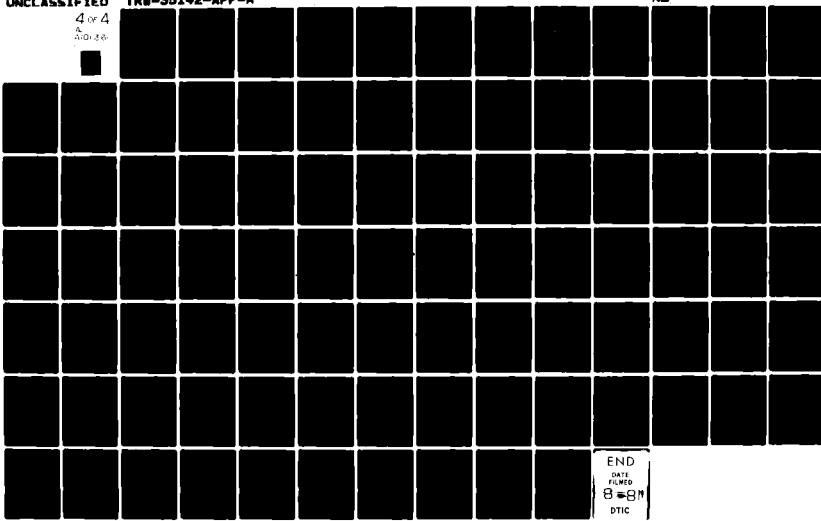
TRW DEFENSE AND SPACE SYSTEMS GROUP REDONDO BEACH CA
EVALUATION OF DCS III TRANSMISSION ALTERNATIVES, PHASE 1A REPORT--ETC(IU)
MAY 80 T M CHU
DCA100-79-C-0044

NL

UNCLASSIFIED

4 or 4

A0144



END
DATA
REMOVED
8-8-81
DTIC

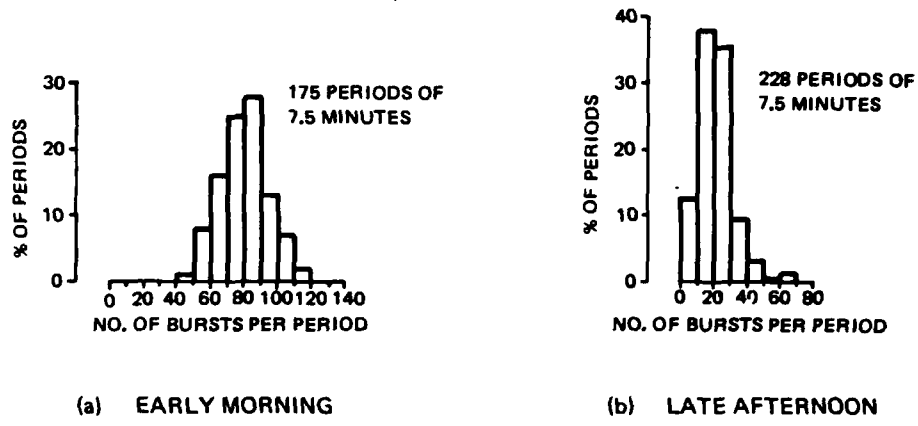


Figure A.11-10. Number of Transmission Burst Per 7.5 Minute Period

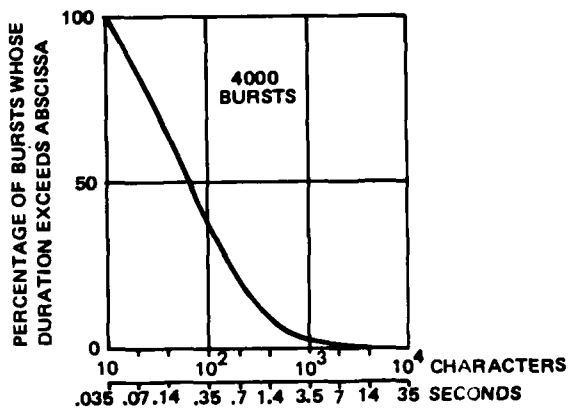


Figure A.11-11. Probability Distribution of Burst Length

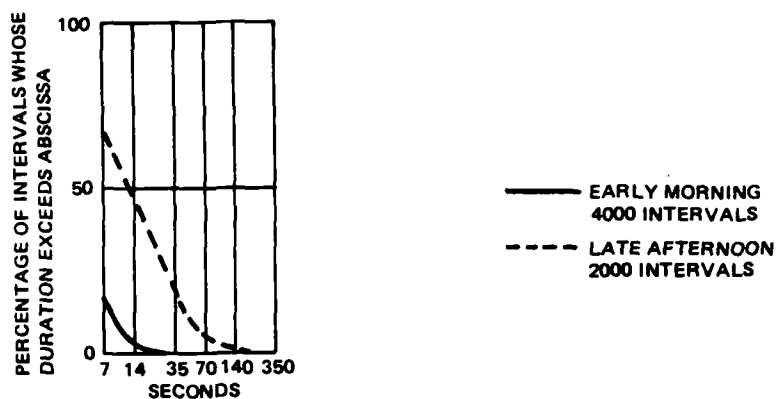
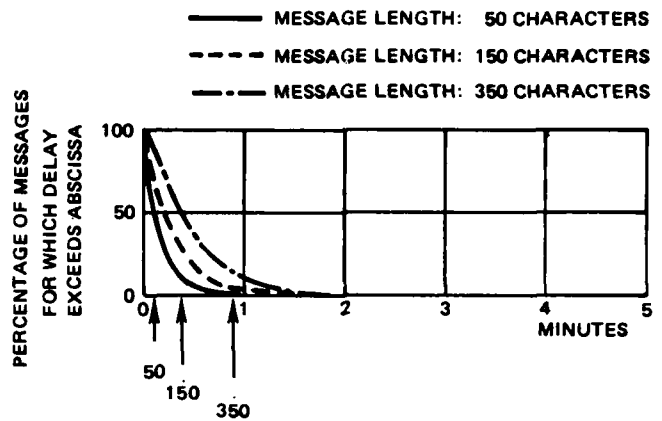
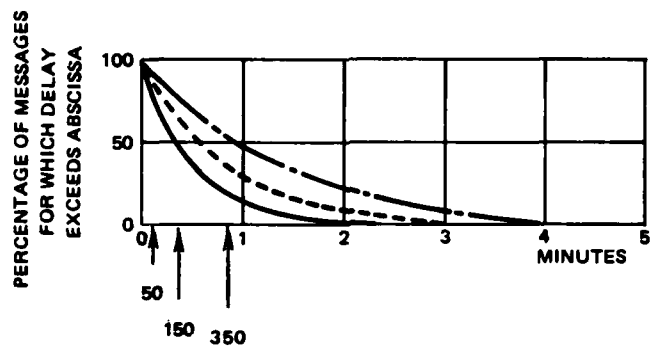


Figure A.11-12. Probability of Distribution of Interval Duration

- c. Transmission Delay. One important statistical aspect of an intermittent communications system is transmission delay, which is defined here as the interval between the moment when a message is available for transmission and the moment when the whole message is received. The transmission delay depends on rate of transmission, message length, distribution of burst occurrence and length, transmitter power, antenna gain and diversity, receiver sensitivity, and system noise. Possibility of distribution of transmission delay for messages of three different lengths of 50, 150, and 350 characters are shown in Figure A.11-13 for the early morning and the later afternoon respectively, and major features of transmission-delay characteristics of the COMET system are summarized in Table A.11-2.



(a) EARLY MORNING



(b) LATE AFTERNOON

TRANSMISSION TIME OF 50 BAUD FOR MESSAGE OF VARIOUS LENGTHS ARE INDICATED BY ARROWS - 50 CH., 7.5 SEC.; 150 CH., 22.5 SEC.; 350 CH., 52.5 SEC.

Figure A.11-13. Probability Distribution of Transmission Delay

Table A.11-2. Transmission-Delay Statistics

Parameter		Description		
Message Length (characters)		50	150	350
Required Transmission Time at 50 bands (sec)		7.5	22.5	52.5
Percentage of Cases with Measured Delay Less Than 50-Band Transmission Time	Early Morning	50	70	85
	Later Afternoon	20	35	50
Average Delay (sec)	Early Morning	10	17	30
	Later Afternoon	30	50	80
Longest Delay (min)	Early Morning	About 1	About 2	About 2
	Later Afternoon	Between 2 and 3	Between 3 and 4	Between 4 and 5

d. Error Rate and Diversity Gain. Various diversity schemes have been tried, and a device called a "multidetector," which checks all receiver outputs and the combiner outputs individually and compares them with each other, was used instead of a conventional combiner. With decision as to the acceptance or rejection of a received signal depending on the outcome of a vote-taking operation which is carried out for every character according to certain rules, the "multidetector" logic was selected as the method that would yield in the greatest gain in time utilization while keeping the error rate below the limit of one in 3000 characters.

With dual-frequency diversity, (i.e., using different frequencies for marking and spacing signals but sharing one antenna), a gain in time utilization of 30 percent over the non-diversity case was obtained. However, with dual-frequency dual-space diversity the optimum "multidetector" produced a gain of 85 percent in time utilization, and very similar results were obtained with height diversity compared with space diversity for the 1000-km link tested. Height diversity nevertheless tends to become less efficient because the length of the circuit is greater than 1500 km.

A.11.3.3 Boeing Data Acquisition System

The Boeing Data Acquisition System was designed to acquire data from a number of battery-powered remote stations. A block diagram of this process, wherein the master station continuously transmits a probing digital signal which includes a preamble, recognition code, and remote station address, is shown in Figure A.11-14. The remote stations are normally in standby mode, but when a probing signal is received the addressed remote station becomes operational and the digital information is decoded. If during the period of decoding it is determined that the addressing is incorrect, the station will return to standby mode. However, if the addressing is correct the remote stations will transmit a block of data to the master station. When the master station receives the remote signal the computer will examine the preamble coding, and if this is found to be correct, will accept the data from the remote station. In addition, the master station features a Nova 12/0 minicomputer for link control, data processing, and printout. Some characteristics of the Boeing system are tabulated in Table A.11-3.

Under a DCA contract, the Naval Ocean System Center (NOSC) recently conducted a study to investigate potential applicability of a meteor-burst communications system to the Minimum Essential Communications Network (MEECN). A portion of this study consisted of a test to demonstrate Boeing Data Acquisition System capability and to evaluate obtained results. For this test, a Boeing master station was located at Elkhorn, Nebraska, one remote station at Ft. Ritchie, Virginia, and one at Colorado Springs, Colorado. Lengths of these two test paths were 1600 km (1000 mi) and 800 km (500 mi) respectively. One additional remote station was deployed at Pueblo, Colorado, which is 80 km (509 mi) at right angles to the Elkhorn-to-Colorado Springs path. The purpose of the Pueblo station was to demonstrate that spacing of this order would cause the two remote stations (Colorado Springs and Pueblo) to use independent sets of meteor trails. These two paths were tested on a 24-hour-a-day basis for two weeks. At the master station, specific information was printed out after reception of each 48-character message, as well as each hour, on the hour, a summary of performance during the past hour as well as cumulative performance since the start of the test.

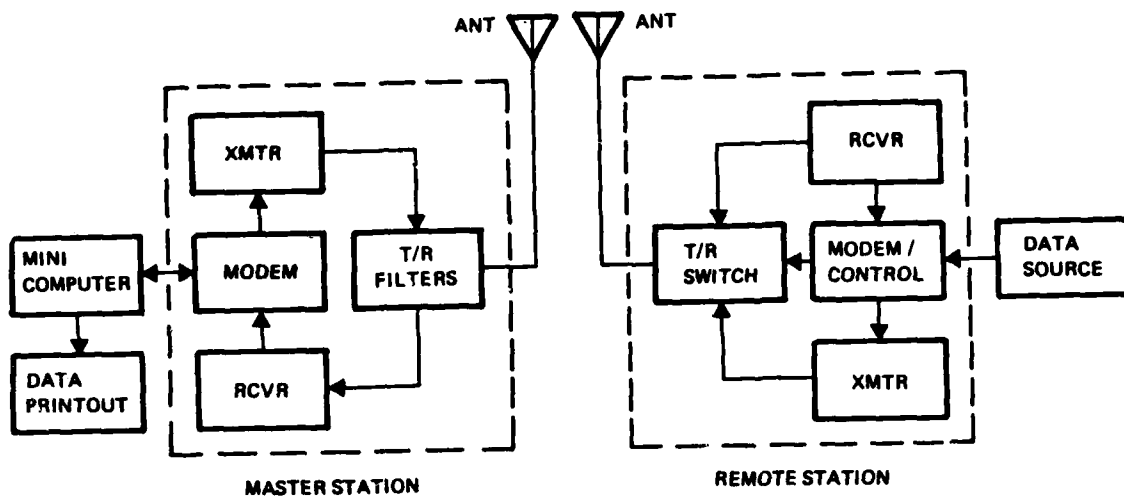


Figure A.11-14. Block Diagram of Boeing Meteor Burst Data Acquisition System

Table A.11-3. Characteristics of Boeing Data Acquisition System

Parameter	Station	
	Master	Remote
Transmitting Frequency (MHz)	46.7	49.7
Transmitter Power (W)	500	300
Antenna	Dual 5-element Yagi, 13-dB gain	Single 5-element Yagi, 8-dB gain
Modulation	PSK	PSK
Data Rate (kbps)	2.0	2.0
Receiver Sensitivity (dBm)	-124	-113
Data Format	--	48 5-bit Baudot characters
Recognition of Probing Signal (ms)	--	18 (12 min; 24 max)
Turn On Responding Signal Code (ms)	--	1
Recognition of Station Code (ms)	7	--
Receive Complete Data Block (ms)	120	--

Figure A.11-15 summarizes waiting-time statistics for the 800-km and 1600-km test paths. Data as presented for six time blocks each of four consecutive hours shows the difference in performance with time of the day. Wait time for delivery of an error-free 48-character message at 95-percent probability of success varies from 1.4 minutes in early morning 6.2 minutes in late afternoon. The waiting time for the 1600-km path is about twice that of the 800-km path.

Direct comparison between the COMET and Boeing systems is not very meaningful due to differences in system design and power level. Nevertheless, Boeing system performance is apparently inferior to that of the STC COMET system, which is specifically designed for two-way data communications.

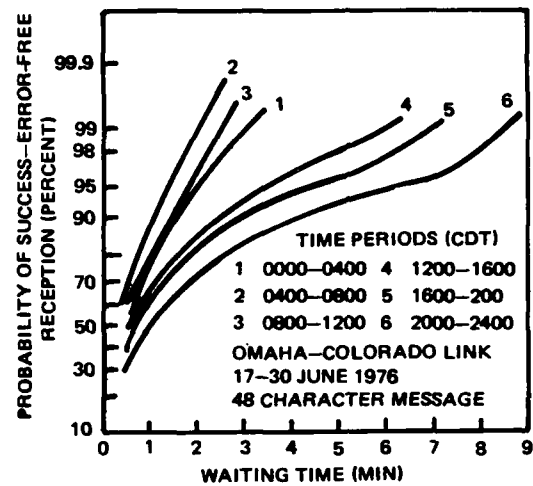
A.11.3.4 Other Related Experimental Systems

In addition to the three meteor communications systems described in the preceding Subsections A.11.3.1 through A.11.3-3, many other studies and experiments relating to this field also were in progress. The following selected tests and experiments and their results are cited either because an obtained experimental result or test performed served to demonstrate a particular feature or useful capability of a meteor system.

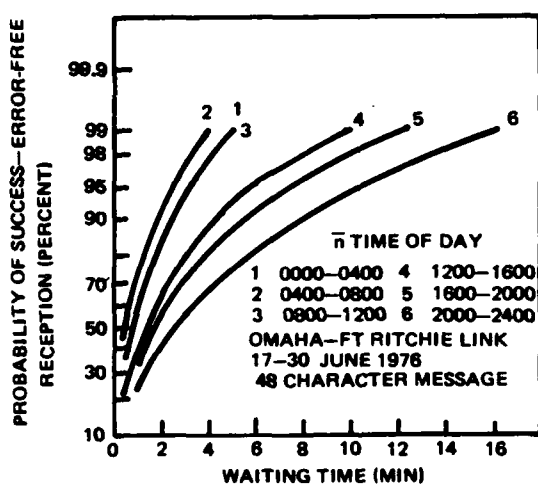
A.11.3.4.1 NBS Meteor Burst Experiment

In connection with the radio-meteor work conducted during the early 1950s by the National Bureau of Standards (NBS), (Refs. A.11-8, A.11-9), transmission measurements over the following three paths were performed continuously for a period of six to fifteen months over the following paths:

- From Long Beach, Illinois to Table Mesa, Colorado, 1295 km (805 mi), east-west path
- From Norman, Oklahoma to Fargo, North Dakota, 1295 km (804 mi), south-north path
- From Point Barrow, Alaska to Kenai, Alaska, 1220 km (759 mi), north-south path.



(a) 800 km (500 mi) LINK



(b) 1600 km (800 mi) LINK

Figure A.11-15. Boeing System Waiting-Time Statistics

Frequencies centering at 30, 49.6, and 73.8 MHz were used for each path simultaneously, with 5-element Yagi antennas tilted 4 degrees with respect to ground and located at a height of 2.4 wavelengths. Transmitters of 2 kw were used for all paths and all frequencies, except a 10-kw transmitter was used for Long Beach-to-Table Mesa path for five months. Both short-term and long-term statistical characteristics of signals were collected and analyzed.

The major conclusion drawn, which is of utmost importance to the present discussion, is that all circuits showed very similar frequency dependence and duty-cycle behavior, establishing that geographical location and path orientation have no significant effect on a meteor-burst communications system.

NBS also conducted teletype meteor-burst communications tests over two circuits between terminal locations at Sterling, Virginia and Walpole, Massachusetts (628 km path) and at Kilbourne, Illinois and Eric, Colorado (1277 km path) (Ref. A.11-10). Each of these circuits has been tested for six months. The two special features of this test meriting attention are the variable threshold level and the variable transmission speed.

During the investigation for various adjustable threshold levels the system was tested for periods of half hours, and the signal duty cycle of each period was measured and recorded. Figure A.11-16 displays the relationship between signal duty cycle and threshold level.

The other noteworthy feature of the NBS system that was observed is that the transmission speeds used were 10, 20, 40, and 80 times the normal 60 words per minute (WPM) teletype rate (i.e., 600, 1200, 2400, and 4800 wpm). Frequency shift keying was used, the frequency shift and receiver bandwidth values being 0.8 and 1.2 kHz for 600 wpm, 2.0 and 3.1 kHz for 1200 wpm, 3.7 and 6.0 kHz for 2400 wpm, and 5.0 and 10.0 kHz for 4800 wpm. Character error rates for various transmission rates also are shown in Figure A.11-17, wherein the double-valued curve for 80X speed should be noted because action of the system control rejects unsuitable signals at the lowest threshold, actually decreasing the system duty cycle in spite of the increased signal duty cycle. It also should be pointed out that the 80X speed data were taken about two months after those of 10X, 20X and 40X. There is reason to believe that substantially increased meteor activity and high incidence of thunderstorms affected the 80X data.

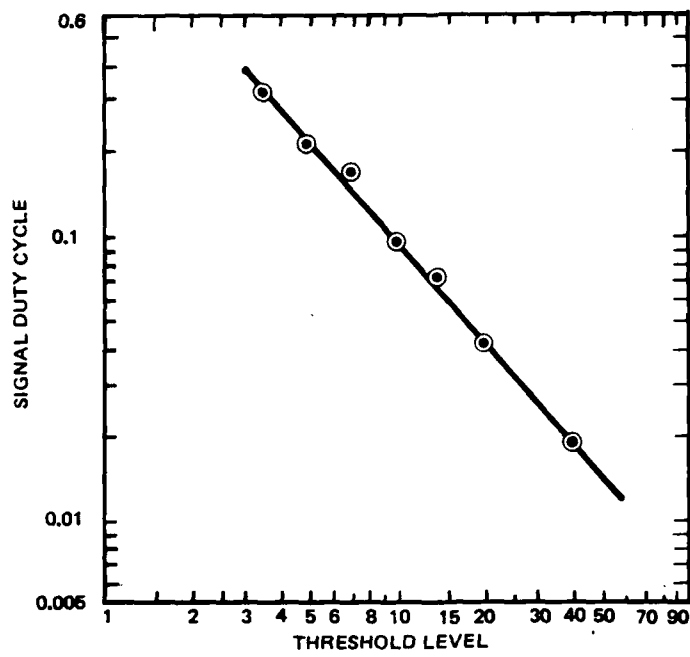


Figure A.11-16. Signal Duty Cycle Versus Threshold Level

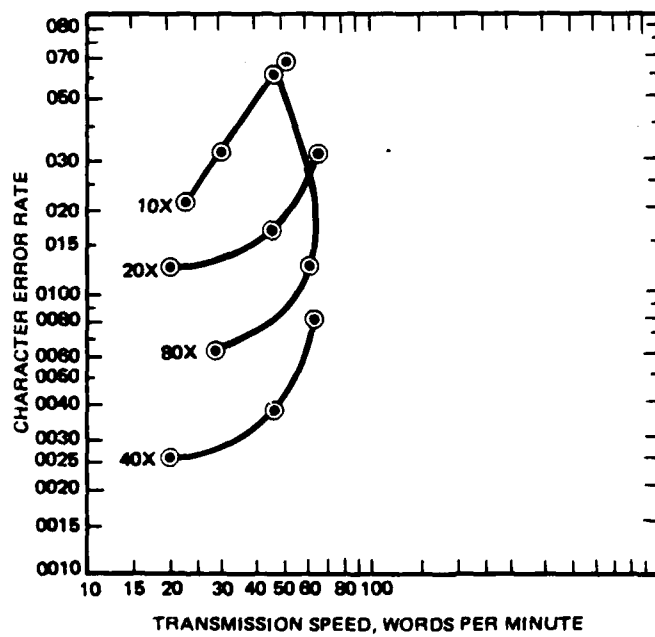


Figure A.11-17. Character Error Rates Versus Transmission Speed

Results indicate that the 40X speed is optimum for the equipment used, and that at this speed a daily average speed of 40 wpm at a character error rate of 0.0035 could be expected.

A.11.3.4.2 SRI Meteor-Burst Voice System

The Stanford Research Institute (SRI) not only conducted pioneer meteor investigation but also performed meteor-burst communications experiments including teletype and voice in the early 1950s (Refs. A.11-11 thru A.11-14). However, the following discussion is limited to description of the meteor-burst voice communications experiment (Ref. A.11-15).

The voice system was tested over a 1318-km (820 mi) circuit between Bozeman, Montana and Palo Alto, California using frequencies of 40.36 and 32.2 MHz. Two three-element Yagi antennas at a height of 9.1 m (30 ft) were used at each terminal for transmitting and receiving.

The block diagram of the SRI meteor-burst voice system as shown in Figure A.11-18 indicates a 1-kW single-sideband (SSB) transmitter at Bozeman that continuously transmits a recognition signal of 100 Watts. When the received signal at Palo Alto is at an acceptable signal level a link-control signal is generated and transmitted which signals the Bozeman station to begin voice transmission.

After the spoken message first enters a microphone the amplified message is fed to a magnetic-tape storage unit and is stored on a continuous loop of magnetic tape. Upon receiving the transmission signal, the recorded voice signal plays back at five times the recorded speed and feeds into the SSB transmitter. The transmitter then radiates a single sideband having a bandwidth of 16.5 kHz to convey normal voice frequencies from 300 to 3300 Hz. The detected fast-speed audio signal is fed to a storage unit and is recorded on a continuous loop of magnetic recording tape.

The tape is played back at one-fifth of recording speed to produce a normal-speed voice message, which is fed to an audio amplifier and loudspeaker for aural monitoring and to a standard tape recorder for permanent recording. It is reported that reliable voice messages have been consistently received.

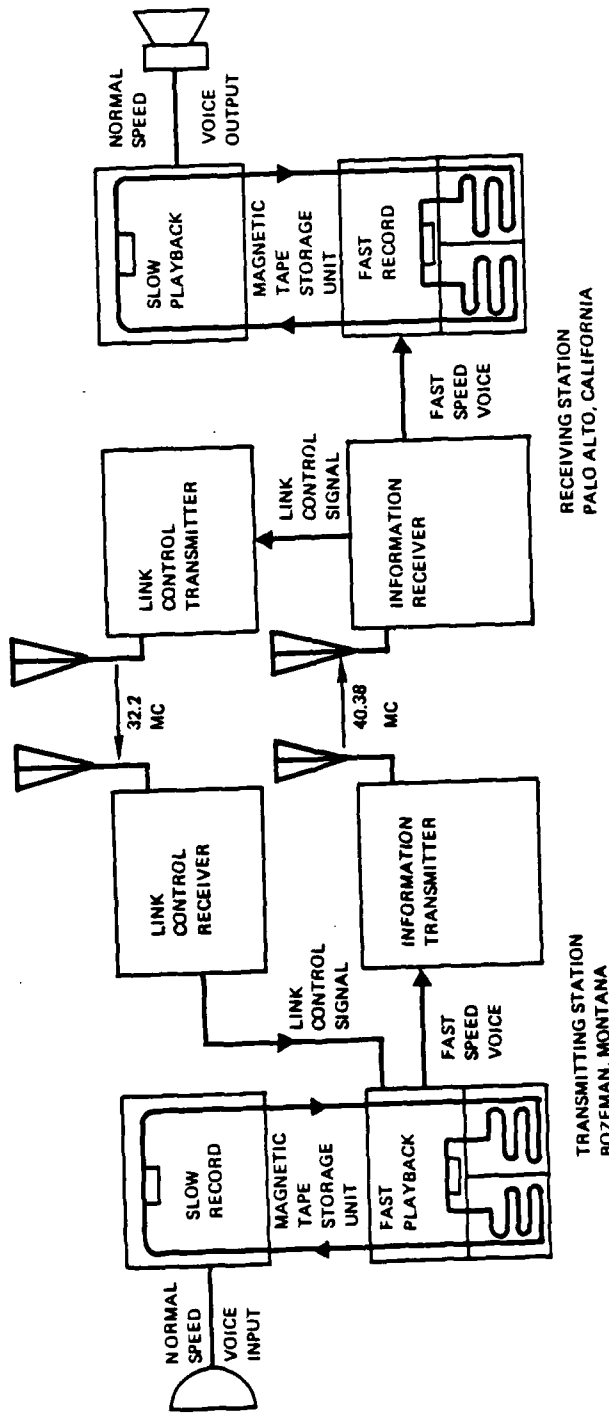


Figure A.11-18. Block Diagram of SRI Meteor Burst Voice System

A.11.4.3.3 RCA Meteor Burst Facsimile Experiment

The Radio Corporation of America (RCA) under sponsorship of the Air Force Cambridge Research Center has conducted a meteor-burst facsimile experiment, preliminary results of which indicate that facsimile transmission using meteor scattered signals is feasible (Ref. A.11-16). The test circuit ran from a National Bureau of Standards transmitting facility at Havana, Illinois to the receiving site at Riverhead, New York over a path length of 1465 km (910 mi). Rhombus antennas 32.0 m (105 ft) long, 25.9 m (79 ft) above ground, and with the main beam at an evaluation angle of 4.5 degrees were used for both the transmitting and receiving terminals, the antennas being oriented approximately 6 degrees to the north of the great-circle path. The transmitter had an output power of 20 kW, operated at 40 MHz, and was frequency-modulated with three levels of shift corresponding to white, black, and horizontal synchronization pulse levels. The modulation index was kept at 0.5 or less. Printed matter with letters of three different sizes was scanned at a rate of two frames per second and transmitted continuously. A resolution of 26.4 elements per cm (67 elements per in) was used. Tests were conducted employing a bandwidth of up to 110 kHz with keying rate up to 73 kHz. The receiver was equipped with both amplitude- and frequency-modulation reception with four selectable intermediate-frequency bandwidths of 27, 55, 110, and 220 kHz, and the receiver noise factor was 4 dB. Thus, with a received output rising above a preset level and accompanied by a synchronization pulse, a cathode ray tube is unblanked, the vertical scan is started, the horizontal scan is synchronized with the received sweep, and the cathode ray tube is modulated by the video information intensity, resulting in facsimile text. A camera then records the picture.

Preliminary results of analyzing some pictures indicate that satisfactory facsimile can be received when the input to the receiver is 26 dB above 1 μ V across 50 ohms for 110-kHz RF bandwidth and the duty cycle is 1 percent. For the system operating at 55-kHz RF bandwidth, a threshold level for satisfactory transmission is about 21 dB at about 1 μ V over 50 ohms, and the duty cycle is about 2 percent. The corresponding data rates for these two bandwidths are 86 kbps and 48 kbps respectively.

A.11.4.3.4 Hughes Air-to-Ground Meteor Scattered System

An air-to-ground meteor scatter communications system has been developed and tested by the Hughes Aircraft Company under U.S. Air Force contract (Ref. A.11-17). Results of these tests indicate that air-ground meteor-burst communications is extremely reliable over ranges of 2080 km (1300 mi), greatly exceeding capability of existing military airborne UHF.

The ground-to-ground and air-to-ground test path selected runs from Bozeman, Montana to Los Angeles, California over a path length of 1456 km (910 mi), and the test system was operated at a fixed frequency of 50 MHz. The ground transmitting site employed a 10-kW transmitter and an antenna array composed of six eight-element Yagi antennas arranged three high by two wide with horizontal and vertical spacing of each antenna of one wavelength. The array was mounted on a tower that extended to 26.8 m (88 ft) above ground, permitting the movable antenna-array center to be varied from two to four wavelengths above ground. The measured horizontal beamwidth was 22 degrees and the gain was 20 dB with respect to a dipole. A dipole antenna was used for reception to simulate an airborne antenna. The receiving system was composed of a specially designed RF preamplifier and converter which caused the incoming RF signal to be converted to a frequency of 26 MHz. The converted signal then was fed into a Hamarlund SP-600 receiver tuned to 261 MHz.

The test system employed a high-speed automatic control circuit to govern duplex operation on a single frequency. The error-correcting code used can correct a single error, and even detects errors for fixed-length code blocks consisting of 11 letters. Messages containing uncorrected errors were automatically repeated until receipt of the corrected message. The code was sufficient to guarantee an effective error rate less than 0.6 percent on an initial point-to-point test.

The ground transmitter probes the medium continuously with a short-pulse code while the aircraft transmitter is silent. On reception of the ground signal the airborne transmitter replies on the same frequency either to send back a message or to invite the ground station to send its traffic. Time sharing of groups of pulses from either end of the link permits single-frequency operation, which of course results in some delay because it is not possible to transmit while receiving, but a high effective transmission rate (2,700 wpm) helps to offset this characteristic.

At the time airborne measurements also were made by Air Force/Cambridge Research Center personnel (Ref. A.11-18) high-power continuous-wave transmissions at 49.6 MHz had been made available for other purposes, with the transmitter located at Cedar Rapids, Iowa and radiation directed toward South Dartmouth, Massachusetts. Transmitter power was 30 kW, and fed into a rhombic antenna having a normal gain of 18 dB with respect to a half-wave dipole.

All signals were monitored simultaneously in an aircraft as well as by the same type of equipment installed at the Air Force Cambridge Research Center, Bedford, Massachusetts, which was just outside of the 3-dB point of the transmitting antenna radiation pattern. A five-element Yagi antenna was used for the receiving terminal. The Bedford antenna was fixed and directed to Cedar Rapids and the airborne antennas was always manually positioned to point at Cedar Rapids. The intent of this experiment was to establish the correlation between signals received on the ground and onboard an aircraft. The correlation ratio for underdense trail burst was found to be from 1.0 to 6.5 approximately, with the distance between the aircraft and the ground station varying from zero to 320 km (200 mi), whereas for overdense trail burst the ratio remained at 1.0 out to a separation of 240 km (150 mi) between receivers and then started to drop to about 0.6 at a separation of 440 km (275 mi). Another interesting finding was that the airborne receiver always received more burst than the ground system.

A.11.4.3.5 Meteor-Burst Broadcast Experiment

All experiments and tests conducted up to this point are associated with point-to-point communications due to the fact that from the very beginning of meteor-burst investigation a meteor-burst system has been conceived to be private system because a meteor-trail scattered signal is direction-dependent, with stations located off the path very rarely intercepting the scattered signals. A concept nevertheless has been suggested that a signal could be scattered by different meteor trails to different directions, which has been validated by an STC experiment using the COMET system described in Subsection A.11.4.2 herein (Ref. A.11-19). Results of the present experiment also indicate that a meteor-burst broadcasting system is indeed possible.

This experiment uses a COMET transmitting terminal at Station B near Toulon, France and a receiving terminal at Station A near The Hague, Netherlands. The other pre-intercept stations are located at Station C near Harrogate, England, Station D near Paris, France, Station E near Freiberg, Germany, Station F near Rome, Italy, and Station G 35 km to the northeast of Station A. Locations of each of these stations are indicated in Figure A.11-19.

Equipments used in the five-intercept stations are essentially the same, antennas consisting of 4-element Yagis with lobes directed toward the ionosphere (80-100 km height) in order to intercept the antenna lobes off the link terminals in the same manner depicted in Figure A.11-19.

The transmitting antenna at Terminal B was pointed in the direction of Terminal A with 3-dB horizontal beamwidth of 50 degrees, and the beam elevation was optimum for the 1000-km length of the link BA. The 4-element Yagi antennas used for the five monitor stations were designed and oriented for maximum overlap with the common-volume scattering of the communication link AB rather than for optimum reception of the transmitter at Station B. Terminal C was within the beam of the transmitter, but the distance from Station B was 400 km longer than optimum and the angle of interception (i.e., the angle between the axis of the transmitting beam and that of the receiving beam) was 23 degrees. Terminals D and E were also within the transmitting beam, but the distances to Station B were 700 km and 500 km and the angles of the interception were 34 degrees and 47 degrees, respectively. Station F was located at a distance of 470 km from terminal B, but the propagation path was of the order of 1000 km and the interception angle was 140 degrees.

Cumulative distribution of propagation percentage of time, P, during which the signal-to-noise ratio exceeds 10 dB, for Terminal A and for the five monitoring stations is shown in Figure A.11-20. This figure also indicates how the propagation conditions differed over the six paths. In order to compare the propagation conditions over the different paths more closely, the values of P for the five monitoring stations were normalized by dividing the value of P measured at Station A over the same period, and the statistical distribution of normalized P is plotted in Figure A.11-21.

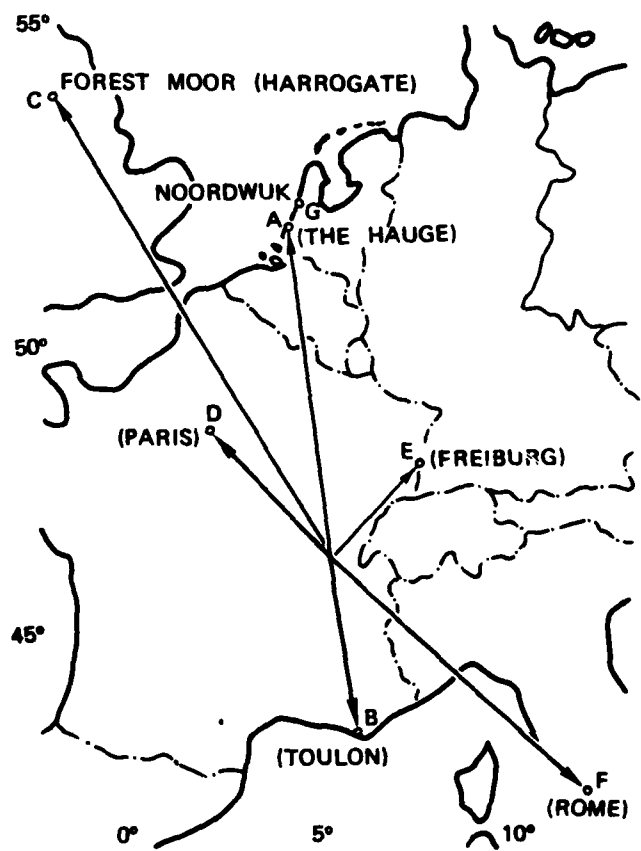


Figure A.11-19. Locations of Meteor Burst Link and Monitoring Stations

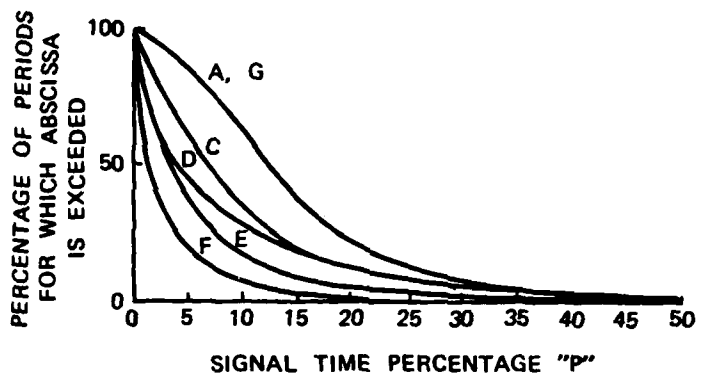


Figure A.11-20. Cumulative Distribution of Propagation Time Percentages for Stations A, C, D, E, and F

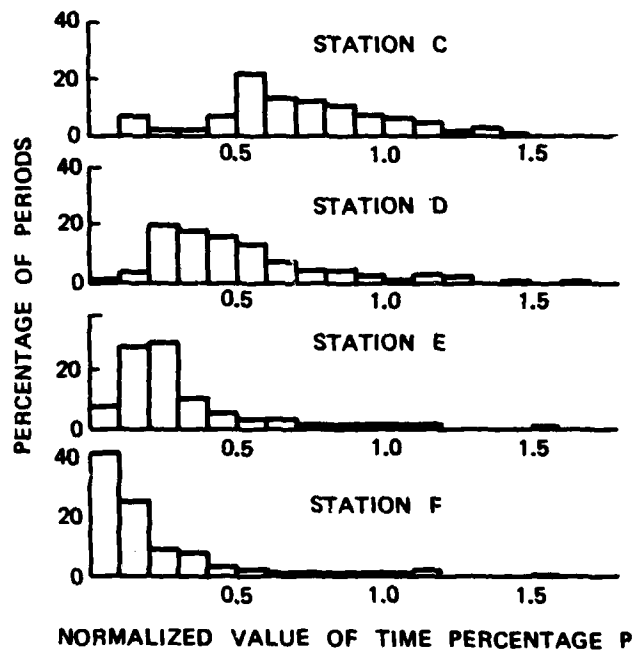


Figure A.11-21. Statistical Distribution of Normalized Values of P for Stations C, D, E, and F

The distribution for Station G, which is the same as that of P for Station A, is not shown. Although these curves do not indicate any close correlation between signals received at the various stations, it nevertheless is apparent that it is possible to communicate by meteor bursts between a point such as Terminal B and a number of others without changing transmitter power and the antenna system.

Interception ratio, defined as the ratio of propagation-time percentage, P , divided by the duty cycle of link AB in the same period, defines the fraction of message passed over the link which has been intercepted by a monitoring station. The cumulative distribution of interception ratios of four stations is depicted in Figure A.11-22. These results thus lead to the conclusions that interreference of meteor scattered signals from far-away stations be ineffective and that meteor-burst propagation can be used for broadcasting applications. However, to provide a nearly equal time percentage of reception at all distances from 200 to 2000 km, three antennas with different vertical radiation patterns would be needed.

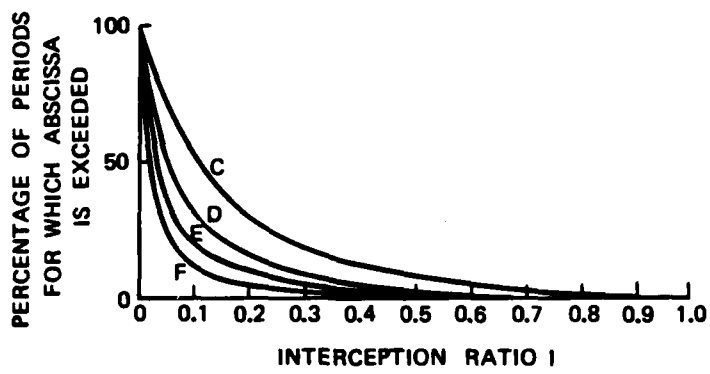


Figure A.11-22. Cumulative Distribution of Interception Ratio for Stations C, D, E, and F

A.12 RADIO FREQUENCY SPECTRUM

Almost all communications are transmitted or carried by radio waves, which may be propagated from the point of generation to the point of reception either through the earth, along the surface of the earth, through the atmosphere, by reflection or scattering from the ionosphere or natural or artificial reflectors within or above the atmosphere, or through the ionosphere.

The particular propagation mechanism or medium used by a radio-communication system depends upon many factors, such as type of information which the service must handle, performance or grade of service which the system is expected to provide, geographic and economic considerations, and availability of the required frequency spectrum.

Radio communication systems can be classified according to the propagation mechanism used into the two broad categories of guided waves and radio waves. In the case of guided waves either a metallic or a dielectric guide is present along which the radio waves propagate. Media discussed this Appendix A (i.e., Section A.1, Coaxial Cable; Section A.2, Millimeter Waveguide; Section A.3, Beam Waveguide; Section A.9, Optical Fibers; and Section A.10, Submarine Cable) all belong to this category. Although radiated waves are ordinarily defined as electromagnetic waves radiated from an antenna and propagated freely in space, this definition of radio waves actually is not very precise. For example, ground waves which propagate along the earth's surface may be classified as guided waves with the earth as a dielectric waveguide. Another is the so-called earth-ionosphere waveguide, which may be considered as a guide for radio waves employed for all ELF/VLF/HF radio communications. The above-noted conventional definition of radio waves nevertheless will be adopted in this section, and waves such as those of the above or similar examples will be regarded as radiated waves.

According to this definition the communications media discussed in Appendix A (i.e., Section A.4, Microwave LOS Relay System; Section A.5, Troposphere Scatter Communications; Section A.6, MM Wave Technology; Section A.7, EHF Satellite Communications; Section A.8, Packet Radio, and A.11, Meteor Burst Communications System) will be considered as systems employing radio waves as transmission media.

The following general discussion is intended to elaborate various aspects of radio waves that have not as yet been addressed.

A.12.1 Radio Wave Propagation

The three major aspects of radio wave propagation are the wave propagation mechanism, the nature of radio signals, and radio-wave characteristics.

A.12.1.2 Wave Propagation Mechanism. Propagation of radio waves as broadly defined above can be categorized into the following processes:

- a. Direct Wave Propagation. So-called line-of-sight propagation
- b. Surface Wave Propagation. Propagation along a surface which separates two media with different characteristics (i.e., wave propagation along the earth's surface)
- c. Reflection. A flat surface with dimensions greater than or comparable to the wavelength and with roughness on a scale much less than the wavelength is capable of reflecting radio waves (i.e., sea and ground surfaces, buildings, tropospheric inversion layers, ionospheric layers, a flat metal plate used for directing radio waves)
- d. Diffraction. Propagation along a curved surface (i.e., the global surface, mountain peaks and ridges)
- e. Ducting. Propagation induced by action of natural phenomena that cause formation of propagation ducts (i.e., tropospheric ducts and ionospheric ducts which provide beneficiary wave-guidance effects. Space between earth and ionosphere usually referred to as earth-ionospheric duct or waveguide)
- f. Scattering. Useful or harmful, forward or backward changes in wave direction caused by various physical or other natural phenomena (i.e., surface protrusions, non-ionized and ionized inhomogeneities in troposphere, and ionosphere).

A.12.1.2 Nature of Radio Signals. To investigate or predict communicate-system performance, knowledge of the received signal is needed for signal design, signal processing, signal combining and detection operations, etc., as well as for selection of terminal equipment or modems. The specular signal model and the diffuse signal model are two basic mathematical models for radio signals in general use.

- a. Specular Signal Model. Letting the signal transmitted or radiated from an antenna be $e(t)$, and assuming that the received signal at a distance is of the form

$$K(t) e [t - T(t)]$$

where $K(t)$ and $T(t)$ are amplitude factor and time delay respectively, then if $K(t)$ and $T(t)$ are substantially constant over a time interval of interest the received signal is basically a replica of the transmitted signal except that the amplitude has been changed by a factor, K , and a time delay, T , has been introduced. This assumed signal is called a specular signal, and the propagation path involved is in general referred to as a specular path. This specular signal model applies frequently to ground-wave propagation, ducting, and diffraction propagation around the earth's surface.

Some received signals can be modeled by using the sum of two specular signals, or

$$K_1(t)e [t - T_1(t)] + K_2(t) e[t - T_2(t)]$$

where K_1 , and K_2 are amplitude factors, T_1 and T_2 are delay times for signals number 1 and 2. It should be emphasized that these four parameters are substantially constant and also that this kind of signal usually exhibits changing amplitude with time at one place, or with range or distance to the transmitting stations at one time. However, because the amplitude fluctuations rates are usually much slower than the slowest message fluctuation of interest, a combination of a diffraction mechanism and a ducting mechanism or of a multiple ducting mechanism can result in two such specular components. A signal consisting of a few specular components, each one with its own amplitude factor and time delay but different from those of the other component, also can occur.

- b. Diffuse Signal Model. A diffuse signal model usually results from a scatter mechanism of propagation. The resulting signal then represents superimposition of a large number of specular signal components without any dominating component. The signal therefore can be expressed as

$$\sum_{i=1}^n K_i(t) e^{j[t - T_i(t)]}$$

The central limit theorem is normally invoked to justify use of the Gaussian process for the resultant signal within a specified time interval. Such a model is physically conceived to result from a large number of non-stationary scatterers.

In practice, the following kinds of signals are commonly found:

- Sum of two diffuse signals model, each one with its own mean time delay and delay spread, and with the difference of the two mean time spreads being a substantial fraction of a few times the delay spread of each of the two.
- Combination of one specular component and one diffuse component. This combination can be expected with high probability in short-range tropospheric propagation.
- Sum of two specular components and one diffuse component. This type of signal occurs also in tropospheric propagation.
- Synthesis of a few quasi-specular signals, of which each one fluctuates slowly relative to the fluctuation of the resulting signal.

A.12.1.3 Characteristics of Radio Waves. The continuous radio spectrum is divided into various bands for convenience, each band covering one decade of frequency, as shown in Table A.12-1. The principal propagation mechanism for each frequency band, the associated signal structures, the fading statistics and fading bandwidth for each band are listed in Table A.12-2.

A.12.2 ELF and VF Propagation Characteristics

The extremely-low-frequency band and voice-frequency voice band encompass the frequency range between 30 Hz to 3000 Hz. Because of the very low information rates which are possible at these frequencies, ELF and VF propagation theory is most often applied to analysis of natural phenomena,

Table A.12-1. Frequency Bands Summary

Band Number	Designation	Frequency Range	Metric Subdivision
2	Extremely Low Frequency (ELF)	30 Hz - 300 Hz	Megametric Waves
3	Voice Frequency (VF)	300 Hz - 3 kHz	--
4	Very Low Frequency (VLF)	3 kHz - 30 kHz	Myriametric Waves
5	Low Frequency (LF)	30 kHz - 300 kHz	Kilometric Waves
6	Medium Frequency (MF)	300 kHz - 3 MHz	Hectometric Waves
7	High Frequency (HF)	3 MHz - 30 MHz	Decimetric Waves
8	Very High Frequency (VHF)	30 MHz - 300 MHz	Metric Waves
9	Ultra High Frequency (UHF)	300 MHz - 3 GHz	Decimetric Waves
10	Super High Frequency (SHF)	3 GHz - 30 GHz	Centimetric Waves
11	Extremely High Frequency (EHF)	30 GHz - 300 GHz	Millimetric Waves
12	--	300 GHz - 3 GHz	Decimillimeter Waves

Table A.12-2. Characteristics of Radio Waves

Frequency Band	Principal Propagation Mechanism	Signal Structure	Remarks
ELF/VLF/LF	Ground waves to a range of a few hundred to a few thousand kilometers (this range is dependent on frequency so that the longer the wavelength, the greater the range); ducting (waveguide modes) between the earth and the ionosphere to beyond the ground-wave range	Specular for ground waves; sum of a few specular components for VLF/LF; some randomness for night-time skywave signal at LF	Non-fading day-time LF ground waves; Rayleigh fading for night-time sky waves; a few-minute fading period
MF	Ground waves to a few hundred kilometers (day and night time); ducting (waveguide modes) between the earth and the ionosphere and ionospheric reflection to beyond ground-wave range (especially at night)	Specular ground waves; specular plus diffused night-time ionospheric signal	Nakagami-Rice fading most frequent for night-time ionosphere wave, with fading bandwidth of a few thousandth Hz
HF	Ground waves to a few tens of kilometers; ionospheric reflection (at frequencies up to MUF); successive ionospheric and ground reflections to thousands of kilometers	Essentially specular for line-of-sight direct ray; discrete and continuous multi-path signals, with each signal exhibiting diffuse plus specular components	Same-time Rayleigh, same-time Nakagami-Rice fading bandwidth of few Hz

Table A.12-2. Characteristics of Radio Waves (Continued)

Frequency Band	Principal Propagation Mechanism	Signal Structure	Remarks
VHF	Direct waves to line-of-sight range for ground-to-ground, ground-to-air, and ground-to-space and vice versa; reflection from sea surface and tropospheric duct to beyond horizon; iono-scatter to 1000-2000 km range for 30-65 MHz; meteor trail scattering to 1000-2300 km for 30-100 MHz, satellite relay for long distance	Similar to HF for line-of-sight propagation; continuum of diffuse signal for trans-horizon propagation; discrete distribution of intermittent signals	For line-of-sight propagation as HF with fading bandwidth of 0.03 Hz at 100 MHz; Rayleigh fading for ionospheric scatter with fading bandwidth about one Hz; 2-15 meteor bursts per minute, each lasting a few seconds
UHF	Direct waves to line-of sight range for ground-to-ground, ground-to-air, air-to ground and vice versa; reflection by artificial reflection or other obstacles, diffraction around the earth's surface to 100 km; diffraction over knife-edge (mountain) obstacles; tropospheric ducting and inversion layer reflection; tropospheric scatter for 80-800 km; satellite relay for long distance	Specular signal component plus discrete and continuous multipath structure for line-of-sight propagation; continuum of diffuse signal with occasional specular signal	Mostly Rayleigh, sometimes Nakagami fading with bandwidth about one Hz

Table A.12-2. Characteristics of Radio Waves (Concluded)

Frequency Band	Principal Propagation Mechanism	Signal Structure	Remarks
SHF	Same as UHF; at frequency bands atmospheric loss (absorption due to water vapor, various kinds of moleculars, etc.) limits the range	Same as UHF	Same as UHF
EHF	Same as SHF; atmospheric loss limits the range except for windows	Same as UHF	Same as UHF

as for example the worldwide distribution of electrical-storms (lightning discharges). The electromagnetic pulses caused by lightning contain considerable energy at these two bands, and this energy forms the natural noise environment not only for these bands but also for higher-frequency bands up to and including the HF band.

The majority of ELF/VF energy is propagated in the terrestrial space bounded by the lower ionosphere boundary and the earth's surface. Both boundaries of these frequencies appear to be good conductors, although the conductivity of either is finite. The earth and ionosphere and the space in between form a finite and reentry waveguide. The propagation of ELF/VF waves in the waveguide is analyzed by using the waveguide-mode theory developed for VLF band (Refs. A.12-1, A.12-2).

A.12.2.1 Boundary Characteristics. Because of the long wavelengths involved, the normal roughness of the earth's surface may be neglected in analyzing long-range propagation of ELF/VF. At these bands the low-conductivity top soil, whose thickness is of the order of a few meters, is very thin electrically. Therefore, the effective conductivity is largely influenced by the more conductive underlying rock and its moisture content, which results in an effective conductivity of the earth's surface of 10^{-4} mhos/m for poorly conducting soil and ice and of 4 mhos/m for sea water. These values are usually appreciably higher than those of the ionosphere boundary, and consequently earth-surface losses usually are much less significant than losses at the ionosphere boundary. In fact, the nature of the dominant waveguide mode is such that the ground may often be taken as having infinite conductivity at ELF.

According to magnetoinic theory (Ref. A.12-3) the ionospheric plasma may be considered as a dielectric medium with a complex permittivity. Assuming the ionosphere to be a homogeneous, isotropic, electric neutral plasma bounded below by a spheric surface, conductivity of the idealized ionosphere then is given by

$$\sigma_i = \frac{\epsilon_0 \omega_p^2}{u + i\omega} \quad (A.12-1)$$

where

- ϵ_0 = permittivity of free space
 ω = angular wave frequency
 v = effective electron-neutra collision frequency
 ω_p = angular electron plasma frequency.

ω_p in turn is related to electron density, N, electron charge, e, and electron mass, M, by the relation,

$$\omega_p^2 = \frac{Ne^2}{\epsilon_0 M} \quad (A.12-2)$$

In the frequency range of interest, $v = W$, which is usually the case in the lower ionosphere, the effective conductivity of the ionosphere, as given by Eq. (A.12-1) becomes

$$\sigma_i \approx \frac{\epsilon_0 \omega_0^2}{v} = \epsilon_0 \omega_r \quad (A.12.3)$$

wherein ω_r is commonly referred to as the effective conductivity parameter. This simplified conductivity parameter has a negligible imaginary part, which implies that the lower ionosphere behaves like a lossy electric conductor at the ELF/VF bands. Typical values for σ_i range from 10^{-6} to 10^{-5} mhos/m. The surface impedance of this ionospheric boundary is given in terms of σ_i by

$$Z_i \approx 120\pi \frac{\epsilon_0 \omega^{1/2}}{\sigma_i} \exp(i\pi/4) \quad (A.12-4)$$

It should be noted that the earth's magnetic field has been omitted and the anisotropy of the ionosphere, which has a relatively small effect over most of the ELF/VF bands has been neglected. The cross-coupling effect (i.e., the coupling between TE modes and TM modes at the ionospheric boundary) may normally be neglected in these bands.

A.12.2.2 Waveguide Modes. The waveguide-mode representation of electromagnetic waves in the earth-ionosphere waveguide has been well developed for VLF propagation (Ref. A.12-1, A.12-2). The electric and magnetic fields are in general representative as an infinite sum of waveguide modes whose propagation characteristics are primarily determined by a set of complex propagation constants, S_n , that may be expressed by

$$S_n = \alpha_n + j\beta_n \quad (A.12-5)$$

where α and β are attenuation constant and phase constant respectively. The attenuation rate, A , and phase velocity, P , of each mode are therefore given by

$$\begin{aligned} A_n &= -0.182/\alpha_n & \text{dB/Mm} \\ P_n &= 3 \times 10^8/\beta_n \end{aligned} \quad (A.12-6)$$

The complexity of the complete mode sum is greatly simplified at ELF/VF because below about 3 kHz, there is only one waveguide mode, TEM above "cutoff." That is, the attenuation rate of the zero-order mode is far below those of the higher order modes over most of the band, and hence the total field may often be represented by this mode alone. At distance less than a hundred kilometers from the source, the higher modes become significantly, and they must be included in the mode sum.

A.12.3 VLF and LF Propagation Characteristics

Very low frequency (VLF-3 kHz to 30 kHz) and low frequency (LF-30 kHz to 300 kHz) radio waves are characterized by their relative stability and reliability of propagation. They are used not only for communication purposes but also for standard time and frequency transmission, and for navigation system. For fixed radiated power, the field strength obtained at a distance increases with decreasing frequency, down to about 10-15 kHz. The propagation also becomes more stable with decreasing frequency, so that the VLF frequencies have been used more extensively, especially in this country. Propagation characteristics and system aspects of VLF and LF band are very similar, therefore, they are discussed together in this section.

A.12.3.1 VLF and LF Propagation Mechanisms. There are three different propagation mechanisms used for propagation studies depending on the frequency and range of interest. They are ground waves, waveguide modes and wave hop or sky waves.

In general, the ground wave consists of three components: the free space component, the ground reflected component and the surface wave component. For ground-based antennas, the free space component and ground reflected component cancel each other almost completely. The surface wave is the wave propagating along a boundary separating two different media--ground and free space, in this case. The field computation can be done by following Norton (Ref. A.12.4) or Wait (Ref. A.12.5). In 1967, the CCIR published ground wave propagation curves (Ref. A.12-6) for frequencies between 10 kHz and 10 MHz. The ground wave propagation depends on frequency, ground conductivity and varies slightly on atmospheric conditions. It is the predominant field component at short ranges.

The waveguide mode approach is useful for lower frequencies and long ranges where only a few lower order modes dominate. For this theory, the total field inside the guide is expressed as a sum of a series of waveguide modes. Each mode has a characteristic field pattern across the transverse plane of the waveguide which does not vary along the direction of propagation. Each mode also has an unique propagation constant which specifies how the phase and amplitude of the mode varies with the distance traveled. The propagation constants are solutions of the modal equation. Solving this equation is the major task of this approach.

The wave hop theory assumes that radio waves propagate along some well defined ray paths. Each ray starts from the transmitter and is reflected back and forth between the ionosphere and the ground on its way to the receiver. For this approach, the first step is to determine possible paths. The transmission loss for each path is then computed. Finally, the total received signal is found by summing the contributions from all paths.

For the VLF band, the wave hop calculation is generally useful for finding the contaminating effects on ground wave field at short range, say 50 km to several hundred km. It also can be used for total field calculation up to 2000 km or 3000 km. Beyond 3000 km, however, the computations are better handled by means of mode theory. The wave hop theory, supplemented by the ground wave contribution at short ranges, is usually used for LF field calculations. In practice, there is no clear cut dividing frequency for the use of waveguide-mode or wave-hop theory.

A.12.3.2 Waveguide Theory. The received total VLF or LF field from a vertical electric dipole can be assumed to be the sum of all modes. At distances more than 500 km, the fields can be accurately represented by the sum of the first few modes. At distances less than approximately 500 km, it is more convenient to represent the field in terms of a geometric series (Ref. A.12-7) where only the terms corresponding physically to the ground wave and the first two sky waves need to be used. This assumes that near-field effects can be neglected. The geometric-optic series is also used at all propagation ranges.

The vertical electric field produced by a vertical transmitting dipole is

$$E_z = \sum_{m=1}^N E_{zm} \quad (A.12-7)$$

where E_{zm} is the field for the m^{th} waveguide mode and N is large enough to include all important contributing modes. The n^{th} mode field is given by

$$E_{zm} = \frac{5.15 (P_r A_{tm} A_{rm})^{1/2} G_{tm} G_{rm}}{(h_t k_r f)^{1/2} (R \sin d/R)^{1/2}} \quad (A.12-8)$$

where

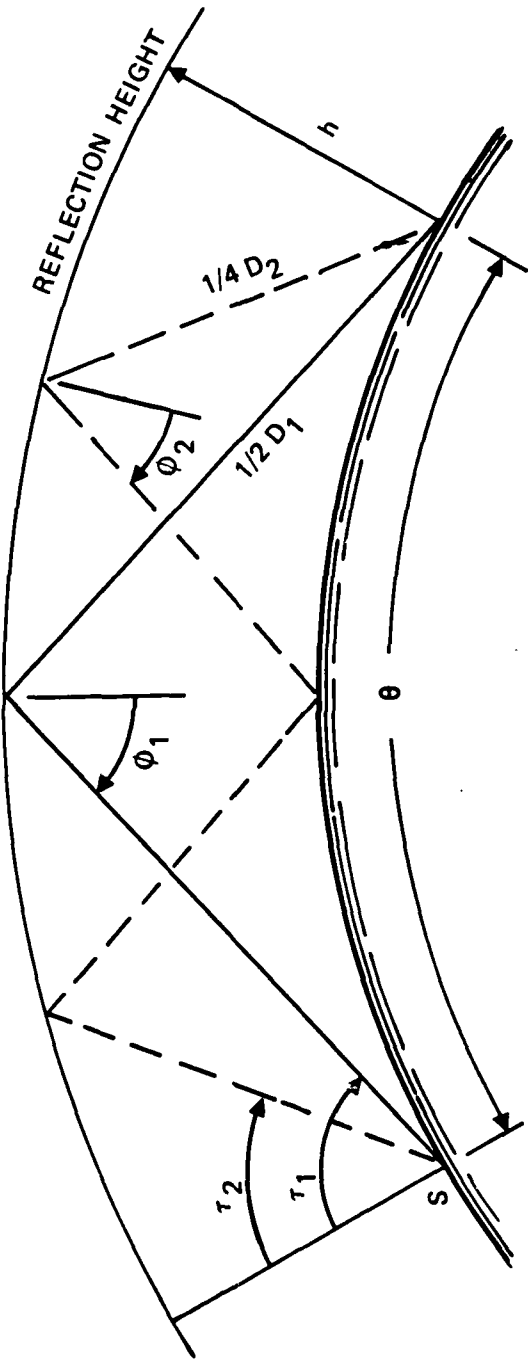
- P_r = radiated power
 A_{tm}, A_{rm} = excitation factor of transmitter and receiver
 G_{tm}, G_{rm} = height gain function at transmitter and receiver
 f = frequency
 h_t, h_r = waveguide height at transmitter and receiver
 d = great circle distance
 R = earth radius
 α = attenuation constant = $8.68 \times 10^3 \operatorname{Im}(S_m)$
 V_m = phase velocity = $c/\operatorname{Re}(S_m)$
 k = wave number
 C = speed of light
 S_m = $\operatorname{Re}(S_m) + j \operatorname{Im}(S_m)$

and S_m is the m^{th} root of model equation. Other mode parameters such as, height gain functions, and excitation functions all depend on the root. The modal equation is quite completed and is omitted here.

Waveguide theory would give quite accurate field prediction if an ionosphere model is available. As previously stated, waveguide theory is very convenient for computing field at long distance for lower frequency because only a few modes are needed.

A.12.3.3 Wave Hop Theory. The geometry of the wave hop theory is shown in Figure A.12-1. The earth is taken as a sphere of radius a with a conductivity σ and relative dielectric constant ϵ . The reflection coefficient of the earth is denoted by $R(\tau)$, where τ is the incident angle. The ionosphere is concentric with known reflection properly characterized by the ionosphere coefficient $R(\phi)$, where ϕ is the angle of incident. The height of ionosphere is h which can be taken as virtual height. Distance d is measured along the spheric ground; angular disrance $\theta = d/a$ is also used.

Figure A.12-1. Geometry for Wave Hop Propagation Model



The total field is the sum of a ground wave component E_0 and skywaves of various number of hops given by

$$E = E_0 + A \sum_1^{\infty} (1 + R_j)^2 T_j^j R_j^{j-1} \exp(-jkD_2)/D_j \quad (\text{A.12-9})$$

where j indicates the number of hops (the number of times the skywave has been reflected by the ionosphere) of the sky wave component considered. A is constant, related to the radiated power. Since both T and R are less than one the series converges. In geometrical optics, T and R are reflection coefficients for an infinite plane wave incident on a plane reflector. This is adequate for distances short enough that the curvature of the earth is not important.

Two corrections are sometimes applied in an attempt to include earth curvature effects. The first is to multiply each term of the Eq. (A.12-9) by a convergence-divergence factor calculated from the geometry. The second correction, the "cutback factor," is motivated as follows. In ray theory, the maximum distance at which the first hop can make a contribution is reached when the ray takes off and returns tangential to the earth. At greater distances, the observer is "in the shadow" for the first hop, and there is no contribution from it. The downcoming wave exits a surface (or creeping) wave on the earth somewhat like an elevated transmitter would. This surface wave propagates into the shadow region. Wait and Conda (Ref. A.12-8) calculated the diffraction around a cylinder of an incident plane wave, and this "cutback factor" has been used by Johler (Ref. A.12-9) and Belrose (Ref. A.12-10) and others, to calculate propagation into the shadow region.

To take account of the continuous creep waves contribution, an integral has to be performed to include all energy that has been reflected from the ionosphere at specified times. Let I_j denote the results for the j -th hop wave, then

$$E = E_0 + \sum_1^{\infty} T_j^j I_j \quad (\text{A.12-10})$$

where I_j is the path integral for the j-th hop wave and does not vary much with time. The ionosphere reflection coefficient, T , changes with time and results in signal amplitude and phase variation.

Several effective methods have been developed for calculating the reflection coefficients of waves incident to the ionosphere. They can be categorized into two basic approaches. In one, the differential equations, which consists of several independent variables, are integrated step-by-step after suitably initializing the calculation at the top of the ionosphere. In the other, the continuously varying medium is approximated by a large number of slabs in whch the physical properties of the slab at any given altitude approximate the properties of the continuously varying ionosphere at that altitude. Due to the mathematical complication of these two approaches, discussion of these approaches is omitted here.

Note that in the waveguide theory discussed in the last subsection, the reflection coefficients are also needed to formulate the modal equation. The approaches are also applicable to that theory.

A.12.4 Medium Frequency Propagation Characteristics

The medium-frquency band (MF), 300 kHz to 3000 kHz, is the transition band between the LF and HF bands. Methodologies used in the LF band, waveguide or wave hop theory and in the HF band, semi-empirical computer code or hand-calculation, are not appropriate for the MF band.

At radio frequencies above 100 kHz the ionosphere no longer acts as a sharp boundary but gradually refracts the wave backward to the earth. This refraction occurs mainly after the wave has penetrated into the ionosphere. The higher the frequency, the greater the penetration. The regions of the ionosphere which mainly affects the propagation of radio wave in the MF band are the D and E regions approximately 70 to 100 km above the earth's surface.

The principal mode of propagation at short distances is ground wave. Its characteristics are generally the same throughout the day and night. The ground wave attenuation is less at the lower frequency end than at the high frequency for the same terrain condition.

As the field intensity of ground wave decreases with increasing range, the sky wave, having been reflected back to the earth by the ionosphere, becomes the dominant one; however, the sky wave is not as stable as the ground wave.

Ground wave computation in MF band is the same as that for VLF, LF, and HF bands. Ground wave field intensity versus distance curves calculated by Norton (Ref. A.12-7) and those of CCIR (Ref. A.12-6) have been widely accepted and used. Sky wave propagation computation in MF band is in general done by using transmission curves. These curves are derived from measurements.

The central portion of MF, namely from 550 kHz to 1650 kHz, is universally used for broadcasting. The lower portion of MF band is allocated for maritime mobile service and radio navigation, and the higher end of MF band is allocated for land mobile service, radio navigation, and aeronautical mobile service.

A.12.5 High-Frequency Wave Propagation Characteristics

Although high-frequency (HF) (3 MHz to 30 MHz) radio waves propagate in essentially the same physical environment as very-low-frequency (VLF) and low-frequency (LF) waves, the propagation of HF waves differ substantially from those of VLF and LF. These aspects of HF waves are briefly summarized in the following Subsections A.12.5.1 through A.12.5.3.

A.12.5.1 HF Propagation Mechanism. Propagating HF waves are bounded by the surface of the earth and by the ionosphere, but the waveguide-mode theory is not at all practical in this band because the earth-ionosphere waveguide is many wavelengths thick, and the waveguide concept also becomes vague for these higher frequencies. This latter effect arises first, because waves whose frequency is higher than the critical frequency will not be reflected back to the space bounded by the lower edge of the ionosphere and the earth's surface and second, because waves below the critical frequency, before being reflected back into the guide, may propagate within the ionosphere (between its lower edge and an altitude of about 350 km or more) while continuously interacting with charged particles. Due to the fact that characteristics of HF waves are modified during this period, it is very difficult to define a boundary impedance to relate incident and reflected waves, as in VLF/LF case.

An HF signal may be comprised of one, two, or three components; each with its own different characteristics. The first component is the ground wave, which provides a very stable signal that is dominant for ranges from a few tens to a few hundred kilometers. The second component, or quasi-specular component may be considered as a combination of a slowly-fading specular component and a rapidly-fading nonspecular component with a Gaussian amplitude distribution. This component follows well-defined paths which can be described by means of ray optics, each path being associated with a reflecting layer with some degree of random irregularity. The third and last component, or the spread component, is the part of the received signal which penetrates deep into the F_2 layer and which has continuous time delay with a spread of up to a few milliseconds.

HF propagation mechanisms or wave paths are shown in Figures A.12-2 and A.12-3. Single-hop transmission paths for the E and F layers are shown in Figure A.12-2 and some multiple-hop F_2 transmission paths are shown in Figure A.12-3. Because earth curvature and the layer height limit the maximum distances which can be reached by reflection from the E and F layers to about 2400 km and 4000 km respectively, the minimum number of hops required for a HF link therefore is the next integer greater than the great-circle distance between transmitter and receiver divided by 2400 for the E layer and by 4000 for the F layer.

The sporadic E layer (E_s) sometimes reflects either down-coming or up-going waves, complicating the path structure. Two typical paths involving E_s layer reflections are shown in Figure A.12-4.

The D layer, which exists only during daytime, is not capable of reflecting HF waves. However, absorption of the wave as it propagates through the D layer is important for transmission-loss calculations.

HF propagation prediction usually is accomplished by first adopting an ionosphere model that describes the ionosphere with respect to time of day, season of the year, solar activity, and the path of the link being investigated. The first few possible low-order paths then are identified, these paths are traced, and the total attenuation for each path is calculated by summing contributions along the path, the total signal strength being the sum of signals contributed by all possible paths. Such computations of course clearly requires use of a digital computer.

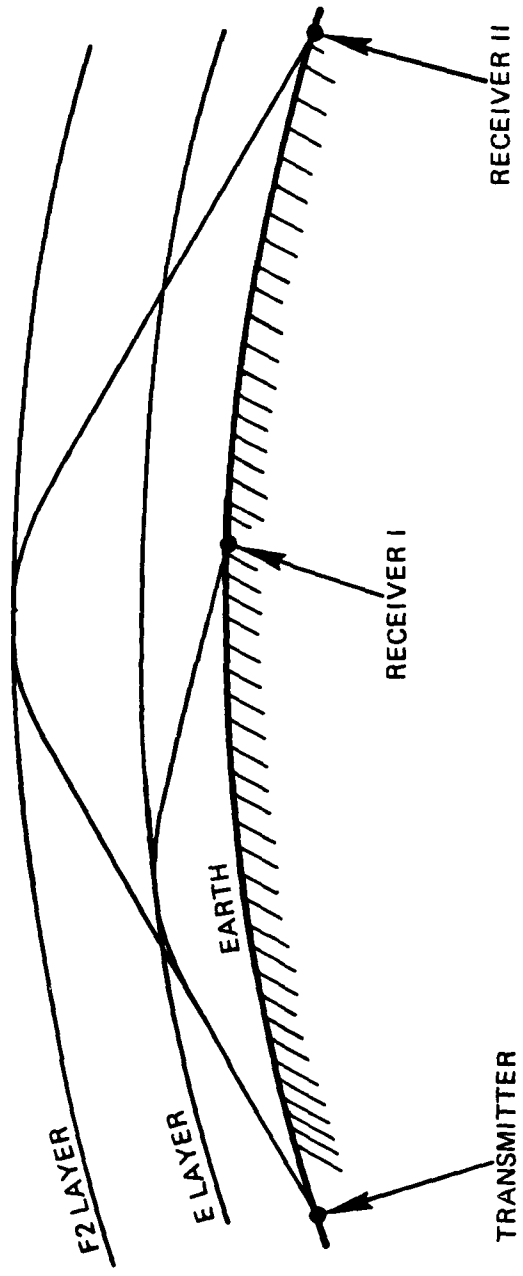


Figure A.12-2. Single-Hop Ionospheric Transmission Paths

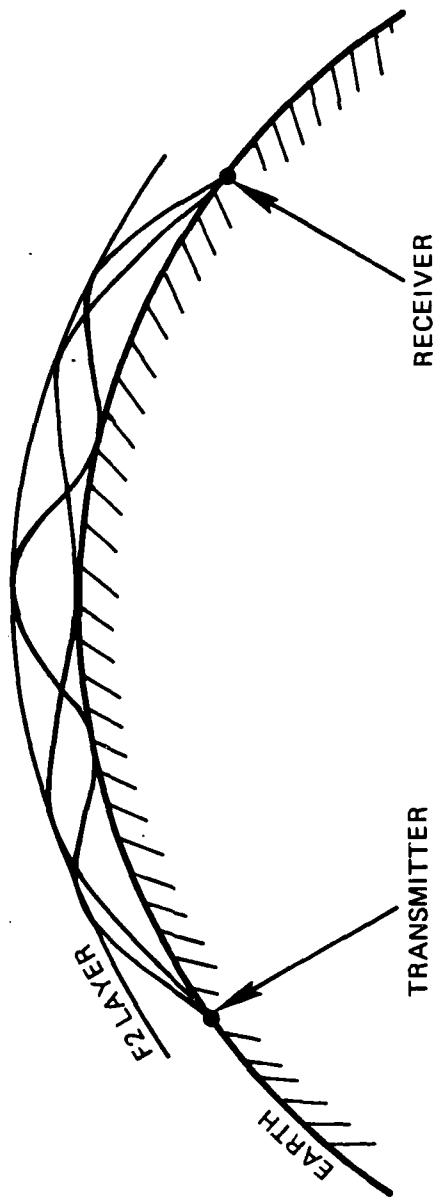


Figure A.12-3. Multiple-Hop Ionospheric Transmission Paths

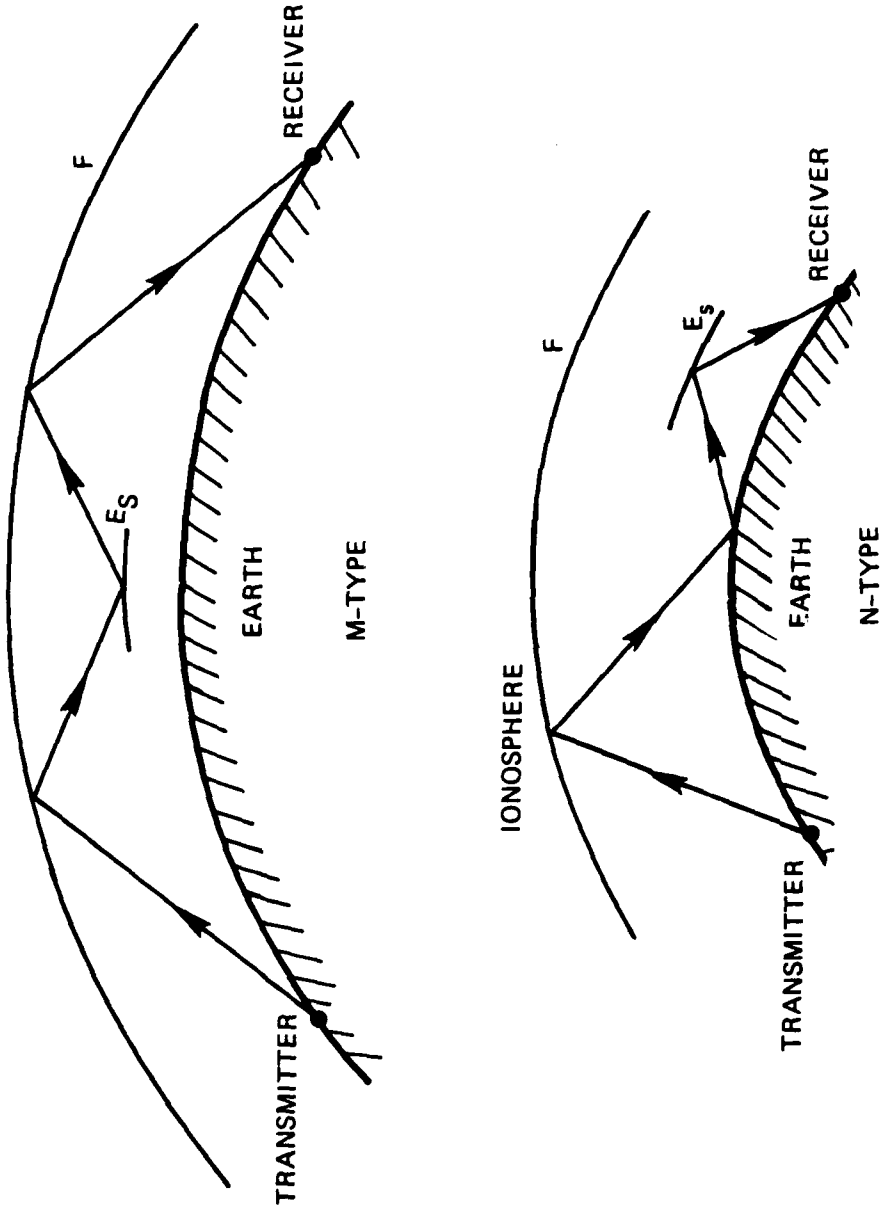


Figure A.12-4. Ionospheric Transmission Paths with Sporadic-E, E_s , Layers Reflection

A.12.5.2 HF Signal Predictions. The computer method referred to in Subsection A.12.5.1 has been highly developed can can be used for long-term prediction. However, short-term variations of a received signal affect performance of a communication system significantly. Therefore a short term model for HF signals also is needed to enable reliable prediction of system performance.

In general, a received HF signal has penetrated deep into the ionosphere before it has been reflected to the ground, so that any temporal or spatial change of ionosphere along the path could produce corresponding variations of signal amplitude and phase. A signal usually also is comprised of a few components, each following a different path, relative variations among these components resulting in fluctuations of the signal. The term fading ordinarily is used to refer to wave amplitude variations of durations of a fraction of a second to a few minutes. Other important qualitative characteristics of fading are depth and speed, time and Doppler spread, and applicable correlation characteristics in space and frequency.

Spatial correlation refers to variation of signal-fading correlation between signals radiated from the same transmitter that are received on different antennas as a function of distance and direction of the antenna separations. Similarly, frequency correlation refers to the variation of signal-fading correlation between signals at different frequencies that are radiated from the same antenna and received on the same antenna as a function of the frequency difference. These correlations coefficients expressed in terms of distance and direction or frequency are important in the design of space- or frequency-diversity systems.

A.12.5.3 HF Frequency Management. Because of the dynamic changes within the ionosphere, which include regular variations such as diurnal, seasonal, solar cyclical, and geographical changes, and irregular variations such as ionospheric-disturbance, sporadic-E, and sporadic-F layers the optimum operating frequency for a particular circuit should change accordingly. Some kind of frequency management consequently is needed for circuits with high reliability requirements. Operators of any circuits may use the graphic or computer methods to identify the optimum frequency, following methods established by the Institute of Telecommunication Science (Ref. A.12-11) based on prediction data provided by the Institute on a quarterly basis or a similar method proposed by CCIR (Ref. A.12-12).

However, a few frequencies are needed for each circuit to guarantee continuous operation, the commonly used frequency complements being the following:

- Two frequency complements (high, and low frequency)
- Three frequency complements (high, middle, and low frequency)
- Four frequency complements (highest, second-highest, third-highest, and lowest frequency).

However, absolute continuity of any radio service, no matter how desirable, is impossible even with an unlimited choice of operating frequencies when HF sky-wave propagation must be relied on. With effective use of optimum frequency prediction (either ITS or CCIR method) and with a few allocated frequencies, link availability of 85 to 95 percent can be obtained, but beyond that level of reliability real-time frequency management and/or an adaptive system as described below must be invoked.

A.12.5.3.1 Real-Time Frequency Management. Real-time frequency management means probing the ionosphere by an oblique and bistatic sounding system. The system now available is the Tactical Frequency Management System (TFMS), AN/TRQ-35(V) manufactured by Barry Research (Ref. A.12-15). The three components of TFMS are a chirpsounder transmitter, a chirpsounder receiver, and a spectrum monitor.

The chirpsounder transmitter sends a low-power 2- to 30-MHz signal, typically 2 watts or less, over the communications path, often using the same antennas as the communications system. In this way antenna patterns are taken into account in addition to the propagation conditions. The test signal is linear FM/CW modulated rather than pulse modulated, thus permitting continuous transmitter output. This technique also permits processing bandwidths of a few Hertz (much narrower than conventional pulse sounders), thus offering immunity to interference from other spectrum users. Further interference rejection is provided by blanking circuits, front-end preselection, and other special circuitry. Using either a 50-kHz/sec or 100-kHz/sec sweep rate, the chirpsounder scans the spectrum from 2 MHz to either 16 MHz or 30 MHz in 4.7 minutes.

The chirpsounder receiver at a distant receiver site tracks the transmitter probing signal. Spectral analysis of the difference frequency between the receiver local oscillator and the incoming signal yields an "oblique ionogram" (i.e., a time-delay-vs.-radio frequency display), and received power vs. frequency is also displayed. From chirpsounder-receiver display of signal amplitude and multipath vs. frequency, the operator then can readily determine channel-to-channel tradeoffs. The cathode ray tube shows, on a real-time basis, what are the propagation conditions and the best frequencies for transmitting. It also indicates mode structure, whether the propagation is in one, two, or more hops, whether the signal is a ground or sky wave, and what particular region of the ionosphere is reflecting the waves, and in addition provides information concerning multipath and time-delay distortions. The receiver can store and display data from up to three separate transmitters. Assigned channels or other specific frequencies of interest can be marked with cursors on the CRT, the frequency of the cursor being read from a digital display.

The third TFMS unit is a spectrum monitor which is used in conjunction with a chirpsounder receiver. It scans the entire HF spectrum every 10 seconds, compiling and continuously updating occupancy statistics (histograms) in 5- and 30-minute time blocks. The receiver gain is automatically adjusted to make the lowest-amplitude threshold of each megahertz segment correspond to slightly above the atmospheric level. Digital readout of the threshold value appears on a cathode ray tube. The spectrum monitor has been design especially for use in locating clean channels within larger frequency bandwidth. Features include a digital readout of center frequency on the cathode-ray-tube spectrum data display and controls to continuously change the displayed center frequency.

The AN/TRQ-35 TFMS has been adopted by the USAF. According to a users report (Ref. A.12-14) reliability of HF communications on links supported by the TFMS has exceeded 99 percent. The set has been successfully deployed in ships and aircraft, and by all four military services and some foreign countries.

A.12.5.3.2 Adaptive HF System. "Adaptive" used in this context implies quite different meanings for different persons. The BR TFMS in a sense is a truly adaptive system which determines an optimum frequency in real time and uses it.

ITT presently is developing a robust communication set operating in the band from 2 MHz to 100 MHz which is called "adaptive HF/VHF set." This set was originally designed to transmit a short and formatted digital message to a small number of users in a nuclear blackout environment (Ref. A.12-15). The frequency used is divided up into a number of subbands, the bandwidth of each varying with the frequency. The message is transmitted over these subbands simultaneously and redundantly, and frequency hopping is used in each subband to provide low probability of interception (LPI) and anti-jamming capability. Four frequency-hopping patterns are employed, the message originator transmits his message using the first hopping pattern, and the nodes receive a correct message and retransmits the message using the second hopping pattern. The nodes which receive the correct message from the second hopping pattern but not from the first one will retransmit the message using the third hopping pattern. The nodes that only receive the correct message from the third hopping pattern will retransmit on the fourth pattern which does not contain any information. Each node that receives a correct message will send an "acknowledgement" which will propagate backward to the message originator in a similar fashion. Each transmission is repeated three times, and an error-correction code also is employed.

As previously noted, this adaptive set is designed for a nuclear environment, the ITT design being based on their observations and measurements during some high-altitude nuclear experiments in the 1960s.

A.12.6 VHF, UHF, and EHF Bands

- In general, electromagnetics waves with frequencies above 30 MHz propagate along a straight line, the so-called line-of-sight transmission which may be employed for terrestrial systems or satellite systems. These applications have been discussed in Sections A.4, Terrestrial Microwave Line-of-Sight Transmission; A.6, Millimeter Wave Technology; A.7, EHF Satellite Communications; and A.8, Packet Radio. The systems discussed in

Section A.5, Tropospheric Scatter Communications and Section A.11, Meteor Burst Communications System are also operating in these frequency bands, but are based on some scattering mechanisms. The former is based on inhomogeneity of the troposphere and the latter on ionized trails due to impinging meteors. This section describes some other transmission modes which occur in these frequency bands.

A.12.6.1 Ionospheric Scattering. In the frequency range of 30-100 MHz, scattering of radio waves from the ionosphere D region which results in a continuous fading signal with superimposed bursts of great strength also is present. The continuous signal can be attributed to scatter from turbulent irregularities in ionization, partial reflection from gradients of ionization, and overlapping reflections from the ionized trails of many small meteors. The ionospheric scattering system utilizes the continuously present but weak variable background scatter signal for continuous transmission at rates of those typical of HF service.

Some VHF ionospheric scattering systems operate in the 35-50 MHz range and use antennas having 20-25 dB gain (relative to an isotropic antenna in free space). The antennas are so sited as to have the radiation pattern main lobe directed to a scattering region about 85 km high at midpath over the great-circle route. A transmitter power of 10-60 kW is required along with dual space-diversity reception and efficient modulation detection methods,, to provide the equivalent of up to sixteen 100-words-per-minute multiplex teleprinter channels having a character error of no more than 10^{-3} for about 99 percent of a year's hours.

The most useful range of frequencies for ionospheric scatter applications is from 30 to 60 Mc/s. However, several considerations affect choice of optimum frequency for a given service. Because propagation loss increases with increasing frequency, the lower part of the band (i.e., below about 40 Mc/s) is preferred to minimize power requirements. At such lower frequencies, frequent propagation of strong signals to great distances by the F₂ layer, nevertheless greatly extends the interference range during years of maximum solar activity and during seasons of highest F₂ MUF, which calls for carefully planned and restricted frequency assignments, as at HF, or changing frequency during interference conditions to frequencies above the F₂ MUF with consequent increased power requirements or reduced channel capability compared to operation at lower frequencies.

A.12.6.2 Sporadic E Propagation. At times the E layer exhibits relatively isolated patches of intense ionization capable of supporting highly efficient reflections in the VHF band. The likelihood and efficiency of propagation by this mode decreases rapidly as frequency is increased, and is of little consequence above 100 MHz. Because of the height of the E layer, the most frequent occurrences are observed over propagation paths of 950 to 2000 km. Seasonally, occurrences peak in summer with the highest incidence in June-July. A less pronounced maximum occurs in December-January. The diurnal pattern within the continental U.S. reveals a broad daytime maximum and a secondary evening maximum. At latitudes about 50° in North America, sporadic E occurs predominantly at night. Shorter distances have a reduced likelihood of propagation due to high radiation angles and long distances are unlikely because the sporadic nature of this mode ordinarily confines transmission to a single hop restricting the interference range to about 2500 km.

Sporadic-E propagation has been treated in detail by Smith (Ref A.12-15) and by Davis et al (Ref A.12-16). However, the point of view taken is that the sporadic-E propagation is treated as a cause of severe interference from distant co-channel stations due to sporadic - E occurrence but not the utility of such propagation.

A.12.6.3 F_2 Propagation. Transmission of VHF radio wave occurs whenever the F_2 layer is sufficiently ionized. F_2 layer propagation rarely occurs above 60 MHz. However, attenuation of F_2 layer propagation is approximately equal to that of free-space propagation. In general, F_2 propagation is most likely during high solar activity at mid-latitudes during winter days. During the period of F_2 propagation, severe interference results from distant radio transmitters, and fixed services will be interrupted and mobile services will suffer sharp reductions in service range. Prediction of possible interference caused by such transmission is available on a monthly basis. However, no attempt has been made to utilize such transmission yet.

A.13 ALTERNATIVES TO ELECTROMAGNETIC COMMUNICATION LINKS

This section identifies possible alternatives to the communications options relying on electromagnetic radiation previously considered in this document. The following discussion briefly reviews the basis for and presents examples of available options and technology outside the realm of electromagnetic waves that may become candidates for support of various communications-system media. The information herein is representative of the current state of physical knowledge.

A.13.1 Basic Considerations

Present physical theory holds that the following four energy-exchange "forces" account for processes occurring within the universe:

- Electric (Coulomb) force
- Strong force
- Weak force
- Gravitational force.

These forces are associated with specific entities identified in Figure A.13-1 that act as carriers of the force. Also, recent work in unified theory appears to support a common origin for the electric and the weak force. Of the four forces, only the strong force (sometimes called the intra-nucleon force) involves a carrier with non-zero rest mass. Gravitons are listed as the carriers of the gravitational force because there are compelling theoretical reasons for their existence, although to the present time no certain direct detections have been observed. In the case of the weak force neutrinos are believed to be the responsible carrier, which, similarly to photons (the carrier of the Coulomb force) have zero rest mass and no electrical charge.

It is the carriers of these exchange forces that directly or indirectly function as the candidate communication carriers, as summarized in Table A.13-1.

ENERGY CAN BE PROPAGATED BY TWO BASIC AGENTS:

- WAVE MOTION

ELECTROMAGNETIC	SPATIAL MODES; DIRECTED BEAMS FOR $\frac{\lambda}{D} < 1$
ELASTIC	
- PARTICLES
 - (FINITE REST MASS, PROPELLED FORCE)

MACROSCOPIC	D IS A CHARACTERISTIC DIMENSION OF THE WAVE OR PARTICLE LAUNCHER
ATOMIC	
SUBATOMIC	DIRECTED MOTION FOR $\frac{\lambda}{D} \rightarrow 0$

Diffusion Corresponds To: Particle Mean Free Path \ll Propagation Distance or
or Absorption Length $<$ Wavelength for Waves

The propagation of odors (molecular species) is an example of particle (finite rest mass) diffusion. The propagation of electromagnetic waves in a medium where the conduction current exceeds the displacement current ($\sigma > \omega\epsilon$) proceeds by diffusion of the electric field (photons).

Figure A.13-1. Energy Propagation Modes

Table A.13-1. Communication Carriers Summary

Phenomenon	Carrier
Electromagnetic Waves	Photons
Elastic (acoustic) Waves	Coulomb force between atoms/photons
Gravity Waves	Gravitons
Charged-Particle Transport	Coulomb-force photons
Neutral-Particle Transport	Neutral particles

The energy associated with physical forces can be considered to be propagated by two agents, as identified in Table A.13-2. For wave motion, isotropic propagation is possible for elastic waves and is nearly isotropic propagation for electromagnetic waves. These waves as well as other waves can also be directed into "beams" or spatial modes. The extent to which this can be done depends upon the ratio of the wavelength, λ , of the waves and the lateral dimension, D, of the wave launcher, and is independent of the specific nature of the waves. A well known example is calculation of the width of an electromagnetic antenna beam in accordance with the relation

$$\theta = \frac{\lambda}{D} \quad (\text{half power beamwidth; radians})$$

In the case of some wave launchers the longitudinal dimensions along the direction of wave propagation as well as the dimensions in the lateral direction contribute to determination of the beamwidth. As the wavelength approaches zero the associated beamwidth (angular divergence) of finite-size launchers also approaches zero. In the limit a unique direction of propagation becomes apparent which is completely analogous to the cases of particle dynamics and of so-called geometrical optics (Ref. A.13-1). Particle propagation is subject to different classes of perturbations than wave-motion propagation, but the dynamics (trajectories) of both phenomena correspond as $\lambda \theta$. Although it is frequently convenient

Table A.13-2. Energy Propagation Modes

Mode	Characteristics
Wave Motion (Spatial Mode): Electromagnetic Elastic Particles	Directed beams for $/D < 1^*$ Finite rest mass propelled by Coulomb force, using directed motion for $/D \geq 0^*$.

*D is a characteristic dimension of the wave or of the particle launcher.

to distinguish between wave and particle types of agents, both can be considered as members of a unifying class (i.e., quantum field) due to the fact that when observed under given experimental arrangements they exhibit wave or particle behavior consistent with the experimental setup.

When energy is propagated in regimes that do not demand quantum considerations, the wave-particle distinction is clear, as for example in the following cases:

- Acoustic (elastic) waves in media of large extent.
(However, acoustic "waves" in crystalline solid-state lattices (phonons) are quantized and are treated as particles carrying energy and momentum to collisions, as evidenced by their scattering with ions in the crystal)
- Electromagnetic waves satisfying the inequality $f \ll kT/h$.

A.13.2 Gravitational Waves and Subnuclear Particles.

Status and expectations of communication schemes using either a modulated source of gravitational energy (Ref. A.13-2) or energetic subnuclear particle beams (Refs. A.13-3 and A.13-4) are summarized in this section.

Radiation of gravitational waves (gravitons) requires creation or annihilation of mass or change in the distance between a mass and a receiver with time. A transmitter concept for gravity waves is a rotating mass whose rotation frequency is variable. Recent highly accurate astronomical observations of eclipsing binary stars have shown that the slow degeneration in the period of a binary system is consistent with the calculated loss of energy by gravitational radiation. However, direct gravitational radiation (gravitons) from cosmic sources remains experimentally unverified at the present time. Operation of current gravity detectors is based on use of piezoelectric strain gages that sense stresses in massive non-magnetic metal blocks. Noise levels of about 0.25 kT , wherein k = Boltzmann constant and T = absolute temperature, have been reported for 1-Hz bandwidth.

Gravity-gradient detectors are used in geophysical prospecting, where masses involved are large and detector-platform motion is used to sense the spatial gradient. This platform motion indicates time variation of the gravitational force and thus provides "signals" that can be detected. The basic detection device is a dumbbell supported on a torsion balance having a time constant of 3 to 10 seconds and a noise level of 1 kT (Ref. A.13-2). The Cavendish experiment which provided the first laboratory measurement of the gravitational constant was of this type. Practical communication ranges using transmitters with feasible masses are less than 10 meters with very narrow bandwidths ($< 0.3 \text{ Hz}$).

Candidate subnuclear particles for communication purposes include mu-mesons (muons), neutrinos, and neutrons, whose properties are given in Table A.13-3 and wherein the quantity m_e^- is the rest mass of the electron.

Table A.13-3. Properties of Various Subnuclear Particles

Particle	Charge	Mass
Muon	e^-	$200 m_e^-$
Neutrino	0	0
Neutron	0	$2000 m_e^-$

Muons have been used in on-off keyed line-of-sight communication experiments (Ref. A.13-3), although range is limited by their relativistic time-dilated lifetime (i.e., their kinetic energy). For example, an energy of 5 Gev corresponds to a vacuum path length of 35 km, at which point a $1/e$ fraction of the initial muon energy has decayed.

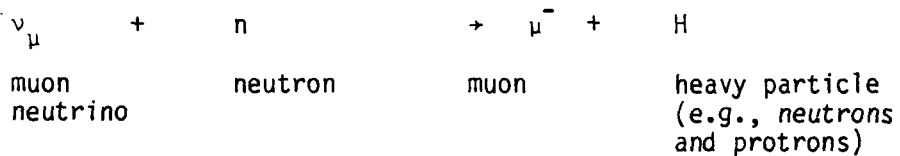
High-energy accelerators can provide muon beams with angular divergences of a few milliradians. If their energy is greater than about 3 Gev, scattering in the troposphere is about the same magnitude. For short ranges of up to 50 km, a detector area (scintillation or Cerenkov counters) of a few hundred square meters would be required. Estimated projected cost of an accelerator (transmitter) capable of supporting long-range (100 km) 50-Gev muon communication is about \$10 million in 1972 dollars (Ref. A.13-2). The accelerator used in the short-range experiments (0.1 km and 1.5 meters of concrete) was the proton synchrotron at the Argonne National Laboratory.

A muon pulse-position modulation system could be used for long-range applications, which in the case of 50-Gev muons would be equivalent to a $1/e$ delay length of about 500 kilometers. However, because muon transit is affected by the geomagnetic field, such long paths might present difficulties requiring very large detector arrays to render such distances feasible. On the other hand, although the cosmic-ray background corresponding to about 1 muon/sec-cm² is the principal noise source for this carrier, direction of arrival, time gating, and energy discrimination could result in a very favorable noise level. A further advantage is that muons can penetrate about 0.5 meters of steel for each Gev of energy.

If dedicated accelerator-transmitter terminals could be built inexpensively this technique could reflect promise for point-to-point communications for data rates of perhaps 100 kbps, as the muon flux levels then would be about equal to the natural background, permitting the propagation path to be obstructed by relatively massive objects with the link remaining closed by the beam. However, the potential of the long-range application nevertheless may be somewhat reduced principally because of the enormous size of the detector array that would be required as well as because of effects of the geomagnetic field. In addition, the accurate pointing (10^{-3} radian) that is needed also mitigates against this application.

Neutrinos in principle are capable of propagating directly along a secant path connecting two points in the earth's surface. Unfortunately, the technology for exploiting this property for communication is of near-heroic proportions (Ref. A.13-4), as summarized below:

- Neutrino beam intensities several orders-of-magnitude greater than those now available from existing accelerators would be needed
- Detector size is very large, with detection capability based on the reaction,



The detection scheme required observation of the visible electromagnetic radiation produced by the Cerenkov effect resulting from impingement of muons from a suitable source into an energy-absorbing body of water. About 10^6 tons of water will be needed for this purpose. Detection is accomplished using Cerenkov radiation detectors that consist of photomultipliers each surveying about 1 sq meter of suitable plastic Cerenkov material. About 80 such detectors would allow perception of 25 events per hour at a range of 10^3 kilometers.

The Fermilab machine can produce 450 pulses per hour of 20-sec duration. Certainly, one bit per pulse could be transmitted and it has been estimated that 15 bits/pulse actually might be transmitted with a $1:10^3$ probability of bit error considering both the cosmic ray background

and the problem of sunlight scattered in the water constituting the detector (Ref. A.13-4). Implicit in this assumption is an angular divergence of the beam from the present value of 3×10^{-3} radians to 1×10^{-3} radians, and transmitter/receiver synchronization also would be needed.

Energetic (≥ 1 Mev) neutrons have absorption lengths in dense matter of at most a few meters, and outside of atomic nuclei have a lifetime of about 13 minutes. Although such relatively long neutron lifetimes allow non-relativistic velocities to provide useful communication ranges, production of highly directive neutron beams nevertheless is challenging in that the basic transmitter technology involved is dependent on performance of a particle accelerator capable of an energy output in the range of a few tens to perhaps 100 Mev. Despite the fact that output would be an electrically neutral beam, which thus implies line-of-sight propagation, losses would result not only from ion production in the atmosphere, but, inasmuch as the neutron has a permanent magnetic moment, also from inhomogeneities in the geomagnetic field which would exert translational forces on the neutrons and contribute to de-collimation of the beam. In addition, neutron detection can be affected by a number of existing electronic detection techniques, and neutrons can induce radioactivity in objects they bombard and thereby impose a health hazard on humans they hit.

A.13.3 Conclusions on Non-Electromagnetic Communications Options

Nonelectromagnetic communication carriers are characterized by certain unique features. However, exploitation of those properties would incur very large costs for both the transmitter and receiver installations, as well as impose further moderate additional costs for training operating and support personnel at appropriate levels. It therefore is unlikely that candidate carriers would override cost-effective support for DCS III requirements.

It nevertheless is possible that the neutral beam technology now under development for controlled nuclear fusion and for weaponry may have applicability to DCS-III needs when survivability and/or stressed conditions are taken into account.

A.14 MANNED AND UNMANNED AIRCRAFT

Various kinds of airborne platform could be used to increase transmission range by extending the local line-of-sight horizon. The following are four types of candidate platforms:

- Manned aircraft
- Unmanned aircraft, i.e., remotely piloted vehicle (RPV)
- Tethered balloon
- High altitude powered platform (HAPP).

The first and second kinds of platform are discussed in this section; and the tethered balloon and HAPP are presented in sections A.15 and A.16, respectively.

Some other airborne platforms which have been either proposed, tested or in use include:

- High altitude powered glider
- High altitude floating balloon
- Rocket or missile
- Cruise missile
- Parachute.

However, by preliminary examination, these kinds of platforms are not suitable for long haul day-to-day communications needs. They will not be discussed in this appendix.

A.14.1 Manned Aircraft

Any high performance and long endurance aircraft can be employed as airborne relay platform. Modification of cabin interior and/or structure of the aircraft may be needed to accommodate communication relaying equipment and its associated auxiliaries. Antennas of relaying purpose have to be mounted in various parts of the aircraft such that coverage will not be obstructed and that interference with other airborne communication, command, and navigation systems will be reduced to the practical minimum.

The approach adapted for the present study is to examine currently existing relay aircraft, to assess their capabilities and then to investigate the feasibility of use such aircraft as DCS III relay platform.

A.14.1.1 EC-135 Aircraft. Various models of EC-135 aircraft are currently employed for Worldwide Airborne Command Post (WWABNCP) to provide support to the Nation Command Authorities (NCA/JCS) and to the Commander-in-Chief of SIUP forces (CINCEUR, CINCPAC, CINCLANT, CINCSAC). This aircraft not only provides space and facility for command and control missions but also for various communications capabilities to support these missions. Only the "Relay" aircraft and "ALCC Relay" aircraft are used for line-of-sight UHF relay and other forms of relay.

The commercial equivalent of EC-135 aircraft is Boeing 707. The major characteristics of the aircraft is tabulated in Table A.14-1.

The model of the relay aircraft is 135 G. In addition to five flight crews, there are three staff onboard to man the radio and electronic equipment and to perform other assigned functions. The major communications media for relay are:

- HF long range voice and digital data
- UHF line-of-sight multi-channel voice and digital data
- UHF satellite digital data.

The major communications equipment complement is tabulated in Table A.14-2.

A.14.1.2 Other Manned Relay Aircraft. Other relay aircraft currently in service is the EC-130Q which supports Navy TACAMO mission since 1962. The EC-130Q is a long range version of the Lockheed Hercules. Specifications of EC-130Q is given in Table A.14-3.

The TACAMO aircrafts are equipped with 20 kW AN/ARC-6 VLF/LF transmitter and associated trailing wire antenna. The aircraft is used to relay certain messages to submarines at wartime at frequencies in VLF/LF band.

Table A.14-1. Major Characteristics of 70

Description	Specification
Wingspan (ft)	130.9
Maximum Length (ft)	145.1
Maximum Height (ft)	43.0
Empty Height (lb)	5,779
Typic Gross Weight (lb)	10,900
Cargo Capacity (lb)	25,000
Number of Flight Crew	3
Power Plant	2 PWC PT6A-28
Maximum Speed (mph)	285
Best Cruise Speed (Mach. No.)	0.8 - 0.83
Landing Speed (mph)	158
Max. Still-Air Range (mi)	6,325

Table A.14-2. Relay Aircraft Communications Equipment Complement*

Equipment	Quantity
AN/ACC Multiplexer Set	2
AN/AIC-10 Interphone	1
AN/AIC-18 Interphone	1
AN/ARC-58 HF Larson Radio	1
AN/ARC-89 Radio Communication System	1
AN/ART-47 UHF Transmitter	5
AN/ART-49 UHF Transmitter Amplifier	5
AN/ART-71 UHF Receiver	6

*Note: Some relay aircraft may have to perform ALCC relay aircraft function, hence, some additional equipment are needed.

Table A.14-3. Specification of EC-130 Q

Description	Specification
Wingspan (ft)	132.6
Maximum Length (ft)	97.8
Maximum Height (ft)	38.4
Empty Weight (lb)	73,618
Gross Weight (lb)	155,000
Power Plant	4 each T56-A-15
Cruise Speed (mph)	360
Range (nmi)	2,050
Cargo (lb)	44,000

Another type of aircraft which is in the process of deployment is the E3-A Airborne Warning and Control System (AWACS). AWACS first became operational in 1977, and more aircraft of standard configuration will be delivered in 1980, 1981, and 1982. The E-3A aircraft is a modified Boeing 707-320B. Besides the addition of a large rotating radome to house its radar, Identification of Friends and FOE (IFF) and data link fighter control (TADILC) antennas, the airplane has more powerful engines than those on commercial aircraft.

Although the primary mission of AWACS is not communication relay, the Joint Tactical Information Distribution System (JTIDS) carried onboard AWACS is of particular interest. The JTIDS is designed to operate in the 960-1215 MHz band and to provide capability of simultaneous multiple radio nets carrying digital messages at the rate of 128 messages per second. Each net will have an information rate of 28.8 kbps in an error detection and correction mode and 57.6 kbps in the non-error detection and correction mode. Time-division multiple access technique is used and the time-slot is 7.8 millisecond (128 time slots per seconds). The number of subscribers of the JTIDS can range from a few to thousands within line-of-sight coverage.

A.14.2.3 Utility of Manned Aircraft for DCS III. It is conceivable that space, weight, power, and cooling capabilities of each type of aircraft should be more than enough to meet the needs of a modern airborne relay platform. However, some difficulties are envisioned at this time; these difficulties are strictly the operational aspects of the aircraft. It should be noted that these difficulties are common for all manned aircraft. They are discussed in the following paragraphs:

- a. Aircraft Endurance. Since the platform is to fulfill a day-to-day communications need, a platform should be always available. This implies that the aircraft should be able to stay on station, by loitering a circle of radius 15 to 30 km, as long as possible. The EC-135 aircraft on station time is about 12-18 hours without aerial refueling depending on the distance between the airbase and the on-air station equipment loads, flying crew, and fuel carried. With on-air refueling, the maximum on-air time is 72 hours, which is set by the requirement of change of oil.
- b. Flying Crew Fatigue. Endurance of a loitering aircraft is restricted more by crew fatigue than by vehicle ability. For example, USAF ASWR-55-1 Weather Reconnaissance Operations restricts the crew duty day to 16 hours. Since this includes pre-flight mission preparation time, normally one to two hours, only 15 hours remains to conduct the flight.
- c. Aircraft Fleet and Logistic Support. A fleet of at least four or five aircraft is needed to maintain continuous on-air relay. One aircraft is on-station, one with flying crew is standby at nearby airbase, the third is for routine maintenance, and the fourth one is used for training the flying crew or for shop-maintenance. Four sets of flying crews are also needed.
- d. Prohibitive Operation Cost. To maintain a fleet of four or five aircraft and four sets of flying crews plus daily fuel consumption, makes the cost of an aircraft relay platform system extremely high if not prohibitive. In addition, there are other costs such as cost incurred by the maintenance, base support, and logistic support.

To estimate the initial operational cost of an airborne platform, the cost data of ECX of Boeing Aerospace Company is used as basis. Since almost all TACAMO aircraft are approaching their end of life span, Boeing has suggested to replace these EC-130Q aircraft by ECX aircraft. Some test have been conducted either by Boeing or by Boeing and the U.S. Navy. The proposed operational plan is to have two aircraft continuously airborne, one in the Pacific area and the other in the Atlantic area. The annual operational costs of EC-130Q fleet and ECX fleet have been estimated by Boeing as shown in Table A.14-4. Note that in that cost estimate, it was assumed the airbases of these fleets are at a distance about 1000 nm from the mission orbiting areas.

Assume an airbase can be located close to the relay orbiting area; utilization of the aircraft can be greatly improved. Based on data given by Boeing, to maintain an aircraft continuously on air for relay five aircrafts are needed which implies an annual operations and support cost of about 30 million dollars. In addition, the acquisition cost of five aircraft is estimated to be 250 million, and the life span of these aircrafts is taken to be 25 years. Therefore, the initial and operations cost of an airborne ECX platform is roughly 40 million dollars per year.

A.14.2 Unmanned Aircraft

A currently available remotely piloted vehicle suitable for communication relay platform is E-System L-450 F. The L-450 aircraft is a multimission, single-engine, high-altitude, long-endurance aircraft which can be operated as either a remotely piloted vehicle or a manned aircraft; L-450 F is the designation for the RPV version. The military designation of L-450 F is XQM 93A. Figure A.14-1 shows major dimensions of the aircraft.

The aircraft can fly slowly in circles at altitudes between 13.7 to 16.8 km (45,000 to 55,000 ft) for 24 hours. It can receive line-of-sight communications for extreme distance and relay those signals to ground stations or other aircraft.

Table A.14-4. Annual Operation and Support Costs*

	EC-130Q	ECX
Number of Aircraft	29	15
Aircraft Utilization (Flying hours/years)	41,600	25,200
Indirect Cost	27.4	9.1
Personnel	36.5	12.9
Radio (AVLF)	19.7	7.9
Aircraft Maintenance	13.0	9.5
Fuel (\$1.24/gallon)	39.2	49.1
Total Annual Costs	135.8	88.5

*Note: Cost is FY dollars and in millions.

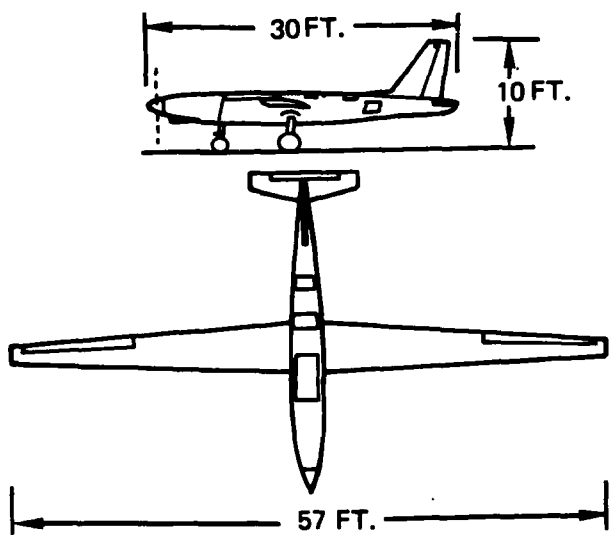


Figure A.14-1. Major Dimensions of L-450 Aircraft

The L-450 payload capacity is 26 cubic feet. About 20 cubic feet is available as one continuous bay aft of the cockpit, and an additional 6 cubic feet is available in a narrow area aft of the primary 20 cubic feet payload bay. For L-450 F, the RPV version, the cockpit provides another 18 cubic feet for payload. The total payload space is 44 cubic feet, and the payload capacity is 1100 pounds. A typical flight profile is shown in Figure A.12-2. Electric power available is 6 kW at 28 volts.

The L-450 aircraft utilizes a high lift-to-drag ratio for maximum endurance. The basic airframe is designed to meet the requirements of Federal Aviation Regulation. The wings have a high aspect ratio, and the aircraft is designed for a 3.8 g load factor. The fuselage is conventional semi-monocoque construction designed to maximize payload capacity.

The autopilot used is a modified version of the Bendix PB-6 Automatic pilot, a self-contained automatic flight stabilization system that is controlled by commands from the ground monitored by a telemetry link.

The L-450 is powered by a PT 6A turboprop engine manufactured by United Aircraft of Canada, Ltd. This engine now has over 10 million flying hours. It has been installed in 2,000 operational aircraft, and it experienced an in-flight shutdown rate of 1 per 100,000 hours operating time. The time between overhaul is up to 7,000 hours. Fuel storage is proved in both wings and fuselage tank. Each wing is capable of holding 1100 pounds of JP-4 fuel, while the fuselage tank has a capacity of 120 pounds.

The major aircraftt parameters given by E-System specification are listed in Table A.14-5.

It should note that the 44 cubic feet, 1100 pounds payload and 6 kW available power are moe than enough for the relay function considered in the main report. An extension of endurance of 6 to 8 hours might be possible by tread-off the unnecessary payload space and weight for fuel capacity.

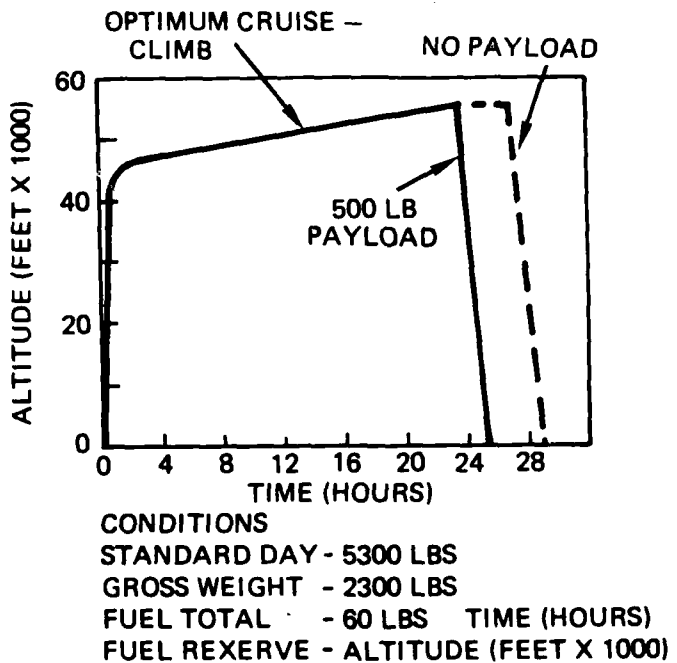


Figure A.14-2. Typical L-450 Flight Profile

The E-system has also developed and manufactured several other types of RPVs, namely E-45, E-50, E-75, E-85, E-100, and E-150 and their variants. These models are much too small in size and with only a few hours endurance and are judged not suitable for airborne relay purpose.

Other types of RPV currently available or under development which could be used for relay platform include YQM-94A, YQM-98A (Compass Cope), etc. They are much larger and heavier aircraft, as shown in Table A.4-6, and may cost more to operate.

E-systems has made a cost estimate for TRW for another study. The system consists of 12 L-450 aircraft, airborne at all times. E-systems pointed out that manned systems significantly improves cost effectiveness over unmanned mode of operation. A fleet of 42 aircraft will be able to provide continuous operation of 12 sites in a time period of 8 years; the total initial cost is 240 million dollars and operations cost per year is 20 million dollars. Therefore, for one continuously on air relay platform, the initial and operational cost is about 3.0 million dollars.

Table A.14-5. L-450 F Specifications

Description	Specification
Endurance	Over 24 hours
Service Ceiling	Over 50,000 feet
Stall Speed	61 knots
True Airspeed (Max. Endurance)	200 knots
Maximum Rate of Climb	3000 feet per minute
Time to 40,000 feet minimum	21 minutes
Takeoff Distance	1200 feet
Gross Weight (manned)	4600 pounds
Gross Weight (unmanned)	5300 pounds
Maximum Payload Weight	1100 pounds
Maximum Payload Volume	44 cubic feet
Positive G Capability	3.80
Negative G Capability	1.52
Turboprop Engine	PT 6A
Available Electrical Power	28 volts, 6 KW

Table A.14-6. Comparison of Three Types of RPVs

	L-450F	YQM-98A	YQM-94A
Overall Length (ft)	29.0	38.7	41.0
Wingspan (ft)	57.0	81.2	90.0
Body Diameter (ft)	--	--	3.7
Launch Weight (lb)	4,500	14,500	14,400
Endurance (hr)	24	24	--

A.15 TETHERED BALLOON CHARACTERISTICS AND CAPABILITY

A.15.1 Tethered Balloon

The aerostat system uses helium-filled tethered balloons as high-altitude platforms to provide reliable and economical communications coverage over large ground areas. Lightweight electronic equipment suspended beneath the aerostat makes point-to-point and omnidirectional communications practicable. The operational altitude is typically between 3 km and 4 km above sea level, from which heights line-of-sight extends to distances of 200 to 250 km from the tether point, and provides ground coverage over areas of from 125,000 to 200,000 sq km.

The maximum operating altitudes for the aerostat are a function of aerodynamic lift and drag, helium volume at altitude, total weight aloft, and environmental factors. Of all the environmental factors, wind has the greatest effect on performance, dynamic pressure at the maximum operating wind velocity constituting the major load on the vehicle and tether. The wind also moves the vehicle slightly downwind, an effect called "blowdown," so that if the vehicle is kept at the same altitude increasing wind speeds cause greater blowdown, which in turn requires more tether to be let out and results in more weight for the vehicle to carry. However, this is more than offset by the aerodynamic lift generated by the vehicle.

Airborne electronic payload equipments are carried in the windscreen compartment under the hull or in the hull. Antennas can be placed on the side of the hull, inside the hull, in the fins, or along the trailing edges of the fins.

A.15.2. System and Components Description.

A.15.2.1 Ballonet System. To maintain the proper aerodynamic shape of the aerostat and to prevent cupping or dimpling of its nose under wind pressure, the pressure within the hull is kept slightly above ambient atmospheric pressure by a ballonet-blower system that consists of a curtained-off volume (within the fixed-volume hull) into which ambient air is pumped. The primary purpose of this air-filled ballonet compartment is

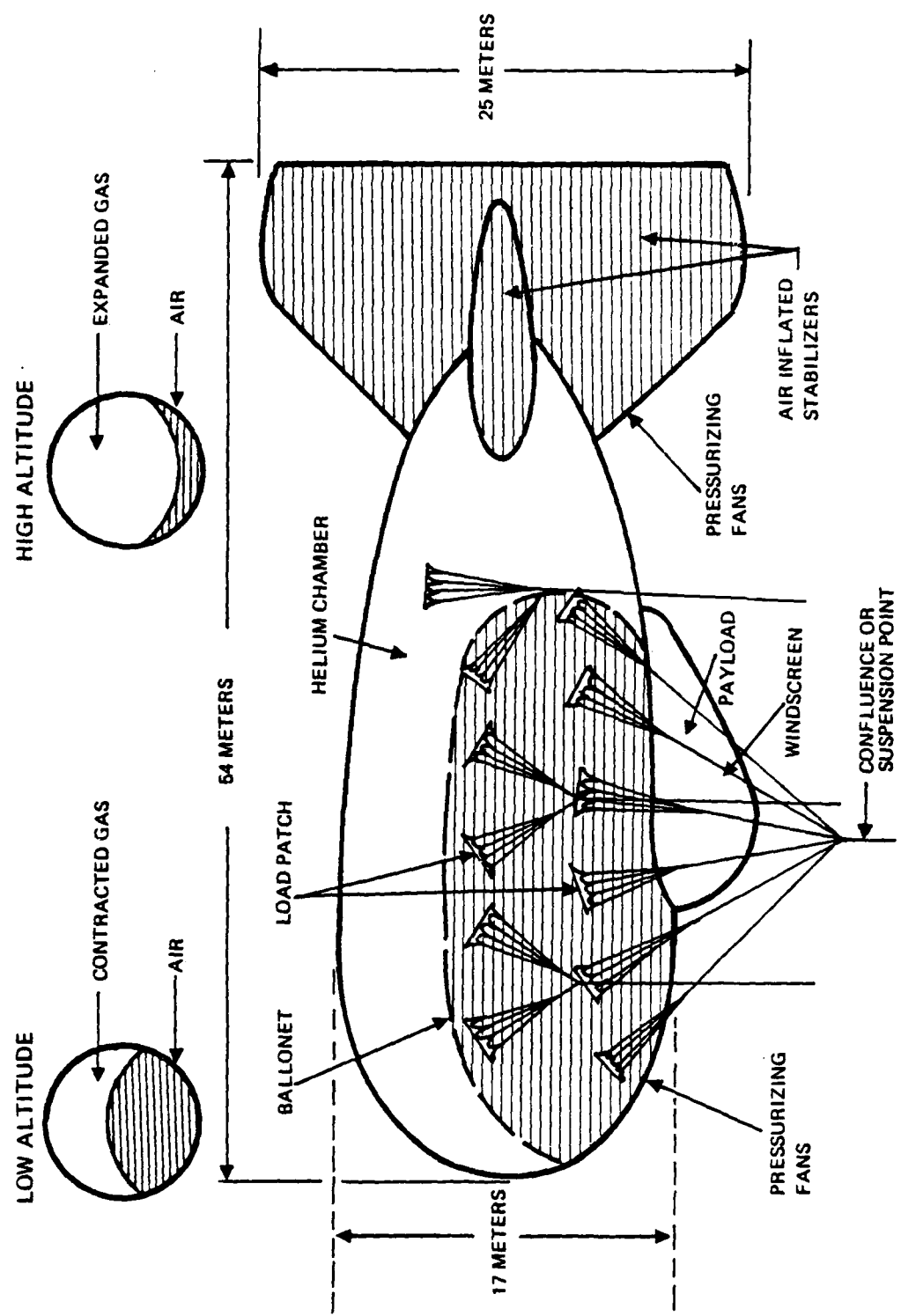


Figure A.15-1. Aerostat Balloon

to provide for expansion and contraction of the helium as the aerostat progresses to and from altitude. As the aerostat ascends, expansion of the helium causes air to be expelled from the ballonet through valves, which increases pressure on the ballonet curtain. As the aerostat is retrieved from altitude the helium contracts, and air is automatically forced into the ballonet compartment by electrically powered blowers. In addition, a series of automatic relief valves are installed in the hull within both the helium and the air compartments to prevent over-pressurization of the vehicle.

A.15.2.2 Stabilizers. As shown in Figure A.15-1, an aerostat is a body of revolution with four tail fins spaced 90 degrees apart on the aft section of the hull. The fins impart static and dynamic flight stability by causing the aerostat to return to its designed equilibrium position if it is displaced from that position by forces such as those exerted, for example, by gusty wind conditions. Selection of the shape and structural type was based on extensive analyses and tests of both rigid and inflatable structures.

Analyses of hard-model wind tunnel tests of the several hull and fin configurations investigated indicated that best aerodynamic performance was obtained by using four airfoil-type fins of elliptic cross-section mounted in cross arrangement with respect to the aerostat hull. It further was concluded from analysis of various structural concepts that a pressurized inflatable structure provides the lightest and most efficient fin. The present design was selected on the basis of all test results that were accumulated.

A.15.2.3 Materials. Present aerostat technology takes advantage of the latest developments in materials engineering in production of the multi-layer laminate material that presently is used for aerostat hulls. This laminate weighs 8.0 ounces per square yard (280 gm/sq m) and consists of adhesive-bonded layers of TEDLAR and MYLAR films that also are bonded to DACRON cloth in the arrangement shown in Figure A.15-2. This type of construction produces a very efficient material with a high strength-to-

weight ratio. The TEDLAR film on the outside surface has both excellent ultraviolet stability and weather resistance, which in turn protects the other components of the laminate and also provides good abrasion resistance. The two MYLAR films serve an efficient gas barrier with low values for helium permeability of less than 25 lb/day. The strong DACRON fabric not only is capable of withstanding loads induced by normal inflation, pressurization, hardware attachments, and inflight loading while providing an appropriate design safety factor, but also has good dimensional stability and imparts a high degree of tear resistance to the multilayer material.

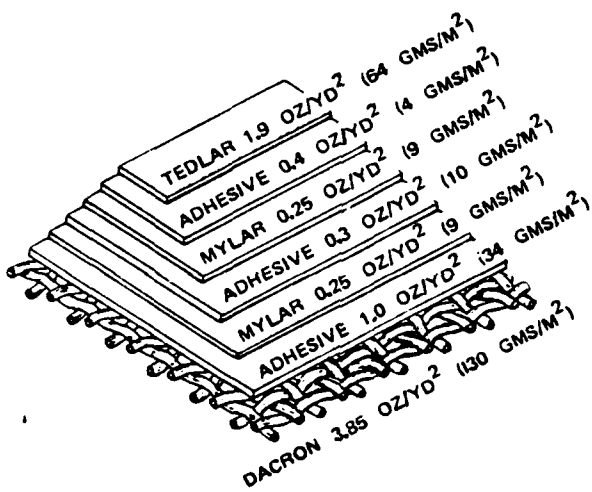


Figure A.15-2. Balloon Hull-Material Construction

Two of the most critical hull-material properties are biaxial tensile strength and tear strength. The tensile strength requirement is 150 lb/in for a 14-day duration at 120° F (including seals), and the tear-strength requirement demands that tears or defects in the material of up to 3/4 inches in length can be sustained without propagating when biaxially loaded to 65 lb/in.

A.15.2.4 Powered Tether System. The powered tether system is capable of supplying up to 31.25 kVA of 40-Hz ground-generated electrical power to a tethered aerostat flying at up to 4.5 km above ground level. The system uses an integral electromechanical cable which serves both as the tethering cable for the aerostat and as a high-voltage transmission line for electrical power supplied to the vehicle. A simplified block diagram of the powered tether system is shown in Figure A.15-3.

On a typical site where reliable commercial power is not available, 50/60-Hz power is generated on-site by diesel-powered engine generator sets which also supply the powered tether system. Motor/generator sets then convert the 50/60-Hz power to 400-Hz low-voltage power, which is transformed to high voltage and is applied to the lower end of the tether electrical conductors. The high voltage received at the upper end of the tether finally is transformed down to low voltage and supplied to the airborne vehicle and its onboard electronic payload equipment.

The tether consists of a 3-conductor high-voltage electrical cable covered with two layers of high-strength steel armor wire which are twisted on the electrical core in opposite directions to render the tether torque balanced, causing the two layers to oppose each others attempt to unwind when loaded and thus to keep the tether from rotating during load application or removal.

On the aerostat, 3-phase power from the tether passes through a power-line-carrier airborne coupler to an airborne transformer. The airborne transformer then steps down the delta-connected high voltage to the wye-connected 120/208 volts required by the aerostat systems and by the electronic payload.

A.15.2.5 Mooring System. The aerostat mooring system is a permanent installation which serves as the ground anchor for the aerostat when it is on-station and as a service and maintenance station for the aerostat between missions. The mooring system consists of a central machinery enclosure and mast mounted on a large central bearing, a horizontal compression member (boom), a circular monorail that supports the boom end,

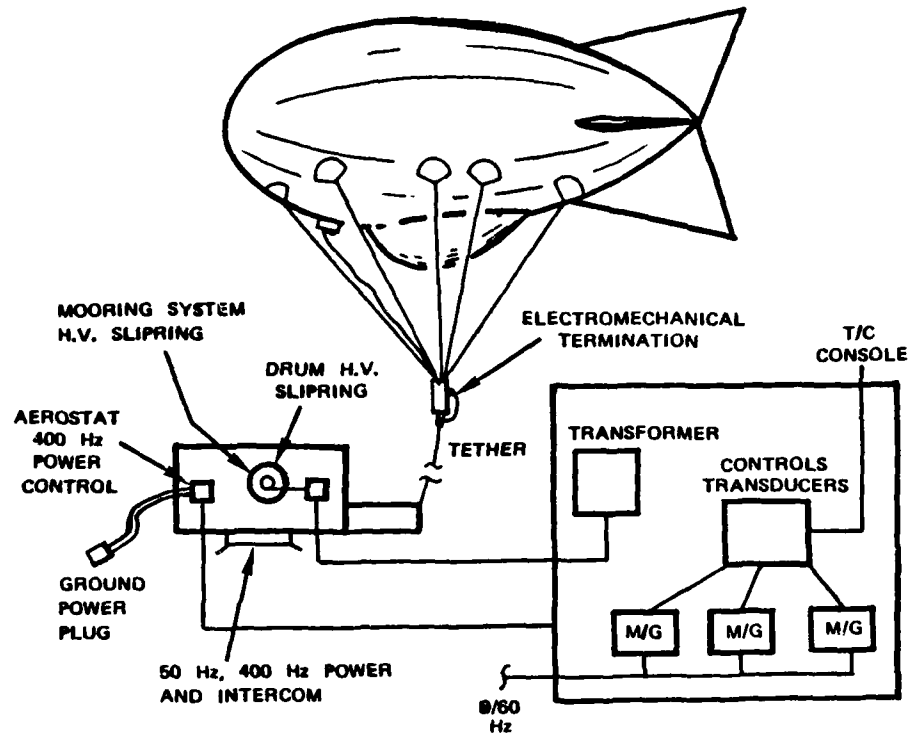


Figure A.15-3. Powered Tethered System

a flying sheave, and close-haul winches on rollers. A mechanical lock with a remote electrical release is provided at the top of the mast. Work surfaces are provided on the top deck of the machinery enclosure, on the boom, and at the location of the aerostat payload when it is moored. A diesel-powered main winch and an auxiliary power unit within the machinery enclosure furnish hydraulic power required to launch and to retrieve and moor the aerostat. The main winch is used to control and store the tether cable during flight operations. In the event the main winch loses hydraulic power the auxilliary power unit can be used to provide backup power. Three smaller winches, one at the base of the mast and two on the circular rail, provide for restraints and control during early stages of launch and during final recovery. A completely enclosed operator cab on the forward side of the machinery enclosure provides visibility to all operational areas.

A.16 HIGH-ALTITUDE POWERED PLATFORM CHARACTERISTICS AND CAPABILITY

A.16.1 Introduction

The High-Altitude Powered Platform (HAPP) is either a balloon or an airplane stationed or orbited over a station at an altitude of approximately 20 km (70,000 ft) for a duration on the order of a year. The operational altitude of 20 km was chosen primarily because wind velocities within the continental United States usually are at their minimum at this altitude. The lighter-than-air platform (balloon) would fly into the wind, whereas the airplane would fly in a tight circle. Both of these platforms would be free-flying and would receive their energy for station-keeping via microwave beam directed upward from the ground. Figure A.16-1 shows the two HAPP concepts. Analysis has indicated that the payload on the platform can be anywhere from 130 to 720 kg (300 to 1600 lb). The two HAPP concepts and the HAPP system baseline design are detailed in Figures A.16-1 and A.16-2 respectively.

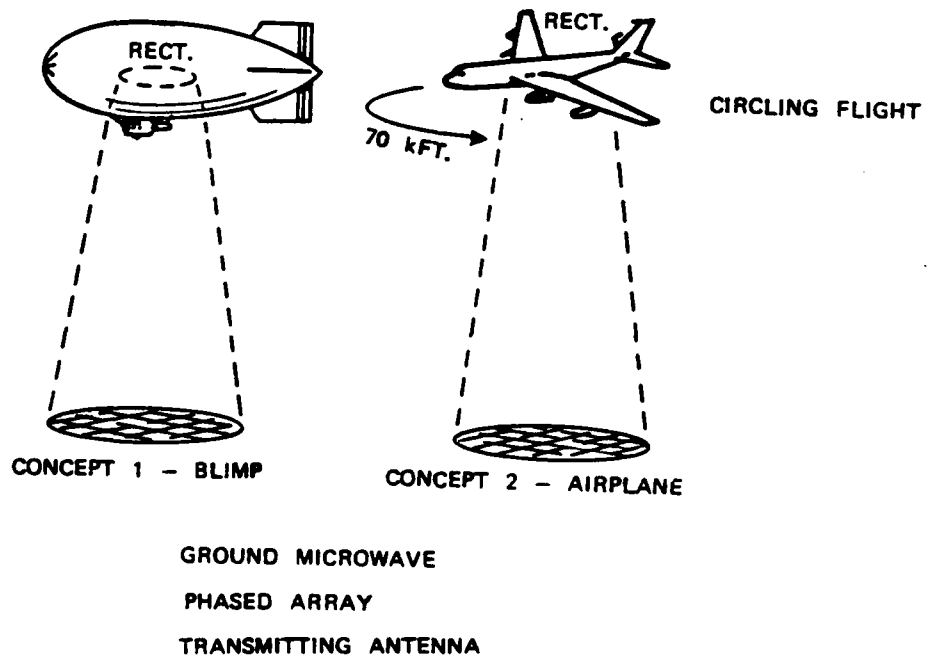
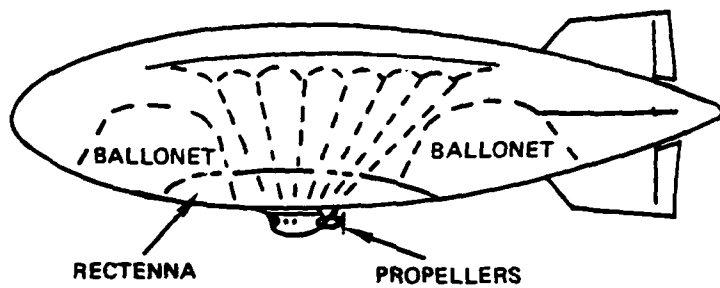


Figure A.16-1. Concepts of High Altitude Powered Platform



Characteristics	Design A	Design B
Payload (kg)	130	720
Hull Mass (kg)	34	610
Rectenna Mass (kg)	278	525
Car Motors (kg)	134	214
Volume (m^3)	14,000	37,000
Fineness Ratio	4	4
C_{DV}	0.06	0.05
Power, Both Motors (kW)	31	46

Figure A.16-2. HAPP Baseline Airship Designs

A.16.2 Power System

The HAPP microwave power system consists of a ground station and a rectenna on the aircraft. The ground station converts conventional electrical power into microwave power that is focused into a narrow beam by the transmitting antenna. The beam is then intercepted by a rectenna (a rectifier/antenna combination on the aircraft) comprising a large number of small antennas which feed a rectifier circuit that converts power from the microwave beam to DC power. Such rectification at each small antenna renders the rectenna relatively insensitive to pointing direction.

Transmission efficiency (the ratio of microwave power impinging on the rectenna to the power output of the microwave power generator) is dependent on the sizes of the rectenna and the transmitting antenna and on the distance over which the power is transmitted. However, efficiency as well as cost increase as the size of the rectenna and transmitting antenna increase, and efficiency decreases when the distance between the transmitter and the rectenna increases.

A number of impressive microwave power-transmission experiments that previously have been performed include achievement of a laboratory DC-to-DC transmission efficiency of 54 percent in 1975, recovery of 30 kW of DC power from a 1.6-km wireless transmission in 1977, and also development of a 90-percent efficient rectenna in 1977. In connection with HAPP efforts, little doubt presently exists regarding the technological feasibility of building a microwave power system capable delivering adequate power to maintain an airship on station, which therefore leaves cost as the biggest uncertainty associated with the required microwave power system. Although currently available dish transmitting antennas could provide adequate performance, the as yet undeveloped retrodirective array could offer significant cost savings. Both the retrodirective array and the receiving rectenna would use electronic components that are currently expensive but that could experience cost reduction of two or more orders of magnitude if produced in large quantities.

A.16.3 Potential Applications of HAPP

Figure A.16-3 indicates the HAPP as a function of coverage diameter and Figure A.16-4 shows the relationship of elevation angle and range. From these curves it may be seen that at zero elevation angle the maximum LOS distance is approximately 620 km and that at an elevation angle of 5° the range will be approximately 200 km, which corresponds to a field-of-view of less than 160° .

The payload capacity of the HAPP is another important consideration. The SRI study indicates that a 6000-kg payload is feasible, which is adequate for almost any foreseeable communications application. In comparison, the NASA ATS-6 advanced communications research satellite weighs 1350 kg (including some hardware not used for communications) and the Comsat Intelsat V weighs 834 kg. Consequently the HAPP vehicle could carry very complex and powerful communications payloads.

Because of the potentially lower cost of the HAPP in comparison with satellites and also because of its ability to provide regional coverage on a frequent basis, interest of potential users has been heightened by realization that the HAPP might fit many of their regional needs. Also, because a HAPP would normally be brought to the ground yearly, users would have opportunity to calibrate and maintain their instruments as well as to replace them with newer devices.

The HAPP looks very promising for communications applications. As a regional broadband communications relay it could provide video channels at a much lower cost than geostationary satellites, and for many other applications at a lower cost than cable or terrestrial microwave links. For direct television broadcasting approximately 80 HAPPs could cover the 48 contiguous states, with all areas having a HAPP more than 5° above the smooth earth horizon. (The 5° angle is a conservatively high estimate as only 13 HAPPs would be required for a 0° angle.)

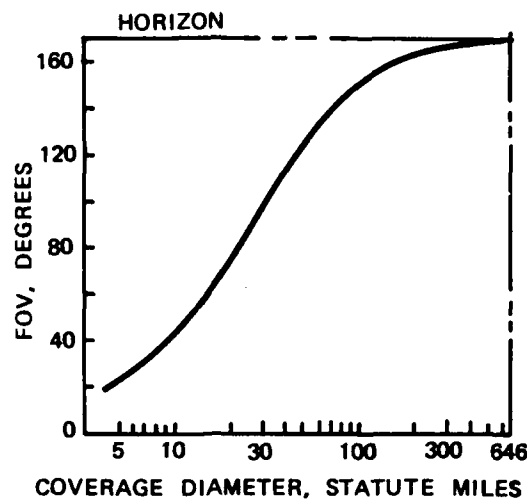


Figure A.16-3. Diameter of Area Seen from a HAPP Versus Sensor Angular FOV (For 70,000 Foot Altitude)

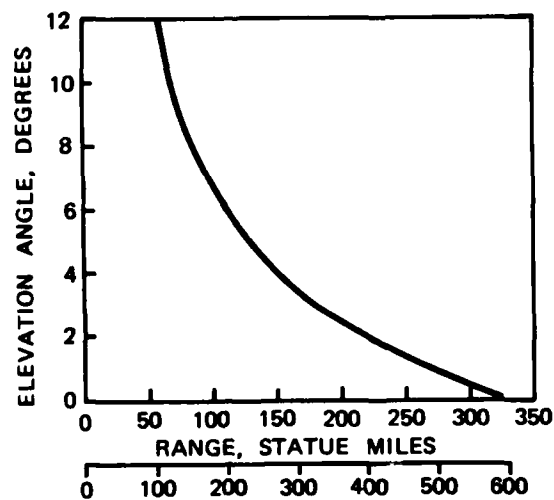


Figure A.16-4. LOS Range as a Function of Ground Antenna Evaluation Angle

A.16.4 Summary

In summary, a platform such as the HAPP would be capable of station-keeping for periods up to a year over a given location, and could perform frequent and repeated high-resolution observations over a given region or serve as a high-altitude regional communications link. The HAPP would combine desirable characteristics of both geostationary satellites (wide-area coverage, frequent observations) and of aircraft (high resolution). In addition, the HAPP could satisfy many remote sensing and communications requirements that are not being fully resolved by means of satellites or aircraft at the present time.

Some of the most promising potential HAPP applications that have been identified include the following:

- Communications (e.g., line-of-sight radio or TV)
- Regional data collection
- Operational uses (e.g., monitoring and sensing)
- Research and development (e.g., serving as a platform for remote sensor and antenna development)
- Navigational aids (e.g., monitoring ice in the Great Lakes, United States rivers, and North Slope waters).

REFERENCES

- A.1-1 Mulcahy, J.W., "The L5E Layout and Description," Paper 18.1, ICC Proc. (1977).
- A.1-2 Martin, J., Future Developments in Telecommunication, Prentice-Hall, Inc., Englewood Cliffs, New Jersey (1977).
- A.1-3 Kaibuchi, S., "The Perspective on Telephone Cables in Japan," Japan Telecommunications Review, 20, 1 (Jan. 1978).
- A.1-4 Simpson, W.G., "Review of Trunk Transmission Planning in UK Post Office," Proc. IEE, 123, 5 (May 1976), pp 393-400.
- A.1-5 "Line Transmission," Orange Book, III-1, Secs. 3-3 and 3-4, CITT Sixth Plenary Assembly, Geneva, Switzerland (Sept.-Oct. 1976).
- A.1-6 Yamada, T., et al, "400d Mbps Digital Transmission System on Coaxial Cable," NEC Res. & Rev., 51 (Oct 1978), pp 56-58.
- A.1-7 Duerdorff, W.T., "Development of Integrated Digital Telecommunication Network," Proc. IEE, 122, 6 (June 1974), pp 56-58.
- A.1-8 Pitroda, S.G., "Telephones Go Digital," IEEE Spectrum, (Oct. 1979), pp 51-60.
- A.1-9 Bruggendieck, S., "Broadband Transmission on Telecommunication Cables," Paper 2.7.2, ICC Proc. (1977).
- A.1-10 Bauch, H., "A 560 Bbps Regenerative Repeater for a Repeater Spacing at 1.6 km along a 2.6.9 mm Coaxial Tube," Paper 2.7.7, ICC Proc. (1977).
- A.2-1 "WT4 Millimeter Waveguide System," Special Issue, Bell System Technical Journal, 56, 10 (Dec. 1977).
- A.2-2 Corazza, G.C., et al, "Characteristics and Prospects of Circular Waveguide Telecommunication Systems," Paper 2.9.2, Proc. IEEE/ICC Conf. (1977).
- A.2-3 Nihei, F., K. Yanagimoto, and F. Ishihara, "Millimeter Waveguide Line in a Cable Tunnel," IEEE MIT International Microwave Symposium Digest, (27-18 June 1978), pp 153-154.
- A.3-1 Boubau, G., Beam Waveguides Advances in Microwaves, 3, Academic Press (1968).
- A.3-2 Steier, W.H., "The Statistical Effects of Random Variations in the Components of a Beam Waveguide," Bell System Technology Journal, 45, (1966), pp 451-471.
- A.3-3 Gloge, D. and W.H. Steier, "Pulse Shutting in a Half-Mile Optical Lens Guide," Bell System Technology Journal, 47, 6 (May-June 1968), pp 767-799.

REFERENCES (Continued)

- A.3-4 Arnaud, J.A. and Ruscio, J.T., "Guidance of 100-Ghz Beams by Cylindrical Mirros," IEEE Trans. MTT-23, 4 (1975), pp 377-379.
- A.3-5 Goubau, G. and Schwering, F., "On the Guided Propagation of Electromagnetic Wave Beam," IRE Trans. on Antenna and Propagation, AP-9, 5 (May 1961), pp 248-256.
- A.4-1 Handbook of Telecommunication Techniques (German), Schiele & Schoen, Berlin (1973).
- A.4-2 GTE Lenkurt, Microwave Radio Products Catalog.
- A.4-3 Uguchi, Bun-ichi, "Microwave Radio System," Telecommunications Journal, 45 (June 1978), pp 323-330.
- A.4-4 Utlant, W.F., "Review of Important Problems in Wave Propagation Affecting Future Telecommunication System Performance," Proc. World Telecommunication Forum Technical Symposium, Geneva, Switzerland (Oct 1975).
- A.4-5 Thelaner, L.G., "Space Diversity, It Design and Implementation," Collins Radio Co., Rapid City, 10 (May 1972).
- A.4-6 Abel, N., "Statistics of Attenuation Due to Precipitation on Terrestrial Radio-Relay Links at 7 to 15 GHz," NTZ (German Publication) (Aug. 1977).
- A.4-7 Brodhage, H. and Hormuth, W., "Planning and Engineering of Radio Relay Links," Siemens AG, May 1968.
- A.4-8 Christopher, N.S., "Reliable Remote Power Source," Telecommunications (March 1979).
- A.4-9 Moxon, R.L., "Problems of Tower Design," (British Paper).
- A.4-10 "Anomalous Propagation," GTE Lenjurt Demodulator (July/Aug. 1975).
- A.4-11 "Microwave Receiver Interference," GTE Lenjurt Demodulator (July-Aug. 1978)
- A.4-12 Harkleroad, A., Mackask, T.T. and Sharma, J.S., "Washington Area Wide-Band System," Telecommunications (June 1979).
- A.4-13 Moskowitz, S., "Military Communications Systems Hop on Digital Bandwagon," Microwaves (May 1979).
- A.5-1 Gunther, F.A., "Tropospheric Scatter Communications - Past, Present and Future," IEEE Spectrum, Vol. 3, No. 9, 1966.
- A.5-2 Picquenard, A., "Radio Wave Propagation," John Wiley & Son, New York, 1974.

REFERENCES (Continued)

- A.5-3 Bergmann, K., "Handbook of Telecommunication Techniques," (German) Schiele & Schoen, Berlin, 1973.
- A.5-4 Hamsher, D.H., "Communication System Engineering Handbook," McGraw Hill, NY, 1967
- A.5-5 "Radio Spectrum Utilization," IEEE/EIA Joint Technical Advisory Committee Report, 1965.
- A.5-6 Rice, P.L., et al, "Transmission Loss Prediction for Troposcatter Communications Circuits," Technical Note 101, National Bureau of Standards, Washington, D.C., 1965.
- A.5-7 Parl, S.A., "New Formulas for Tropospheric Scatter Path Loss," Radio Science, Vol. 14, pp 47-57, 1979.
- A.5-8 SKingley, B.S., "Spectrum Efficiency Key to North Sea Tropo Network," Microwaves, Vol. 5, No. 11, 1976.
- A.5-9 Brodhage, H., and Hormuth, W., "Planning and Engineering of Radio Relay Links," Siemens A.G. Report, May 1968.
- A.5-10 Gough, M.W., Rider, C.G., and Larsen, R., "Troposcatter Angle Diversity in Theory and Practice," AGARD Conf. Proc. 244, Aspects of Electromagnetic Wave Scattering in Radio Communications, Cambridge, MA, 3-7 Oct. 1977, pp 29-1 through 29-14.
- A.5-11 Monsen, P., "Spectrally Efficient Digital Troposcatter," Paper 3, IEEE/IEEE & AFCEA Conf. Proc. Digital Tropospheric Scatter Systems NATO, Brussels, Belgium, 26 March 1980.
- A.6-1 Read, M.E. (Principal Investigator), "Ultra-Wideband Gyrotron Studies," Report No. CLN40J (Accession No. DN8755730), pp 6, DCA/DLA Work Unit Summary, Alexandria, VA (12 Oct 1978) and Private Communication with Dr. R.A. Smith, TRW/DSSG, Redondo Beach, CA.
- A.6-2 Barnett, L., Naval Research Laboratory, Washington, D.C., Private Communications with Dr. R.A. Smith, TRW/DSSG, Redondo Beach, CA (Nov. 1979).
- A.6-3 Moncrief, F.J., "Japan's Attention Turns to GaAs FETs as Low-Noise Devices Reach Maturity," Microwaves, 19, 2 (Feb. 1980), pp 36.
- A.6-4 Elta, M.E. and Haddad, G.I., "High Frequency Limitations of IMPATT, MITATT, TUNNETT Mode Devices," IEEE Trans. on Microwave Theory Technology, MTT-27, (May 1979, pp 442-449.

REFERENCES (Continued)

- A.6-5 Nishitanai, K., et al, "High Power GaAs IMPATT Amplifier," IEEE Trans. on Microwave Theory Technology, 59, (Jan. 1971), pp 973-977.
- A.6-6 Kurokawa, K. and Megathae, F.M., "An X-Band 10 Watt Multiple-IMPATT Oscillator," Proc. IEEE, 59, (Jan. 1971), pp 102-103.
- A.6-7 Alder, R., "A Study of Locking Phenomena in Oscillators," Proc. IRE, (June 1946), pp 351.
- A.6-8 Kunao, M.J. and Fong, T.T., "Solid State MM-Wave Sources and Combiners," Microwave Journal, (June 1979), pp 47.
- A.6-9 Gewartowski, J.W., "Progres with CW IMPATT Diode Circuits at Microwave Frequencies," IEEE Trans. on Microwave Theory Technology, MTT-27, (May 1979), pp 434-441.
- A.6-10 Nishizawa, J., et al, "GaAs TUNNETT Diodes," IEEE Trans. on Microwave Theory Technology, MTT-20, (Dec. 1978), pp 1029-1035.
- A.6-11 Juneo, H.J. and Fond, T.T., "Solid State MM-Wave Sources and Combiners," Microwave Journal, 22, (June 1979), pp 47-75.
- A.6-12 Bosch, F. and O.G. Peterson, "Switching Performance of MM-Wave Pin Diodes for Ultra-High Data Rates," IEEE Int'l. Microwave Symposium, San Diego, CA (1977).
- A.6-13 Leichti, C., Proc. 4th European Microwave Conf., Montreux, Switzerland (1974).
- A.6-14 Kennedy, W.K., "MW Semiconductor and Solid State Components," Microwave Journal, 21, 11 (Nov. 1978), pp 66-69.
- A.6-15 Barrers, J.S., "GaAs FETs Promise Much as They Come of Age," Microwaves, 19, 2 (Feb. 1980) pp 67.
- A.6-16 "Mission Analysis on Command and Control Communications," Communications Technologies, IV, 1, USAF/AFSC Study Facility, Hanscom Field (Nov. 1971) (S), pp 80 (U).
- A.6-17 Richards, P.L. and Shen, T.M., "SIS Quasiparticle Junctions as Microwave Photon Detectors," to be published in Apl. Phys. Lett. (1980).
- A.6-18 Calveillo, J.A., "GaAs Schottky Barrier Devices and Components," Microwave Journal, 22, (Sept. 1979), pp 92.
- A.6-19 Payne, J.M. and Wordeman, M.R., "Quasi-Optical Diplexer for Millimeter Wavelengths," Rev. Sci. Instrum., 49, (Dec. 1978), pp 1741-1743.

REFERENCES (Continued)

- A.6-20 "Millimeter Microwave Components," TRG Division, Alpha Industries, Inc., Woburn, MA.
- A.6-21 Weibel, G.E. and H.O. Bressel, "Propagation Studies in Millimeter Wave Link Systems," Proc. IEE, 55, (April 1967), pp 497-513.
- A.6-22 Morgan, L.A. and Ekdahl, C.A., Jr., "Millimeter Wave Propagation," DDC Accession No. AD 489424.
- A.6-23 Davies, A.R., "Estimates of Satellite-to-Earth Microwave Attenuation by Cloud, Rain, Oxygen and Water Vapor," (April 1977), DDC Accession No. ADA 052581.
- A.6-24 Zhevakin, S.A. and Naumov, A.P., "Propagation of Centimeter, Millimeter and Submillimeter Waves in the Earth's Atmosphere," (1967), DDC Accession No. AD-694411.
- A.6-25 Stutzman, W.L. and Bostian, C.W., "A Millimeter Wave Attenuation and Depolarization Experiment Using COMSTAR and CTS Satellites," DDC Accession No. AD 069583.
- A.6-26 Young, G.D. and Hrycenko, G., "Statistical Investigation of the Effect of the Troposphere on Millimeter Wavelength Radiation and Coherence," (1969), DDC Accession No. AD-685246.
- A.6-27 Tatarski, V.I., Wave Propagation in a Turbulent Medium, McGraw Hill, NY (1961).
- A.7-1 Trewartha, G.T., Elements of Physical Geography, McGraw Hill, NY (1957).
- A.7-2 Dougherty, H.T. and Dulton, E.J., "Estimating Year to Year Variability of Rainfall," IEEE Trans. on Communications, COM-26, 8 (Aug 1978).
- A.7-3 Sums, A.L. and Jones, D.M.A., "Climatology of Instantaneous Precipitation Rates," Illinois State Water Survey Final Report, No. AF CRL TR-73-0171 (March 1973).
- A.7-4 "Communications Satellite System Survivability Analysis," Report No. 24904-6593-XF-00, Appendix B, TRW Systems Group, Redondo Beach, CA (1977).
- ... , J.G., et al, "Multiple Access Techniques for Commercial Satellites," Proc. IEEE, 59, 2 (Feb. 1971).
- ... , ... and Wessler, B.D., "Computer Network Development and Resource Sharing," AFIPS Proc. SJCC, pp 543-549,

REFERENCES (Continued)

- A.8-2 Kahn, R.E., "Resource-Sharing Computer Communication Network," Proc. IEEE, Vol. 60, pp 1394-107, 1972.
- A.8-3 Kahn, R.E., Gronemeyer, S.A., Burchfield, J., and Kunzelman, R.C., "Advances in Packet Radio Technology," Proc. IEEE, Vol. 66, pp 1468-1569, 1978.
- A.8-4 Abramson, N., "The ALOHA System - Another Alternative for Computer Communications," AFIPS Conf. Proc., Vol. 37, pp 281-285, 1970.
- A.8-5 Kahn, R.E., "The Organization of Computer Resources Info A Packet Radio Network," Proc. Natl. Computer Confo., pp 177-186, 1975.
- A.8-6 Dixcon, R.C., Spread Spectrum System, John Wiley & Sons, New York, NY 1976.
- A.8-7 AGARD-LS-58, Spread Spectrum Communications, AGARD Lecture Series, May 1973.
- A.8-8 Kleinrock, L., and Lam, S.S., "Packet Switching in a Multi-Access Broadcast Channel Performance Evaluation," IEEE Trans., Vol. COM-23, pp 410-422, 1975.
- A.8-9 Abramson, N., "The Throughput of Packet Broadcasting Channels," IEEE Trans., Vol. COM-25, pp 117-128, 1977.
- A.8-10 Kleinrock, L., and F. Tobagi, "Packet Snitching in Radio Channels: Part I - Carrier Sense Multiple Access Modes and Their Throughput Characteristics," IEEE Trans., Vol. COM-23, pp 1400-1416, 1975.
- A.8-11 Togabi, F.A., Berla, M., Peebles, R.W., and Manning, E., "Modeling and Measuring Techniques in Packet Communication Networks," Proc. IEEE, Vol. 66, pp 1423-1447, 1978.
- A.8-12 Jacobs, I.M., Binder, R., and Hoversten, E.V., "General Purpose Packet Satellite Network," Proc. IEEE, Vol. 66, pp 1448-1467, 1978.
- A.8-13 Lincoln Laboratory, MIT, "Network Speech Processing Program," Annual Report, ESD-TR-78-361, September 1978.
- A.9-1 Maimon, T.H., "Stimulated Optical Radiation in Ruby," Nature (London), Vol. 6, pp 106, 1960.
- A.9-2 Javan, A., Bennet, W.R., Herriott, D.R., "Gas Optic Lasers," Phys. Rev. Lett., Vol. 6, pp 106, 1961.
- A.9-3 Kompfner, R., "Optical Communications," Science, Vol. 150, pp 149-155, 1965.

REFERENCES (Continued)

- A.9-4 Miller, S.E., and Tillobon, L.C., "Optical Transmission Research," *Appl. Opt.*, Vol. 5, pp 1538-1549, 1966.
- A.9-5 Kao, K.C., and Hockham, G.A., "Dielectrics - Fiber Surface Waveguides for Optical Frequencies," *Proc. IEE*, Vol. 113, pp 1151-1158, 1966.
- A.9-6 Kapron, F.P., Keck, D.B., and Maurer, R.D., "Radiation Loss in Glass Optical Waveguides."
- A.9-7 Miyashita, R., Miya, T., and Nakahara, M., "An Ultimate Low Loss, Single-Mode Fiber at 1.55 mm," Topic Meeting on Optical Fiber Communication (Optical Society of America), Washington, D.C., March 1979.
- A.9-8 Horiguichi, M., "Spectral Losses of Low-OH-Content Optical Fiber," *Electron Lett.*, Vol. 12, pp 310-312, 1976.
- A.9-9 Hartman, R.L., Schumaker, N.E., and Dixon, R.W., "Continuously Operated (Al, Ga) As Double-Heterostructure Laser with 70° Lifetime as Long as Two Years," *Appl. Phys., Lett.*, Vol. 31, pp 756-759, 1972.
- A.9-10 Basch, E.E., and Beaudette, R.A., "The GTE Fiber Optic System," National Telecommunication Conference Record, pp 142, 1977.
- A.9-11 Jacobs, I., "Lightwave Communications Passes Its First Test," Bell Labs Record, Vol. 54, pp 290-297, 1976.
- A.9-12 Chang, K.Y., Marthaler, E., and Basmadjian, H.K., "An Overview of a Fiber Optic Exploratory Trail in Montreal," *Proc. Internation Communication Conference*, pp 6.1.1-6.1.6, 1978.
- A.9-13 Akiyama, S., Otsuka, T., Sekiguchi, M., Fukushima, Hamanaka, T., and Nishimuro, K., "3-Channel TV Transmission on Optical Fiber," *Proc. Int. Conf., Integrated Optics and Optical Fiber Communications*, Paper C6.5, pp 481, 1977.
- A.9-14 Sanband, E.P., "Optical Fiber Communications in UK," *Proc. Int. Conf., Integrated Optics and Optical Communications*, Paper 8.2, pp 507, 1977.
- A.9-15 Schwartz, M.I., Reenastia, W.A., and Mullins, J.H., "The Chicago Lightwave Communications Project," *Proc. Int. Conf., Integrated Optics and Optical Communicataions*, Paper P14, 1977.
- A.9-16 Brace, D., and Cameron, K., "BPO 8448 16K Bits/s Optical cable Feasibility Trail," *Proc. European Conference Optical Communications 3rd*, pp 237, 1977.

REFERENCES (Continued)

- A.9-17 Berry, R.W., Brace, D.J., and Ravensdroft, I.V., "Optical Fiber System Trail at 8 Mbits/s and 140 Mbits/s," IEEE Trans., Vol. COM-26, pp 1020-1027, 1978.
- A.9-18 Hill, D.R., Jessop, A., and Howard, P.J., "A 140 Mbits/s Field Demonstration System," Proc. European Conference Optical Communications 3rd, pp 240, 1977.
- A.9-19 Cocito, G., et al, "COS 2 Experiment in Turin: Field TEst on an Optical Cable Duct," IEEE Trans., Vol. COM-26, pp 1028-1035, 1978.
- A.9-20 Giallorengi, T.G., "Optical Communication Research and Technology: Fiber Optics," Proc. IEEE, Vol. 66, pp 744-780, 1978.
- A.9-21 Gloge, D., "Weakly Guiding Fibers," Appl. Opt., Vol. 10, pp 2252-2258, 1971.
- A.9-22 Morslowski, S., "High Capacity Communications Using Moromode Fibers," Proc. 2nd European Conference Optical Fiber Transmission, Paris, France, pp 373, 1976.
- A.9-23 Ollshansky, R., and Keck, D.B., "Pulse Boarding in Graded Index Optical Fibers," Appl. Opt., Vol. 15, pp 481-491, 1976.
- A.9-24 Maurer, R.D., "Introduction to Optical Fiber Waveduiges," in Introduction to Integrated Optics, Barnoski, M., Ed. Plenum Press, New York, 1974.
- A.9-25 Li, T., "Optical Fiber Communication - The State-of-the-Art," IEEE Trans., Vol. COM-26, pp 946-955, 1978.
- A.9-26 Keck, D.B., Maurer, R.D., and Schultz, P.C., "On the Ultimate Lower Limit of Attenuation in Glass Optical Waveguide," Appl. Phys. Lett., Vol. 22, pp 307, 1973.
- A.9-27 Carson, D.S., and Maurer, R.D., "Optical Attenuation in Titania Silica Glasses," J. Non-Cryst. Solids, Vol. 11, pp 368, 1973.
- A.9-28 Maurer, R.D., Schiel, E.J., Kronenberg, S., and Lux, R.A., "Effect of Neutron and Gamma-Radiation on Glass Optical Waveguide," Appl. Opt., Vol. 12, pp 2024, 1973.
- A.9-29 Aggerwal, I.D., Macedo, P.B., and Montrose, C.J., "Light Scattering in Lithium Aluminosilicate Glass System," American Ceramic Society Meeting, Bedford Springs, PA, 1974.
- A.9-30 Crow, J.D., "Power Handling Capability of Glass Fiber Lightguides," Appl. Opt., Vol. 13, pp 469, 1974.

REFERENCES (Continued)

- A.9-31 Dyott, R.B., and Stern, J.R., "Group Delay in Glass Fiber Waveguide," Electron. Lett., Vol. 7, pp 82-84, 1971.
- A.9-32 Malitson, J.H., "Interspecimen Comparison of the Refractive Index of Fused Silica," J. Opt. Soc. Am., Vol. 55, pp 1205-1209, 1965.
- A.9-33 Fleming, J.W., "Material and Mode Dispersion in $\text{GeO}_2 \cdot \text{B}_2\text{O}_3 \cdot \text{SiO}_2$ Classes," J. Am. Ceram. Soc., Vol. 59, pp 503-507, 1976.
- A.9-34 Fleming, J.W., "Material Dispersion in Lightguide Glass," Electron. Lett., Vol 14, pp 326, 1978.
- A.9-35 Cohen, L.G., and Lin, C., "Pulse Delay Measurement in the Zero Material Dispersion Wavelength Region for Optical Fibers," Appl. Opt., Vol. 16, pp 3136-3139, 1977.
- A.9-36 Personick, S.D., "Time Dispersion in Dielectric Waveguide," Bell Sys. Tech. J., Vol. 51, pp 1199-1232, 1972.
- A.9-37 Katsuyama, Y., Ishida, Y., Ishihara, K., Miyashita, T., and Tsuchiyi, H., "Suitable Parameters of Single-Mode Optical Fiber," Electron. Lett., Vol. 15, pp 94-95, 1 Feb. 1979.
- A.9-38 Miller, S.E., "Light Propagation in Generalized Lens-Like Media," Bell Sys Tech. J., Vol. 44, pp 2017-2064, 1965.
- A.9-39 Marsue, D., "Pulse Propagation in Multimode Dielectric Waveguide," Bell Sys. Tech. J., Vol. 51, pp 1199-1232, 1972.
- A.9-40 Kapron, F.P., and Deck, D.B., Pulse Transmission Through a Dielectric Optical Waveguide," Appl. Opt., Vol. 10, pp 1519-1523, 1971.
- A.9-41 Kimura, T., and Daikoku, K., "A Proposal on Optical Fiber Transmission System in a Low Loss 1.0-1.4 mm Wavelength Region," Oppt. and Quant. Elect., Vol. 9, pp 33, 1977.
- A.9-42 Li, T., "Optical Fiber Communication - The State-of-the-Art," IEEE Trans., Vol. COM-26, pp 946-955, 1978.
- A.9-43 Muska, W.M., Tingye, L., Lee, T.P., and Dentai, A.G., "Material Dispersion - Limited Operation of High-Bit-Rate Optical Fiber Data Links Using LEDs," Elect. Lett., Vol. 13, pp 605-607, 1977.
- A.9-44 Ettenberg, M., Kressel, H., and Wittke, J.P., "Very High Radiance Edge - Emitting LED," IEEE Jour., Vol. QE-12, pp 360, 1976.

REFERENCES (Continued)

- A.9-45 Horikoshi, Y., Takanshi, T., and Iwane, G., "High Radiance Lighting Emitting Diodes," Japan J. Appl. Phys., Vol. 15, pp 485, 1976.
- A.9-46 Wittke, J.P., Ettenberg, M., and Kressel, H., "High Radiance LED for Single Fiber Optic Link," RCA Review, Vol. 37, pp 159-183, 1976.
- A.9-47 O'Connor, P.B., MacChesney, J.B., and Melliar-Smith, C.M., "Large-Cove High-NA Fiber for Data Link Application," Electron. Lett., Vol. 13, pp 170, 1977.
- A.9-48 Botez, D., and Ettenberg, M., "Comparison of Surface- and Edge-Emitting LEDs for Use in Fiber Optical Communications," IEEE Trans., Vol. QE-26, pp 1230-1238, 1979.
- A.9-49 Paloi, T.L., "Depolarization of the Lasing Emission from CW Double-Heterostructure Lasers," IEEE Trans., Vol. QE-11, pp 489, 1975.
- A.9-50 King, F.D., "High Radiance LEDs," Electronics, pp 93, 1976.
- A.9-51 Kressel, H., and Battler, J.K., Semiconductors Laser and Heterojunctions LEDs, Academic Press, New York.
- A.9-52 Lee, T.P., and Dentai, A.G., "Power and Modulation Bandwidth of GaAs-AlGaAs High-Radiance LEDs for Optical Communication System," IEEE Jour., Vol. QE-24, pp 150, 1978.
- A.9-53 Paloi, T.C., "Modulation of Diode Laser," Laser Focus, Vol. 13, pp 54, 1977.
- A.9-54 Hishi, H., Kawahara, H., Hanamita, K., and Kudo, K., "Semiconductor Laser with Flat Frequency up to 2 GHz," Proc. Int. Conf., Integrated Optics and Optic Fiber Communications, Tokyo, Japan, Paper A53, pp 73, 1977.
- A.9-55 Burns, J., Danielsen, M., Jeppesen, P., Mengel, F., Moeskjor, H., and Ostaich, V., "On the Dynamic and Spectral Behavior of Double Heterojunction Stripe Laser Modulation with Subnano-Second Pulses," Proc. 2nd Eur. Conf., Optical Fiber Transmission, pp 231, 1976.
- A.9-56 Melchior, H., "Detector for Lightwave Communications," Physics Today, Vol. 30, pp 32-39, 1977.
- A.9-57 Melchior, H., "Semiconductor Detector for Optical Communications," Conf. Laser Eng. Appl., Abstract in IEEE Trans., Vol. QE-9, pp 659, 1973.

REFERENCES (Continued)

- A.9-58 Anderson, K.K., McMullin, P.G., D'Asaro, L.A., and Goetzberger, A., "Microwave Photodiodes Exhibiting Microplasma-Free Carrier Multiplication," *Appl. Phys. Lett.*, Vol. G, pp 62, 1965.
- A.9-59 Nishida, K., "Avalanche-Noise Dependence on Avalanche-Photodiode Structures," *Electron. Lett.*, Vol. 13, pp 419, 1977.
- A.9-60 Conradi, J., and Webb, P.P., "Silicon Reach-Through Avalanche Photodiodes for Fiber Optic Application," *Proc. Eur. Conf. Opt. Fiber Comm.*, pp 128, 1975.
- A.9-61 Melchior, H., Misher, M.B., and Abrams, F., "Photodetectors for Optical Communication Systems," *Proc. IEEE*, Vol. 48, pp 1466-1468, 1970.
- A.9-62 Muller, J., and Ataman, A., "Double-Mesa Thin-Film Reach-Through Silicon Avalanche Photodiodes with Large Gain Bandwidth Product," *Tech. Dig. Int. Electron Devices Meeting*, pp 416, 1976.
- A.9-63 Kaneda, T., Mizushima, T., and Kajigama, K., "Silicon Avalanche Photodiodes with Low Multiplication Noise and High Speed Response," *IEEE Trans.*, Vol. ED-3, pp 1337, 1976.
- A.10-1 Powerlly, J., "International Integrated Civil Communication System," *Electronics and Power*, 6 March 1975, pp 249-252.
- A.10-2 Baras, C.C., Submarine Telecommunication and Power Cables, Peter Peregrinas Ltd., Stevenage, Harts, England, 1977.
- A.10-3 Easton, R.L., "Undersea Cable Systems - A Survey," *Communications Society*, Vol. 13, No. 5, 1975, pp 12-15.
- A.10-4 Dawidziuk, B.M., "Global Submarine System: What's Happening on the Sea Bottom?", *Telephony*, 24 September 1979.
- A.11-1 Meteor-Burst Communications Papers, *Proc. IRE*. Vol. 45, No. 12, pp 1642-1736, 1957.
- A.11-2 Forsyth, C.A., Vegan, E.L., Hansen, D.R., and Hines, C.O., "The Principles of JANET - a Meteor Burst Communications System," *Proc. IRE*, Vol. 45, pp 1642-1657, 1957.
- A.11-3 Kaiser, T.R., "Radio Echo Studies of Meteor Ionization," *Advances in Physics*, No. 12, 1952.
- A.11-4 Mannings, L.A. and Eshleman, U.R., "Meteor in the Ionosphere," *Proc. IRE*, Vol. 47, pp 191, 1959.
- A.11-5 Crystale, J.H., "Analysis of the Performance of the Edmonton-Yellowknife JANET Circuit," *IRE Trans.*, Vol. CS-8, pp 33-40, 1960.

REFERENCES (Continued)

- A.11-6 Bartholome, P.J., and Vogt, I.M., "COMET - A New Meteor Burst System Incorporation ARQ and Civersity Reception," IEEE Trans., Vol. COM-16, pp 268-278, 1968.
- A.11-7 Heritage, J.L., Bickel, J.E., and Kugel, C.P., "Meteor Burst Communication in Minimum Essential Emergency Communication Network (MEECN)," NOSE TR-138, August 1977.
- A.11-8 Hornback, C.E., "The NBS Meteor-Burst Propagation Project - A Progress Report," NBS Boulder, Colorado, Tech. Note 86, March 1960.
- A.11-9 Sugar, G.R., "Radio Propagation by Reflection from Meteor Trail," Proc. IEEE, Vol. 52, pp 116-125, 1964.
- A.11-10 Carpenter, R.J., and Oche, G.R., "High Resolution Pulse Measurements of Meteor-Burst Propagation at 41 Mc/s Over 1295 km Path," Jour. Res NBS, Vol. 66D, pp 249, 1962.
- A.11-11 Eshelman, V.R., "Mechanism of Radio Reflection from Meteoric Ionization," Stanford University Electronics Res. Lab., Rep. 49, 1952.
- A.11-12 Villard, O.G., Jr., Peterson, A.M., Manning, L.A., and Eshelman, V.R., "Extended-Range Radio Transmission by Oblique Reflection from Meteoric Ionization," J. Geophys. Res., Vol. 5-8, pp 83-93, 1953.
- A.11-13 Eshelman, V.R., and Manning, L.A., "Radio Communication by Scattering from Meteoric Ionization," Proc. IRE, Vol. 42, pp 530-536, 1954.
- A.11-14 Eshelman, V.R., and Mlodnosky, R.F., "Directional Characteristics of Meteor Propagation Derived from Radar Measurements," Proc. IRE, Vol. 52, pp 1715-1723, 1957.
- A.11-15 Vincent, W.R., Wolfram, R.T., Sifford, B.M., Joyce, W.E., and Peterson, A.M., "A Meteor-Burst System for Extended Range VHF Communications," Proc. IRE, Vol. 45, pp 1695-1700, 1957.
- A.11-16 Blis, W.H., Wagner, R.J., and Wickizer, G.S., "Experimental Facsimile Communication Utilizing Intermittent Meteor Ionization," Proc. IRE, Vol. 52, pp 1734-1735, 1957.
- A.11-17 Honnum, A.J., Evans, G.L., Chambers, J.T., and Otten, K., "Air-to-Ground Meteoric Scatter Communication System," IRE Trans., Vol. CS-8, pp 113-133, 1960.
- A.11-18 Casey, J.P., and Holladay, J.A., "Some Airborne Measurements of VHF Reflection from Meteor Trails," Proc. IRE, Vol. 52, pp 1735-1736, 1957.

REFERENCES (Continued)

- A.11-19 Ince, A.N., "Spatial Properties of Meteor-Burst Propagation," IEEE Trans., Vol. COM-28, pp 841-849, 1980.
- A.12-1 Wait, J.R., "Electromagnetic Waves in Stratified Media," 2nd Edition, Pergamon Press Inc., New York, NY, 1970.
- A.12-2 Galejs, J., "Terrestrial Propagation of Long Electromagnetic Waves," Pergamon Press Inc., Oxford, England, 1972.
- A.12-3 Ratcliffe, J.A., "The Magento-Ionic Theory and Its Application to the Ionosphere," Cambridge University Press, London, 1959.
- A.12-4 Norton, K.A., "Low and Medium Frequency Radio Propagation," in Electromagnetic Wave Propagation, Editor, Desirant, M., and Michiels, J.L., Academic Press, 1960.
- A.12-5 Wait, J.R., "Introduction to the Theory of VLF Propagation," Proc. IRE, Vol. 55, pp 1624-1647, 1962.
- A.12-6 CCIR Recommendation 368, "Ground Wave Propagation Curves for Frequency Below 10 MHz," Document of XIth Plenary Assembly, 1966, Vol. II, pp 17-23.
- A.12-7 Johler, J.R., "Concerning Limitation and Further Corrections to Geometric - Optical Theory for LF, VLF Propagation Between the Ionosphere and the Ground," Radio Science, Vol. 68D, 1964.
- A.12-8 Wait, J.R., and Conda, A.M., "Pattern of an Antennas on a Curves Lossy Surface," IRE Trans., Vol. AP-6, pp 348, 1958.
- A.12-9 Johler, J.R., "Propagation of the Low Frequency Radio Signal," Proc, IRE, Vol. 50, No. 4, 1962.
- A.12-10 Belrose, J.S., "Low and Very Low Frequency Radio Wave Propagation," in AGARD Lecture Series XXIX, Radio Wave Propagation, AGARD, 1968.
- A.12-11 Institute for Telecommunication Sciences, "Telecommunication Research and Engineering Report 13, Ionospheric Predictions, Vol. 1, 2, 3 and 4," Office of Communications Institute for Communications Science, OT/TRE 13, Boulder, Colorado, 1971.
- A.12-12 CCIR, "CCIR Atlas of Ionospheric Characteristics," CCIR Report 340, 1966; ITU, Geneva, 1967.
- A.12-13 Fenwick, R.B., "Real-Time Frequency Management for Military HF Communications," pp 25, March 1980.
- A.12-14 Beach, J., "Assessing HF Propagation Conditions in Real-Time," Defense Electronics, pp 21, May 1980.

REFERENCES (Concluded)

- A.12-15 DCA, "Advanced High Frequency Communications Concept Formulation," DCA TM 120-76, May 1976.
- A.13-1 Goldstein, H., "Classical Mechanics," Addison Wesley, 1951.
- A.13-2 Forward, R. L. Hughes Research Laboratories, Private Communication.
- A.13-3 Arnold, R.C., "Telecommunications with Muon Beams," Science, Vol. 177, pp 163, 1972.
- A.13-4 Saenz, A.W., et al., "Telecommunication with Neutrino Beams," Science, Vol. 198, pp 295, 1977.